Magnetite and Green Rust: Synthesis, Properties, and Environmental Applications of Mixed-Valent Iron Minerals

Muhammad Usman, J M Byrne, A Chaudhary, S Orsetti, Khalil Hanna, C Ruby, A Kappler, S B Haderlein

Magnetite and green rust: synthesis, properties and environmental applications of mixed-valent iron minerals

M. Usman[1, 2*], J. M. Byrne[3], A. Chaudhary[1,4], S. Orsetti[1], K. Hanna[5], C. Ruby[6], A. Kappler[3], S. B. Haderlein[1]

[1] Environmental Mineralogy, Center for Applied Geosciences, University of Tübingen, 72074 Tübingen, Germany
[2] Institute of Soil and Environmental Sciences, University of Agriculture, Faisalabad–38040, Pakistan
[3] Geomicrobiology, Center for Applied Geosciences, University of Tübingen, 72074 Tübingen, Germany
[4] Department of Environmental Science and Engineering, Government College University Faisalabad, Pakistan
[5] Univ Rennes, École Nationale Supérieure de Chimie de Rennes, CNRS, ISCR – UMR6226, F-35000 Rennes, France

[6] Laboratoire de Chimie Physique et Microbiologie pour l'Environnement, UMR 7564 CNRS-Université de Lorraine, 54600 Villers-Lès-Nancy, France

* Corresponding author:
M. Usman
Research Fellow (Alexander von Humboldt-Foundation)
Environmental Mineralogy, Center for Applied Geosciences,
University of Tübingen
Hölderlinstr. 12, 72074 Tübingen, Germany
Email: muhammad.usman@uaf.edu.pk or: musmanch@yahoo.com
Phone No.: +49 70 71 29 78 924
Fax: +49 70 71 29 50 59

Abstract

Mixed-valent iron [Fe(II)-Fe(III)] minerals such as magnetite and green rust have received a significant amount of attention over recent decades, especially in the environmental sciences. These mineral phases are intrinsic and essential parts of biogeochemical cycling of metals and organic carbon and play an important role regarding the mobility, toxicity, and redox transformation of organic and inorganic pollutants. The formation pathways, mineral properties, and applications of magnetite and green rust are currently active areas of research in geochemistry, environmental mineralogy, geomicrobiology, material sciences, environmental engineering, and environmental remediation. These aspects ultimately dictate the reactivity of magnetite and green rust in the environment, which has important consequences for the application of these mineral phases, for example in remediation strategies. In this review we discuss the properties, occurrence, formation by biotic as well as abiotic pathways, characterization techniques, and environmental applications of magnetite and green rust in the environment. The aim is to present a detailed overview of the key aspects related to these mineral phases which can be used as an important resource for researchers working in a diverse range of fields dealing with mixed-valent iron minerals.

Contents

1. Introduction

Iron (Fe) is the fourth most abundant element in the earth crust with an average mass concentration of 5.6% and is the second most abundant metal after aluminum.[1] Fe exists in almost all aquatic and terrestrial environments. Fe is commonly found to form together with O, and/or OH either oxides, hydroxides or oxide-hydroxides which are collectively referred to as 'iron oxides' in this review article. There are 16 known iron oxides (Table 1) having different crystal structure, chemical composition and, Fe valence state.[2] Iron oxides are categorized into three different groups based on Fe oxidation state including: (i) ferric oxides bearing only trivalent Fe(III), including ferrihydrite, goethite, hematite, lepidocrocite etc., (ii) very rare ferrous oxides containing exclusively divalent Fe(II), with only examples of Fe(II)O and $Fe(II)(OH)_2$, and (iii) mixed-valent iron oxides containing both Fe(III) and Fe(II) in their structure which include magnetite and green rust (GR). Iron predominantly exists as Fe(III) oxides especially near the surface of Earth's crust due to the presence of oxygen. However, under appropriate redox conditions in aquatic or terrestrial environments, Fe(III) oxides can serve as electron acceptors for microbial respiration or react with Fe(II) or other reductants to form mixed-valent Fe minerals such as magnetite and GR which are the focus of this review. Magnetite [$Fe(II)Fe(III)_2O_4$], a black ferromagnetic mineral, is a member of the spinel group of minerals while GRs are layered double hydroxides.[3] GRs appear in intense bluish green colors. Structurally, GRs contain both Fe(II) and Fe(III) cations in brucite-like layers along with intercalated anions. Most common types of GRs are hydroxysulfate GR [$GR(SO_4^{2-})$], hydroxycarbonate GR [$GR(CO_3^{2-})$], and hydroxychloride GR [$GR(Cl^-)$] according to the type of intercalated anions, i.e., sulfate (SO_4^{2-}), carbonate (CO_3^{2-}), or

chloride (Cl^-), respectively. A detailed description of structural properties of both magnetite and GR is presented in the section 2 of this review.

Table 1: Overview of iron oxides. Reproduced with permission from Ref. 2. Copyright 2003 Wiley-VCH Verlag GmbH & Co. KGaA.

Oxide-hydroxides and hydroxides	**Oxides**
Goethite α-FeOOH	Hematite α-Fe_2O_3
Lepidocrocite γ-FeOOH	Magnetite Fe_3O_4
Akaganéite β-FeOOH	Maghemite γ-Fe_2O_3
Schwertmannite $Fe_{16}O_{16}(OH)_y(SO_4)_z \bullet nH_2O$	β-Fe_2O_3
δ-FeOOH	ε-Fe_2O_3
Feroxyhyte δ'-FeOOH	Wüstite FeO
High pressure FeOOH	
Ferrihydrite $Fe_5HO_8 \bullet 4H_2O$	
Bernalite $Fe(OH)_3$	
$Fe(OH)_2$	
Green rusts $Fe(III)_xFe(II)_y\ (OH)_{3x+2y-z}(A^-)_z$; $A^- = Cl^-$; 1/2 SO_4^{2-}	

Mixed-valent Fe minerals are amongst the most reactive iron compounds due to their role in biogeochemical cycling of trace elements, their ability to affect the mobility, redox transformation, and toxicity of various organic and inorganic pollutants, and their use in various environmental remediation strategies. A large amount of research concerning mixed-valent iron oxides has been carried out in recent decades, but despite the immense amount of collected research data, no comprehensive review of this topic has been published. Our review article is intended to compile the research data related to all aspects of mixed-valent Fe minerals (magnetite and GR) including their characteristics, presence, formation, and role in the environment.

Only narrow aspects of this wide research field were reviewed so far. For example, a very recent review article by Su C.[4] describes the environmental applications of engineered magnetite nanoparticles and its hybrid composites. Munoz et al.,[5] in 2015, reviewed various methods to form magnetite-based catalysts followed by their

efficiency to improve Fenton oxidation for treatment of industrial wastewater. In 2013, Tang et al.[6] presented a comprehensive review of various factors to be considered for sustainable environmental application of magnetic nano-materials like magnetite, maghemite, and zero-valent iron (Fe^0). Another review article in 2012 discussed the catalytic role of various iron oxides to improve Fenton oxidation.[7] In 2008, Trolard et al.[8] reviewed the iron cycle with a special focus on the GR and consequences of its reactivity on geochemical cycles of Fe and other elements. The monography by Cornell and Schwertmann[2] (first published in 1996 and revised in 2003) is by far the most comprehensive document on iron oxides that compiles all related aspects in one volume. In 2001, Hansen[3] reviewed the environmental chemistry of GRs with focus on their formation, stability and environmental applications. In addition to these reviews, mixed-valent iron oxides were also discussed as a part of review articles along with other reactive minerals.[9-13] It should be noted that biomedical applications of magnetite are not within the scope of this review and thus are disregarded as well as modified forms of these minerals or pure end member minerals such as Fe(III) oxides (e.g. goethite) with adsorbed Fe(II).

Here, we compile the research data from numerous publications working on different aspects related to magnetite and GR in the environment. As a first part of this review, the properties of these mixed-valent Fe minerals are discussed. Depending on the nature of the initial precursor, routes of synthesis can be tailored to tune the properties of the final product. This connection to the structural properties, magnetic measurements, redox potential, and stoichiometry (i.e., the relative proportions of Fe(II) and Fe(III)) is critically illustrated in the properties section. Next the occurrence of these mixed-valent Fe minerals is discussed both in near surface natural settings and engineered systems (as the corrosion of manmade materials) in

environment. Note that reactions and formation of these minerals in deep geological settings at high temperature or pressure are outside the scope of this work. Common methods of synthesizing mixed-valent Fe minerals are outlined including abiotic (co-precipitation, Fe(II) oxidation, Fe^0 oxidation, and transformation of Fe(III) oxides) and biotic techniques (bacterial Fe(II) oxidation or Fe(III) reduction). The synthesis section highlights various mechanisms involved in the formation of mixed-valent Fe minerals. The characterization section describes various techniques which are frequently used to identify the mineralogy or morphology of the target minerals. The environmental applications section reviews the use and efficiency of mixed-valent Fe minerals to remediate pollutant contamination via sorption, reductive transformation, and advanced oxidation processes. This review article intends to provide an authoritative reference for the numerous researchers working on various aspects of mixed-valent Fe minerals in near surface environments.

2. Properties of mixed-valent iron minerals

2.1. Structural properties

Magnetite

Magnetite is a member of spinel class of minerals (named after spinel; $MgAl_2O_4$) that contain mixed anions and cations. The general formula for spinels is AB_2O_4 where A and B designate divalent and trivalent metallic cations, respectively. A spinel structure contains all divalent cations on tetrahedral sites while all trivalent cations are in octahedral coordination. However, in an "inverse" spinel structure, octahedral sites are shared by divalent and trivalent cations. Magnetite is an inverse spinel and its structural formula can be written as $Fe(III)_{tet}[Fe(II)\ Fe(III)]_{oct}O_4^{2-}$. Structurally, it contains two iron sub-lattices (Figure 1) including a tetrahedral coordination (Fe_{tet})

occupied by Fe(III), and an octahedral coordination (Fe_{oct}) bearing Fe(II) and Fe(III).[14] Alternating planes of Fe_{tet} and Fe_{oct} are stacked along [111] in magnetite structure (Figure 1). Magnetite exhibits the highest electrical conductivity (1 – 10 Ω^{-1} m^{-1}) among iron oxides[2] which is attributed to the rapid migration of mobile charges by electron hopping on Fe occupied sites[14] or by hopping of mobile Fe(II) between unoccupied lattice sites.[15]

It is interesting to point out that many studies have evidenced that iron dissolution in magnetite preferentially occurs at Fe_{oct} in mildly acidic medium (pH 2 – 2.5).[16-18] Only octahedral Fe was preferentially exchanged when magnetite is reacted with aqueous Fe(II).[16-18] However, Gorski et al.[15] did not indicate any preferential exchange of octahedral or tetrahedral sites when ^{56}Fe(II) was reacted with magnetite at circumneutral pH. In this regard, they proposed two mechanisms (Fe atom diffusion and bulk electron conduction) that might be responsible for atom exchange of aqueous Fe(II) and magnetite.[15]

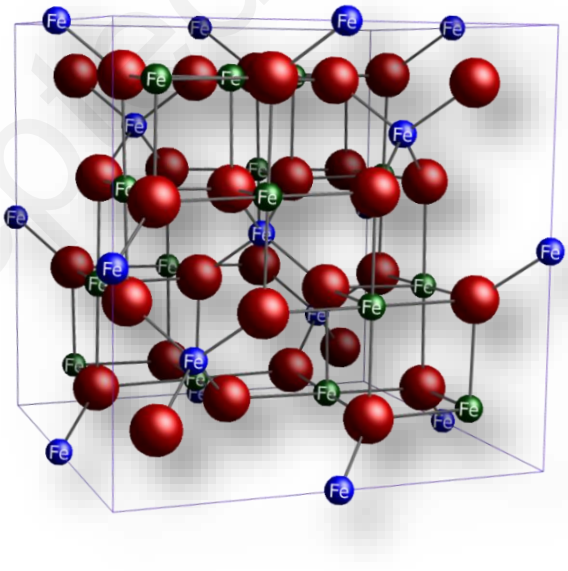

Figure 1: Ball and stick model of the unit cell of magnetite. Octahedral Fe ions are in green, tetrahedral Fe ions are in blue, oxygen ions are in red. Created using CrystalMaker® for Windows version 2.2.

Green rust: chemical composition of the interlayer and structural models

The general structural formula of GRs can be written as $[Fe(II)_{1-x}\ Fe(III)_x(OH)_2]^{x+}$. $[(x/n)\ A^{n-},\ m\ H_2O]^{x-}$ where A^{n-} denote intercalated anions and x represents the molar fraction of trivalent cation that usually ranges from 0.25 – 0.33. Structurally, GR consist of brucite-like layers containing both divalent and trivalent cations that are interlayered by anions and structural water. Owing to this type of layered structure, GRs are placed in layered double hydroxides class of minerals, also known as anionic clays. Detailed description of iron based layered double hydroxides has been provided by Ruby et al.[19] Metal hydroxide sheets have a positive charge which is correlated to the partial replacement of divalent by trivalent metal cations. There are a variety of anions which are intercalated in GR structure including (i) simple monovalent anions (e.g. Br^-, Cl^-, F^-), (ii) divalent oxo-anions, (e.g. CO_3^{2-}, SO_4^{2-}), (iii) organic anions of varying sizes (e.g. $HCOO^-$, $C_2O_4^{2-}$, $CH_3(CH_2)_{10}COO^-$), and surfactants. The chemical formula, space group, cell parameters, and interlayer distance of $GR(SO_4^{2-})$, $GR(CO_3^{2-})$, and $GR(Cl^-)$ are summarized in Table 2. GR intercalating other anions such as selenite,[20] formate,[21] C_9-C_{14} linear alkyl carboxylates,[22] and oxalate[23] can be obtained by oxidation of $[Fe(OH)_2, Fe(II)]$ mixtures (Section 4.1.2).

Table 2: Crystallographic data of three types of green rust (GR). The values of *a* and *c* are the cell parameters and d_0 corresponds to the interlayer distance.

Type of green rust	**$GR(SO_4^{2-})$**	**$GR(CO_3^{2-})$**	**$GR(Cl^-)$**
Chemical formula	$Fe(II)_4Fe(III)_2(OH)_{12}SO_4,8H_2O$	$Fe(II)_4Fe(III)_2(OH)_{12}CO_3,3H_2O$	$Fe(II)_3Fe(III)(OH)_8Cl,\sim1.5H_2O$
Space group	P-3m1	R-3m	R-3m
***a* (Å)**	5.5524 [24]	3.1759 [25]	3.19 [26]
***c* (Å)**	11.011 [24]	22.7123 [25]	23.85 [26]
***d_0* (Å)**	11.011	7.57	7.95

The structure and composition of GRs is dependent on the nature of intercalated anions. For instance, Bernal et al.[27] divided the GR family into two groups based on their X-ray diffraction (XRD) data: GR-I with a rhombohedral unit cell and GR-II with a hexagonal unit cell. Planer or spherical anions (e.g. CO_3^{2-}, Br^-, Cl^-) lead to GR-I consisting of three repeat units (Figure 2a) and three dimensional anions (e.g. SO_4^{2-}, SeO_4^{2-}) are indicative of GR-II that are composed of 2 repeat units (Figure 2b).[24,26,28,29] These types represent quite different interplanar distances of the stacking sequence along the c axis (d_0 7.6 – 8 Å and 10.9 Å for GR-I and GR-II, respectively). The hydroxide sheets in GR-II are separated by interlayers composed of two adjacent planes of anions and water molecules, as compared to the one plane in GR-I.[24] In an elementary stratum of GR-II, stacking sequence is described as *AcBij*. . ., where A and B denote planes of OH^- ions, c represents that of Fe cations and i, j denotes interlayers planes. In this stratum, molecules of i and j planes are located close to the positions of A and B [(~ A) and (~ B)], respectively, yielding a hexagonal close-packed stacking of oxygen atoms *AcB(~A)(~B)* . . . On the other hand, *AcB(~B)* . . ., is the sequence in an elementary stratum of GR-I where water molecules in interlayers are located vertically above OH^- ions of adjacent hydroxide layers.[24,26]

The successive strata are also arranged differently in crystal structure of both GRs that is due to location of intercalated water molecules.[24] Simon et al.[24] proposed that the *AcB(~B)* . . . sequence in GR-I induces a three-layer repeat *AcB(~B)BaC(~C)CbA(~A)A* . . . leading to a rhombohedral structure. In GR-II, only one single-layer repeat is induced by *AcB(~A)(~B)* . . . sequence yielding a primitive hexagonal cell. However, Christiansen et al.[30] proposed a different structural model with Na inside structure based on their data for GR-II (GR-SO_4) (contrary to the model by Simon[24] et al. without Na). Structural model by Christiansen et al.[30] proposed different orientation

of SO_4^{2-} anions and inclusion of Na atoms in the interlayer. They pointed out that SO_4^{2-} tetrahedra bases were nearest to the hydroxide layers; their apices point into the interlayer space and they are surrounded by three water molecules. However, Simon et al.[24] oriented the SO_4^{2-} so the apical oxygen was nearest to the hydroxide layer to achieve best refinement results. It should be noted that solid was prepared in the presence of Na in both cases. Christiansen et al.[30] proposed its chemical formula as $NaFe(II)_6Fe(III)_3(SO_4)_2(OH)_{18}.12H_2O$ that lead to to a $Fe:SO_4^{2-}$ ratio of 9 : 2 = 4.5 due to an excess of Na inside the structure. However, this ratio was found very close to 6 : 1 (without Na) in another laboratory measurement[31] as proposed in the previous formula of $Fe(II)_4Fe(III)_2(OH)_{12}SO_4.H_2O$ by Simon et al.[24] Some quantity of Na (< 3 at. %) is often found associated to GR as observed by transmission electron microscopy coupled with an energy dispersive X-ray system (TEM-EDX)[32] but there is no clear evidence that the Na atoms are located in the interlayer. Based on this disagreement in literature, further research should be conducted to identify a definitive structural model. It should be noted that if alkaline metal cations are part of the GR interlayer, then many chemical compositions reported in the literature should be reconsidered.

Génin et al.[33] described GR-I with stacking sequence of *AcBiBaCjCbAkA*…, where *A–C*, *a–c* and *i–k* denote OH^- planes, metal cation layers and intercalated layers, respectively.[24,34]

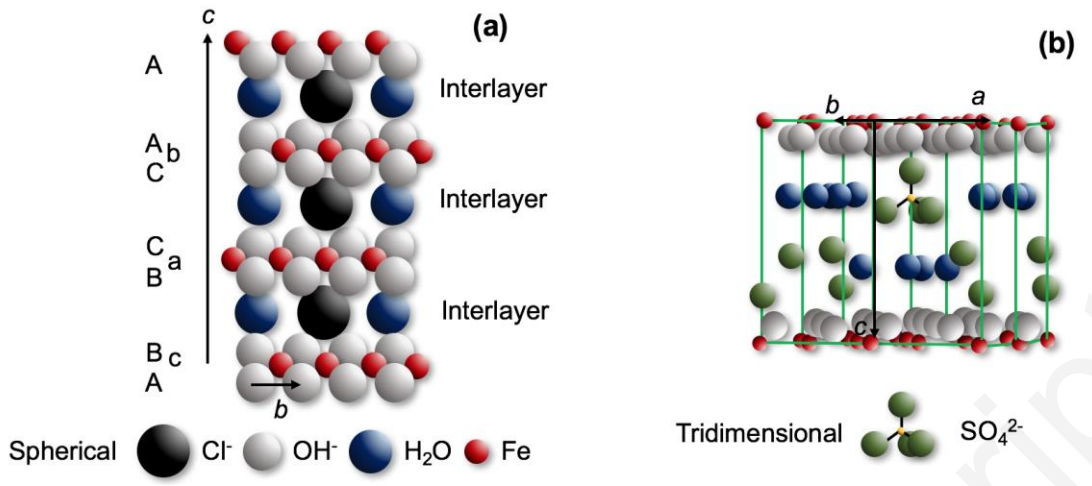

Figure 2: General view of the crystal structure of green rusts: (a) GR-I (Cl^-) (b) GR-II (SO_4^{2-}). Image (a) is adapted with permission from Ref. 26. Copyright 1998 Elsevier. Image (b) is adapted with permission from Ref. 24. Copyright 2003 Elsevier Masson SAS.

2.2. Fe(II) : Fe(III) ratio

Mixed-valent Fe minerals can have a range of oxidation states dependent upon the amount of structural Fe(II) which can be discussed quantitatively as their stoichiometry (x = Fe(II)/Fe(III)).[35] Magnetite containing ideal Fe(II) contents (x = 0.5) is known as stoichiometric magnetite (assuming $Fe(II)Fe(III)_2O_4$ formula). In stoichiometric magnetite, Fe(III) occupies both tetrahedral and octahedral sites equally, while Fe(II) is only located in the octahedral sites. However, stoichiometric GRs (~ $3 \leq x \leq 2$) contain at least two times more Fe(II) than stoichiometric magnetite. Oxidation of mixed-valent Fe minerals causes a decrease in Fe(II)/Fe(III) ratio ($x < 0.50$ and $x < 2$ for magnetite and GR respectively) which is denoted as a partially oxidized or nonstoichiometric phase. Stoichiometry is also defined in the literature as R = (Fe(III) / (Fe(II) + Fe(III)) and its value is 0.67 and 0.25–0.33 for stoichiometric magnetite and GR.[36] The structure of nonstoichiometric magnetite is often expressed as $Fe_{3-\delta}O_4$, where δ represents the departure from stoichiometry. Its

(δ) value can range from zero (stoichiometric magnetite) to 1/3 (completely oxidized). Complete oxidation of magnetite (x = 0) yields maghemite. This formula can be written as $Fe(III)_{tet}[Fe(II)_{1-3\delta}\, Fe(III)_{1+2\delta}\square_{\delta}]_{oct}O_4$, where □ are vacancies formed in the crystal structure to account for charge balance.[35] For magnetite, the following equation can be used to easily convert the stoichiometry to and from the different notations:[35]

$$x = \frac{Fe(II)}{Fe(III)} = \frac{1-3\delta}{2+2\delta} \quad (1)$$

Stoichiometry is mainly dictated by the synthesis method, source, experimental conditions, and aging time, etc.[36,37] For example, Zegeye et al.[36] reported that the stoichiometry was different when magnetite was formed from lepidocrocite by bioreduction (δ ~ 0) or by abiotic Fe(II)-induced mineralogical transformation (δ ~ 0.05). In case of biogenic magnetite, the value of δ was very low (0.025) after one day of incubation but a full stoichiometric magnetite (δ ~ 0) was obtained after one month of incubation.[36] The stoichiometry of the final mineral phase was also found to be dependent on the nature of the initial ferric oxides when magnetite was formed by abiotic transformations of ferrihydrite (δ ~ 0.04), lepidocrocite (δ ~ 0.05), and goethite (δ ~ 0.08).[37]

The stoichiometry of mixed-valent Fe minerals dramatically influences their reactivity and structural properties including crystalline structure,[38] reduction potential,[39,40] sorption capacity,[41] catalytic ability in advanced oxidation processes.[42-45] Stoichiometric phases (δ = 0) or the ones containing higher Fe(II) contents are considered as the most reactive phases in this regard while non-stoichiometric phases have lost their reactive nature.[39,43,44] A detailed description of the effect of stoichiometry of mixed-valent Fe minerals on their reactivity is presented in Section 6. Exposing non-stoichiometric magnetite to a Fe(II) source can restore its

stoichiometry (x = 0.5 or δ = 0) through oxidation of adsorbed Fe(II), accompanied by reduction of the octahedral Fe(III) in the underlying magnetite to octahedral Fe(II).[40] The extent of aqueous Fe(II) uptake depends on the stoichiometry of magnetite. Gorski and Scherer[40] showed that Fe(II) uptake by the least stoichiometric magnetite (x = 0.28) was four times higher than by the most stoichiometric phase (x = 0.48). However, uptake of Fe(II) was limited by formation of stoichiometric magnetite.[40] Owing to the strong influence of stoichiometry, an accurate and precise measurement of stoichiometry is crucial in characterization of mixed-valent Fe minerals. There are various methods which are commonly used to measure their stoichiometry including (i) complete acidic dissolution,[17,40,42,44] (ii) ^{57}Fe Mössbauer spectroscopy,[36,37,46] (iii) powder XRD,[46,47] and (iv) X-ray magnetic circular dichroism (XMCD).[48] Acidic dissolution is a simple way to measure stoichiometry but care should be taken to avoid oxidation of Fe(II) in air. This method has limited application in natural and mixed phases containing redox-active compounds or functional groups that are attached to the particle surface.[35] For such samples, spectroscopic techniques are preferred because samples can be characterized without any additional pretreatment (such as washing). To measure stoichiometry, Mössbauer spectroscopy (Section 5.2 for details) relies on the hyperfine parameters extracted from mineral spectra (relative area of Fe(II) and Fe(III) doublets) by appropriate fitting models.[2,36] Powder XRD is based on the unit-cell length of magnetite which becomes smaller upon oxidation due to the lower size of Fe(III) as compared to the Fe(II) and formation of vacancies.[35] XMCD provides precise information of the relative site occupancies in spinels[49,50] which can be used to determine the stoichiometry of magnetite, especially at the surface of the mineral.[48] A detailed description of the XMCD technique is provided in Section 5.4. It should be noted that many reported stoichiometry measurements of

mixed-valent Fe minerals have relied mostly on singular techniques without validation by secondary analyses.[36,37,44,51] Gorski et al.[35] indicated an excellent agreement between stoichiometry of magnetite measured by acidic dissolution and Mössbauer spectroscopy. A significant linear correlation was also reported between the unit-cell length of magnetite measured by powder XRD and magnetite stoichiometry measured by acidic dissolution or Mössbauer spectroscopy.[35]

2.3. Redox potential

In aqueous environments, the reactivity of a Fe mineral is strongly dependent upon its ability to undergo reduction (gain electrons) and oxidation (lose electrons) in redox reactions. As electrons do not freely exist in aqueous solution each reduction must be coupled to an oxidation and vice versa.[52] The tendency of a mineral to gain or lose electrons is commonly referred to as the redox potential (E) which is reported in volts (V) or millivolts (mV). The more positive the redox potential is, the stronger the oxidizing power of the mineral is, whilst by contrast the lower (more negative) the redox potential is, the strongest the reducing power of the mineral is. Redox potentials depend strongly upon several factors including pH, temperature, and concentration of reactants. For example the self-induced redox potential reported for magnetite reduction to aqueous Fe(II) by White et al.[53] is seen to vary from +0.38 V at pH 3 to +0.27 V at pH 7. The presence of dissolved Fe(II) is a particularly important factor, since Fe minerals become significantly more reducing even in the presence of small Fe(II) concentrations. Due to the semiconducting properties of Fe minerals, there are several processes that might take place upon sorption of Fe(II) to the solid, including electron transfer, conduction, dissolution, atom exchange and formation of secondary minerals. Gorski and Scherer presented a revised conceptual framework where the Fe(II) becomes oxidized upon sorption to Fe(III) minerals and different possible fates

for the lost electron are presented.[54] The exact mechanism of this process is still under discussion. Furthermore, the redox potentials of solid oxides varies with crystal phase and grain size.[55]

Whilst there is extensive research into redox potential measurements of minerals, an in-depth understanding of mineral redox processes is still difficult to achieve. There are two main classic techniques to determine the redox potential of minerals: non-invasive electrochemical methods (e.g. redox electrodes) and dissolving the mineral to quantify the ratio of oxidized and reduced species and using these to calculate a theoretical Nernstian potential. Metallic redox electrodes commonly used to estimate redox potentials (such as Pt ring) usually do not provide reliable measurements in the case of minerals due to a number of factors such as sorption of mineral to the electrode, lack of redox equilibria between the analyte and the electrode and absence of active species in solution, among others.[56] On the other hand, dissolving the sample and quantifying the activity of redox active species is a time consuming and experimentally troublesome method, where anoxic conditions are required for satisfactory results.

Nevertheless, in order to determine redox potentials of minerals, many studies have developed indirect measurements such as through reactions between the Fe minerals and probe compounds (e.g. nitrobenzene and quinones).[56,57] Alternatively, mediated electrochemical techniques make use of dissolved redox active compounds, which facilitate electron transport between mineral and electrode.[58] Consequently, through various theoretical and measurement based techniques,[58,59] the standard redox potentials of a number of different Fe(III) minerals have been determined for their reduction to Fe(II) (Table 3).

Table 3: Standard redox potentials (E^0) of iron minerals (vs SHE). "Theoretical" refers to values calculated from free standard enthalpies of formation;[59] "Chemical

reduction" refers to experimental quantification of ferrous iron after reduction of minerals with H_2;[59] "Mediated potentiometry" refers to values obtained by measuring redox potential of mineral suspensions using a Pt redox electrode in the presence of a soluble electron transfer mediator.[58] $Fe(OH)_3$ is a generic form of a more complex structure of ferrihydrite which is still under debate.

	Ferrihydrite	**Lepidocrocite**	**Goethite**	**Hematite**
Reaction	$Fe(OH)_3 + e^- + 3H^+ = Fe^{2+} + 3H_2O$	γ-$FeOOH + e^- + 3H^+ = Fe^{2+} + 2H_2O$	α-$FeOOH + e^- + 3H^+ = Fe^{2+} + 2H_2O$	0.5α-$Fe_2O_3 + e^- + 3H^+ = Fe^{2+} + 1.5H_2O$
Theoretical[59]	1.06 V	0.86 V	0.71 V	0.73 V
Chemical reduction[59]	0.939-1.031 V	0.892-0.938 V	0.720-0.790 V	0.764-0.828 V
Mediated potentiometry[58]	-	-	0.768 V	0.769 V

The redox behavior of the mixed-valent mineral magnetite, however, remains relatively poorly understood. This is in part due to the complication that more than one redox-active species (e.g. Fe(II) and Fe(III)) at different potentials are present in magnetite at the same time, which can lead to "mixed potentials" which simultaneously contribute to the net measured potential.[60] Similar observations have been reported for iron-bearing clays at different Fe(II) to Fe(III) ratio, where a distribution of redox potentials was modelled.[61] Therefore, a wide range of redox potentials for magnetite at neutral pH have been quoted in the literature including +0.27 V,[53] -0.314 V,[55] -0.38 V[62] when measured against the standard hydrogen electrode (SHE). The reason for this discrepancy in redox potentials for magnetite has been suggested to be due to variations in the Fe(II)/Fe(III) ratio of the samples under investigation.[39] Gorski et al.[39] measured the redox potential in terms of the open circuit potential (E_{OCP}) of a wide range of magnetite's with different stoichiometry. The study found that stoichiometric magnetite (Fe(II)/Fe(III)=0.5) had the lowest redox potential whilst the fully oxidized end member maghemite (Fe(II)/Fe(III)=0) had the highest redox potential (Figure 3). This linear relation between redox potential

and stoichiometry also has important implications in the ability for magnetite to be used as a remediation agent for different environmental pollutants.[40,63]

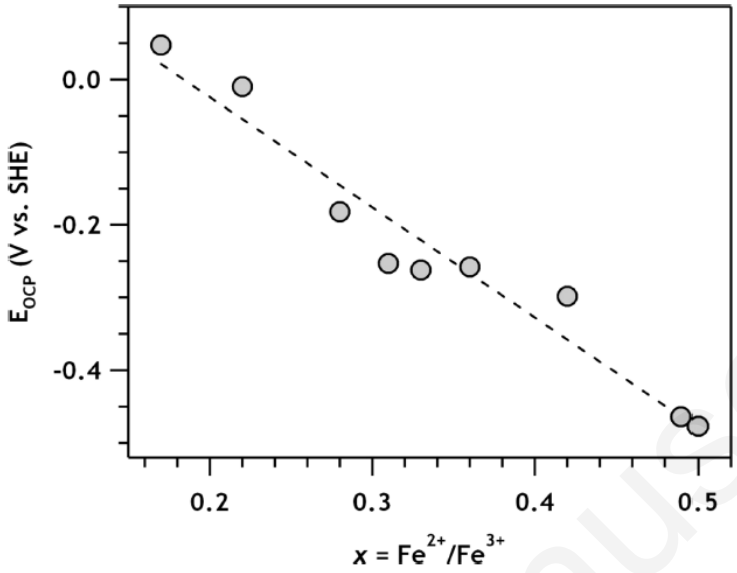

Figure 3: Open circuit potentials (E_{OCP}) of magnetite as a function of stoichiometry (Fe(II)/Fe(III) ratio). Reproduced from Ref. 39. Copyright 2009 American Chemical Society.

2.4. Magnetic properties

This section will focus primarily on the magnetic properties of magnetite (also known as Lodestone) which is thought to be the oldest magnetic material known to man and has been described as the most important magnetic mineral on Earth. In the environment, iron deposits can be naturally magnetized though lightning strikes, however, it is also derived from a number of different sources including the breakdown of igneous rocks (e.g. basalt), from volcanic eruptions, Fe(III)-reducing, Fe(II)-oxidizing, and magnetotactic bacteria (see section 4.2), as well as though anthropogenic pollution.[64] The magnetic properties of these types of magnetite are hugely diverse making it challenging to specify any one particular type being more environmentally relevant than the other. For instance, titanium substituted magnetite

(ülvospinel) typically forms via magmatic processes as oppose to microbiological pathways or during sedimentation. Nevertheless, it is often reported as the most common magnetic mineral and is the main source of rock magnetism on Earth[65] however, its inclusion in this review is restricted.

To most effectively understand the reasons why magnetite is magnetic, it is important to consider the general crystal structure of the mineral. Magnetite has an inverse spinel crystal structure with a cubic unit cell (a = 8.396 angstroms) in which 32 oxygen ions are arranged in an approximately close packed array (Figure 1). Iron ions fill some of the spaces between the oxygen ions. Specifically, eight Fe(II) and eight Fe(III) ions are arranged in octahedral (B) coordination surrounded by six oxygen ions, and eight Fe(III) ions are arranged in tetrahedral (A) coordination surrounded by four oxygen ions. This means that the ratio of Fe(III) to Fe(II) is 2:1 which maintains charge neutrality in combination with the O^{2-} ions. Each Fe(II) and Fe(III) ion has a magnetic moment of 4 and 5 μ_B respectively. Magnetic exchange interactions exist between neighboring Fe ions in which the A site ions are arranged in antiparallel orientation to the B site ions. This results in the magnetic spin orientations of all A site ions being arranged in parallel and opposite directions to magnetic spin orientations of all B site ions. Since Fe(III) ions occupy A and B sites equally, there is no net magnetization from these ions because their spin states cancel each other out. This gives rise to a net magnetization due to the Fe(II) ions in the B site which for bulk magnetite is reported as 92 $Am^2\ kg^{-1}$.[66] As a result of this distribution of magnetic ions within the mineral any changes to the Fe(II)/Fe(III) ratio can have a significant effect on the bulk magnetic properties of the magnetite. For example, maghemite ($Fe(III)_{Tet}[Fe(III)_{5/3}\square_{1/3}]_{Oct}O_4$) is the fully oxidized form of magnetite, containing no Fe(II), and is known to have a lower bulk saturation magnetization (M_s)

of ~75 Am^2 kg^{-1} at room temperature. Other factors which also influence the magnetic properties of the mineral include the particle size[67] and the inclusion of transition metals such as cobalt, zinc, and titanium.[68,69] For zinc, Zn(II) ions replace Fe(III) in tetrahedral lattice sites which suppresses part of the antiparallel magnetic moment. This means that the magnetic moment of the octahedral lattice becomes larger relative to the tetrahedral moment and the Zn doped magnetite becomes more magnetic. In the case of cobalt, Co(II) replaces octahedral Fe(II) which should in principle make the mineral less magnetic, however due to the magnetic moment of the Co(II) ion, this decrease is relatively minor. Instead, the presence of Co(II) increases the coercitvity of the Co doped magnetite which makes it harder to switch the magnetization direction of the mineral. Such a property is advantageous for biomedical applications such as cancer therapy or targeted drug delivery.[70] In titanomagnetite, Ti(IV) are situated in the B sites which means that in order to maintain overall charge neutrality, some of the Fe(III) ions must be replaced to Fe(II). Ülvospinel (Fe_2TiO_4) consists of Fe(II) ions on the A site, and an equal amount of Fe(II) and Ti(IV) on the B site. Since Ti(IV) has no magnetic moment, the net magnetization of ülvospinel is consequently much lower than that of magnetite (Table 4).

Several of the magnetic properties of magnetite depend upon temperature with one of the most characteristic features of magnetite referred to as the Curie temperature (T_c). T_c corresponds to the temperature above which magnetite is no longer magnetic and acts as a paramagnet. Essentially, above this temperature there is sufficient thermal energy for the magnetic ions within the mineral to become randomly orientated to each other, resulting in zero net magnetization. T_c can be determined through the measurement of magnetic susceptibility over a range of temperatures and is generally

observed to take place at ~580 °C. For a sample of pure stoichiometric magnetite, when the temperature is decreased again, the susceptibility curve will follow the heating curve. When these curves do not match, this could indicate the presence of non-stoichiometry or the presence of impurities in the mineral.[65]

A second important characteristic temperature dependent feature of magnetite is called the Verwey transition (T_v). The transition is often characterized by a significant step in the magnetization of magnetite at ~120 K and is a result of magnetite undergoing a transition from cubic crystal symmetry to a lower symmetry (likely monoclinic) structure.[71] T_v is known to be sensitive to the presence of additional elements, e.g. Ti(IV)[72] and Al(III),[73] as well as Fe(II)/Fe(III) ratio[74] whilst its dependence upon size is less clear, especially in the superparamagnetic regime[75] and for many synthetic magnetite does not appear to be present at all.[76] This transition is also observable to some extent using Mössbauer spectroscopy and is thought to correspond to the point at which electron hopping between Fe(II) and Fe(III) sites within the A site no longer takes place. Within Mössbauer, this is characterized by the requirement to add an additional sextet during fitting.

Ultimately, it is possible to identify the presence of different mixed-valent minerals, in particular magnetite and minerals from the spinel group, within environmental samples through the use of magnetic characterization methods.

Table 4: Magnetic properties of some typical environmental minerals[77]. T_c – Curie temperature, M_s – saturation magnetization

Mineral	Formula	T_c (°C)	M_s (Am^2 kg^{-1})
Iron	Fe	770	218
Magnetite	Fe_3O_4	575-585	90-922
Ülvospinel	Fe_2TiO_4	-153	0
Jacobsite	$MnFe_2O_4$	~300	77
Trevorite	$NiFe_2O_4$	585	51
Greigite	Fe_3S_4	~333	~25

2.5. Thermodynamic properties

The standard Gibbs energy of formation ($\Delta G°_f$) of the synthetic GR minerals were most often determined by redox potential measurements performed during oxidation of [$Fe(OH)_2$, $Fe(II)_{aq}$] mixtures by dissolved O_2 in contact with ambient air (detailed in Section 4.1.2). As discussed in a recent re-evaluation of thermodynamic data concerning GR($C_2O_4^{2-}$),[23] the position of the redox potential plateau is used for the determination of the value of $\Delta G°_f$(GR). These authors indicated that the equilibrium potential of the $Fe(OH)_2$ / GR couple should be determined under anoxic conditions and should be calculated by using the same initial value of the Gibbs energy of $Fe(OH)_2$, *i.e.* ($\Delta G°_f(Fe(OH)_2) = -490 \pm 1$ kJ mol^{-1}.[29] The values of $\Delta G°_f$ of both GR intercalating different anions and stoichiometric magnetite[78] are given in Table 5. The $\Delta G°_f$ value of anhydrous GR(SO_4^{2-}) is very reliable since it was determined independently by Ayala Luis et al.[79] and Refait et al.[29] by using a completely different experimental approach, i.e. slow acid titration of GR(SO_4^{2-}) and oxidation of [$Fe(OH)_2$, $Fe(II)_{aq}$] mixtures. GR is thermodynamically metastable in comparison with magnetite. Indeed, Refait et al[80] showed that if GR(SO_4^{2-}) and magnetite are considered in a Eh-pH Pourbaix diagram, the large stability domain of magnetite will always overlap the stability domain of GR(SO_4^{2-}). For kinetic reasons, GR can form much more rapidly than magnetite, in particular in Fe(II)-rich aqueous medium as observed in co-precipitation experiments[81] and during transformation of ferric minerals[51]. However, in strongly alkaline solution (pH > 10) or acidic solution (pH < 5), GRs rapidly transform either into [Fe_3O_4, $Fe(OH)_2$] or [FeOOH, $Fe(II)_{aq}$] mixtures, respectively.

Table 5: Gibbs standard energy of formation (ΔG^0_f) of the dehydrated (anhydrous) forms of green rust and magnetite.

Mineral type	**$\Delta G°_f$ (kJ mol^{-1})**	**Ref.**
$Fe(II)_4Fe(III)_2(OH)_{12}SO_4$	– 3790 ± 10	[29]
$Fe(II)_4Fe(III)_2(OH)_{12}SO_4$	– 3819.44 ± 6.44	[79]
$Fe(II)Fe(III)_2(OH)_{12}CO_3$	– 3590 ± 10	[23]
$Fe(II)_6Fe(III)_2(OH)_{16}C_2O_4$	– 4712 ± 9	[23]
$Fe(II)_3Fe(III)(OH)_8Cl$	– 2146 ± 5	[23]
Fe_3O_4	– 1012.57	[78]

3. Occurrence of mixed-valent iron minerals in the environment

Mixed-valent Fe minerals are commonly present under very diverse environmental and geochemical conditions, or as the products of the corrosion of manmade materials. The occurrence of these mineral phases is discussed below.

3.1. Natural environments

The occurrence of Fe(II)/(III) hydroxides, termed 'green rusts', was mentioned for the first time in a PhD dissertation by Keller in 1948 (cited by McGill et al.[82] and Bearcock et al.[83]). The mineralogist Reginald Taylor was the first to propose that the bluish-green color in hydromorphic gleysol (Figure 4) could be associated to the presence of GR.[84] For the first time in 1997, Trolard et al.[85] identified GR in hydromorphic soil sampled from forest of Fougères (Brittany, France) by using Mössbauer and Raman spectroscopies. In recognition of its original sampling location, this GR sample has been named fougèrite which was approved by the International Mineralogical Association in 2004.[86,87] Feder et al.[87] used a miniaturized Mössbauer spectrometer (MIMOS) for an in-situ study of gleysol. Formation of

fougèrite was observed by coprecipitation of Fe(II), Fe(III), and Mg(II) when soil is oversaturated with water and dissolved O_2 enters the system. The authors linked GR formation to the interconversion of lepidocrocite and fougèrite due to seasonal fluctuations and soil medium characteristics (dissolved O_2, higher organic matter supply, alternating oxic/anoxic conditions). Feder et al.[87] also observed that Fe(II)/Fe(III) of fougèrite increases with depth as x, i.e. the Fe(II)/Fe(III) ratio, was 0.5 in upper soil horizon displaying oximorphic characteristics but increased to 2 in the deepest horizons showing reductomorphic properties.

Owing to its high reactivity and poor stability, the occurrence of GR has rarely been reported in natural settings. More recently, the occurrence of GRs have also been reported in five other natural environments: (i) within ochreous sediments from an abandoned coal mine drainage system where GR layer was formed below (4 mm) the surface (South Wales, UK),[83] (ii) in groundwater sampled below the water table from an artesian well in a chalk aquifer and from deep granite fractures in an underground tunnel (Denmark),[88] (iii) in the iron(II)-rich stratified (oxic/anoxic) lake Matano (Indonesia),[89] in CO_2-rich soils on a mofette field (Czech Republic),[90] and in metal polluted uranium mine drainage crossing the transition zone between anoxic subsurface and the oxic surface (Thuringia, Germany).[91] Similarly, putative identifications of GR-like phases were reported in buried 700,000 year old lacustrine deposits (Ohio, USA),[92] in iron-rich sediment cores from a water reservoir (California, USA),[93] and in redoximorphic soil downhill from a perennial spring (Iowa, USA).[94] GRs in soil and water can form under circumneutral to alkaline conditions in anoxic or reduced environments by different abiotic or biotic processes which are described in detail in Section 4. Keeping in view the order of preference for interlayer ions to replace each other ($CO_3^{2-} > SO_4^{2-} > Cl^-$),[95] Christiansen et al.[88]

proposed that the formation of GR(CO_3^{2-}) would be favored in freshwaters having abundant CO_3^{2-}. However, SO_4^{2-} dominates in replacement order when SO_4^{2-}/CO_3^{2-} is high and therefore will favor the formation of GR(SO_4^{2-}) in saline water because of higher SO_4^{2-} contents.[88,96]

Figure 4: Soil containing fougèrite with bluish-green color. From Trolard et al.[86] (2007, Figure No. 1). Reproduced with kind permission of The Clay Minerals Society, publisher of *Clays and Clay Minerals*.

In contrast to GR, magnetite has widespread occurrence in natural environments due to higher stability and has been identified in multiple locations such as in river bed sediments (USA),[97] in well-drained soils (UK, USA),[98,99] in semi-arid wetland soils (Israel),[100] in gleysol (Germany),[101] in Chinese loess and paleosols,[102] in tholeiitic basalt (Brazil),[103] in Proterozoic zoned carbonatites (India),[104] in sand fraction of deeply-weathered oxisol in savanna ecosystem (Brazil),[105] in alluvial soils near Fe–Pb mining site (Bulgaria),[106] in tropical lateritic soil profiles from southern India,[107] in sediments of three different Asian rivers draining into the South China Sea,[108] and in Fe-rich hydrocarbon contaminated soils and sediments from a former oil field (Germany)[109] and hydrocarbon contaminated sediments form a former military air

base[110] and in soils of a mofette field[90] (Czech Republic). Recently, magnetite has been suggested to have also precipitated in early Archean ocean environments.[111]

Magnetite usually exists in the sand and silt fractions of soil rather than the clay fraction and is generally considered to have been inherited by weathering of the parent rock.[105,112] Both biotic[101] and abiotic[98] pathways were proposed to be relevant for magnetite formation in soils (for details, see Section 4). However, a pedogenic origin for magnetite has been invoked by studies such as Viana et al.[105] where magnetite and hematite were identified in an oxisol which has been developed form magnetite-free parent materials. Previously, Auerswald et al.[100] suggested formation of pedogenic magnetite by fire under reducing conditions in soil. Oldfield and Crowther[113] proposed distinctive magnetic measurements to differentiate the magnetite formed by weathering and pedogenic magnetite formed by burning. Geiss et al.[114] proposed anhysteretic remanent magnetization ratios and coercivity distributions to estimate pedogenic magnetite and this estimation was suggested as a tool to reconstruct past climate during paleosol formation.

Owing to the wide spread occurrence and stability in natural environments, reactivity of natural magnetite has been explored for environmental remediation *via* sorption,[115-118] reduction,[119] and chemical oxidation (for details, see Section 6).[120]

3.2. Corrosion products in engineered systems

Magnetite and GR have been observed as corrosion products of elemental iron in many engineered systems. In 1969, Stampfl[121] discovered GR(CO_3^{2-}) as corrosion product in municipal water pipes. McGill et al.[82] reported the formation of GR, magnetite and γ-FeOOH by corrosion of cast iron. Boucherit et al.[122] used Raman spectroscopy for the first time to identify GR in the pitting corrosion films. Génin et al.[96] reported the coexistence of GR(SO_4^{2-}), magnetite and sulfate-reducing bacteria at

steel piles corroded in a harbor area. Abdelmoula et al.[123] identified a layer of GR(CO_3^{2-}) on the surface of metallic iron corroded in $NaHCO_3$ solution (0.1 M). Only GR(CO_3^{2-}) was noted even when samples were corroded at higher Cl^-/HCO_3^- of 40. However, corrosion of mild steel in bicarbonate solution (0.1 M $NaHCO_3$) in the presence of Cl^- (0.15 M) and SO_4^{2-} (0.1 M) generated GR(Cl^-) and GR(SO_4^{2-}), respectively.[124] When both Cl^- (0.15 M) and SO_4^{2-} (0.1 M) were present along with bicarbonate, pitting corrosion product was a mixture of GR(Cl^-) and GR(SO_4^{2-}) as revealed from *in-situ* investigations by Raman spectroscopy.[124] However, the presence of Cl^- ions was necessary to induce pitting in phosphate buffer (0.1 M) as no pitting was observed by SO_4^{2-} alone (i.e. without Cl^-). Marine corrosion of steel immersed above the mudline for more than two decades resulted in rust layers which contained GR(SO_4^{2-}) (outer strata), Fe(III) (oxyhydr)oxides (intermediate strata), and magnetite (inner strata).[125] Pineau et al.[126] identified GR(SO_4^{2-}) during marine corrosion of steel at three French harbors and associated its formation with the presence of SO_4^{2-}-reducing bacteria.

Neff et al.[127] identified magnetite as the dominant corrosion product in iron archaeological artefacts buried in soil for centuries. Colomban et al.[128] identified the corrosion products for steel sheets either from automobiles in circulation for years or from sheets corroded in laboratory. GR was only observed in the latter case; however, magnetite was present along with other iron oxides in both cases.

GR has also been observed as a corrosion product in Fe^0 permeable reactive barriers.[129] The mineralogy of the corrosion products was correlated to the chemical composition of the water, type of water contaminants, amount of dissolved O_2 and presence of sulfate-reducing bacteria.[129,130]

4. Synthesis of mixed-valent iron minerals

This section describes various routes through which mixed-valent Fe minerals can be synthesized including abiotic and biotic pathways. A brief sketch of these pathways is provided in the Figure 5 which are detailed in the following subsections.

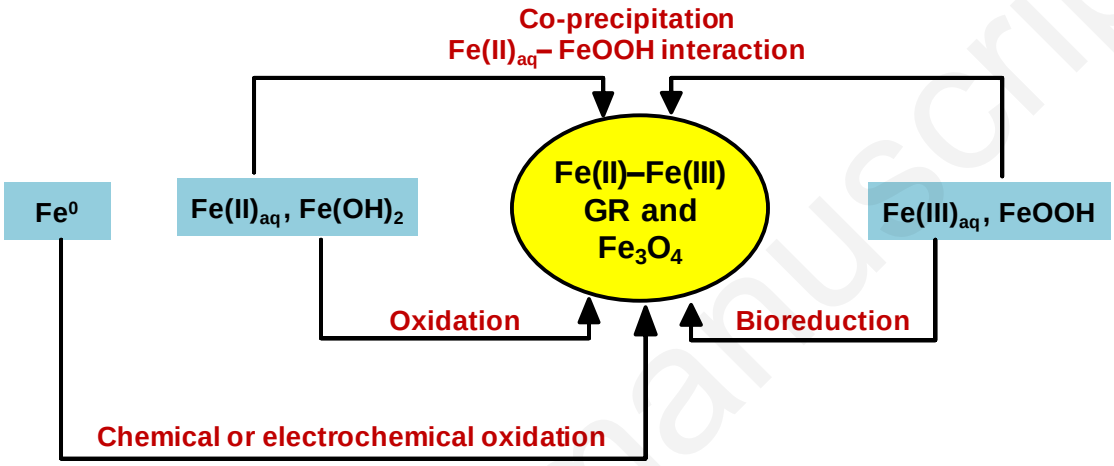

Figure 5: Overview of different pathways for the formation of magnetite (Fe_3O_4) and green rust (GR).

4.1. Abiotic synthesis of mixed-valent iron minerals

4.1.1. Co-precipitation of dissolved Fe(II) and Fe(III) species

Among various techniques to synthesize mixed-valent Fe minerals, co-precipitation is widely recognized as a convenient method due to ease, simplicity, and lack of any toxic intermediates.[17,31,81,131] This method involves the mixing of a base with an aqueous mixture containing dissolved species of Fe(II) and Fe(III) at room temperature. Experiments are conducted under an inert atmosphere to prevent the inclusion of oxygen that is known to rapidly oxidize Fe(II) at circumneutral pH.[132]

Formation of mixed-valent Fe minerals depends on Fe(II)/Fe(III) ratio, concentration of total Fe, pH, ionic strength, and the identity of present anions such as chloride, carbonate or sulfate (in the case of GR).[17,133] The co-precipitation route used to synthesize mixed-valent Fe minerals can be explained by a mass-balance diagram (Figure 6) which was created to interpret pH titration curves obtained during the co-precipitation of Fe(II) and Fe(III) soluble species in sulfate solutions.[81] In this diagram (Figure 6), the ordinate $R = n(OH^-)/[n(Fe(II)) + n(Fe(III))]$ denotes the number of OH^- species per mole of Fe that are consumed during the formation of a given mixed-valent iron mineral. The abscissa $x = n(Fe(III))/[n(Fe(II)) + n(Fe(III))]$ denotes the molar fraction of trivalent cations. This mass-balance diagram allows visualization of the identity and relative extents of the Fe phase that may form depending upon the ferric molar fraction x of the initial reactants[31] and the quantity of base added, *i.e.* the value of R. The formation of a biphasic system (A, B) is expected when the experimental point P(x, R) is situated on a segment joining both P_A and P_B, where P_A and P_B correspond to the position of the compounds A and B in the mass balance diagram, respectively. The formation of a mixture of 3 phases [A, B, C] is expected if the experimental point P(x, R) is located inside the triangle (P_A, P_B, P_C). The relative proportions of iron present in each phase can easily be determined by using the lever rules well known for equilibrium binary and ternary phase diagrams.[31] By using the values of P(x, R) of the equivalent points of various titration curves combined to quantitative measurements performed with Mössbauer spectroscopy, it was demonstrated that GR(SO_4^{2-}) exists with a unique ferric molar fraction of x = 1/3 (*i.e.* Fe(II) : Fe(III) = 2 : 1). For x values higher and lower than 1/3 the formation of [GR(SO_4^{2-}), Fe_3O_4] and [GR(SO_4^{2-}), $Fe(OH)_2$] mixtures was observed. On the contrary to GR(SO_4^{2-}), GR(CO_3^{2-}) was synthesized by co-precipitation with variable

ferrous to ferric molar ratios ranging from $x \sim 1/4$ (Fe(II) : Fe(III) ~ 3 :1) to $x = 1/3$.[32] Formation of GR occurred in two steps: (i) the precipitation of a disordered solid compound and, (ii) an interfacial reaction between clusters of hydroxylated ferrous species and the surface of the disordered solid compound leading to the formation of the GR crystals. GR(SO_4^{2-}) and GR(CO_3^{2-}) suspensions were shown to be unstable in strong alkaline condition (pH >10) and both transform abiotically into [Fe_3O_4, $Fe(OH)_2$] and [Fe_3O_4, $FeCO_3$] mixtures, respectively.

The formation of magnetite by co-precipitation of dissolved Fe(II) and Fe(III) species was studied in detail for a stoichiometric ferrous to ferric molar ratios, $x = 0.67$, i.e. Fe(II) : Fe(III) = 1 : 2.[134] The experiments were performed at 25 °C by maintaining a constant pH with various types of base (NaOH, NH_3, and $N(CH_3)_4OH$). The size of the magnetite spheroidal crystals were kept in the range of ~ 1.5-12.5 nm by controlling the pH and the ionic strength of the solution. Interestingly, a critical pH, named pH* and situated in a narrow range of 10.3 to 10.7 that depended on the value of the ionic strength, was identified. For pH values higher than pH*, the secondary particle growth by Ostwald ripening did not occur anymore and thermodynamically stable nanocrystals of magnetite were obtained due to a lowering of the interfacial tension γ induced by the adsorption of chemical species such as HO^- or cations of the electrolyte. For this reason, a strong decrease of crystal size was observed in the medium containing the smallest cations, *e.g.* Na^+ as compared to $[N(CH_3)_4]^+$, these species being the best screening ions.

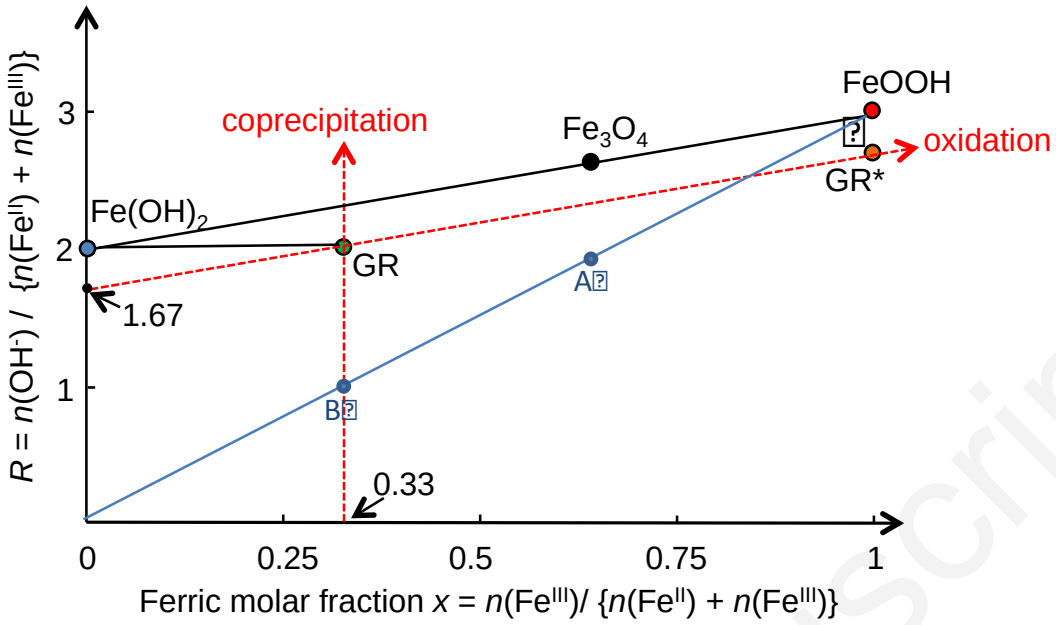

Figure 6: The mass-balance diagram representing the synthesis of magnetite (Fe_3O_4) and green rust *via* co-precipitation and oxidation. GR correspond to green rust and GR* to the fully oxidized form of GR, *i.e.* Mössbauerite. Point A correspond to the mixture [2/3 FeOOH, 1/3 Fe(II)] and point B is mixture [1/3 FeOOH, 2/3 Fe(II)]. Adapted with permission from Ref. 31. Copyright 2006 Elsevier Masson SAS.

4.1.2. Partial oxidation of hydroxylated dissolved Fe(II) and ($(Fe(II)_{aq}$, $Fe(OH)_2$) mixture

Formation of green rust. The kinetics of oxidation of dissolved Fe(II) species by dissolved O_2 was studied by several authors[135-137] with the general goal to obtain a better understanding of the behavior of Fe in natural aquatic environments. In their early work,[135] Stumm and Lee demonstrated that the kinetics of oxidation of dissolved Fe(II) species by air-O_2 at low concentration of Fe(II) (~ 10^{-5} M) was strongly dependent on the pH. The oxidation kinetics were accelerated by a factor of ~100 when the pH was increased by one unit in a narrow pH range situated between 7 and 8. In this range of pH, it was shown before[138] that fully hydroxylated dissolved Fe(II) species, *i.e.* $[Fe(OH)_2]^0_{aq}$, are predominant as compared to other species such as

$[Fe(OH)]^{+}_{aq}$ and $Fe(II)_{aq}$, these being more stable at acidic pH. Interestingly, Stumm and Lee[135] note also that the oxidation of Fe(II) species may occur "in a stepwise fashion over the mixed iron(II)-iron(III) hydroxide" as suggested by Feitknecht and Keller.[139] This observation was confirmed later by Bernal et *al.*[27] who showed that GR compounds may incorporate various type of anions (Cl^-, Br^-, F^-, and SO_4^{2-}) when formed by aeration of ferrous salts solution and partially precipitated by NaOH. GR intercalating other anions such as selenite,[20] methanoate,[21] C_9-C_{14} linear alkyl carboxylates,[22] and oxalate[23] were also obtained by oxidation of [$Fe(OH)_2$, Fe(II)] mixtures.

Other studies have also focused in depth on aeration of [$Fe(OH)_2$, Fe(II)] mixtures[140,141] with Genin et al.[142] able to determine that an accurate OH^- : Fe(II) ratio of 5 : 3 (or 1.67) was necessary to fully transform the initial [$Fe(OH)_2$, Fe(II)] mixture into a single phase of $GR(SO_4)$. As later explained by Ruby et al.,[143] the oxidation reaction is represented by a line of slope 1 in the mass balance diagram (Figure 6) and corresponds to a chemical reaction that is independent of the pH. In the case of $GR(SO_4)$, this reaction can be written as following:

$$5Fe(OH)_2 + Fe(II)_{aq} + (1/2)O_2 + 9H_2O + SO_4^{2-} = Fe(II)_4\,Fe(III)_2\,(OH)_{12}\,SO_4.\,8H_2O \quad (2)$$

The reaction was monitored by recording both the pH and redox potential E_h of the suspension and equilibrium condition leading to the observation of well-defined pH and E_h plateaus. By using this methodology, the Gibbs standard energy of formation ΔG^o_f of $GR(SO_4^{2-})$, $GR(CO_3^{2-})$, and $GR(Cl^-)$ was determined (Table 5).

Formation of magnetite

Ferrous hydroxide was easily transformed into magnetite during its oxidation by air at low temperature situated in a range between 25 – 65 °C.[144-146] Similarly to the

reaction leading to GR, the OH^-:Fe(II) ratio used for the precipitation of the ferrous soluble species was shown to have a strong influence on the nature of the final products. For instance, an OH^- : Fe(II) ratio lower than 2 can lead to the formation of ferric (oxyhydr)oxides such as goethite (α-FeOOH) or lepidocrocite (γ-FeOOH) with GR as an intermediate compound. Both Olowe et al.[145] and Domingo et al.[146] demonstrated that pure magnetite is most frequently obtained for an initial OH^- : Fe(II) ratio of 2, corresponding to the stoichiometric ratio leading to the formation of $Fe(OH)_2$. In the presence of an excess of base (OH^- : Fe(II) >2), either (Fe_3O_4, α-FeOOH) mixture or single phase of α-FeOOH were observed. In order to better control the shape and the size of the magnetite crystals, other oxidants, most frequently nitrate (NO_3^-),[147-149] were chosen to oxidize ferrous hydroxide. As proposed in the pioneering work of Sugimoto and Egon,[147] these experiments need to be performed at a temperature of ~90 °C. Vereda et al.[149] showed recently that the presence of an excess of OH^- species in the initial solution promotes the formation of nanometric magnetite crystals (30-100 nm), whilst micrometric crystals (0.4-1.1 μm) with increasing surface roughness were obtained in the presence of an excess of Fe(II) species.

4.1.3. Chemical or electrochemical oxidation of zero-valent iron

Electro-generation of green rust

Electro-generated GR was often synthesized by controlling the redox potential of the zero-valent anode (potentiostatic mode) while on the contrary, electro-generation experiments leading to magnetite were performed at an imposed current density (galvanostatic mode). Legrand et al.*[150]* studied in a systematic way the nature of the oxidation products formed on Fe^0 in carbonated solutions. Voltammograms exhibited

active domains with anodic peaks situated in a redox potential range situated in between ~ –0.55 V/SHE and ~ –0.45 V/SHE. For such values of redox potential imposed at the zero-valent anode, the chronoamperometric measurements exhibited a decrease of the current density showing that Fe^0 surface was rapidly covered by solid oxidation products. Depending on the concentration of carbonate species varying in a range situated in between $5x10^{-2}$ M and 1 M, the pH and the temperature (25 °C < T < 90 °C), 3 types of oxidation products, *i.e.* siderite ($FeCO_3$), GR(CO_3^{2-}) and an amorphous ferric oxyhydroxide were observed. The formation of GR(CO_3^{2-}) as a single phase were observed in the whole temperature range at the lowest carbonate concentration for a pH range situated in between 8.4 and 9.8. For higher carbonate concentration, an imposed pH higher than 9 was necessary to avoid the formation of siderite. Refait *et al.*[151] performed similar experiments (applied potential of ~ –0.6 V/SHE) in an aqueous medium containing a mixture of Cl^-, SO_4^{2-}, and CO_3^{2-} anions in a relative molar proportion of 50 : 3 : 0.3 respectively. Such an aqueous medium was used to mimic the condition found in seawater. It led to the formation of GR(SO_4^{2-}) with some traces of GR(CO_3^{2-}). As expected from the general trends observed for other layered double hydroxides, monovalent ions such as Cl^- were not preferentially intercalated into GR. Another study of Antony et al.[152] performed on a gold anode was devoted to determining the Fe(II) : Fe(III) ratio of electro-generated GR. It was shown that for both GR(SO_4^{2-}) and GR(CO_3^{2-}) this ratio was always very close to 2 : 1 in agreement with the values determined for GR synthesized by coprecipitation or by air oxidation of $Fe(OH)_2$.[24,149] The lower Fe(II) : Fe(III) value of 1 : 1 observed previously[153] was later attributed to the formation of an oxidized form of GR, a Fe(II)-Fe(III) oxyhydroxycarbonate named recently Mössbauerite,[154] that

can be easily synthesized by oxidizing GR *in situ* without dissolution-reprecipitation.[143,152]

Electro-generation of magnetite

The formation of magnetite on the surface of Fe^0 electrodes has been the subject of several studies.[155-157] The control of the imposed electro-oxidation current density, the type of anions present in the electrolyte and the distance between the anode and the cathode were shown to be crucial for obtaining both magnetite as a single phase and a relatively narrow crystals size distribution. The presence of complexing agents, *e.g.* thiosulfates,[155] amine surfactants[156] were used to obtain nanoparticles of magnetite in a size range situated in between ~ 20 and ~ 45 nm. In a more recent study,[157] it was demonstrated that nanoparticles of magnetite can also be easily synthesized in surfactant-free electrolyte. The size of the crystals generally increased with increasing current density or by decreasing the distance between the anode and the cathode. The formation of a ferric precursor (γ-FeOOH) that formed before magnetite, was identified by X-ray diffraction[155] and later confirmed by Cabrera et al.[156] by analyzing the electrolyte suspension by UV spectroscopy. The role of the OH^- species generated by the reduction of water at the cathode or by adjusting the pH of the electrolyte with an alkaline solution was investigated more recently. It was suggested that the diffusion of OH^- species from the cathode to the anode governed the formation of the ferric precursor and finally magnetite. Indeed, the ferric precursor was proposed to be formed by the oxidation of ferrous hydroxide by dissolved O_2 at the surface of the Fe^0 anode. The reaction was kinetically governed by both the rate of dissolution of Fe^0 species into $Fe(II)_{aq}$ species from the anode and by the diffusion of OH^- species produced on the cathode. The formation of magnetite was proposed to be due to

"coprecipitation" between $Fe(OH)_2$ and the ferric precursor FeOOH at the surface of the Fe^0 anode.[157]

Controlled chemical oxidation of zero-valent iron

The oxidation of Fe^0 at the open circuit potential, *i.e.* without any applied current or potential, may also lead to the formation of magnetite or GR as single phases. Abdelmoula et al.[123] demonstrated that an α-iron(0) disk immersed in either an aerated 0.1M $NaHCO_3$ solution at a pH of 8.3 is covered after 5 days of reaction by a thick green film that was characterized to be GR(CO_3^{2-}) by conversion electron Mössbauer spectroscopy (CEMS) performed at 78 K. The reaction of Fe^0 powder in contact with a flow of deaerated water solution containing carbonate and calcium ions was studied in column experiments by Jeen et al.[158] Raman spectroscopy revealed that magnetite was formed at the surface of iron with $Fe(OH)_2$ forming as an initial precursor. Huang and Zhang[130] studied the role of dissolved Fe(II) species during the oxidation of Fe^0 by dissolved oxygen and NO_3^-. It was shown that the oxidation of Fe^0 by dissolved oxygen was strongly enhanced by the presence of dissolved $Fe(II)_{aq}$ leading to the formation of a bilayer structure consisting of an inner layer of magnetite and an outer layer of γ-FeOOH. The study of the kinetics of formation of the corrosion products indicated that γ-FeOOH was formed initially at the Fe^0 surface and was progressively replaced by Fe_3O_4 concomitantly to the decrease of DO observed during the oxidation reaction. The formation of magnetite was suggested to occur at the Fe^0/ γ-FeOOH layer by the autoreduction of γ-FeOOH by Fe^0. After 24 hours of reaction, γ-FeOOH disappeared completely and magnetite as a single phase was observed on the Fe^0 surface.

4.1.4. Interaction of Fe(II) with Fe(III) (oxyhydr)oxides

Interaction of ferric (oxyhydr)oxides with aqueous Fe(II) can transform them into other ferric and/or mixed-valent phases. The synthesis procedure involves introduction of dissolved Fe(II) species into a suspension of ferric (oxyhydr)oxides at neutral pH. At this pH, the hydroxylation rate of the Fe(II) species is sufficient which is required to initiate the transformation process. However, to form mixed Fe(II)-Fe(III) oxides, a specific Fe(II)/Fe(III) ratio (2 for GR and 0.5 for magnetite), and hydroxylation ratio (R = OH^-/Fe) (1 for GR and 2/3 for magnetite) is required (Reactions 3 and 4). The values of *R* can be easily visualized on the Fe(II)-Fe(III) mass balance diagram by the segment joining points A and B to points Fe_3O_4 and GR, respectively (Figure 6).

The extent of such mineralogical transformations is controlled by various factors including the nature of the initial ferric mineral, Fe(II)/Fe(III) ratio, reaction pH, OH^-/Fe ratio and ligands. For example, at low Fe(II) levels, ferrihydrite was transformed either into lepidocrocite,[159,160] goethite,[47,159,161,162] or hematite[163]. At high Fe(II) concentrations, mixed-valent Fe minerals such as magnetite[17,37,47,160,164-169] or GR[51,81,170,171] were formed from different ferric (oxyhydr)oxides. For example, Ishikawa et al.[165] investigated the transformation of various ferric oxides (Fe(II)/Fe(III) ratio of 0.5) under changing OH^-/Fe ratios (0–4). They reported that transformation of ferric oxides into magnetite was highest at OH^-/Fe = 2 and was in the order of akaganéite > lepidocrocite > goethite. Similarly, Hansel et al[172,173] reported that at low Fe(II) concentration (<1.0 mmol Fe(II)/g ferrihydrite), ferrihydrite was transformed into lepidocrocite and goethite while magnetite formation was favored at elevated Fe(II) concentration (>1.0 mmol Fe(II)/g ferrihydrite). In another study by Pedersen et al.[160] at pH of 6.5, ferrihydrite was

completely transformed into other stable phases like lepidocrocite at low Fe(II) contents (Fe(II)/Fe(III) = 0.4) or goethite at higher Fe(II) concentration (Fe(II)/Fe(III) = 1). At high Fe(II) levels, lepidocrocite was transformed into magnetite while it remained untransformed at low Fe(II) levels. Goethite or hematite were not transformed either at lower (Fe(II)/Fe(III) = 0.4) or at higher Fe(II) concentration (Fe(II)/Fe(III) = 1) which was attributed to their strong stability and crystallinity.[160]

When experimental conditions were fully controlled to form stoichiometric magnetite[37] or GR[51] through the following reactions, significant amount of goethite was transformed into mixed Fe(II)-Fe(III) oxides.

$2Fe(III)OOH + Fe(II) + 2OH^- \Rightarrow Fe(II)Fe(III)_2O_4 + 2H_2O$ (for magnetite formation) (3)

$2Fe(III)OOH + 4Fe(II) + 6OH^- + 2\ H_2O + SO_4^{2-} \Rightarrow Fe(II)_4Fe(III)_2(OH)_{12}SO_4$ (for GR formation) (4)

However, the kinetics of magnetite formation was much slower than that observed for GR under similar experimental conditions (Figure 7). The extent of ferrihydrite transformation into magnetite and GR was 91 and 100%, respectively. In contrast, only 4% of goethite was transformed into magnetite whilst the extent of goethite transformation was higher (62%) when GR was formed.[51] This difference in formation kinetics could be correlated to structural differences between both GR and magnetite. GR is an "open" and hydrated phase which might develop much more rapidly in aqueous solution. Conversely, magnetite is a very dense and compact iron oxide and its formation requires full deprotonation of the initial Fe(II) and Fe(III) species. Therefore, it is considered that the formation of GR is favored when dissolved Fe(II) species interact with ferric (oxyhydr)oxides in anoxic environments.[51]

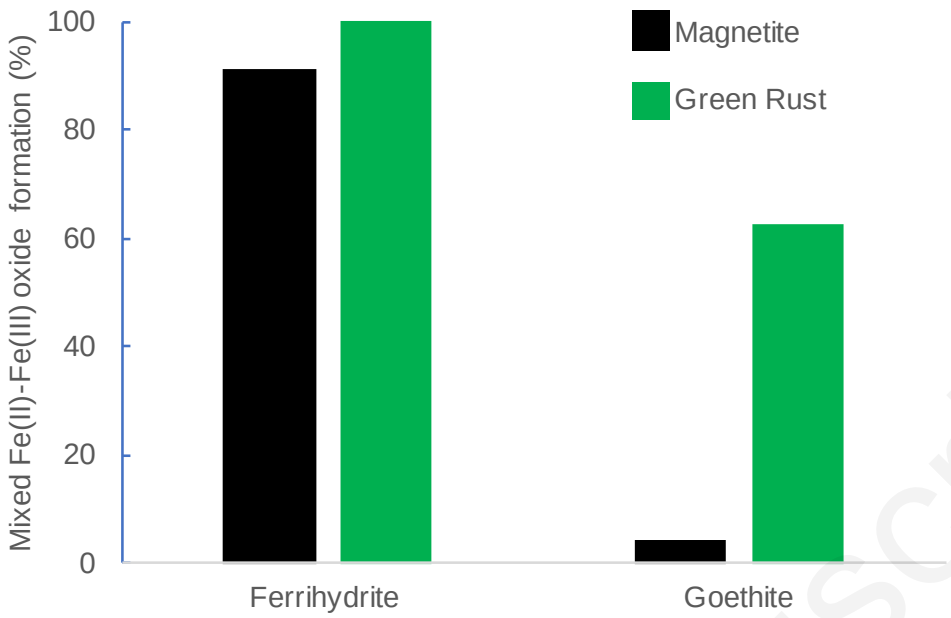

Figure 7: Transformation extent of ferrihydrite and goethite into mixed-valent iron minerals (magnetite and green rust) measured by Mössbauer Spectroscopy. Ferrihydrite and goethite were reacted with stoichiometric amounts of soluble Fe(II) and NaOH to form magnetite and green rust according to the reaction 3 and 4. Figure prepared by using the data reported in Table 2 of Ref. 51.

The exact mechanism of these transformations is not yet well understood. However, as summarized in the literature,[2,169] the Fe(II)-induced mineralogical transformations of ferric (oxyhydr)oxides can be represented as (i) topotactic transformation (also called solid-state conversion or structural rearrangement) or as (ii) reconstructive/re-crystallization (dissolution/re-precipitation). Each of these processes are supported by sometime contradictory evidence. Topotactic conversions involve the transformation of ferric oxides without dissolution and magnetite formed through this pathway retains the particle size and morphology of initial phase (Figure 8).[37,47,51,160,174] Formation of GR via topotactic transformation of ferrihydrite following Fe(II) sorption has also been proposed.[167] Topotactic transformations are initiated by surface adsorption of Fe(II) and interfacial transfer of electrons.[17,47,175] On the contrary in

reconstructive process, a complete breakdown of initial iron phases proceed *via* their dissolution followed by the precipitation of new secondary phases. Interfacial electron transfer between iron (oxyhydr)oxides and adsorbed Fe(II) initiates the reductive dissolution and then re-precipitation of the adsorbed Fe(II) on oxides particle surfaces.[47] However, both transformation pathways involve the adsorption of Fe(II) onto ferric (oxyhydr)oxides followed by electron transfer from the sorbed Fe(II) to structural Fe(III) in ferric minerals.[176] Williams and Scherer[177] provided spectroscopic demonstration of reduction of structural Fe(III) in the presence of adsorbed Fe(II) and electron transfer therein. They exposed ferrihydrite (made from ^{57}Fe) and exposed it to aqueous Fe(II) (made from ^{56}Fe) considering that Mössbauer spectroscopy will detect the structural ^{57}Fe(III) but not the adsorbed ^{56}Fe(II). Obtained Mössbauer results clearly indicated appearance of ^{57}Fe(II) line which provides evidence for reduction of structural ^{57}Fe(III) in ferrihydrite and electron transfer between adsorbed Fe(II) and the underlying Fe(III) oxide. Similarly, enriched Fe isotope experiments have shown compelling evidence for the exchange of aqueous Fe(II) with structural Fe(III) in ferrihydrite, goethite and hematite.[176,178,179]

Transformation of Fe(III) (oxyhydr)oxides is mainly initiated by adsorption of Fe(II) to singly coordinated sites forming inner-sphere surface complexes. The key role of Fe(II) sorption has also been highlighted when the formation of magnetite was inhibited due to the inclusion of organic matter[180] or phosphate[168] in transformation experiments. Microbial transformation of ferrihydrite to magnetite was inhibited when instead of Fe(II), humic substances were adsorbed onto the surface sites of ferrihydrite.[180] Similarly, phosphate forms very strong inner sphere complexes with the iron (oxyhydr)oxide surface and therefore its presence decreased the adsorption of Fe(II) and thus consequently hindered interfacial electron transfer and the solid-state

reaction.[168,181-184] Loosely-bound ligands such as salicylate anion did not significantly affect the magnetite formation[168] which is perhaps explained by the fact that the affinity of phosphate to the surface of iron (oxyhydr)oxide was much stronger than salicylate (i.e. intrinsic constant of surface complexation of phosphate lies at $\log K_{int}$ = 30, while that of salicylate is around $\log K_{int}$ = 8).[185,186]

Mössbauer spectroscopy has been used to experimentally monitor the result of mineralogical transformation from interfacial electron transfer reactions between ferric (oxyhydr)oxide and adsorbed Fe(II).[177,187] Transfer of electrons between sorbed Fe(II) and ferric crystal can be affected by microscopic sorption mechanism (i.e. inner- or outer-sphere complexation).[177,187] However, Yang et al. argued against relying completely on surface sorption in transformation and pointed out the importance of semiconductor properties of ferric (oxyhydr)oxides to determine their reaction via an electron transfer mechanism.[169] As the inner-sphere complexes are most likely to form on surfaces with singly coordinated surface groups, adsorption of Fe(II) on these sites should be the key step for interfacial electron transfer and ultimately the mineralogical transformations *via* both processes.[187,188] Therefore, the transformation extent of different kinds of goethite was found directly correlated to their site density of the singly coordinated surface groups.[168] Moreover, variation in crystal faces of ferric minerals also influences their transformation extent by affecting the nature of surface complexes (bidentate or tridentate) between Fe(II) and the ferric mineral. Higher transformation extents can be obtained when specific crystal faces are present, which promote the development of inner-sphere complexes and ultimately interfacial electron transfer. The adsorption behavior of divalent cations may probably be dominated by the crystal faces terminating the chains (021/001 like faces) and formation of bidentate or tridentate complex is favored due to the presence of the face

021 or 121.[188-190] Indeed, 021 crystal faces are highly reactive and usually denote the main growth direction of crystallites.[189] Owing to the much lower surface area of 021 faces as compared to that of the 100 and 110 faces, 021 faces are characterized by higher growth velocity and relatively higher affinity surface sites to sorb cations.[188,189,191] In addition to the 021 face, the 110 face was likely implied in the adsorption of the Fe(II) especially at a high Fe(II) level.[192] Owing to these differences, goethite with higher proportions of 021 or 121 faces was more likely to transform into magnetite than goethite which had a lesser amount of these crystal faces.[168]

It should be noted that studies on surface-mediated transformation of iron (oxyhydr)oxides have been conducted primarily in model systems devoid of natural organic matter. In natural systems, however, mineral surfaces are inevitably in contact with organic matter and iron (oxyhydr)oxides that rarely exist as pure phases. The existence of organic matter-iron oxides co-precipitates is therefore expected in soils, sediments and subsurface aquifers. The presence of associated organic matter (adsorbed or coprecipitated) is likely to influence heterogeneous electron transfer processes and formation of reactive Fe(II) surface sites. For example, it was demonstrated that the presence of coprecipitated organic matter caused a linear decrease in ferrihydrite transformation with increasing C/Fe amount because presence of organic matter improves the stability of ferric minerals.[193] Coprecipitated organic matter also inhibited the growth of ferric minerals as coprecipitated ferrihydrite has smaller particle size and greater structural disorder than organic-free ferrihydrite.[194] Coprecipitation of organic matter could lead to higher organic matter contents in Fe minerals as compared to simple adsorption of OM due to the fact that coprecipitated OM is more strongly bound to the mineral and more difficult to desorb from the mineral surface.[195] Such minerals also have lower surface area than pure ones as

mineral surface sites are blocked by organic matter with lower specific surface area.[194-196] Similar is also true for biogenic minerals[197] (See Section 4.2).

In subsurface environments, iron (oxyhydr)oxides generally do not occur as homogeneous assemblages. Frequently iron (oxyhydr)oxides can exist as coatings on less reactive or less soluble soil particles such as quartz sand or clay.[198] In addition, the iron can be found in assemblages of different iron (oxyhydr)oxides coatings which form the interface between mineral grains and groundwater.[198] Therefore, mineralogical transformations of ferric (oxyhydr)oxide coatings have been investigated in many studies devoted to form mixed-valent Fe minerals.[168,199,200] The extent of mineralogical transformations can vary depending upon the nature of support. For example, coating of ferrihydrite onto quartz sand (10% w/w) did not influence its subsequent transformation extent to magnetite.[200] Similar trends were observed for goethite coated onto sand.[168] However, the use of clay (kaolinite) as a support for goethite resulted in decreased transformation extent into magnetite under similar experimental conditions.[168] As Si may inhibit the direct adsorption of aqueous Fe(II) onto Fe(III) minerals, it is possible silicate release from Si-bearing minerals may hinder the solid-state transformation of coating phases.[201] The sorption of silicate resulted in an approximate 10-fold decrease in the rate of the Fe(II)-catalyzed process.[201] Thus, the presence of inorganic or organic ligands might act to retard the transformation of ferric minerals.

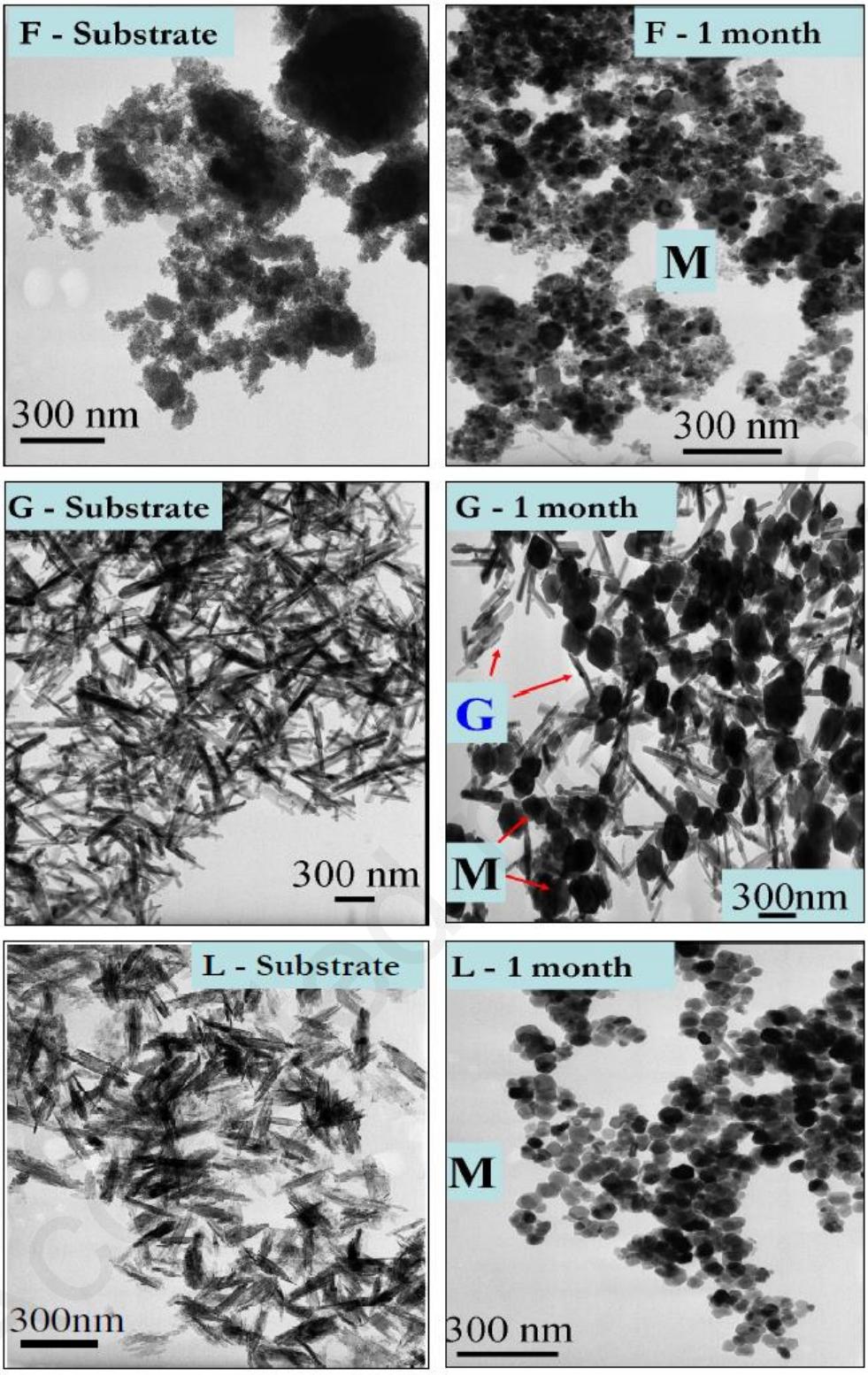

Figure 8: Bright field transmission electron microscopy images showing initial ferric (oxyhydr)oxides (ferrihydrite-F, lepidocrocite-L and goethite-G) and their transformations products after their reaction with suitable amounts of Fe(II) and OH^- to form stoichiometric magnetite (M). Transformation product of G indicates the presence of M and untransformed G. Reproduced with permission from Ref. 37. Copyright 2012 Elsevier.

4.2. Synthesis of mixed-valent iron minerals by microbial activity

The ubiquity of iron in the environment, in particular on early Earth when the atmosphere was anoxic and Fe was more available in its reduced and mobile form,[202] has led to the evolution of microorganisms with enzymatic pathways used to access different oxidation states of Fe as either an electron donor for Fe(II) oxidation or as an electron acceptor for Fe(III) reduction. Microbial Fe mineralization mechanisms are key components in the global iron cycle and link different biogeochemical cycles, including the iron, carbon, and nitrogen cycles.[203]

Through microbial iron redox transformations, a variety of different Fe minerals are formed, several of which contain both Fe(II) and Fe(III) and thus can be considered to be mixed-valent, e.g. magnetite or GR. Some of these minerals are persistent in the environment for billions of years, i.e. in banded iron formations (BIFs),[204,205] and as such represent important biomarkers for the understanding of how life emerged on Earth. Others, such as GR, are very reactive and have a much shorter life-time before they convert into more stable mineral phases.[33]

Here we detail the different pathways through which microbial processes induce the formation of such mixed-valent Fe minerals including through microbial Fe(III) reduction and Fe(II) oxidation. This will be complemented by a summary of magnetite biomineralization by magnetotactic bacteria, i.e. microorganisms that synthesize magnetite not as part of their catabolism but rather for navigation purposes using the magnetic properties of this mineral.

4.2.1. Synthesis by bacterial Fe(III) reduction

Physiology and diversity of Fe(III)-reducing bacteria

Microbial Fe(III) reduction occurs in almost all natural environments including sediments and soils and involves the oxidation of organic matter (e.g. acetate or

lactate) or hydrogen which act as electron donors coupled to the reduction of Fe(III) which acts as the terminal electron acceptor. Most of our knowledge on this process stems from studies with microorganisms belonging to the groups of *Geobacter* sp. and *Shewanella* sp (*Geobacter metallireducens* strain GS-15, *Geobacter sulfurreducens*, *Shewanella oneidensis* MR-1, *Shewanella putrefaciens* strain 200 and strain ATCC 8071) and from *Desulfuromonas acetoxidans.*[206-211] These heterotrophic Fe(III)-respiring bacteria are able to use various electron donors including a broad range of organic compounds as well as H_2 at neutral pH.[208,212-215] The organic compounds used as electron donor include simple fatty acids such as acetate and lactate but also more complex organic molecules such as aromatic compounds. Some of the Fe(III)-reducing microorganisms are unable to degrade their organic electron donor completely, usually accumulating acetate.[214] In recent years, some evidence for coupling the microbial reduction of ferric iron to the oxidation of ammonium has been found.[216-218] Similarly, lab and field experiments have suggested the coupling of anaerobic methane oxidation to ferric iron reduction.[219-221] However, no pure cultures of microorganisms have been isolated yet that are able to catalyze and grow by these two processes.

Fe(III)-reducing microorganisms can reduce Fe(III) that is in solution or present as poorly soluble ferric iron minerals. At neutral pH in the absence of organic ligands, Fe(III) is poorly soluble and precipitates as Fe(III) mineral. However, in the presence of citrate, nitrilotriacetate, or other ligands (including humic substances), Fe(III) can form soluble complexes and can serve as terminal electron acceptor in anaerobic respiration for Fe(III)-reducers.[222] Examples of Fe(III) minerals that can be reduced are poorly crystalline (oxyhydr)oxides such as ferrihydrite, lepidocrocite, schwertmannite, and goethite but also more crystalline representatives such as

hematite.[223-226] Mixed-valent Fe(II)/Fe(III) minerals such as magnetite and Fe(III) present in clay minerals can also be microbially reduced.[227-231].

Due to the poor solubility of Fe(III) (oxyhydr)oxides, electrons have to be transferred from the microbial cells to the Fe(III) mineral either via direct cell contact (involving transfer of the electrons from the cell interior to cell surface c-type cytochromes) or via different mechanisms for extracellular electron transfer (Figure 9).[232] Although the currently described electron transport pathways in different Fe(III)-reducing microorganisms including *Shewanella* and *Geobacter* sp. contain similar components, they are considerably different suggesting that electron transport for Fe(III) reduction can occur via many different biochemical pathways including electron shuttling via dissolved or solid-phase electron shuttles, Fe(III) solubilization or the use of conductive cell-appendages, so-called microbial nanowires (summarized recently by Melton et al., and Shi et al.).[232,233]

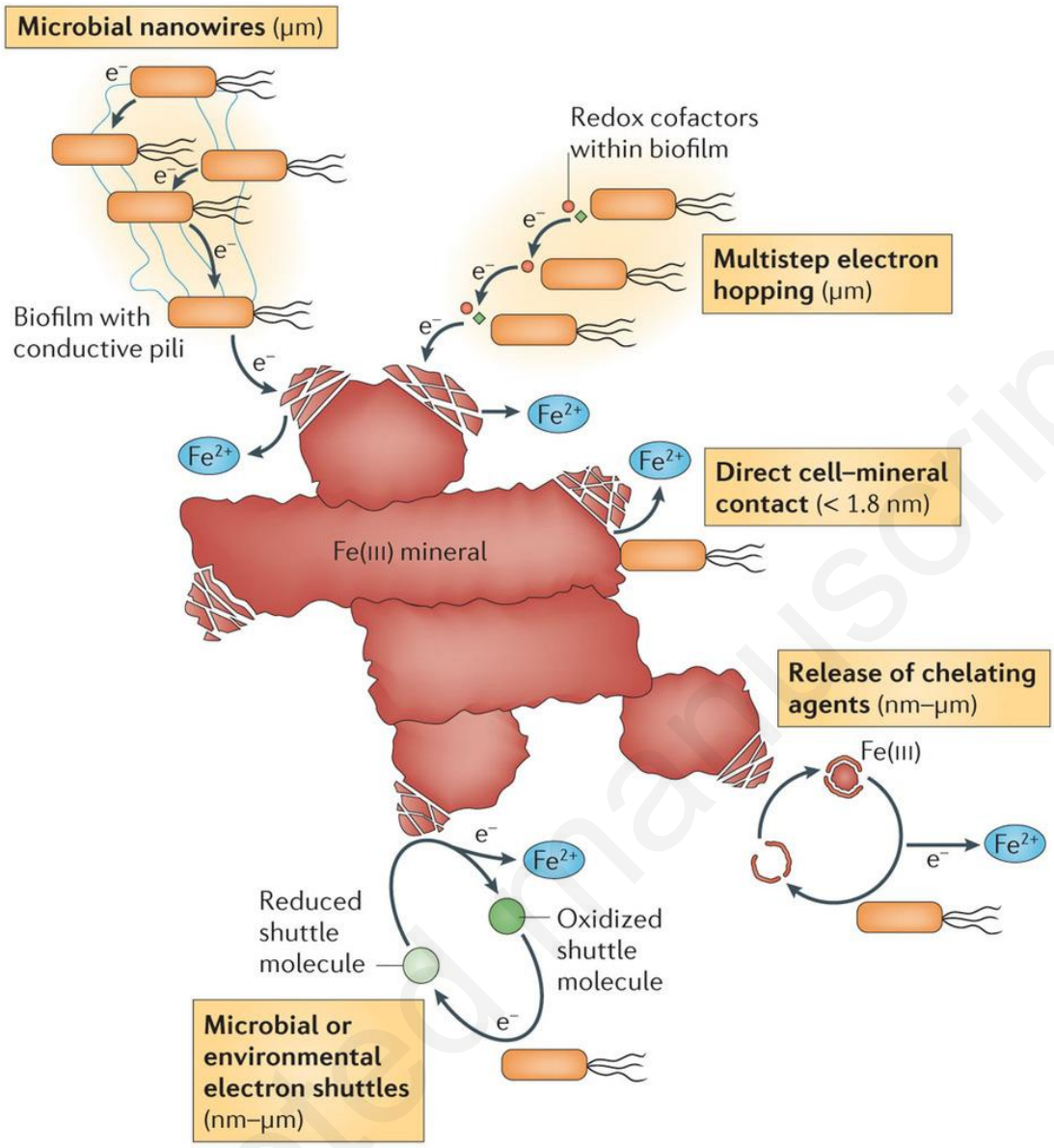

Figure 9: Possible electron transfer pathways during Fe(III) reduction. Direct contact between the Fe(III) minerals and the bacterial cell facilitates Fe(III) reduction over short distances. Bacteria secrete chelating agents or exploit microbial or environmental redox-active electron shuttles (such as flavins or dissolved and solid-state humic substances, respectively) to facilitate electron transfer over short (nm) and long (µm) distances. Electrically conductive pili and multistep electron hopping via redox cofactors that are present in biofilms have been implicated in long-distance extracellular electron transfer. Reproduced with permission from Ref. 232. Copyright 2014 Nature Publishing Group.

Formation of mixed-valent iron minerals during microbial Fe(III) reduction

Following microbial Fe(III) mineral reduction, Fe(II) is released into solution and either remains dissolved, precipitates as a Fe(II) mineral phase or can further react with remaining Fe(III) precipitates. Commonly, it is seen that ferrihydrite can undergo microbial Fe(III) reduction leading to the formation of goethite, magnetite or siderite with the exact nature of the minerals dependent upon a number of different physical and geochemical parameters such as Fe(III) reduction and Fe(II) formation rates, pH, temperature, cell density or Fe(III) concentration.[172,173,180,234,235] Piepenbrock et al.[180] showed that a certain Fe(II)/Fe_{tot} ratio is required during Fe(III) reduction to trigger the formation of magnetite and the presence of organic matter such as humic substances can also inhibit the formation of the mixed-valent mineral. Such humic substances have been shown to be able to shuttle electrons to and from both biogenic and chemically synthesized magnetites.[236] Furthermore, the identity of the mineral phases produced by the Fe(III)-reducing strain *Shewanella oneidensis* MR-1 has been shown to be dependent upon other physico-geochemical factors including geometric orientation of the bottles that the bacteria and minerals are incubated in, with magnetite formation favoured when the ferrihydrite pellet was most dense.[235] In the environment, microbial magnetite has been shown to form at hydrocarbon-contaminated field sites and was even used by its magnetic signal to locate the hotspot of microbial activity.[237] In the deep ocean, iron reduction by *Shewanella piezotolerans* WP3, which was isolated from the Pacific Ocean at a water depth of ~1914 m, has also been shown to produce magnetite via reduction of hydrous ferric oxide at rates much faster than many other known iron(III)-reducing bacteria.[238] *Shewanella putrefaciens* has been shown to be able to reduce magnetite to GR.[239] This study shows agreement with the fact that GR(CO_3^{2-}) formation can occur via Fe(III)

reduction by *Shewanella putrefaciens* when lepidocrocite is the starting Fe(III) phase.[240,241]

The physical and chemical characteristics of mixed-valent minerals produced by bacteria are highly dependent upon their formation conditions. This includes the effect of cell density on particle size. By increasing the cell concentration, the reduction of the ferrihydrite starting material proceeds faster and small magnetite nanoparticles (d ~12 nm) are produced. When low cell numbers are present, however, the reduction takes place more slowly leading to the formation of larger grains of magnetite (d ~40–50 nm).[234] It was also shown by Zhang et al[242] that larger grained magnetite (d >30 nm) is produced by thermophilic Fe(III)-reducing bacteria in contrast to the often superparamagnetic magnetite produced by other Fe(III)-reducing strains.

4.2.2. Synthesis of mixed-valent iron minerals by bacterial Fe(II) oxidation

Fe(II)-oxidizing bacteria are capable of drawing energy and/or electrons for growth by oxidizing ferrous iron to ferric iron.[243] At low O_2-concentrations and neutral pH, a habitat is called microoxic and molecular oxygen can serve as terminal electron acceptor for Fe(II) oxidation. The microorganisms catalyzing this process use the Fe(II) as electron and energy source and are called microaerophilic Fe(II)-oxidizers.[244] As soon as O_2 is consumed and the geochemical conditions become anoxic, Fe(II)-oxidizing microorganisms need to use other terminal electron acceptors. Photoautotrophic Fe(II)-oxidizers can use light as energy source and transfer the electrons from Fe(II) to carbon dioxide for biomass synthesis. In contrast, nitrate-reducing Fe(II)-oxidizers use Fe(II) as an electron and energy source to reduce nitrate as terminal electron acceptor producing different N-species as intermediates

and metabolic products. For the described microbially catalyzed Fe(II) oxidation processes, until now no general biogeochemical mechanisms are known, i.e. the proteins involved in Fe(II) oxidation and their genetic information is mostly unclear. Limited information on Fe(II) oxidation enzymatics and genetics is available only for individual strains.[245,246]

Although microaerophilic Fe(II)-oxidizing bacteria such as *Gallionella* sp., *Leptothrix* sp. or the known marine strains (*Mariprofundus* sp.) can produce unique cell-mineral structures of organic templates associated with Fe(III) minerals (twisted stalks and elongated sheaths), the identity of the biomineral produced is relatively simple. So far mainly poorly crystalline Fe(III) (oxyhydr)oxides including ferrihydrite, goethite, and lepidocrocite have been described.[247,248] No strong and convincing evidence for mixed-valent Fe minerals such as magnetite or GR has so far been published, although in a few rare cases greenish minerals have been seen by eye and some magnetite particles have been found in deep sea samples that contained microaerophilic Fe(II)-oxidizers (C. Chan and D. Emerson, personal communication). However, one can imagine that microbial reduction of the poorly crystalline Fe(III) (oxyhydr)oxide biominerals could potentially lead to the formation of magnetite or GR, although the presence of organic biomolecules is certainly expected to slow down or even prevent the formation of magnetite.[194,196,249,250]

Anaerobic nitrate-reducing Fe(II)-oxidizing bacteria have been detected in soils, freshwater, and marine habitats.[251-255] Microbial Fe(II) oxidation coupled to nitrate reduction produces Fe(III) minerals and dinitrogen or intermediates of the denitrification reaction including NO_2^-, NO, and N_2O.[256,257] Interestingly, almost all described nitrate-reducing Fe(II)-oxidizers are mixotrophic, meaning that they require an organic co-substrate to allow for continuous cultivation and Fe(II)

oxidation.[251,253,257-261] In the last two decades, a large number of mixotrophic nitrate-reducing Fe(II)-oxidizers has been described, however, examples of autotrophic ones are rare. The enrichment culture KS described by Straub et al.[254] is the first described culture that can oxidize Fe(II) autotrophically and can be maintained under chemolithoautotrophic conditions continuously. Since then a few more strains capable of autotrophic nitrate-reducing Fe(II) oxidation have been described in different studies.[262-269] However, the capability for continuous Fe(II) oxidation and growth under autotrophic conditions over several generations has not been demonstrated for all of these cultures.

When nitrate-reducing Fe(II) oxidation occurs at neutral pH, the produced Fe(III) is poorly soluble and precipitates rapidly as Fe(III) mineral. Interestingly, cells in all described mixotrophic strains heavily encrust in Fe(III) minerals[261,270,271] while the autotrophic culture KS does not form any cell encrustation under autotrophic conditions.[272] From these observations it was concluded that in the autotrophic nitrate-reducing Fe(II)-oxidizing cultures the Fe(II) is oxidized enzymatically and directly coupled to nitrate reduction while under mixotrophic conditions the nitrate is reduced coupled to oxidation of the organic co-substrate thus producing reactive nitrite (NO_2^-) that oxidizes the Fe(II) abiotically.[260,261,273]

These two biotic and abiotic Fe(II) oxidation mechanisms also have consequences for the identity of the minerals formed during nitrate-reducing Fe(II) oxidation: while for the autotrophic culture KS the poorly crystalline Fe(III) mineral ferrihydrite has been observed,[272] for the mixotrophic strains (and for some of the ones where it is currently unclear whether they are autotrophic or mixotrophic) more crystalline minerals (such as goethite) and even mixed-valent Fe(III) minerals such as magnetite and GR have been observed: Kappler et al.[252] described the formation of goethite for *Acidovorax*

sp. strain BoFeN1 and later Pantke et al.[274] showed that this goethite formation goes via a green-rust intermediate (Figure 10). This has been confirmed by Etique et al. for *Klebsiella mobilis*[275] and by Miot et al. for *Acidovorax* sp. strain BoFeN1[276] who furthermore demonstrated that the GR can also turn into magnetite. GR formation has also been observed recently by the heterotrophic co-culture strains in the autotrophic nitrate-reducing enrichment culture KS.[272] Magnetite formation by nitrate-reducing Fe(II)-oxidizers was first suggested by Chaudhuri et al.[277] Furthermore, it has been demonstrated that magnetite formation can even be initiated under conditions under which magnetite does usually not form, simply by the addition of magnetite crystals.[278] These magnetite nucleation sites function as seeds for more magnetite formation by lowering the activation energy for magnetite precipitation. One can easily imagine that this plays an important role in the environment where Fe(III)-reducing or even magnetotactic bacteria are responsible for providing such magnetite nucleation sites.

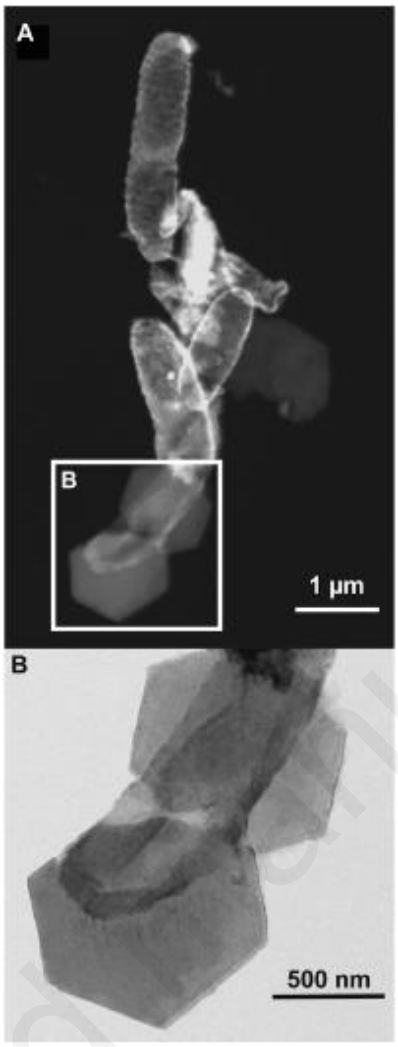

Figure 10: Scanning transmission electron microscopy (STEM) image of BoFeN1 culture suspension after 2 days measured in the high angular annular dark field mode (HAADF) (A). Magnified transmission electron microscopy image of BoFeN1 cell with hexagonal carbonate GR flakes measured in brightfield mode (B). Reproduced from Ref. 274. Copyright 2012 American Chemical Society.

Although biogenic magnetites (or other mixed-valent Fe(II)-Fe(III)-phases) produced by Fe(II)-oxidizing bacteria have not been systematically studied in environmental samples, in part because they are hard to distinguish from the abiogenic counterparts, it can be expected that their properties are distinctly different from abiotic ones. First, the association with organic matter (similar as the association with other geochemical species such as silicates) has the potential to stabilize and preserve them to a larger extent than expected.[279] Second, compared to synthetic minerals, the mixed-valent

phases produced by Fe(III)-reducing and magnetotactic bacteria have been shown to have a higher Fe(II) content than abiogenic Fe(II) / Fe(III) minerals.[280,281]

In addition to microaerophilic and nitrate-reducing microorganisms, phototrophic Fe(II)-oxidizing bacteria also oxidize Fe(II) to Fe(III) with the potential for the formation of mixed-valent Fe(II)-Fe(III) minerals including GR and magnetite. For most of these so-called photoferrotrophs, including representatives of the purple non-sulfur, the purple sulfur, and the green-sulfur bacteria, the precipitation of poorly crystalline ferric (oxyhydr)oxides (including ferrihydrite and goethite) has been described in both freshwater and marine media conditions.[282,283] For one of the freshwater strains, *Rhodopseudomonas palustris* TIE-1, and also for one of the marine strains, *Rhodovulum iodosum*, the formation of small amounts of magnetite has been observed.[284,285]

Evidence for GR formation by phototrophic microorganisms in the environment might come from studies of Archean ocean model environments, such as Lake Matano in Indonesia. In this lake, an anoxic water later with Fe(II) in the photic zone and the abundance of phototrophic Fe(II)-oxidizing bacteria has been described and GRs have been identified as minerals formed potentially by the activity of the Fe(II)-oxidizers but maybe also by Fe(III)-reducers using the Fe(III) minerals produced by the Fe(II)-oxidizers.[89,286,287]

4.2.3. Magnetotactic bacteria

Whilst the formation of magnetite outside of the cellular membrane by Fe(III)-reducing and Fe(II)-oxidizing bacteria can be considered to be a biologically induced mechanism, magnetotactic bacteria (MTB) are able to produce magnetite, greigite or both[288,289] internally via biologically controlled mechanisms. These bacteria produce chains of magnetite or greigite within individual membranes (denoted

magnetosomes), which are small vesicles containing grains of magnetic mineral. When placed under the influence of a magnetic field, the bacteria propel themselves along the field lines at speeds of 100 μm/s using flagella[65] and are thus considered to use the magnetosomes for a form of navigation along the Earth's magnetic field (magnetotaxis). Whilst these organisms were first identified in the 1960's, it was not until they were later re-discovered by Blakemore (1975)[290] in a marine sediment that MTB started to gain widespread attention. Since then it has been shown that MTB are ubiquitous and can grow in almost any aquatic environment, with strains identified in freshwater ponds, river sediments, soils, marine waters, and marine sediment.[291] Most MTB exist at the oxic-anoxic interface, (i.e. microoxic environments) where oxygen concentrations are much lower than that of the atmosphere.[292] In most cases, oxygen is the terminal electron acceptor used during respiration of the bacteria and small concentrations of O_2 are required for magnetite formation. *Magnetospirillum magnetotacticum* MS-1 is able to use NO_3^- as an electron acceptor for respiration, however, it has been observed that at least 1% O_2 is required for the formation of magnetosomes to occur.[293]

In terms of understanding the mechanisms of formation of magnetosomes, two of the most frequently studied strains include *Magnetospirillum magneticum* AMB-1 (AMB) and *Magnetospirillum gryphiswaldense* MSR-1 (MSR)[294] due to their ability to be cultivated in reasonable quantities. Over 30 genes have been identified within MTB that regulate the uptake of iron, deposition, and controlled precipitation of mineral within the magnetosome membrane.[295] It appears that whilst the formation of magnetosome membranes occurs even when magnetite does not form, magnetite cannot be produced in mutant strains which do not possess the membrane.[296-298] This suggests that the magnetosome acts as a specialized nanoreactor in which optimum

redox and pH environments (pH > 7, low redox potential) can be strictly regulated in order to promote magnetite formation. This formation is thought to take place either through the co-precipitation of Fe(II) and Fe(III), or via the secondary transformation of a precursor mineral such as ferrihydrite.[288] In total, the Fe contained within all of these magnetosomes accounts for >4% of the cell's mass (dry cell weight) and for more than 99.5% of the iron content of the bacteria.[299,300]

Magnetites formed within MTB are notable for their high chemical purity,[301] though it has been shown that additional metal cations (e.g. Cu, Mn, and Co) can be incorporated into the mineral.[302-304] Depending upon the strain, the size of the magnetosomes can vary between 10 and 120 nm, and almost all with very narrow size distributions.[294,305] A number of different shapes have been observed including cuboctahedral, elongated prismatic, tooth shaped and bullet shaped (Figure 11).[294,306] Currently, however, the genetic factors which affect the size and shape of the magnetosomes are not well understood. Many of these particles are single domain at room temperature[307] which helps to ensure they retain a remanent magnetization and the magnetic moment is dictated by the number and size of the magnetosomes. Since the magnetic dipole is effectively fixed within the cell, when the magnetic field changes direction, so do the bacteria.

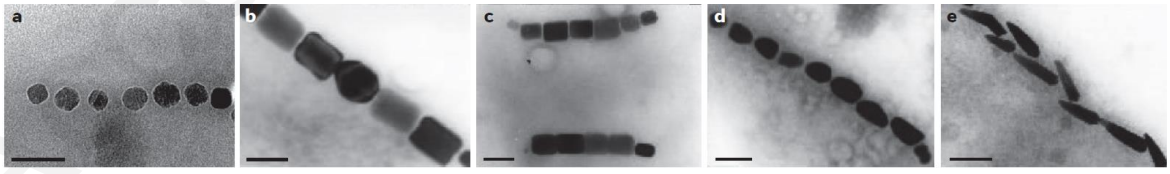

Figure 11: Different morphologies of magnetite produced by MTB's. Reproduced with permission from Ref. 294. Copyright 2016 Nature Publishing Group.

It is generally regarded that the use of magnetosomes within MTB is in order to provide an internal compass for navigation. More specifically, MTB orient themselves via magnetotaxis along the Earth's magnetic field. This reduces a three-

dimensional coordinate-based movement to a one dimensional problem, i.e. if the bacteria know the position of north, south, east and west they are then able to consider movement in the vertical water column, likely along chemically stratified inclines to search for redox gradients. This is further supported by the fact that both north seeking and south seeking MTB have been found living in the Northern and Southern hemispheres, respectively.[292] However if such a mechanism is so beneficial for MTB, why do other bacteria not also form magnetic particles for navigation? Also, many of these bacteria are able to survive without forming magnetite within their magnetosomes which might suggest that the magnetite is also able to provide other uses. For instance, other potential advantages of producing magnetosomes which have so far been suggested include: (i) For detoxification of metal ions, or reactive oxygen species which can form during oxygen respiration and can react with magnetite.[308,309] (ii) As a store for Fe in a compact, non-hydrated, inert and non-toxic form although to date no evidence has been able to suggest such a mechanism.[310] (iii) For electron storage in which, depending upon the geochemical conditions, the magnetite (or greigite) could be used as either an electron donor or an electron acceptor.[311,312] Whilst this theory has so far not been proven, recent evidence has shown that Fe(III)-reducing and Fe(II)-oxidizing bacteria can use magnetite in such a capacity (termed biogeobattery).[48,313] Furthermore, it is known that environmental conditions can influence the interior of the magnetosome membrane directly, thus what happens outside of the cell can affect the contents of the magnetosome.[297,314]

From an environmental perspective, the magnetite formed by MTB has been frequently suggested as a potential biomarker (microfossil) which can be used to reconstruct geochemical conditions from ancient Earth. The idea is that when the bacteria die the biological component degrades and the magnetite is incorporated into

the sediment and eventually sedimentary rocks, forming a significant contribution to their magnetic properties.[315-317] Magnetotactic bacteria have even been suggested to be the source of chains of magnetite found within the Martian meteorite ALH84001[318] although this study was heavily debated and much doubt surrounds the claims.[319] Potential problems for using the magnetic properties as biosignatures includes the fact that they are almost indistinguishable from abiotic magnetite or magnetite produced by Fe(II)-oxidizing and Fe(III)-reducing bacteria.[284,320,321] Furthermore, diagenetic or metamorphic processes might result in changes to the magnetic properties of the mineral inclusions. It has recently been suggested that a combination of physical, mineralogical and chemical characterization could be used to identify magnetite with trace element incorporations. Specifically, Amor et al.[302] looked the incorporation of 34 trace elements into magnetosomes formed by *Magnetospirillum* AMB-1 and identified the fact that biogenic magnetite incorporates 100 times less trace elements than synthetic magnetite. Alternatively, mass-dependent and -independent fractionation of Fe isotopes within magnetosomes might also be used as a potential proxy to investigate their ability to serve as biomarkers.[322]

5. Identification and quantification techniques

This section is devoted to illustrate various methods and techniques that are frequently used to identify the mineralogy or morphology of mixed-valent Fe minerals. We have focused on XRD, Mössbauer spectroscopy, vibrational spectroscopy including Raman and infra-red (IR), synchrotron methods such as extended X-ray absorption fine structure (EXAFS), X-ray absorption near edge spectroscopy (XANES), scanning transmission X-ray microscopy (STXM), XMCD, magnetic measurements as well as imaging techniques including Transmission Electron Microscopy (TEM) or Scanning Electron Microscopy (SEM). Combined, these powerful techniques can provide accurate quantitative determination of particle size, mineralogy, morphology and stoichiometry.

5.1. X–ray diffraction

This technique is commonly considered to be one of the most effective and rapid methods of mineral identification as diffraction data is able to provide information on mineral composition, crystallinity, and unit cell parameters.[2] The XRD diffraction patterns of magnetite and GRs have been well studied with corresponding reflections are shown in Figure 12.

The diffractogram of magnetite is typically characterized by several well defined reflections (Table 6), the most intense of which occurs at 0.253 Å (311). Magnetite has a cubic crystal structure with *d*-spacing of 8.397 Å. One complication which can arise when identifying magnetite through XRD is due to the similarity of its diffractogram to that of maghemite. Both iron oxides have almost identical lattice parameters and spinel structure (Figure 12) and consequently their respective

reflections heavily overlap.[2,323-326] Minor differences in the diffractogram of maghemite exist in the form of additional reflections at 0.373 Å (210) and 0.340 Å (213). These reflections can possibly be used to distinguish magnetite from maghemite but in reality their intensities are too weak (~5%) for the positive identification of the maghemite phase. Moreover, even if these reflections are successfully observed, it does not necessarily guarantee the sample to be single-phase maghemite since it could be a mixture of both magnetite and maghemite mineral phases.[326] Thus, distinction of both phases is difficult by using XRD. Recent studies have, however, (very few in number) showed the possibility of quantitative determination of both phases in their mixture by using X-ray diffraction data. For example, Kim et al.[323] proposed the use of high-angle diffraction peaks as (511) and (440) to quantify magnetite and maghemite in their mixture by constructing a calibration curve using the pure phases. Mikhaylova et al.[325] used a Rietveld XRD method to quantify both phases in magnetite-maghemite mixture and the obtained data matched that of Mössbauer spectroscopy. Furthermore, Pearce et al.[327] were able to show a relationship between mineral stoichiometry and *d*-spacing using the following relationship:

$$R = 0.89598 / \left(\frac{0.1989}{(\alpha - 8.3344)} - 1 \right)^{1/1.1988} \qquad (5)$$

Where R = Fe(II)/Fe(III) and α is the cell parameter (*d*-spacing) in angstroms. Using such a relationship could provide information about whether the mineral is fully reduced (i.e. magnetite), fully oxidized (i.e. maghemite) or somewhere in between (i.e. mixture of phases or partially oxidized magnetite).

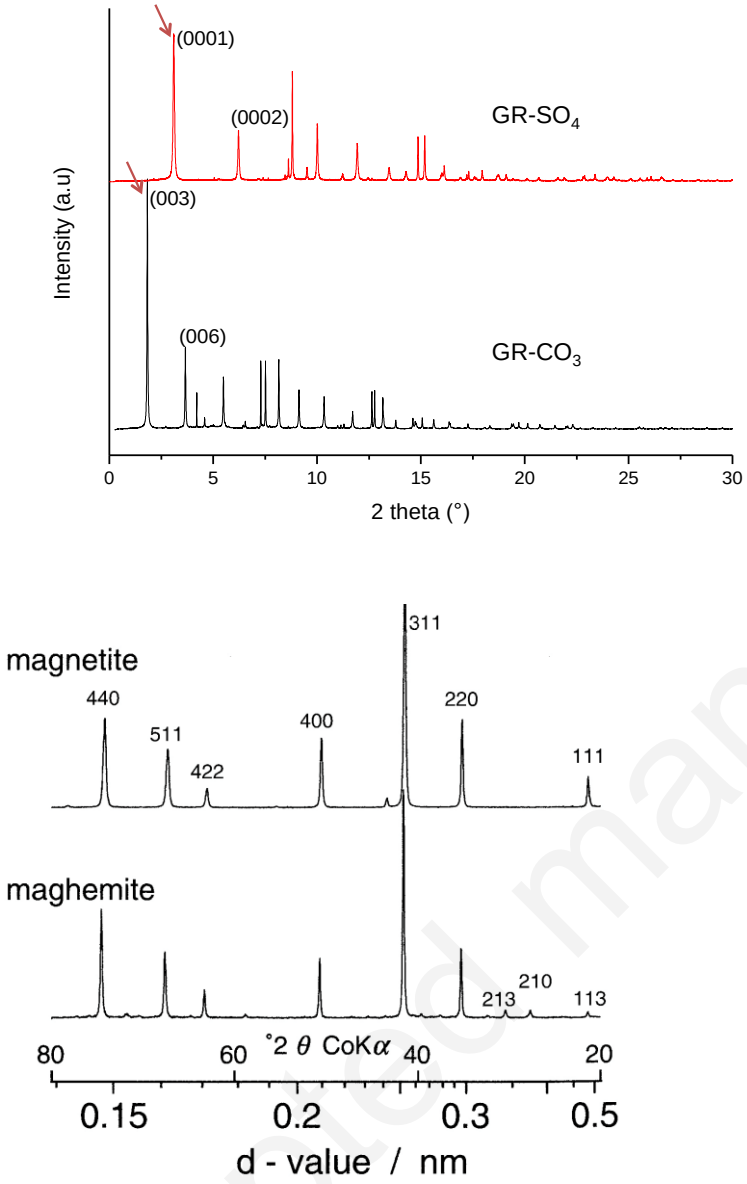

Figure 12. X-ray diffractograms of green rusts namely GR(SO_4^{2-}) and GR(CO_3^{2-}), magnetite, and maghemite. Diffractograms of GR(SO_4^{2-}) and GR(CO_3^{2-}) are reproduced with permission from Ref. 19. Copyright 2010 Elsevier. Diffractograms of magnetite and maghemite are reproduced with permission from Ref. 2. Copyright 2003 Wiley-VCH Verlag GmbH & Co. KGaA.

In the case of GRs, samples need to be carefully prepared to protect samples against oxidation during XRD analysis, for example through preparation and analysis under anoxic conditions and/or by coating samples with glycerol during analysis.[42,328-330] The XRD diffractograms of GR are typically characterized by reflections at low 2-theta values (Figure 12) with *d*–spacing of 7–10 Å (Figure 13). Different GRs can

easily be distinguished by the position of intense reflections in XRD diffractograms and corresponding parameters (Table 6). For example, the position of the most intense (003) reflection of GR(CO_3^{2-}) (*d*–spacing 7.57 Å) is located at a much lower angle than corresponding reflection (0001) of GR(SO_4^{2-}) (*d*–spacing 10.96 Å) simply because of different *d*−spacing (Figure 13).[19]

Table 6: X-ray powder diffraction data for magnetite and both kinds of green rusts (GR-I and GR-II)

Magnetite[a]			**GR-I**[27]			**GR-II**[27]		
d Å	**i**	**hkl**	**d Å**	**i**	**hkl**	**d Å**	**i**	**hkl**
4.85200	8	111	8.02	vs	003	10.92	vs	001
2.96700	30	220	4.01	v	006	5.48	s	002
2.53200	100	311	2.701	m	102	3.65	s	003
2.42430	8	222			104			
2.09930	20	400	2.408	m	105	2.747	m	004
1.71460	10	422			107			100
1.61580	30	511	2.037	w	108	2.660	ms	101
1.48450	40	440	1.598	mw	101	2.459	ms	102
1.41920	2	531			110			
1.32770	4	620	1.567	mw	113	2.195	ms	005
1.28070	10	533						103
1.26590	4	622	1.487	w	116	1.938	ms	104
1.21190	2	444						
1.12210	4	642				1.712	w	105
1.09300	12	731						
1.04960	6	800				1.587	w	110
0.98960	2	660				1.570	w	111
0.96950	6	751						
0.96320	4	662				1.525	w	112
0.93880	4	840						
0.89520	2	664						
0.88020	6	931						
0.85690	8	844						
0.82330	4	1020						
0.81170	6	951						
0.80800	4	1022						

[a] Natl. Bur. Stand. (U.S.) Monogr. 25, volume 5, page 31 (1967)

For GRs, quantification of the *d*–spacing value is perhaps the most important information to extract from XRD diffractograms in order to determine the nature and size of the intercalated molecules. The *d*−spacing's obtained from GR diffractograms typically increase through the incorporation of large organic anions in GR structure.

For example, XRD data revealed very high *d*−spacing (42 Å) when GR was synthesized by incorporating bulky alkyl anions.[22] A range of *d*−spacings corresponding to different GRs is provided in Figure 13 to illustrate the impact of the incorporated anions on the *d*−spacing values.

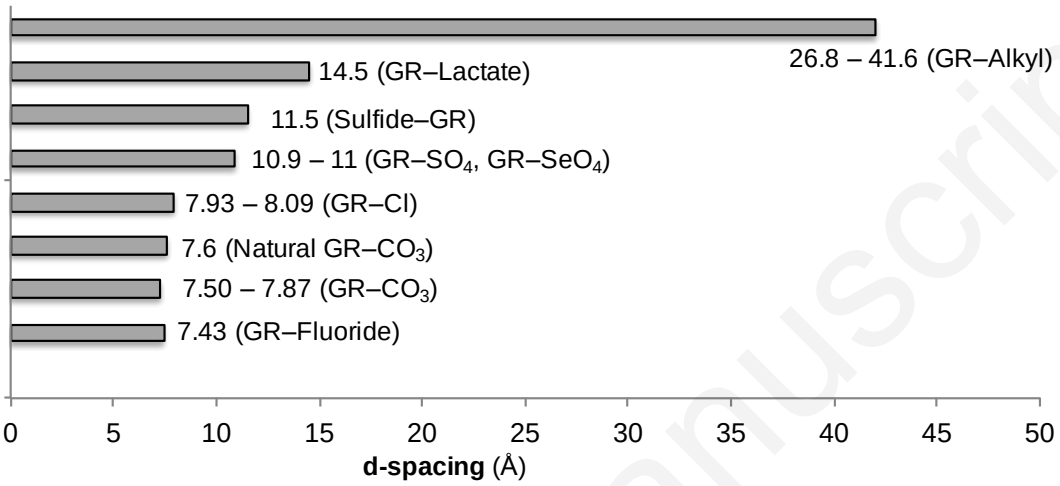

Figure 13: Variation of *d*−spacings in XRD parameters of different GRs depending upon their type and nature of intercalated molecules. This figure is based on the data compiled in previous studies[22,26,88,331,332] and references cited therein.

5.2. Mössbauer spectroscopy

Since its discovery in 1958,[333] Mössbauer spectroscopy has established itself as an important technique for determining the mineral composition, oxidation state, and even crystallinity of Fe minerals. The technique has increasingly been applied to different areas of geoscience, especially with regard to biogeochemistry, nanomaterials and Mars.[334,335]

The Mössbauer effect is based upon the resonant absorption of γ−radiation by atomic nuclei. In the case of ^{57}Fe Mössbauer spectroscopy, a radioactive ^{57}Co source (often embedded in a Rubidium matrix) decays to ^{57}Fe, resulting in the emission of γ−rays of 14.4 keV which are then absorbed by an absorber nucleus (i.e. the sample). The simplest Mössbauer spectrum can be described as having a Lorentzian line shape with half width at half maximum (HWHM) of 0.097 mm/s. The HWHM is limited by

Heisenberg's uncertainty principle although instrumental broadening will often lead to a slightly larger value. To change the energy range over which the γ−radiation is absorbed by a sample, the source is moved back and forth to take advantage of Doppler Effect. Consequently, Mössbauer spectra are routinely shown with *x*-axis units in mm/s which refers to the velocity of the moving source.

Hyperfine parameters

The formation of hyperfine interactions (parameters) are key characteristics of the Mössbauer effect. These parameters are related to the local coordination environment of the atoms in a sample and can be used to determine both the mineralogy and redox state of a sample. The main parameters that are routinely considered include the isomer shift (δ), quadrupole splitting (ΔE_Q), quadrupole shift (ε) and the magnetic hyperfine splitting (B_{hf}) (Figure 14).

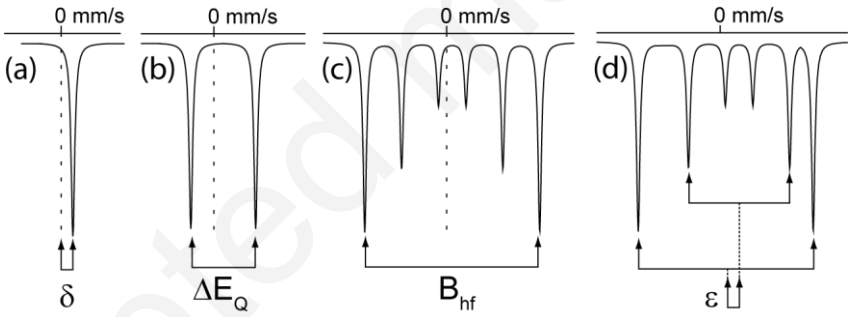

Figure 14: Mössbauer parameters, (a) isomer shift δ, (b) quadrupole splitting ΔE_Q, (c) magnetic hyperfine field B_{hf}, (d) quadrupole shift ε.

The **isomer shift (δ)** is an observable shift in the center of the absorption lines of a Mössbauer spectrum from the center of the absorption spectrum of reference material, commonly α−Fe(0) that is defined as 0 mm/s. It arises due to the s-orbital electron cloud of an absorber atom interacting with its nucleus and can be used to provide information on the electron density at the nucleus and chemical changes in the atom or lattice. The s-electron density depends upon the bonding environment of an atom,

which means that different compounds or minerals have different δ. Since Fe(III) and Fe(II) ions have different numbers of *d*-electrons (5 and 6 respectively), the nucleus is shielded from s-electrons to different extents meaning that in general, Fe(II) ions thus have larger values for δ than Fe(III) ions, although this is not necessarily the case for all minerals (see example of pyrite).

The **quadrupole splitting (ΔE_Q)** emerges in the case of asymmetric (i.e. non-spherical) absorber nuclei which includes almost all Fe minerals. The interaction presents itself as two clearly resolved symmetrical absorption lines (denoted a doublet) the distance between which is highly dependent upon oxidation state. In general high spin Fe(III) atoms show much lower ΔE_Q than high spin Fe(II) atoms which means that ΔE_Q can often be readily used for the determination of oxidation state in environmental samples without any additional treatment. Conversely, however, low spin Fe(II) atoms (e.g. in pyrite and other iron sulfur minerals) tend to have very low ΔE_Q meaning that caution should be taken when assigning the oxidation state to different doublets.

The **magnetic hyperfine field (B_{hf})** is a measure of the magnetic field at an atom which emerges either due to intrinsic magnetization or through the application of an external magnetic field. The B_{hf} is a very convenient parameter for mineral identification with many minerals showing distinct values. In essence, the hyperfine field manifests as a six-line spectrum (sextet) with is symmetrical about the isomer shift with B_{hf} defined as the distance between the outermost peaks. In powdered samples, the relative intensities of peaks 1 to 6 are 3:2:1:1:2:3 respectively. A parameter which is related to the quadrupole splitting and is only observable in the case of a magnetic hyperfine field is the **quadrupole shift (ε)**. This occurs when the peaks of the sextet are not equidistant, with peaks 1 and 6 moving in the opposite

velocity direction to peaks 2, 3, 4 and 5 (Figure 14). **ε** is related to ΔE_Q by the expression $\varepsilon = \Delta E_Q/2$, however it is often very small in comparison to B_{hf}. Combined with other parameters however it is able to provide valuable information for mineral identification, (e.g. for goethite or hematite).

Determination of oxidation state

The ability to distinguish between oxidation states, most notably Fe(II) and Fe(III), and their local atomic coordination is one of the most powerful aspects of ^{57}Fe Mössbauer spectroscopy. This applies in particular to soils and sediments. In general, the redox state of Fe affects the δ and ΔE_Q values of the paramagnetic part of each sample. A δ value of <0.8 mm/s combined with a ΔE_Q <1 mm/s is characteristic for Fe(III). In contrast, high spin Fe(II) shows δ values >1.05 mm/s and ΔE_Q >1.3 mm/s.[336] It is important, however, to note that certain ferrous phases, in particular low spin octahedral Fe(II) exhibit low δ and ΔE_Q. Such phases include pyrite (FeS_2) which contains Fe(II) covalently bonded to sulfur atoms and has ΔE_Q of 0.61 mm/s.[337] Another point to consider is that in cases where samples are magnetically ordered, ΔE_Q is often smeared out by the hyperfine field however the isomer shift remains a valid indicator of oxidation state.

Mineral Identification

Through the comparison of hyperfine parameters against established databases, it is possible to use ^{57}Fe Mössbauer spectroscopy for mineral identification. This is particularly useful when other mineralogical techniques cannot provide such information, for example when using XRD on samples which are dominated by non-Fe containing mineral phases. Furthermore, Mössbauer spectroscopy is particularly useful for measuring short range ordered minerals (poorly crystalline phases), or samples which are x-ray amorphous, though this often applies to Fe(III)

(oxyhydr)oxides rather than to mixed-valent Fe minerals. Some examples of Mössbauer spectroscopy being used for mixed-valent minerals include magnetite, GR, greigite and phyllosilicates which will be briefly discussed here.

Table 7 includes the key Mössbauer mineral parameters of magnetite and GR. The Mössbauer spectrum for **magnetite** is characterized by two overlapping sextets corresponding to the tetrahedral lattice (tet) which is comprised of only Fe(III), i.e. $Fe(III)_{tet}$ and the octahedral lattice (oct) which is comprised of both Fe(II) and Fe(III), i.e. Fe(II) $Fe(III)_{oct}$. Full details of the crystallographic structure of magnetite are provided in section 2.1. The presence of just one sextet for both octahedral ions is attributed to the existence of electron hopping between the Fe(II) and Fe(III) within the octahedral lattice,[338] although this hopping becomes less prevalent at low temperatures. The spectrum at 140 K for stoichiometric magnetite has an $Fe(II)Fe(III)_{oct}$ sextet with δ ~0.72 mm/s, ε ~−0.02 mm/s and B_{hf} of 47.4 T combined with a Fe_{tet} sextet with δ ~0.38 mm/s ε ~0.00 mm/s and B_{hf} of 50.2 T.[35] As the measurement temperature decreases below the Verwey transition (~121 K), the $Fe(II)Fe(III)_{oct}$ splits into two sextets, resulting in the low temperature spectrum having at least three distinct sextets.[339] It is possible to calculate the Fe(II)/Fe(III) ratio from a magnetite spectrum based on the relative areas of the $Fe(II)Fe(III)_{oct}$ and $Fe(III)_{tet}$ sextets[35] according to the formula $Fe(II)/Fe(III)=(0.5* Fe(II)Fe(III)_{oct})/(0.5* Fe(II)Fe(III)_{oct}+Fe(III)_{tet})$. However, the calculation is most effectively applied when the sample is fully magnetically ordered and above T_v, thus ideally a spectrum obtained at 140 K is considered to be the most effective for determining Fe(II)/Fe(III).[35] The incorporation of additional transition elements into the magnetite crystal lattice can also be probed using Mössbauer spectroscopy, which is directly

relevant to processes which can occur in the environment. Such incorporations of Zn or Co can lead to changes in δ, ε, and B_{hf}.[68,69]

The presence of both Fe(II) and Fe(III) in **GR** lends to its suitability for Mössbauer spectroscopy as both sites are observable as distinct doublets. Several studies have even tried to distinguish the different anion groups within different GRs, which has been summarized by Genin et al.[340] Sulfate GR(SO_4^{2-}) comprises of Fe(II) and Fe(III) doublets with Fe(II)/Fe(III) of 1.9. Carbonate GR(CO_3^{2-}) requires a third Fe(II) doublet and also has Fe(II)/Fe(III) of 1.9. Chloride GR(Cl^-) comprises of three doublets, though with a Fe(II)/Fe(III) of 2.7. These values of Fe(II)/Fe(III) depend upon level of oxidation and should be noted that many of the parameters of GR are often indistinguishable from Fe-bearing clays.[94]

Table 7: A table of Mössbauer parameters for mixed-valent Fe minerals magnetite and green rust (GR). δ – isomer shift, ΔE_Q – quadrupole splitting ($\Delta E_Q=2\varepsilon$) where ε is quadrupole shift, B_{hf} – hyperfine field, R.A. – relative abundance. The reference corresponding to each set of mineral parameters is also included.

Mineral	**T**	**Oxidation state**	**δ**	**ΔE_Q**	**B_{hf}**	**R.A**	**Ref.**
	K		mm/s	mm/s	T	%	
Magnetite	140	$Fe(III)_{Td}$	0.38	0.00	50.2	35.9	35
		$Fe(II)Fe(III)_{Oh}$	0.72	-0.04	47.4	64.1	
GR(SO_4^{2-})	78	Fe(II)	1.27	2.88		66	340
		Fe(II)	0.47	0.44		34	
GR(CO_3^{2-})	78	Fe(II)	1.27	2.93		51	340
		Fe(II)	1.28	2.64		15	
		Fe(III)	0.47	0.42		34	
GR(Cl^-)	78	Fe(II)	1.26	2.80		36	340
		Fe(II)	1.27	2.55		37	
		Fe(III)	0.47	0.44		27	

5.3. Vibrational spectroscopy

Raman and infrared spectroscopies are commonly used to qualitatively identify the iron phases on corrosion products.[341-345] Normally, the vibrational characteristics of a solid are affected by crystallinity, particle size and temperature. To accurately quantify the iron oxides and hydroxides, the use of vibrational spectroscopy is, however, not common.[341-345]

Raman spectroscopy is generally the vibrational spectroscopy of choice to characterize oxide powders and films as distinct Raman signatures are displayed by various iron oxide polymorphs and it is possible to take benefit of so-called phonon confinement for better assessment of the sample crystallinity.[341,346-349] Several Raman bands are identified for magnetite where the most representative band is found at about 667 cm^{-1}.[349,350] An overview of Raman mode frequencies at room temperature reported in different studies[122,346,351-357] is shown in Table 8. Generally, the Fe−O bond of bulk magnetite is characterized by the two distinct absorption bands at 570 and 375. For nanosized magnetite, the two bands at 632 and 585 arise due to split of the band at 570 and shift to higher wavenumbers, and the band at 440 results when the 375 band is shifted to a higher wavenumber. There is some confusion over the assignments of the phonons for magnetite, particularly the Raman-active phonons. When interpreting Raman data, De Faria et al.[341] highlighted the importance of considering laser power to interpret the Raman data. Magnetite can be converted to hematite and maghemite by moderate laser power or heating and therefore, some of the earlier Raman data evidenced the attribution of phonons of maghemite or hematite impurity to the parent magnetite phase. Findings of De Faria[341] were confirmed when laser-induced thermal effects on magnetite were studied by Shebanova and Lazor.[349] Figure 15 shows the Raman spectrum of natural sample of GR (called fougerite),

extracted in the forest of Fougères (Brittany-France). This spectrum displays the same characteristic bands at 518 and 427 cm^{-1} as the synthetic GR(CO_3^{2-}) or GR(Cl^-).[85]

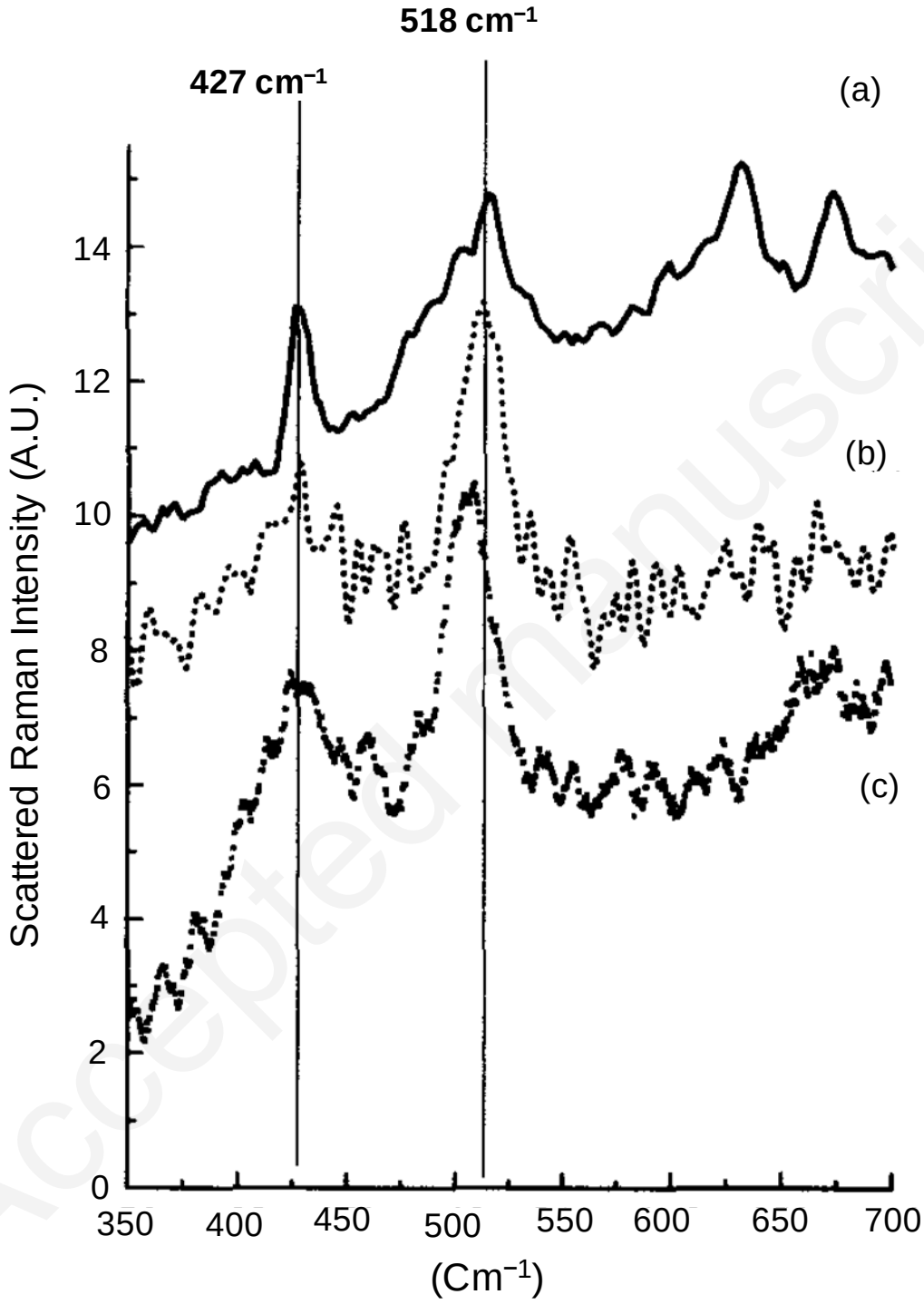

Figure 15: Microprobe Raman spectra of different green rusts (GRs): (a) natural GR, (b) synthetic GR(CO_3^{2-}) and (c) correspond to synthetic GR(Cl^-). Reproduced with permission from Ref. 85. Copyright 1997 Elsevier.

Although IR is less frequently used, some works reported two IR bands for magnetite located between 360 and 800 cm^{-1}, e.g. bands at 360 cm^{-1} and 565 cm^{-1}, and/or a band at 570 cm^{-1}.[342,343] Oxidation of magnetite to maghemite leads to the change in the IR spectra where the number of bands significantly increases signaling a transition to a structure of lower symmetry.[148]

Table 8. Raman mode frequencies and IR bands of magnetite.

	Raman Shift (cm^{-1})							Ref.
Magnetite	670	550 560						122,346
	676	550	470	418	319	298		351
	665	540						352
	662.7	533.6			301.6			341
	670	540			308		193	353
	706	570	490		336		226	354
	665	540			311			355
	669	540		410	300			356
	668	538			306		193	349
	666	541			311			357
	IR bands (cm^{-1})							
		560						346,353
		560		350				347
		572 with a shoulder around 700 (nano-sized)						*a*
		570 (nano-sized)		375				*b*
		570		400				148

[a] Li Y.-S.; Church, J. S.; Woodhead, A. L. Infrared and Raman Spectroscopic Studies on Iron Oxide Magnetic Nano-particles and their Surface Modifications. *J. Magn. Magn. Mater.* **2012,** *324*, 1543-1550.

[b] Zhang, J.; Srivastava, R. S.; Misra, R. D. K. Core-shell Magnetite Nanoparticles Surface Encapsulated with Smart Stimuli-responsive Polymer: Synthesis, Characterization, and LCST of Viable Drug-targeting Delivery System. *Langmuir* **2007,** *23*, 6342-6351.

For GR, the Raman or IR analysis focused mainly on the interlayer anion,[331,358-365] which are generally used to distinguish the formation of GR(SO_4^{2-}) and GR(CO_3^{2-}). Zegeye et al.[36,366] pointed out that a typical IR spectrum of GR(SO_4^{2-}) contains bands due to brucite-like sheets at 515, 780, 880 and 1550 cm^{-1} and bands arising from

intercalated SO_4^{2-} at around 620/660 and 1105/1138 cm^{-1}. Two bands, at 1100 and 1145 cm^{-1}, were recorded by Peulon et al.[367] for GR-II when deposited electrochemically on inert gold substrate, and assigned them to the split ν_3SO_4 mode. In a GR-I structure, a very intense peak at 1351 cm^{-1} was recorded with a shoulder at 1395 cm^{-1} assigned to the intercalated CO_3^{2-}.[358]

5.4. Synchrotron X-ray absorption

In recent decades, synchrotron-based analytical methods have become extensively used within the geosciences for the analysis of environmentally relevant elements in natural soils and sediments. Synchrotron radiation lends itself towards this field due to its element specificity combined with spatial resolution for analysing either bulk or nanoscale materials. Synchrotron radiation is produced when electrons are accelerated in circular paths at speeds close to the speed of light, resulting in the release of X-rays (photons) which are then used for probing a sample. In the most basic setup, a sample is irradiated with monochromatic X-rays at a specific energy. As the energy increases, atoms of a specific element absorb the X-rays at an absorption edge. A wide range of techniques making use of this principle are available including XANES, EXAFS, XMCD, and STXM which are discussed below. For more detailed information, Templeton and Knowles[368] provide an excellent overview of the use of synchrotron based methods for microbes, minerals and metals.

The XANES is a general term which is often used when describing absorption edge spectra collected at the *K*-edge. The XANES spectrum is generated when photons are absorbed by an element of interest at its respective absorption edge (for Fe the *K*-edge ~7112 eV) causing a core electron to be excited into an unoccupied orbital or ejected from the atom. Information about the oxidation state of Fe mineral phases at the *K*-edge can be obtained by probing the pre-site features which are obtained in typical

XANES spectra (Figure 16a). The energy of an absorption edge shifts to higher values as the oxidation state increases so Fe(II) mineral phases have a lower absorption energy than Fe(III) mineral phases. The method to obtain the element oxidation state from XANES requires the normalization of the absorption pre-edge feature which is located ~15−20 eV before the main K-edge (see inset Figure 16a). From the normalized pre-edge spectrum, the centroid (for more details see Wilke *et al.*[369]) is compared against the integrated pre−edge intensity to reveal both oxidation state and coordination environment (Figure 16b). The separation between the pre-edge centroids of Fe(II) and Fe(III) is reported to be 1.4+/−0.1 eV.[369,370] Using this approach ThomasArrigo *et al.* (2014) were able to observe small traces of Fe(II) in association with Fe(III) minerals in iron-rich organic floc material isolated from a wetland in Switzerland.[371]

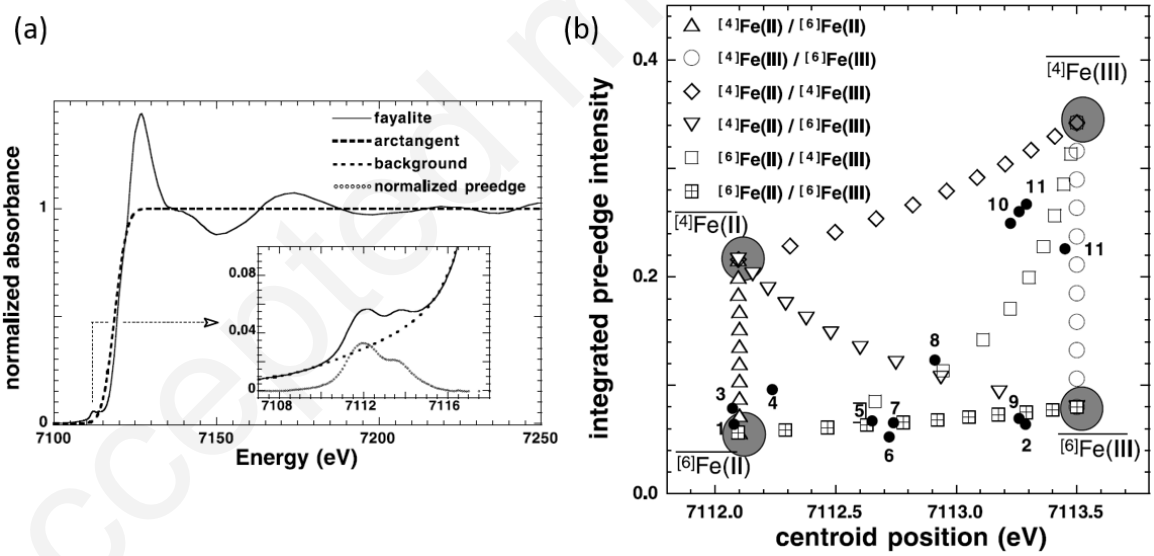

Figure 16: (a) The Fe K-edge absorption spectrum. The inset figure shows the pre-edge feature, which when normalized can be used to calculate the centroid position and integrated pre-edge intensity. (b) Comparison between pre-edge intensity and centroid position (eV) for different oxidation and coordination states of Fe in various Fe minerals. Black circles are 1 humite; 2 rhodonite no. 1; 3 rhodonite no. 2; 4 dumortierite; 5 potassian kaersutite; 6 kaersutite; 7 vesuvianite no. 1; 8 vesuvianite no. 2; 9 franklinite, 10 magnetite no. 1 & no. 2; 11 labradorite; 12 maghemite. Both (a) and (b) are reproduced with permission from Ref. 369. Copyright 2001 Mineralogical Society of America.

The EXAFS is also often collected in addition to XANES. EXAFS spectra provide information about the local coordination environment of atoms in a mineral. The EXAFS spectra are characterized by spectral oscillations which are generated when a photoelectron is backscattered by surrounding atoms. The wave patterns of these backscattered electrons interfere with the wave patterns of the outgoing electrons resulting in fine structural differences at energies just above the absorption edge. EXAFS is used to provide information about coordination number, nearest and next-to-nearest neighbor atom positions and their interatomic distances. Pantke et al. used EXAFS to find that GR is produced as an intermediate phase during the oxidation of Fe(II) to goethite by the nitrate-reducing bacteria *Acidovorax* sp. BoFeN1.[274]

The XMCD is a form of X-ray absorption spectra (XAS) which utilizes soft X-rays (typically at energies below 10 keV) to investigate the oxidation and coordination state of magnetic minerals. The ferrimagnetic properties of magnetite arise due to the anti-parallel alignment of Fe cations within the crystal lattice sites. Specifically, this includes Fe(II) and Fe(III) in octahedral coordination (oct), and Fe(III) in tetrahedral coordination (tet). XAS collected under the application of oppositely polarized magnetic fields (−0.6 T and +0.6 T parallel and anti-parallel to the direction of the beam respectively), will yield small differences (provided that the X-rays are circularly polarized either left or right). Subtraction of one of these spectra from the other results in the origin of the XMCD. Careful analysis of XMCD spectra can be used to reveal changes in magnetization, valence state (i.e. number of *d* electrons), site location and provide information about magnetic cations with different oxidation states at different lattice sites.[372] For instance fitting of the Fe $L_{2,3}$ edge XMCD to atomic multiplet calculations,[373,374] can be used to determine the cation distribution of Fe(II) and Fe(III) in oct and tet sites. Each peak corresponds to a different lattice site

with the first negative peak corresponding to Fe(II) in octahedral environment, the middle positive peak corresponding to Fe(III) in tetrahedral coordination and the third (negative) peak corresponding to Fe(III) in octahedral coordination. In the case of titanomagnetite, the XMCD spectra contains an additional positive peak which occurs at the low energy side of the Fe−L_3 edge corresponding to Fe(II) in tetrahedral coordination.[375] XMCD can thus provide unambiguous determination of the relative site occupancies in spinels[49,50] which can be used to obtain information about the Fe(II)/Fe(III) ratio of magnetite, especially at the surface of the mineral.[48] XMCD has been utilized for the investigation of biogenic magnetite formed through the reduction of ferrihydrite by Fe(III)-reducing bacteria.[280] Using the technique it is also possible to determine how different metals are incorporated into the mineral structure including arsenic,[376] chromium,[377-380] cobalt,[69,381,382] manganese, nickel, technetium[378] and palladium[383] zinc, which have all been investigated. Furthermore, greigite has also been probed using XMCD[384-386] which furthermore demonstrates the versatility of the technique for magnetic mixed-valent minerals.

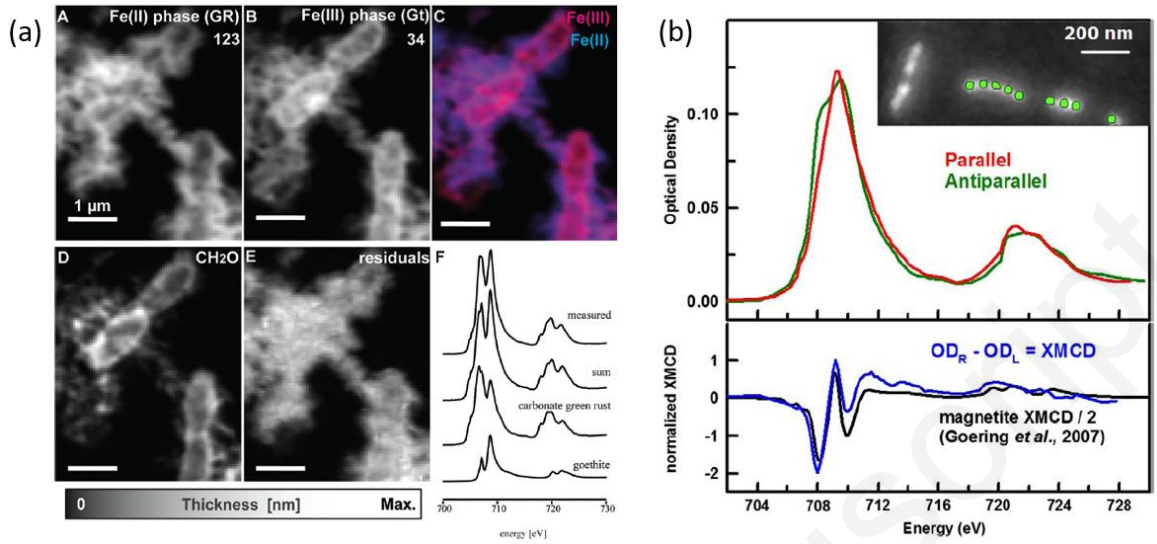

Figure 17: (a) The formation of mixed-valent green rust as an intermediate phase before goethite formation during microbial Fe(II) oxidation was shown using STXM Reproduced from Ref. [274]. Copyright 2012 American Chemical Society. (b) STXM can be combined with XMCD to provide the cation distribution of Fe(II) and Fe(III) in individual magnetosomes formed within magnetotactic bacteria. Reproduced with permission from Ref. [281]. Copyright 2010 Elsevier.

The STXM combines chemical speciation with microscopy at resolutions down to 12 nm.[387] It is advantageous over more conventional electron microscopies (e.g. scanning and transmission electron microscopies) because it is able to provide information on the distribution, oxidation state and coordination environment of different elements. STXM uses soft X-rays and can measure dry samples, hydrated polymers or biological material which means it is highly suited to measuring environmentally relevant samples. The basic setup of a STXM beamline enables monochromated X-rays to pass through a zone plate which focuses the x-ray beam onto a single spot (i.e. pixel). Each single pixel then contains a distinct absorption spectra (or XANES) which can be analyzed. Von der Heyden et al.[387] used STXM on trace amounts of Fe minerals which were extracted from the euphotic zone in the Southern ocean. In this study, XANES were collected at the Fe L_3 absorption edge (~710 eV). The energy

difference (ΔeV) and intensity ratios of the two primary peaks in the L_3 edge, corresponding to Fe(II) (lower energy) and Fe(III) (higher energy), were compared to obtain information on the oxidation state, coordination number and mineral identity of individual grains of Fe minerals at resolutions of ~12 nm.[387] Other studies using STXM have been able to observe the formation of GR by the nitrate-reducing Fe(II)-oxidizing bacterium *Acidovorax* sp BoFeN1 (Figure 17a).[274] Aqueous Fe(II) was oxidized, leading to the formation of the GR as an intermediate phase which then in turn underwent transformation to goethite. It has also been shown that STXM can be combined with XMCD to determine the cation distribution of Fe(II) and Fe(III) within individual magnetosomes grown inside magnetotactic bacteria (Figure 17b).[281] The study confirmed that the magnetic moment of the individual magnetosomes were aligned in the same direction and was also able to show that magnetosomes were slightly enriched in Fe(II) (i.e. they were reduced). The cation distribution within magnetite produced via dissimilatory Fe(III) reduction by *Shewanella oneidensis* have also been analyzed using this combination of STXM and XMCD.[388]

5.5. Transmission electron microscopy and scanning electron microscopy

The morphology of mixed-valent iron oxides is routinely examined by TEM and SEM.[2] These imaging techniques provide insights into the micron and nanoscale structure of these minerals. TEM usually provides 2D image while SEM can provide more information on topology (i.e. pseudo 3D).[2] Shape of GR particles varies from hexagonal to rhombohedral (Figure 18) while magnetite can have commonly cubic, octahedral or hexagonal crystal structure (Figure 8, Figure 19).[31,37,51] GRs typically have thin, plate-like hexagonal crystals (Figure 18) however, crystals of GR(SO_4^{2-}) have been observed to be much larger[31] and flatter[32] than GR(CO_3^{2-}).

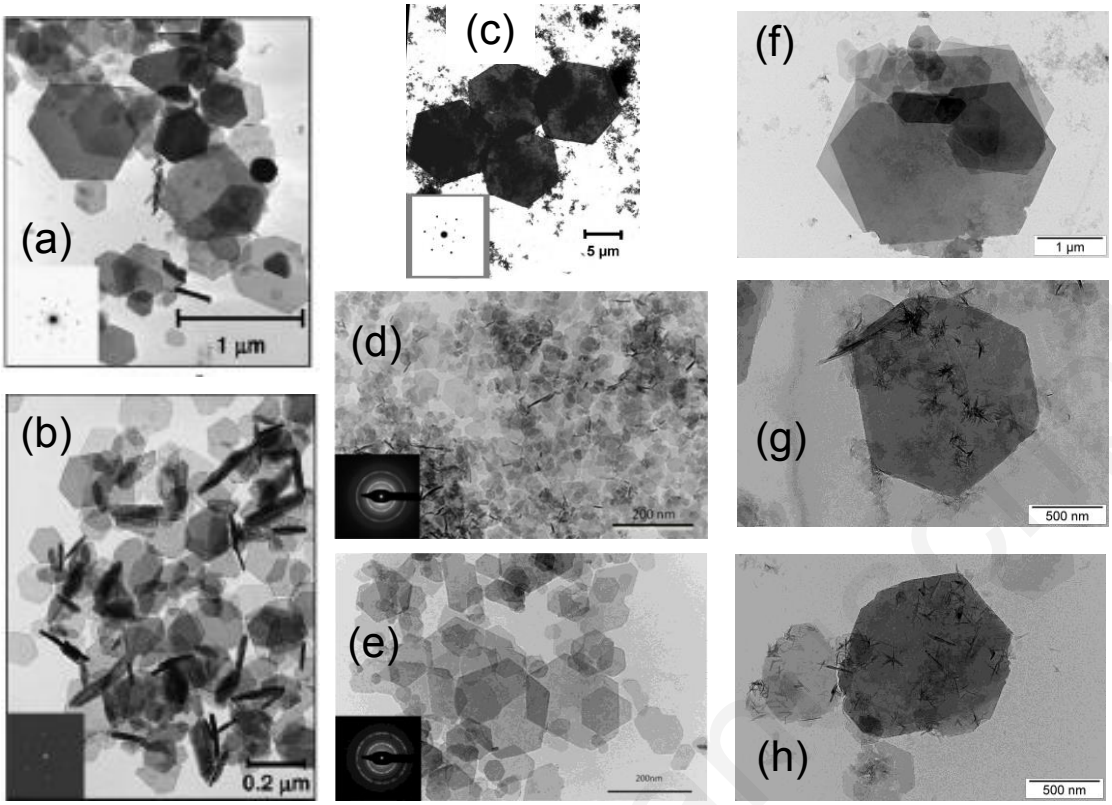

Figure 18: TEM images of different green rusts formed by different procedures. (a) GR(SO_4^{2-}) and (b) GR(CO_3^{2-}) were formed by coprecipitation.[31] Reproduced with permission from Ref. 31. Copyright 2006 Elsevier Masson SAS. (c) GR(CO_3^{2-}) formed by bioreduction of lepidocrocite.[389] Reproduced from Ref. 389. Copyrights 2002 American Chemical Society. (d) and (e) correspond to GR(CO_3^{2-}) formed by coprecipitation but samples were aged for 0 h and 24 h respectively.[390] Reproduced with permission from Ref. 390. Copyright 2012 Elsevier. (f), (g) and (h) correspond to the GR(SO_4^{2-}) formed by abiotic mineralogical transformations of ferrihydrite, goethite and hematite respectively where traces of goethite and hematite are still visible in (g) and (h), respectively.[51] Reproduced with permission from Ref. 51. Copyright 2012 Elsevier.

It should be noted that the morphology of magnetite or GR can vary significantly with the method of formation and other reaction conditions. Hexagonal platelets are the typical crystal habit of GR however slight variations in GR morphology varied according to the method of synthesis as evident from TEM images of GRs formed by various methods (Figure 18). Owing to the strong diffraction behavior of these plates, derived structural data is often comparable to that obtained through XRD. Similarly, magnetite occurs most commonly as octahedral crystals[2] but varying methods of

synthesis can yield different crystal habits (Figure 19). For example, magnetite crystals obtained by slow oxidation of a $FeCl_2$ solution at room temperature were round shaped[391] as compared to the octahedral particles which were formed by oxidation of a $FeSO_4$ (0.5 M) solution with KNO_3 in KOH (1.43 M) at 90 °C.[2,392] Recently, Byrne et al.[48] modified the later synthesis method where a $FeSO_4$ solution (absence of Fe(III) was ensured by storing it with Fe^0 for one month prior to oxidation) was oxidized in alkaline solution of KNO_3 at 90 °C under strict N_2 atmosphere. Obtained product was micromagnetite (d ~ 100−200 nm) with rounded particles along with some squared ones. However, nanosized magnetite particles (d ~ 12 nm) with similar shape (rounded with squared) were obtained by Byrne et al.[48] when anoxic solution of 1 M $FeCl_2$, 2 M $FeCl_3$ in 0.3 M HCl was added dropwise into 25% NH_4OH solution. Usman et al.[37] reported that magnetite formed by abiotic mineralogical transformations of ferrihydrite, lepidocrocite and goethite, have different morphologies, particle size and surface area (Figure 8). They reported that magnetite formed ferrihydrite was characterized by smaller particles with non-uniform shape and size (<50 nm). However, when magnetite was formed from lepidocrocite or goethite, shape of its particles varied between hexagonal to octahedral (Figure 8). Moreover, size of magnetite particles was 70–80 nm and 200–300 nm when formed from lepidocrocite and goethite, respectively.[37]

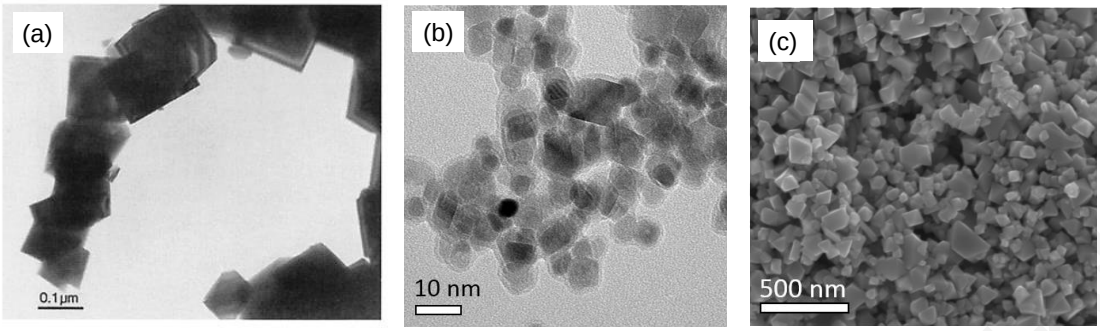

Figure 19: TEM images of magnetites synthesized by different procedures. (a) Magnetite synthesized by Schwertmann and Cornell[392] from $FeSO_4$ solution. Reproduced with permission from Ref. 392. Copyright 2000 John Wiley and Sons. (b) Nano-magnetite synthesized by Byrne et al.[48] from $FeSO_4$ solution by modifying method of Schwertmann and Cornell[392], and (c) micro-magnetite synthesized by Byrne et al.[48] from $FeCl_2$ and $FeCl_3$ solution. Both (b) and (c) images are reproduced with permission from Ref. 48. Copyright 2016 Nature Publishing Group. TEM images of magnetite formed by abiotic transformation of ferrihydrite, lepidocrocite and goethite can be seen in Figure 8.

5.6. Magnetic measurements

The ubiquity of magnetic minerals in almost all natural environments means that magnetic based measurements provide a powerful tool for investigating past and present changes to the Earth's geology, ocean currents, windblown deposits, pollution and climate. For example, the use of magnetic methods on soils taken from the Chinese Loess Plateau has enabled changes to the extent of ice age glaciers to be determined throughout time by probing the type of magnetic material deposited during warm and moist conditions compared to cold and dry conditions.[393] Furthermore, magnetic measurements are also being used to measure the effects of anthropogenic pollution in plant matter as well as to human health.[64,394]

Magnetism is dependent upon the movement of electrons around an atom which generates a magnetic dipole (or magnetic moment). The magnetic behavior of Fe minerals, particularly mixed-valent magnetite and greigite mean that a number of

different magnetic based measurements can be used to obtain information about their relative abundance, grain size, chemical composition and stoichiometry. Here we present a very brief overview of some of the parameters typically investigated using magnetic measurement techniques as well as a short introduction to some of the instruments such measurements can be performed with.

The most commonly occurring magnetic minerals are Fe minerals but within most of these minerals the magnetic moments of the Fe atoms do not interact with each other and are randomly orientated due to thermal energy. Consequently, the magnetic moments cancel each other out resulting in paramagnetism (e.g. ferrihydrite). In ferromagnetic materials, the magnetic moments of each atom are coupled together and are aligned parallel to one another leading to strong magnetic behavior. In some minerals coupled layers of Fe atoms form in which the net magnetic moment of these layers are in anti-parallel orientation to each other, thereby cancelling each other out and resulting in no overall magnetization (anti-ferromagnetism), though in some cases these moments are slightly misaligned and result in canted anti-ferromagnetism (e.g. hematite). Magnetite is a ferrimagnetic mineral in which Fe(II) and Fe(III) ions exist in octahedral coordination with magnetic moments anti-parallel to Fe(III) in tetrahedral coordination leading to a cancellation of the Fe(III) moments and an overall net magnetic moment due to only Fe(II) atoms. Superparamagnetism describes materials which are small enough so that at room temperature show no residual magnetic behavior, however when cooled through their blocking temperature (T_B) show very strong magnetic characteristics (e.g. nanomagnetite).

Several different techniques are used for measuring magnetic properties including several temperature dependent tools. A hysteresis loop (Figure 20) contains information about the magnetization M of a mineral when it is subject to an applied

magnetic field *H*. The point at which all magnetic moments within the mineral are aligned and there is no increase in *M* is called the saturation magnetization (M_s). If a sample retains magnetic ordering at room temperature, this is called the remanent magnetization (M_r). The field required to ensure a sample has no magnetization is called the coercivity (H_c). A superparamagnetic material is one which has no coercivity (i.e. *H*c=0). The applied field required to remove remanence one the magnetic field is removed is called the coercivity of remanence (H_{cr}). Finally the susceptibility (χ) describes the initially linear increase in magnetization in a low field.

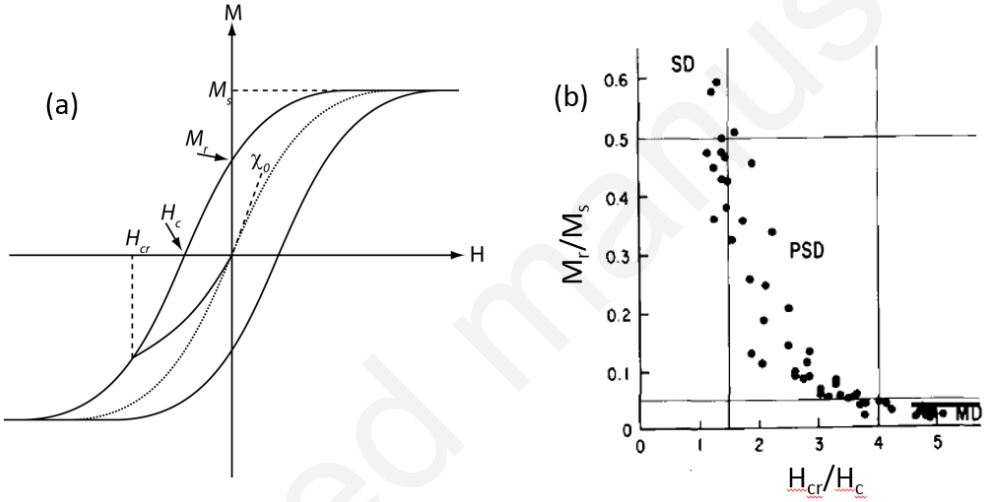

Figure 20: (a) A hysteresis loop shows how the magnetization (*M*) of a sample changes with applied field (*H*). From the loop it is possible to determine saturation magnetization (M_s), remanent magnetization (M_r), coercivity (H_c), coercivity of remanence (H_{cr}) and susceptibility. (b) Data from a hysteresis loop can be inserted into a Day plot to show the approximate grain size of magnetite in a sample. Reproduced with permission from Ref. 395. Copyright 1977 Elsevier.

Hysteresis loops can also be used to approximately determine the grain size of a mineral under investigation by following the definitions of superparamagnetic (SP), pseudo single domain (SD) and multidomain regimes (MD) as outlined previously.[395] SP describes magnetite with particle size d < 30 nm, $M_r/M_s << 0.01$ and $H_{cr}/H_c > 10$. PSD magnetite falls within the range of 30 < d < 100 nm and has $0.1< M_r/M_s < 0.5$, $2 < H_{cr}/H_c < 4$ combined with 10 mT < H_c < 15 mT. Finally MD magnetite has d > 100

nm, $M_r/M_s < 0.1$, $H_{cr}/H_c > 4$ and $H_c < 10$ mT.[396] Such a method is particularly useful in environmental samples where it is not possible to isolate individual magnetic grains to determine their particle size by microscopy. This approach, however, can be affected by mixtures of particles with different size distributions. Several types of instruments can be used to obtain a hysteresis loops including Alternating gradient force magnetometer (AGFM), Vibrating Sample Magnetometer (VSM), or superconducting quantum interference device (SQUID) magnetometer. These different techniques are often coupled with cryostats or furnaces to obtain temperature dependent measurements.

Other techniques frequently used within geosciences focus on the determination of magnetic susceptibility (χ), often in the form of volume dependent magnetic susceptibility (κ). This technique applies a low AC magnetic field (e.g. 300 A/m with frequency of 875 Hz) onto a sample which is held within a pick-up coil. For example Porsch et al.[231] used volume-dependent magnetic susceptibility to track Fe(III) mineral reduction by the Fe(III)-reducing bacteria *Shewanella oneidensis* MR−1. Over time it was shown that κ increased as the mineral sample transformed from paramagnetic ferrihydrite to ferrimagnetic magnetite (Figure 21a). A small decrease in κ after the magnetite formation was ascribed to be due to either siderite formation or the increase in magnetite grain size. This is because κ is related to grain size with superparamagnetic particles exhibiting higher susceptibility than single domain magnetite.[397] Using κ has also been used to determine regions of high magnetic content in hydrocarbon contaminated soils which was suggested to be due to microbial activity.[109,237] Furthermore, κ was recently used to observe redox changes (i.e. oxidation or reduction) in magnetite induced by Fe(II)-oxidizing or Fe(III)-reducing bacteria under the influence of different geochemical conditions (Figure

21b). Thus, using such techniques offer non-invasive, rapid and inexpensive approaches to quantifying relative changes to the magnetic content of a sample which can often include cores and complex model environments.

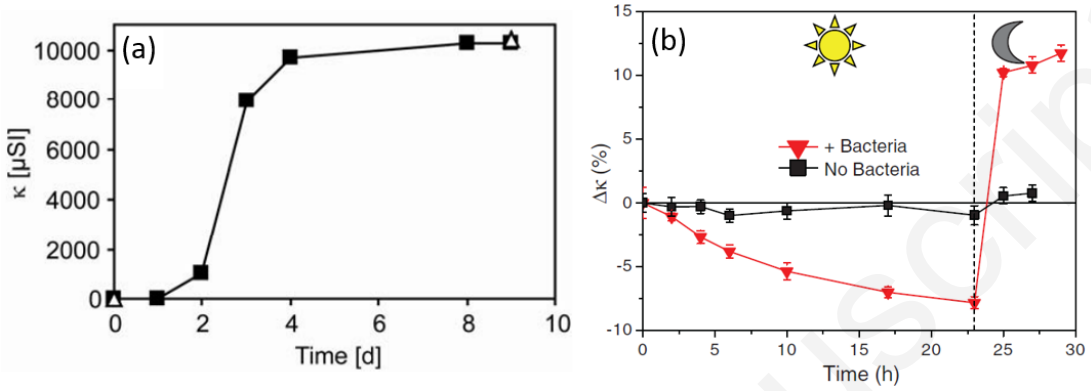

Figure 21: (a) Changes to volume-dependent magnetic susceptibility (κ) during microbial reduction of ferrihydrite to magnetite.[398] Reproduced from Ref. 398. Copyright 2010 American Chemical Society. (b) Relative changes to κ during the incubation of magnetite with Fe(II)-oxidizing and Fe(III)-reducing bacteria. Decreases in κ correspond to oxidation whilst increases in κ correspond to reduction.[313] Reproduced with permission from Ref. 313. Copyright 2015 The American Association for the Advancement of Science.

6. Application of mixed-valent iron minerals for environmental remediation

This section illustrates the role of mixed-valent Fe minerals in biogeochemical cycling of trace elements, their ability to affect the mobility, redox transformation and toxicity of various organic and inorganic pollutants, and their use in various remediation strategies for contaminated water and soils. Mineral properties such as surface area, particle size, and stoichiometry, have a dramatic impact on their efficiency in such applications and that will also be highlighted. Due to the presence of structural Fe(II), mixed-valent Fe minerals are considered as highly reactive to catalyze chemical oxidation (Fenton-like, persulfate and photo-catalytic) of organic pollutants at circumneutral pH and that is discussed as a last part of this section.

6.1. Sorption of contaminants

Mixed-valent Fe minerals play a significant role in the sorption of organic and inorganic compounds in the environment, and thus influence the transport and mobility of contaminants in natural and engineered systems. For instance, magnetite commonly occurs in natural and engineered settings,[99] and due to its reactive and high surface area, it plays a significant role in the sorption of environmental pollutants (Table 9). Magnetite is used in analytical chemistry to separate a wide variety of substances, such as dissolved metal species, organic and biological materials.[399] From an engineering point of view, the magnetic properties of magnetite and its thermodynamic stability make it very suitable for its use as sorbent in environmental remediation processes. Indeed, the use of magnetite in wastewater treatment, *in situ* groundwater remediation and for recovery of valuable metals from mine waters has several advantages over conventional techniques. Owing to its ferromagnetic

character (further details in section 2.4), it can be used to treat contaminated water supply where it can be kept in place using a magnetic trap or can be separated by using a magnet with low field strength. Magnetic separation offers quick recovery and reuse of magnetite for further remediation.[400] The removal of particles from solution with the use of magnetic fields is therefore likely to be more efficient, selective and much faster than filtration or centrifugation.[400]

The GRs have been widely reported to transform several inorganic and organic contaminants through redox processes (see section 6.2), however, this has led to a distinct lack of information of the sorption ability of GR which is rarely investigated independently of the redox reaction. Indeed, as the binding of substrate to oxide surfaces is a prerequisite to induce heterogeneous reduction reactions, both of these processes are often considered together in published reports, particularly in the case of redox-active elements. Despite this lack of understanding of sorption behavior, GRs are anion exchangers and clearly represent potential sorbents in anoxic environments. Due to the amphoteric surface hydroxyl groups, GR can also sorb anions (organic and inorganic) and cationic metals. Similarly to hydrotalcite, GR may also sorb acidic compounds, which typically exist in anionic form at neutral pH. This adsorption may proceed through: (i) anion exchange, or (ii) ligand exchange or surface complexation reaction on external sites.[401-403]

To best describe the sorption properties of mixed-valent Fe minerals, this section has been subdivided into: (i) sorption of inorganic compounds including oxyanions, heavy metals and radionuclides; (ii) sorption of organic compounds including naturally occurring ligands and emerging contaminants. Salient sorption studies in environmental and engineering contexts using GR and unsubstituted pure magnetite are summarized in Table 9.

6.1.1. Inorganic compounds

Recently, there has been a growing interest in the use of magnetite in the removal of metals and oxyanions from water, with the aim of developing new cost effective, non-toxic, magnetic filtration/sorption remediation strategies.[404-408] Magnetite nanoparticles have shown to be very efficient for the removal of arsenic (As) and chromium (Cr) from water, as the adsorption capacity generally increases with decreasing particle size.[409,410] Magnetite showed high affinity for both arsenite-As(III) and arsenate-As(V)[411] in comparison to conventional techniques (ion exchange, coagulation, adsorption onto activated alumina) which require pre-oxidation of As(III) to As(V) in order to enhance sorption efficiency.[412] Variations in pH, temperature, and ionic strength can also affect the speciation and adsorption of oxyanions to magnetite.[413] The adsorption of As(III) as well as As(V) onto magnetite (point of zero charge ~7) was found to be pH dependent.[116,406] Arsenic sorption decreased with increasing ionic strength, probably due to compression in diffused double layer, increase in particle aggregation and decrease in the available surface area for arsenic adsorption. High adsorption of arsenic was observed at high temperatures, which may be due to an increase in the kinetic activity or increase in the mass transfer rate from solution to surface.[410]

From a microscopic perspective, Jönsson and Shermann[414] pointed out that As(V) sorbs to magnetite and GR(CO_3^{2-}) by forming inner-sphere surface complexes resulting from corner sharing between AsO_4 groups and FeO_6 octahedra. GR and magnetite strongly sorb As(V) with sorption capacities greater than 100 μmol As g^{-1} around pH 7, with no indication of abiotic reduction of adsorbed As(V) by structural Fe(II). For the very first time, Wang et al.[415] showed the predominant formation of tridentate As(III)O_3 complexes occupying the vacant tetrahedral sites on (111)

surfaces of magnetite. The EXAFS spectra by Liu et al.[411] suggested the existence of bidentate binuclear corner-sharing complexes for As(V), and tridentate hexanuclear corner-sharing complexes for As(III) on magnetite surfaces. However when sorption of arsenic was studied onto GR(Cl^-), As(V) sorbs more efficiently than As(III).[416] Both arsenic species formed inner sphere complexes at surface coverages of 0.27 and 2.70 μmol m^{-2}. With EXAFS derived data for As(V), they proposed the presence of monodentate mononuclear corner-sharing complexes and binuclear bidentate double-corner complexes. However, they suggested the predominant binding of As(III) pyramids to the edges of GR(Cl^-) layers by corner sharing with FeO_6 octahedra.[416] Other inorganic ligands such as silicate and phosphate have also been shown to sorb to the external faces of GR.[403,417]

Studies have shown the ability for magnetite nanoparticles to sorb heavy metals such as Pb(II), Cu(II), Zn(II) and Mn(II).[418,419] The adsorption capacity of magnetite nanoparticles towards metal ions was found dependent on the electronegativity of these ions. Moreover, the adsorption capacity of heavy metals strongly varied according to the pH and temperature of solution. The adsorption mechanism seems to be mainly an electrostatic attraction between metal ions and the magnetite affected by the hydrated ionic radius of the metal cations. Modification of magnetite particles by coating with humic acid or chitosan has also been reported for enhancing removal of cationic metals such as Cd(II), Cu(II), Hg(II), Pb(II), and Ni (II) from water.[420,421]

Numerous studies have focused on using magnetite to target the migration and fate of persistent radionuclides in the environment, especially in the context of nuclear waste disposal.[422-427] This is of particular interest because it is thought that magnetite formation may occur during the anoxic corrosion of steel containers used to store nuclear waste. Environmental factors strongly affect the sorption of elements onto

magnetite. For instance, Catelette et al.[423] reported that magnetite has a high retention capacity for Ba(II) and Eu(III), whilst Cs(I) is sorbed on magnetite only if magnetite contains some impurities such as silica. The sorption of ^{137}Cs and ^{90}Sr increases with pH, with higher sorption for ^{90}Sr than that for ^{137}Cs at any pH.[422] Both of these radionuclides were sorbed primarily by electrostatic interaction between the positively charged cation and the negatively charged magnetite surfaces (pH ≥ PZC). Magnetite showed strong sorption of the tetravalent radionuclide, $^{141}Ce(IV)$, at all pH values, with the sorption being nearly independent of ionic strength, advocating the participation of inner sphere type of coordination between the metal ion and the surface sites or surface precipitation.[422] In Martinez et al.,[405] the variation of the sorption of selenium (Se) on magnetite with pH has been described as two inner-sphere complexes for Se(IV), and an outer-sphere complex for Se(VI). Magnetite nanoparticles have been also used to remove U(VI) from contaminated waters.[428,429] Das et al.[430] showed that high adsorption of U was observed at neutral pH, whereas reduced species U(IV) on the magnetite surface was detected by X-ray photoelectron spectroscopy (XPS). Adsorption and reduction of U(VI) and subsequent growth of UO_2 nanoprecipitates have also been reported using XANES and atomic force microscopy (AFM).[431,432]

Adsorption of naturally occurring inorganic ligands such as carbonate, sulfate, silicate and phosphate have been largely studied at both macroscopic and molecular levels, and are known to be strong competitors of oxyanions (e.g. As or Cr) for sorption on magnetite surfaces.[433-438] XPS, Mössbauer and IR spectroscopies have provided evidence that Fe(III) in octahedral sites is involved in phosphate adsorption with formation of protonated binuclear species,[434] while outer-sphere complexation was rather suggested for ligands such as sulfate and carbonates.

6.1.2. Organic compounds

In contrast to inorganic compounds, only few studies are available on the mechanism and extent of sorption of organic contaminants (classical or emerging) on magnetite or GR. Generally, binding of organic compounds proceed through hydrogen bonding, van der Waals interactions and surface complexation reactions with magnetite surfaces or external sites of GR,[328,439-442] interlayer anion exchange only in case of GR,[328,442] and hydrophobic interactions to engineered systems such as organic-amended magnetite and surfactant-interlayered GRs.[4,443-446]

Adsorption of citric acid, gallic acid, poly(acrylic acid), poly(acrylic-co-maleic acid) and humic acid onto magnetite nanoparticles have been investigated at neutral pH commonly prevailing in natural waters.[447] The adsorption of organic matter such as humic acid on magnetite particles is further considered in the context of colloidal stabilization, as it prevents particle aggregation in a wide range of pH and enhances salt tolerance.[448] The adsorption of bacterial cells to magnetite has been investigated with the aim to develop water purification methods,[449] or for the removal of lindane (γ–HCH) from water by microbial cells immobilized on magnetite.[450] Magnetite has been efficiently used to remove tetracyclines (antibiotics) from aqueous media.[439,440] Kinetics and extents of sorption of nalidixic acid (quinolone antibiotic) on magnetite have been recently investigated by Usman et al.[441] While the effect of ionic strength was of less significance, the adsorption was found to be strongly affected by particle size and surface properties of magnetite.[441] Very recently, magnetite stoichiometry has been shown to strongly influence the capacity of magnetite to bind organic and inorganic compounds (e.g. quinolone antibiotics, natural organic matter and dissolved silicates).[451] Binding of tested ligands was enhanced with an increase in stoichiometry of magnetite by Fe(II) recharge.

Kone et al.[328] reported that pentachlorophenol can bind to the external surface of GR although no reductive transformation was observed. Pentachlorophenol cannot penetrate the GR interlayer and displace anion from the interlayer. At neutral pH, pentachlorophenolate adsorption proceeds probably through electrostatic attraction between the anionic sorbate and the positively charged centers in the hydroxide sheets of GR. Liang and Buttler[442] studied the sorption of various carboxylic acids onto GR(Cl^-) and reported that carboxylic ligands sorb on the internal as well as external surface sites of the GR. It was suggested that carbon tetrachloride transforms only on external surface sites of GR, since this compound does not enter GR interlayers.[442,452] Due to the hydrophilic surface of magnetite, it is unable to efficiently uptake organic compounds and so consequently, chemical modifications to make the magnetite surface more suitable for retention of hydrophobic compounds have recently been attracting attention.[4] For instance, the formation of mixed hemimicelles from adsorption of cation surfactants - cetyltrimethylammonium bromide (CTAB) and cetylpyridinium chloride (CPC) - on magnetic nanoparticles, can enhance sorption of organic compounds by strong hydrophobic and electrostatic interactions.[443] Alternatively, non-toxic ligands may also appear as an environmentally friendly approach to remove organic pollutants. For instance, 6-Deoxy-6-ethylenediamino-β-cyclodextrin grafted thiodiglycolic acid modified magnetic nanoparticles were used to effectively remove pharmaceutically active compounds and endocrine disrupting compounds such as naproxen and carbamazepine and bisphenol A.[444] Activated carbon combined with magnetite or magnetite-immobilized Chitin has also been investigated in order to produce magnetic adsorbents of volatile organic compounds and chlorinated compounds.[453,454]

In general, magnetite and GR likely play a considerable role in the sorption and immobilization of inorganic and organic compounds in the environment. Table 9 summarizes the studies which have determined the adsorption parameters for magnetite or GR.

Table 9: Summary of quantitative findings of sorption of different compounds to magnetite or GR. The source of magnetite (natural or synthetic) is indicated, while all GR samples were lab-synthesized. Studies are arranged according to their order of appearance for inorganic and organic compounds.

Sorbent type	**Target pollutant & its initial concentration**	**Experimental conditions**	**Extent / rate of adsorption**	**Ref.**
Magnetite (natural) < 180 µm,18.3 $m^2\ g^{-1}$	Cs (I): 2×10^{-5} mol L^{-1}, Ba (II): 5×10^{-5} mol L^{-1}) Eu (III): 2×10^{-4} mol L^{-1}	pH 3 – 11, magnetite 2 g L^{-1}, ionic strength (I) = 10^{-2} and 10^{-1}.	90% for Ba (II) at I = 10^{-1} and pH > 11, 100% for Eu (III) at pH > 7 and I = 10^{-1}. < 50% of sorption for Cs(I) which was independent of pH	423
Magnetite (natural) 33.3 µm; 1.8 $m^2\ g^{-1}$	Yb(III): 2.10^{-5} mol L^{-1} Ni(II): 2.10^{-5} mol L^{-1} Cs(I): 4.10^{-5} mol L^{-1}	pH 3 – 11, $NaNO_3$ = 0.1 mol L^{-1} for Yb(III) and Ni(II), 0.01 mol L^{-1} for Cs(I) Magnetite = 12 g L^{-1} for Yb(III) and Cs(I), 8 g L^{-1} for Ni(II)	100% for Yb(III) and Ni(II) (pH = 7) and negligible for Cs(I) (<10%).	117,118
Magnetite (commercial) 0.1 µm; 2 $m^2\ g^{-1}$	Cs, Sr, and Co 1000 ppm each	pH 6 – 9 (for Cs and Sr) and 5 – 8 (for Co), magnetite 10 g L^{-1}, $NaNO_3$ = 0.01 N	q_{max} (µmol m^{-2}) = 0.70 (Cs, pH 6), 3.92 (Sr, pH 7) and 3.88 (Co, pH 8)	424
Magnetite (lab synthesized) 50-200 nm; 8.5 $m^2\ g^{-1}$	U(VI) 4.4×10^{-7} mol L^{-1}	pH 6 I = 0.1 mol L^{-1} Solid/Liquid ratio 2 g L^{-1}	90% after 1 day	407
Magnetite (lab synthesized) 90 $m^2\ g^{-1}$	As(III) and As(V) 100 µM As(III)	pH 9, magnetite 0.5 g L^{-1}, 0.01 M $NaClO_4$	Maximum sorption density 140 µmol g^{-1} after 24 h for As(III).	406
Magnetite (natural) < 5 µm; 0.89 $m^2\ g^{-1}$	Se(IV) and Se(VI) 3×10^{-6} – 5×10^{-4} dm^3 mol^{-1}	pH 4, 5 g L^{-1} magnetite, reaction time 30 h	K_L (dm^3 mol^{-1}) = 3×10^5 and 1.19×10^6 for Se(VI) and Se(IV) respectively with maximum sorption (mol m^{-2}) of 3.5×10^{-6} and 3.13×10^{-6}.	405

Magnetite (commercial) < 5 μm; 1.58 $m^2\ g^{-1}$	U(VI) 10^{-4} mol L^{-1}	1 g of magnetite, acidic pH, 0.1 mol L^{-1} $NaClO_4$	Existence of both U(IV) and U(VI) during uranium sorption, which was correlated to the reduction of U(VI) to U(IV) by magnetite.	[425]
Three kinds of magnetite M1: Lab-synthesized 11.72 nm; 98.8 $m^2\ g^{-1}$ M2 : Commercial 20 nm; 60 $m^2\ g^{-1}$ M3 : Commercial 300 nm; 3.7 $m^2\ g^{-1}$	As(III) and As(V) 0 – 250 μmol L^{-1}	pH 4.8, 6.1 and 8, Magnetite = 0.1 g L^{-1} for M1 and M2 and 2.5 g L^{-1} for M3 0.01 M $NaNO_3$	q_{max} (μmol g^{-1}) for As(III) = 20 (M3), 388 (M2) and 1532 (M1) after 24 h	[409,410]
Magnetite (lab synthesized) 40 nm; 31 $m^2\ g^{-1}$	Phosphate 0 – 1600 mg L^{-1}	pH 3, magnetite 1 g L^{-1}, 24 h	Maximum adsorbed amount is 5.2 mg g^{-1} at equilibrium P concentration above 300 mg L^{-1}.	[434]
Magnetite (commercial) 1.6 $m^2\ g^{-1}$	H_4SiO_4 1.85×10^{-4} mol L^{-1}	pH 7, magnetite 4 g L^{-1}, I = 10^{-2} M ($NaNO_3$)	Magnetite sorbed almost 40% of silicates after one week (equilibrium reached).	[433]
Magnetite (natural) 0.1 mm; 0.89 $m^2\ g^{-1}$	As(III) and As(V) 2×10^{-5} M	pH 6.5, magnetite 5 g L^{-1}, 0.1 mol L^{-1} NaCl	Sorption rate constant k ($m^2\ mol^{-1}\ h^{-1}$) was 0.82 and 0.47 for As(III) and As(V), respectively. K_L ($dm^3\ mol^{-1}$) = 2.50×10^4 for As(III) and 1.4×10^5 for As(V).	[116]
Magnetite (commercial) 20 nm; 60 $m^2\ g^{-1}$	As(III) and As(V) 100 μg L^{-1}	pH 8, magnetite 0.5 g L^{-1}	>90% removal of both species within 2 h. Values of k_{SA} (L $min^{-1}\ m^{-2}$) were 0.0055 and 0.0064 for As(V) and As(III), respectively.	[413]
Magnetite (lab synthesized) 12 nm; 74 $m^2\ g^{-1}$	Radionuclides ^{137}Cs (4×10^{-10} M), ^{90}Sr (4×10^{-10} M), ^{154}Eu (2×10^{-9} M),	pH 7, magnetite 2 g L^{-1}, I = 0.01 M ($NaClO_4$)	Sorption extent was 30% (Cs), 60% (Sr), 100% (Eu and Ce)	[422]

	^{141}Ce (7.5×10^{-8} M)			
Magnetite (commercial) 1.59 $m^2 g^{-1}$	Th(IV) 1.1×10^{-6} M	pH 3, magnetite 10 g L^{-1}, I = 0.01 M ($NaClO_4$), T = 298 K	Maximum sorption (almost 100%) after 14 days.	426
Magnetite (commercial) 720 nm; 1.68 $m^2 g^{-1}$	Sulfate 1.5×10^{-5} M	pH 4, magnetite 10 g L^{-1}, I = 0.001 M (KCl), T = 25 °C	A constant concentration of sorbed sulfate (0.35 at nm^{-2}) was attained quickly (within 24 h)	436
GR(Cl^-) (lab synthesized) 49 $m^2 g^{-1}$	As(III) and As(V) 1.67 mM	pH 7.2, T = 25 °C, GR 12.5 g L^{-1}, I = 0.1 M (NaCl), anoxic conditions	Sorption extent was almost 100% for both species after 24 h.	416
Magnetite (lab synthesized) 50-100 nm	U(VI) 30 mg L^{-1}	pH 7, magnetite 1 g L^{-1}, I = 0.01 mol L^{-1} ($NaClO_4$)	Quick sorption (5.5 mg g^{-1}) attained after 4 – 6 h.	430
Magnetite (commercial) 23-50 nm; 52.5 $m^2 g^{-1}$	U(VI) 0.5 mg L^{-1}	pH 8.5, magnetite 0.25 g L^{-1}	Approximately 20% removal of uranium after 48 h.	429
Magnetite (natural)	U(VI) 0.1 mM	pH 5 and 10 1 mM $NaNO_3$ Anaerobic conditions	Sorption loadings (µmol m^{-2}) were 22.34 (pH 5) and 25.23 (pH 10) after 12 h of exposure.	431,432
Three kinds of magnetite (lab synthesized) 1) 8 nm; 190 $m^2 g^{-1}$ 2) 12 nm; 110 $m^2 g^{-1}$ 3) 35 nm; 46 $m^2 g^{-1}$	Ni(II) 41.87 mg L^{-1}, Cu(II) 47.44 mg L^{-1}, Cd(II) 45.87 mg L^{-1} and Cr(VI) 43.61 mg L^{-1}	pH 4, T = 20 °C, magnetite 25 g L^{-1} was used to treat wastewater containing all the target metals.	M1 showed the highest sorption efficiency (mg L^{-1}): 0.86, 0.13, 0.89 and 1.62 for Ni(II), Cu(II), Cd(II) and Cr(VI), respectively.	b
Magnetite (lab synthesized) 8 nm; 95.5 $m^2 g^{-1}$	Pb(II), Cu(II), Zn(II) and Mn(II) 150 mg L^{-1}	pH 5.5, T = 298 K magnetite 4 g L^{-1}	The maximum adsorption capacities ranged between 0.14 to 0.18 mmol g^{-1} for these metals.	418

Magnetite (natural) 20-40 nm; 11.9 m^2 g^{-1}	As(III) 5 mg L^{-1}	pH 7.9, magnetite 8 g L^{-1} (mechanically activated)	Maximum sorption efficiency of 96% was obtained after 6 h.	[c]
Two kinds of magnetite (lab synthesized by different methods) 1) 25 nm 2) 27 nm	Cr(III) and Cr(VI) 100 ppb	pH 4, magnetite 2.5 g L^{-1}	More than 90% was observed for both species after 1 h.	[d]
Magnetite (lab synthesized) 2 and 7 nm 125 m^2 g^{-1}	Cr(VI) 100 mg L^{-1}	pH 5.5, magnetite 2 g L^{-1}	88% of pollutant was removed after 1 h (equilibrium).	[419]
Magnetite (lab synthesized) 34 nm; 39 m^2 g^{-1}	As(III) and As(V) 0.75 mM	pH 5, T = 25 °C I = 0.01 M ($NaNO_3$) magnetite 1 g L^{-1}	Adsorption rate was 7.7 and 6.7 mmol g^{-1} h^{-1} for As(V) and As(III), respectively. k_2 (g $mmol^{-1}$ h^{-1}) = 192 for As(V) and 179 for As(III).	[411]
Magnetite (lab synthesized) 15 nm	Ce(IV) 50 mg L^{-1}	pH 3.8, T = 25 °C magnetite 250 mg L^{-1}	Maximum sorption capacity was 160 mg g^{-1} (equilibrium reached in 60 min).	[427]
Magnetite (commercial) < 50 nm 40 m^2 g^{-1}	Oxytetracycline 2 mM	pH 5.55, T = 35 °C magnetite 20 g L^{-1}, I = 0.01 M (KCl)	> 90% was sorbed within 25 minutes. Pseudo-first-order rate coefficient = 8×10^{-5} s^{-1}.	[439]
Magnetite (lab synthesized) 10 nm; 127 m^2 g^{-1}	Chlorotetracycline 5 mg L^{-1}	pH 6.5, T = 298 K magnetite 0.05 g L^{-1}, I = 10 mM (NaCl)	Maximum adsorption capacity was 476 mg g^{-1} with K_L value of 23,051 L mg^{-1}.	[440]
Magnetite (commercial) 4 μm; 2.4 m^2 g^{-1}	Pentachlorophenol 50 mg L^{-1}	pH 7, T = 20 °C magnetite 2 g L^{-1}	Langmuir maximum sorbed amount = 0.023 mmol m^{-2} and K_L = 10.5 L $mmol^{-1}$.	[455]

GR(Cl^-) (lab synthesized) 19.1 $m^2\ g^{-1}$	Benzoic acid, phthalic acid and mellitic acid 0.1 – 5 mM	pH 8 GR 10 g L^{-1} I = 50 mM (NaCl)	$q_{max-Langmuir}$ (mmol g^{-1}) = 4.18×10^{-3} for benzoic acid, 2.7×10^{-2} for phthalic acid and 2.56×10^{-1} for mellitic acid. K (L $mmol^{-1}$) = 0.58 for benzoic acid, 21 for phthalic acid and 218 for mellitic acid.	442
Magnetite (lab synthesized) 95.3 $m^2\ g^{-1}$	Gallic acid and humic acid 10 mmol L^{-1}	pH 6.5, room temperature, magnetite 1 – 20 g L^{-1}, I = 0.01 M NaCl	Highest sorption was observed in case of humic acid (0.9 mmol g^{-1}) vs < 0.4 mmol g^{-1} for gallic acid.	447,448
Three kinds of magnetite: 1) Lab-synthesized 30 nm; 103 $m^2\ g^{-1}$ 2) Lab synthesized 60 nm; 25 $m^2\ g^{-1}$ 3) Commercial 1.5 µm ; 1.7 $m^2\ g^{-1}$	Nalidixic acid 200 µM	pH 6.5, T = 20 °C, magnetite 0.5 g L^{-1}, I = 10^{-2} M (NaCl)	Maximum sorbed amount (µmol g^{-1}) was in the following order: M1 (172 µmol g^{-1}) > M2 (74 µmol g^{-1}) > M3 (16 µmol g^{-1}) with K_2 (g $\mu mol^{-1}\ min^{-1}$) values of 1.85E – 04 (M1), 1.26E – 03 (M2) and 2.22E – 02 (M3)	441

[a] Randall, S. R.; Sherman, D. M.; Ragnarsdottir, K. V. Sorption of As(V) on Green Rust ($Fe_4(II)Fe_2(III)(OH)12SO_4 \cdot 3H_2O$) and Lepidocrocite (γ-FeOOH): Surface Complexes from EXAFS Spectroscopy. *Geochim. Cosmochim. Acta* **2001,** *65*, 1015-1023.

[b] Shen Y. F.; Tang, J.; Nie, Z. H.; Wang, Y. D.; Ren, Y.; Zuo, L. Preparation and Application of Magnetic Fe_3O_4 Nanoparticles for Wastewater Purification. *Sep. Purif. Technol.* **2009,** *68*, 312-319.

[c] Bujňáková, Z.; Baláž, P.; Zorkovská, A.; Sayagués, M. J.; Kováč, J.; Timko, M. Arsenic Sorption by Nanocrystalline Magnetite: An Example of Environmentally Promising Interface with Geosphere. *J. Hazard. Mater.* **2013,** *262*, 1204-1212.

[d] Parsons, J. G.; Hernandez, J.; Gonzalez, C. M.; Gardea-Torresdey, J. L. Sorption of Cr(III) and Cr(VI) to High and Low Pressure Synthetic Nano-Magnetite (Fe_3O_4) Particles. *Chem. Eng. J.* **2014,** *254*, 171-180.

6.2. Reductive transformation of inorganic and organic contaminants

Abiotic reductive transformation processes play a crucial role in the fate, mobility and toxicity of redox sensitive contaminants in natural and engineered systems. Such reactions often lead to less toxic, more bioavailable and easy-to-degrade species than the parent pollutant. The prominent role of Fe(II) in reductive transformation of pollutants is evident from the large number of laboratory and field studies. Generally, structural Fe(II) or Fe(II) complexes with oxygen ligands are more reactive than aqueous Fe(II).[456-458] Therefore, mixed-valent Fe minerals have been widely used to transform numerous inorganic[431,459-463] and organic contaminants[39,40,170,452,464] through redox processes. In general, reduction of contaminants by mixed-valent Fe minerals follow first order law in contaminant concentration.[458]

Very recently, Latta et al.[465] presented a comprehensive survey of literature which highlighted that GR is involved in cycling of 35 elements (Table 10). These elements can interact with GR through four major pathways (Table 10), (i) adsorption onto the external surface of GR, (ii) interlayer incorporation of anions and monovalent cations, (iii) incorporation of divalent and trivalent metals into the octahedral sheets, and (iv) redox transformations.[465] A compilation of studies reporting the use of GR or magnetite for reduction of various pollutants is provided in Table 11.

Table 10: A table depicting reactive elements towards GR and the type of reactions. It is based on the data compiled by Latta et al.[465]

Elements	**Type of interaction with green rust**			
	Adsorption	Redox transformation	Octahedral incorporation	Interlayer incorporation
As, Mo, P, W, Si	√			
Cr, Hg, Np, Sb, U	√	√		
Se	√	√		√
Ag, Au, Cu, Tc		√		
Fe, O		√	√	
C, N		√		√
Al, Co, H, Mg, Ni, Zn			√	
Na, K, Rb, Cs, S, F, Cl, Br, I				√

Due to its high content of structural Fe(II), most of the reduction studies focused on the reactivity of GR. There are, however, other factors that contribute to the high reactivity of GR, such as the bonding environment of Fe(II). Magnetite contains strong ionic bonds between Fe(II) and O whereas in GR layers, OH^- and Fe(II) are bound by weaker ionic bonds. Sharing of electrons with O by hydrogen weakens this bond and thus GR is easy to oxidize.[466] Moreover, the cubic structure of magnetite is closely packed with similar appearance in every direction. Therefore, the amount of available surface Fe(II) is lower compared to GR which has a looser structure and platy crystals with a high fraction of structural Fe(II) available for reduction. Higher interlayer thickness also facilitates the exchange of even relatively large compounds.[460,467] Hence, magnetite is known for its stability during reduction (apart from small passivation layer)[468] while GR quickly transforms into other products such as ferrihydrite,[469] goethite,[328,467] magnetite[133,328,452,467,470,471] or mixtures of lepidocrocite and magnetite.[472] Similar oxidation products (magnetite and

lepidocrocite) were formed from three types of GR with decreasing yields of magnetite as oxidation product followed the order GR(CO_3^{2-}) > GR(SO_4^{2-}) > GR(Cl^-).[472]

Reduction rates of Fe(II)-bearing minerals increase with their Fe(II) content. For example, Lee and Batchelor[473] showed that the reduction rate for chlorinated ethylenes and Cr(VI) was highest for GR(SO_4^{2-}) (Fe(II):Fe(III) = 464:212) followed by magnetite (Fe(II):Fe(III) = 206:516), pyrite (Fe(II):Fe(III) = 94.8:120), biotite (Fe(II):Fe(III) = 114:3.1), montmorillonite (Fe(II):Fe(III) = 1.2:6.3), and vermiculite (Fe(II):Fe(III) = 14.2:42.5). Similar results were found for magnetite with different Fe(II):Fe(III) stoichiometries. Gorski and Scherer[40] demonstrated that Fe(II) contents of magnetite strongly influences the rate of nitrobenzene reduction. Partially oxidized or sub-stoichiometric magnetite ($x < 0.5$) slowly reduced nitrobenzene (first order rate coefficient, k_{obs}, = 5.36×10^{-6} min^{-1}) while reduction by stoichiometric magnetite ($x = 0.50$) was much more rapid (k_{obs} = 0.20 min^{-1}). Gorski et al.[39] also observed increased rates of nitrobenzene reduction with increasing Fe(II) stoichiometry in magnetite from $x = 0.31$ to $x = 0.50$. Half-lives of nitrobenzene were 1.2 min, 3.5 min, 74 min, 3.8 days, 90 days with magnetite $x = 0.50$, 0.48, 0.42, 0.36, and 0.31, respectively.[39] Similarly, Latta et al.[63] found that the extent of U(VI) reduction was highly dependent upon magnetite stoichiometry. They reported that stoichiometric ($x = 0.5$) or partially oxidized magnetite ($x = 0.42$ and 0.48) completely reduced the U(VI) while very little to no reduction was observed with more oxidized magnetite with $x < 0.33$ after one week. However, a rapid rate of reduction was re-established by oxidized magnetite when it was reacted with aqueous Fe(II) to form stoichiometric magnetite upon Fe(II) uptake.[39,40,63] Reaction of non-stoichiometric magnetite with aqueous Fe(II) can recharge its Fe(II) contents and increase its reactivity, thus

aqueous Fe(II) content and magnetite stoichiometry should always be reported in comparative reactivity studies.[40] Rates of nitrobenzene reduction by initially stoichiometric magnetite were comparable to non-stoichiometric magnetite recharged with Fe(II) underscoring the significance of structural Fe(II) contents.[40] Therefore, recharge of structural Fe(II) in magnetite was proposed to stimulate reduction of contaminants like chlorinated ethylenes,[474] Cr(VI),[475] U(VI),[63] NO_3^-,[468] and nitroaromatic compounds[39,40,464] in various studies. Note that, Fe(II) bound to magnetite resulted in significant reduction of nitroaromatic compounds while negligible transformation occurred by aqueous Fe(II) or magnetite alone.[464,476] Thermodynamic calculations indicate that aqueous Fe(II) is capable of reducing some organic pollutants in the absence of Fe minerals, for example nitroaromatic compounds.[58] However, numerous experimental evidence has shown that the reaction is exceedingly slow in the absence of Fe minerals and that the amount of oxide-associated Fe(II) controls the reaction rate.[477,478] Whether the mineral acts as a heterogeneous catalyst by forming surface complexes or by enhancing the electron transfer steps has not been elucidated until now.

The limiting step in the electron transfer process from magnetite to contaminants has not been conclusively identified yet. Recent studies[39] propose conceptual models that combine mass and electron transfer processes. Experimental evidence is still not decisive towards whether Fe(II) diffusion through magnetite structure or charge transfer is the rate limiting step.

Regarding GR, reduction of inorganic compounds such as nitrogen and chromium species, were among the first reactions studied.[458,469,470,479] Both NO_3^- and NO_2^- can be reduced by GR[470,479] or magnetite,[468] though the reaction of NO_3^- was slower compared to NO_2^-.[470,479] While GR(SO_4^{2-}) and GR(CO_3^{2-}) (Fe(II):Fe(III) ratio of 2:1)

had the same reduction rate for nitrate,[470,479] GR(Cl^-) with a Fe(II):Fe(III) ratio of 3:1 exhibited a five times higher reduction rate.[133]

When the interlayer Cl^- was exchanged by SO_4^{2-} to obtain GR(SO_4^{2-}) with similar Fe(II):Fe(III) ratio (3:1), reduction of NO_3^- by the resulting GR(SO_4^{2-}) was six times slower as compared to the original GR(Cl^-).[133] These studies[133,470,479] applied NO_3^- from a sodium salt ($NaNO_3$) and interpreted the results in terms of reactions taking place at the external mineral surface. However, reactivity studies of GR(SO_4^{2-}) with nitrate in the presence of different counter-cations, i.e., $NaNO_3$ and $Ba(NO_3)_2$ at similar initial NO_3^- concentration (14 mM), the rate of reaction increased by 40 times in the presence of Ba^{2+}.[460] This difference was attributed to the forced exchange of SO_4^{2-} by NO_3^- in the GR interlayer due to the formation of $BaSO_4$ precipitates which is not the case for $NaNO_3$.[460] Recently, Etique et al.[480] investigated the reduction of NO_3^- by GR(SO_4^{2-}) in the presence of phosphate anions. They showed that increasing phosphate concentration significantly impaired the NO_3^- reduction probably due to the adsorption of phosphate on lateral surface sites of GR crystal that restrains the interaction of NO_3^- with Fe(II) species. Phosphate surface complexes preferentially form at the lateral sites due to the presence of mono- and di-coordinated OH^- surface groups of [1010] faces which is known to stabilize GR.[32] The presence of phosphate or bacterial cells (which can also stabilize GR[481]) also affected the reduction of methyl red and Hg(II).[482] However, the effects of stabilizing agents were dependent on the nature of the target pollutant as reduction of methyl red was more affected than Hg(II). Moreover, different types of GRs (chemically synthesized GR(CO_3^{2-}) vs. GR(SO_4^{2-}) vs. biogenic GR(CO_3^{2-})) showed similar reactivity towards these pollutants when rate constants were normalized to the concentration of structural Fe(II) of the GRs.[482]

The reduction of Cr(VI) by GR has been studied at different experimental conditions to analyze effects of pH, surface area of mineral and initial metal concentration. For example, at low Cr(VI) concentrations, the rate of metal reduction by GR(CO_3^{2-}) was proportional to the surface area of GR[458,483] whereas reduction rates became more complex at higher Cr(VI) concentration. At higher GR concentrations in terms of specific surface area (8.3 m^2 L^{-1} and 16.7 m^2 L^{-1}) first-order kinetics was observed while zero-order kinetics was obtained at low surface area concentration of GR (4.2 m^2 L^{-1}).[458] These findings can be rationalized by surface site saturation by Cr(VI) or surface passivation by oxidized precipitates that physically cover the otherwise available Fe(II) on the surface of GR. Electron transfer within the GR lattice (Fe(II) to Fe(III)) and in the interlayer region have been proposed.[472,483] Surface passivation of magnetite was also suggested as the limiting factor during the reduction of Cr(VI).[41,484] A recent study compared the Cr(VI) reduction by various natural and synthetic magnetites having different particle sizes (and thus also different surface areas) and found that considerable reduction was obtained only by the finest magnetite.[119]

Bond and Fendorf[472] compared the reduction rates of Cr(VI) by various GRs and reported the order GR(Cl^-) > GR(CO_3^{2-}) > GR(SO_4^{2-}) on mass basis and proposed a second order rate law $d[Cr(VI)]/dt = -k[Cr(VI)][GR]$ to describe the reaction kinetics at different Cr(IV) concentrations. Both, Fe(II):Fe(III) ratio and accessible surface area may contribute to the observed reduction rate of GR minerals. While the Fe(II):Fe(III) ratio was highest in GR(Cl^-) (3.1:1), followed by GR(CO_3^{2-}) (1.9:1) and GR(SO_4^{2-}) (2.0:1) the role of external surface area was more important than Fe(II):Fe(III) ratio within a structural group (GR1 or GR2). Reported values of surface area were 30.1, 19.0 and 3.6 m^2 g^{-1} for GR(CO_3^{2-}), GR(Cl^-) and GR(SO_4^{2-}),

respectively. However, Skovbjerg et al.[467] argued that a single model may not be appropriate for three different types of GRs due to structural differences among them. Reduction of Cr(VI) by GR(CO_3^{2-}) involves reactions at the external surface only where a Cr-monolayer accumulated and progressively decreased the reactivity of GR(CO_3^{2-}).[483] In GR(SO_4^{2-}), however, Cr(VI) penetrates into the interlayer (due to higher *d*-spacing) by replacing SO_4^{2-} before reduction.[467] This penetration offers quick access to large domains of the GR(SO_4^{2-}) structure that leads to fast reduction kinetics. Entry of Cr(VI) is then blocked by sparingly soluble precipitates of Cr and further reduction of Cr(VI) occurs at the GR solid/solution interface.[467] Recently, Latta et al.[465] reported a complete reduction of U(VI) by GR(SO_4^{2-}) and GR(Cl^-) whilst the amount of reduction ranged from 34 to 63% by GR(CO_3^{2-}). However, little impact of anions was observed for uptake of U(VI) at pH 8.0[465] and that of Cr(VI) at pH 7.[472]

Mixed-valent Fe minerals have also been used to reduce chlorinated organic compounds such as CCl_4 and chlorinated ethylenes (vinyl chloride, cis-dichloroethylene, trichloroethylene, and tetrachloroethylene).[452,473,485,486] The presence of transition metal cations such as Ag, Au and Cu enhance the reductive dechlorination of CCl_4 by acting as catalysts. GR amended with such metals have been proposed for remediation of CCl_4 contamination in anoxic environments.[487]

While reduction alone has shown strong potential to remove pollutants from contaminated matrices, it also can be coupled with other remediation techniques to improve treatment efficiency.[328,488] Such combined approaches as well as the impact of natural ligands on the reactivity of mixed-valent Fe minerals should be further evaluated in the future.

Table 11: Summary of studies using mixed-valent Fe minerals for redox transformation of pollutants in contaminated matrices. Stoichiometry of magnetite or GR is missing from literature where it was not reported. All experiments were performed in batch reactors. Studies are arranged according to their order of appearance, first for magnetite and then for GR.

Type of mixed-valent Fe mineral	Target Pollutant and its initial concentration	Experimental conditions	Extent / rate of pollutant degradation	Mineral stability/Fe leaching	Ref.
Magnetite as reductant					
Magnetite (commercial) 44 $m^2\ g^{-1}$ + 0.27mmol g^{-1} Fe(II)	Hexahydro-1,3,5-trinitro-1,3,5-triazine (RDX) 50 µM	Magnetite 44 $m^2\ L^{-1}$, pH 7 (HEPES)	100% after 3 days Pseudo-first order kinetics initially, k_{obs} 1.0x10^{-1} h^{-1}	N. D.	464
Magnetite (lab synthesized), 57.2 $m^2\ g^{-1}$ Fe(II):Fe(III) = 206:516	Chlorinated ethylenes (PCE) and Cr(IV) (51.5 mM)	Magnetite = 0.1 w/w pH 7, no buffer 10 mM NaHCO3	Reductive capacity for Cr(VI) 3-16 times higher than for PCE.	N. D.	473
Two magnetites (lab synthesized) a) 9 nm, 63.5 $m^2\ g^{-1}$ b) 80 nm, 14.5 $m^2\ g^{-1}$	CCl_4 114 µM	Magnetite 5 g L^{-1} pH 7.8 (HEPES) 0.1 M NaCl	First order kinetics k_{obs} 0.29 h^{-1} (a) 3x10^{-3} h^{-1} (b)	N. D.	485
Magnetite (lab synthesized) 18 $m^2\ g^{-1}$	CCl_4 20 µM	Magnetite 25 g L^{-1} pH 6-10 0.1 M NaCl	Pseudo first order k_{obs} 7x10^{-6} – 1.1x10^{-4} L m^{-2} h^{-1}	N. D.	486
Magnetite (lab synthesized) 20 nm 54 – 72 m2 g−1 Fe(II):Fe(III): 0.28 – 0.48	Nitrobenzene 40 µM	Magnetite 1 g L^{-1} pH 7.2 (MOPS)	First order (x = 0.48) k_{obs} = 0.20 min^{-1} No significant reaction for x=0.28	N. D.	39,40
Magnetite (commercial) 1.54 $m^2\ g^{-1}$	Nitrate (NO_3^-) and nitrite (NO_2^-)	Magnetite 10 g L^{-1} pH 5.5 – 7.5	NO_3^- k_{obs} (1.2-0.6)x10^{-3} h^{-1} (pH 5.5 – 7.5)	N. D.	468

Fe(II)/Fe(III) = 0.47 + Fe(II)	0.5 mM		+Fe(II): k_{obs} (3.2-1.3) x10^{-3} h^{-1} (pH 5.5 – 7.5) NO_2^- k_{obs} 1.4x10^{-4} h^{-1} (pH 5.5)		
Magnetite (lab synthesized) 26.1 m^2 g^{-1}	Cr(VI) 1 mM	Magnetite 1:100 w/w pH 1, 7 and >13	100% Cr(VI) oxidation in <50 h (pH1) and 400 h (pH7). Only 20% oxidation after 800h at pH>13	goethite	484
Magnetite (lab synthesized) (+ Fe(II) 86 mg L^{-1})	Cr(VI) 80 mg L^{-1}	Magnetite 6.5 g L^{-1} pH 7.2	80% Cr(VI) oxidation in 1 h (magnetite+Fe(II)) 60 % Cr(VI) oxidation in 1 h (magnetite only)	N. D.	475
Seven different magnetites - 05 samples (natural) 39 – 52 nm, 1.4 – 7.6 m^2 g^{-1} - 02 samples (commercial) 20 nm (39.3 m^2 g^{-1}) & 41 nm (7.3 m^2 g^{-1}) + Fe(0)	Cr(VI) 50 mg L^{-1}	Magnetite 6 g L-1 pH 4, 6 and 8 NaCl 10 mM	>85% Cr(VI) oxidation pH 4 commercial magnetite 20 nm (25 days) No extensive reduction for other magnetite samples. +Fe(0): General increase in reduction rates	N. D.	119
Magnetite (lab synthesized) Different stoichiometries and origins a) x = 0 (maghemite) b) x = 0.33 c) x = 0.43 (biogenic magnetite) d) x = 0.50 + Fe(II) for x<0.50	U(VI) 500 µM	Magnetite 5 g L-1 pH 7.2 (MOPS or $NaHCO_3$)	Complete U(VI) reduction for x > 0.42, no significant U(VI) reduction for x < 0.42 after one week.	magnetite	63
Green Rust (GR) as reductant					
GR(SO_4^{2-}) (lab synthesized)	NO_3^- 14.28 mM	pH between 7 – 8.5, T 25 °C,	Pseudo first-order rate constant k_{obs} 1.161 x 10^{-5} s^{-1}.	GR oxidized to magnetite.	460,479

		1 mmol of GR, Fe(II) in GR (t = 0) = 6.63			
a) GR(Cl^-) (lab synthesized) Fe(II):Fe(III) = 3:1 b) GR(Cl^-) modified to GR(SO_4^{2-}) with similar Fe(II):Fe(III) ratio	NO_3^- 14.28 mM	pH 8.2, T 25 °C, 2.5 mM GR	k_{obs} (s^{-1}) = 30.8 ±10.4 x 10^{-5} for GR(Cl^-) and 4.7 x 10^{-5} for $GR_{Cl \rightarrow SO4}$.	GR transformed to magnetite.	133
GR(CO_3^{2-}) (lab synthesized) Fe(II):Fe(III) = 2:1	NO_3^- 3.2 mM	pH 10.5, T 25 °C, initial Fe(II) concentration by GR = 167 mM,	Nitrate removal efficiency was 91%.	Magnetite as the main oxidation product.	480
GR(CO_3^{2-}) (lab synthesized) 47 m^2 g^{-1}, Fe(II):Fe(III) = 5:1 (Initial solutions)	Cr(VI) 192 µM	pH 7, 0.25 g L^{-1} GR,	k_{obs} is 3.3 x 10^{-3} s^{-1}.	N.D.	458
a) GR(SO_4^{2-}) (lab synthesized) Fe(II)/Fe(III) = 2 b) GR(Cl^-) (lab synthesized) Fe(II)/Fe(III) = 2.3	Cr(VI) Fe(II)/Cr(VI) = 6	pH 8, Fe(II)/Cr(VI) = 6	Complete reduction of Cr(VI) to Cr(III) in < 2.5 h.	Cr(III)-Fe(III) oxyhydroxide, similar to the “2 line ferrihydrite” was obtained in both cases.	469
Three types of GR (lab synthesized) a) GR(Cl^-) 19.0 m^2 g^{-1}, Fe(II):Fe(III) = 3.1:1 b) GR(SO_4^{2-}) 3.6 m^2 g^{-1}, Fe(II):Fe(III) = 1.9:1 c) GR(CO_3^{2-}) 30.1 m^2 g^{-1}, Fe(II):Fe(III) = 2:1	Cr(VI) 192 µM	pH 7, 0.5 g L^{-1} GR	k_{obs} is 3.66 x 10^{-2} s^{-1} for GR(Cl^-), 2.39 x 10^{-2} s^{-1} for GR(CO_3^{2-}) and 1.81 x 10^{-2} s^{-1} for GR(SO_4^{2-}).	Magnetite and lepidocrocite were observed as oxidation products in all.	472
GR(CO_3^{2-}) (lab synthesized) Fe(II)/Fe(III) = 2	Cr(VI) 111 µM	pH 9.3, 25 °C, 1000 µmol of Fe in GR(CO_3^{2-})	Complete removal of Cr(IV) within 20 minutes.	Chromium containing ferric oxyhydroxycarbonate as oxidation	483

				product.	
GR(SO_4^{2-}) (lab synthesized)	Cr(VI) Cr(VI)/Fe(II) 5 to 110 %	Cr(VI)/Fe(II) 5 to 110 %	Complete removal of Cr(VI) in 5 minutes for Cr(VI)/Fe(II) < 100%	Cr-substituted goethite	467
GR(SO_4^{2-}) (lab synthesized) 86.3 m^2 g^{-1} Fe(II):Fe(III) = 464:212	Chlorinated ethylenes: 0.19 mM tetrachloroethylene (PCE), 0.25 mM trichloroethylene (TCE), 0.41 mM cis-dichloroethylene (cis-DCE), and 0.40 mM vinyl chloride (VC)	pH 7, GR 7 g L^{-1}	Rate constants k^c for reductive dechlorination were: 1.59 day^{-1} for PCE, 0.90 day^{-1} for TCE, 0.59 day^{-1} for cis-DCE and 0.94 day^{-1} for VC.	Oxidation product was magnetite and/or maghemite.	474
GR(SO_4^{2-}) (lab synthesized) 86.3 m^2 g^{-1} Fe(II):Fe(III) = 464:212	PCE (10 equiv mol^{-1} of ethane) and Cr(IV) (51.5 mM)	pH 7, Solid/liquid ratio = 0.007 for GR	Reductive capacity for Cr(IV) was ~1400 µeq g^{-1} and for PCE was ~90 µeq g^{-1}.	N.D.	473
GR(SO_4^{2-}) (lab synthesized) Fe(II):Fe(III) = 2:1	CCl_4 20.7 – 264 mM	pH 8, 25 °C, 4 – 8 mM Fe(III) from GR	First order rate constant ranged k_{obs} ranged from 0.47 x 10^{-5} s^{-1} to 2.18 x 10^{-5} s^{-1}.	GR was oxidized to magnetite.	452
Three GRs (lab synthesized) a) GR(SO_4^{2-}) b) GR(CO_3^{2-}) c) GR (Cl^-)	U(VI) 400 µM	pH 8, GR 5 g L^{-1}	k_{obs} was 8.3 x 10^{-4} s^{-1}, 7.3 x 10^{-4} s^{-1} and 5.4 x 10^{-4} s^{-1} for GR(CO_3^{2-}), GR(SO_4^{2-}) and GR(Cl^-), respectively.	N.D.	465

Two GRs (lab synthesized) a) GR(SO_4^{2-}) b) GR(CO_3^{2-})	$[TcO_4]^-$ 0.076 mM	pH 7 – 8 , GR 15 g L^{-1}	Complete reduction	GR was oxidized to goethite.	463
GR(SO_4^{2-}) (lab synthesized)	Se(VI) 1.13 mM (pH 3.8) 44 µM (pH 6.8 and 9.3)	pH 3.8, 6.8 and 9.3	No Se(VI) reduction at pH < 4 (no GR, all Fe(II) dissolved) Se(VI) reduction faster when it was present during GR formation (first order rate)	Magnetite, lepidocrocite	471
Two GRs (lab synthesized): a) GR(SO_4^{2-}) 20 m^2 g^{-1}, Fe(II):Fe(III) = 2:1 b) GR(CO_3^{2-}) 36 m^2 g^{-1}, Fe(II):Fe(III) = 2:1	Hexahydro-1,3,5-trinitro-1,3,5-triazine (RDX) 100 µM	pH 7, GR 2 g L^{-1} in 0.1 M KBr	>90 of RDX removed by both GRs in 60 min.	No transformation or surface passivation occurred after reaction.	170
GR(SO_4^{2-}) (lab synthesized)	Ag^{I}, Au^{III}, Cu^{II}, and Hg^{II} (400 µM)	GR 5 g L^{-1}	Concentrations of Ag, Au, Cu, and Hg were decreased to 890 nM, 360 nM, 1.2 µM, and 1.7 µM, respectively.	Magnetite	462

6.3. Use of mixed-valent iron minerals to promote advanced oxidation processes

Advanced oxidation processes (AOPs) are emerging as viable remediation technologies for soils and water contaminated with recalcitrant organic pollutants. These processes generally use a combination of oxidants and catalysts to generate highly reactive radicals having strong ability to degrade organic pollutants. The catalytic ability of mixed-valent Fe minerals is well documented to promote two major oxidation reactions using hydrogen peroxide (Fenton-based oxidation) and persulfate (Table 12). Provided below is a brief discussion of the role of pure magnetite and GR in these processes.

Fenton oxidation is a complex catalytic reaction of hydrogen peroxide (H_2O_2) with iron (mostly Fe(II) ion) in acidic solution that predominantly generates highly reactive hydroxyl radicals ($HO^{\bullet}$). This process is based on Fenton's pioneering work (first report in 1876 followed by a deep study in 1894) which suggested the use of an aqueous mixture of H_2O_2 and Fe(II) salt (Fenton's reagent) to oxidize tartaric acid.[489,490] Later in 1934, Haber and Weiss proposed a radical mechanism for this process and suggested that $HO^{\bullet}$ radical is the actual oxidant.[491] The simplest and most widely accepted form of this process is described as:[490,492]

$$Fe(II) + H_2O_2 \rightarrow Fe(III) + HO^- + HO^{\bullet} \quad (6)$$

Reaction (6) is a stoichiometric process, but Fe is often used in catalytic amount because of the subsequent pathways of H_2O_2 decomposition,[493] which regenerate Fe(II) through the classical Haber-Weiss cycle:

$$FeOH^{2+} + H_2O_2 \rightarrow Fe(II) + HO_2^{\bullet} + H_2O \quad (7)$$

$$FeOH^{2+} + HO_2^{\bullet} \rightarrow Fe(II) + O_2 + H_2O \quad (8)$$

The $HO^{\bullet}$ radical is among the most powerful oxidizing agents (E^0 = 2.8 V) with strong potential to instantaneously react with organic pollutants and thus are widely

used in remediation studies.[492] Despite many advantages, conventional Fenton oxidation is mainly limited by the optimum pH (< 4, required to keep metal ions in solution) and associated drawbacks such as the cost of initial acidification, negative impacts on native biota and formation of Fe(III) sludge.[494] Similar process (modified Fenton) can take place at circumneutral pH if chelating agents (CAs) are used along with soluble Fe(II) but the use of CAs is linked to higher cost, elevated toxicity and potentially negative effects on oxidation efficiency due to their non-productive consumption by oxidants.[495,496] These drawbacks can be avoided by using Fe minerals instead of soluble Fe(II) to generate $HO^{\bullet}$ radicals at circumneutral pH in the Fenton-like oxidation reaction.[497]

A more recent oxidant used for AOPs is the persulfate ($S_2O_8^{2-}$) that can be chemically or thermally activated to produce the sulfate free radical ($SO_4^{\bullet-}$) which is a stronger oxidant (E^0 = 2.6 V) than the persulfate anion (E^0 = 2.01 V).[498] Generation of sulfate radical by Fe(II) activation is achieved through the following reaction:

$$S_2O_8^{2-} + Fe(II) \rightarrow SO_4^{\bullet-} + SO_4^{2-} + Fe(III) \quad (9)$$

Fe minerals have shown strong capacity to activate both oxidants (H_2O_2 and $S_2O_8^{2-}$), leading to the production of highly reactive radicals ($HO^{\bullet}$ and $SO_4^{\bullet-}$) at circumneutral pH. Moreover, mineral catalyzed chemical oxidation shows better oxidant stability and pollutant degradation than by soluble Fe(II) activation as the latter is prone to precipitation at circumneutral pH.[499-501] Mineral-catalyzed chemical oxidation is widely studied to remediate contaminated soils and water by using various Fe minerals including ferrihydrite,[502-504] goethite,[503-506] hematite,[503,504,507] lepidocrocite,[503,504] magnetite,[499,503,504,507-513] and GR.[42,328,514-516] Mixed-valent Fe minerals show higher catalytic efficiency than ferric minerals to promote chemical oxidation of organic pollutants which is correlated to the presence of structural

Fe(II).[503,504,507,517] For example, Matta et al.[503,504] showed that magnetite (with 85% pollutant removal) was more effective than ferric oxyhydroxides (ferrihydrite, goethite, hematite and lepidocrocite) (with <10% of pollutant removal) for oxidative degradation of 2,4,6-trinitrotoluene.

Even if the ability of magnetite or GR to promote Fenton oxidation is mainly dictated by its Fe(II) content, implications of Fe(III) in oxidation reaction cannot be ignored. Indeed, Kwan and Voelker[518] have suggested the following chain of reactions in mineral catalyzed oxidation system:

$$\equiv Fe(III) + H_2O_2 \rightarrow \equiv Fe(III)H_2O_2 \quad (10)$$

$$\equiv Fe(III)H_2O_2 \rightarrow \equiv Fe(II) + HO_2 + H^+ \quad (11)$$

$$\equiv Fe(II) + H_2O_2 \rightarrow \equiv Fe(III) + HO^- + HO^\bullet \quad (12)$$

The mineral catalyzed reaction is a chain of reactions occurring on the surface where the regeneration of Fe(II) (eqs. 10 and 11) is the rate limiting step. If only Fe(III) is initially present, Fe(II) is slowly generated by reactions 10 and 11 initiating oxidation reactions. But in the case of iron (II) bearing minerals, presence of iron (II) can enhance the production rate of $HO^\bullet$.[503,507,519] By analogy to the Fenton-like system, Liu et.al.[520] have proposed a one-electron reduction of ≡Fe(III) surface site, which result in the formation of persulfate radical ($S_2O_8^{\bullet-}$):

$$\equiv Fe(III)OH + S_2O_8^{2-} \rightarrow \equiv Fe(II)OH + S_2O_8^{\bullet-} \quad (13)$$

This radical $S_2O_8^{\bullet-}$ can be involved in radical chain reactions with water, while freshly generated Fe(II) react with $S_2O_8^{2-}$ to generate radical sulfate $SO_4^{\bullet-}$ through:

$$\equiv Fe(II)OH + S_2O_8^{2-} \rightarrow \equiv Fe(III)OH + SO_4^{2-} + SO_4^{\bullet-} \quad (14)$$

The catalytic ability of magnetite and GR to promote advanced oxidation strongly depends on their structural and surface properties, Fe(II)/Fe(III) ratio and solution chemistry.[42-45] In this regard, Xue and colleagues[43] investigated the efficiency of two different kinds of magnetite (M1 and M2) to promote Fenton-like oxidation of Rhodamine B at neutral pH in aqueous solution. Both M1 and M2 exhibited different properties like Fe(II)/Fe(III) ratio (0.24 ± 0.2 and 0.43 ± 0.2, respectively while similar contents of total Fe: 70 ± 2 wt.%), mean particle diameter (<50 nm and <5 μm, respectively) and SSA (40 ± 3 and 2.4 ± 0.2 m^2 g^{-1}, respectively). The results indicated that M2 exhibited better oxidation efficiency than M1 at all tested ranges of H_2O_2/Fe ratio (5–150) due to the higher Fe(II) content. For example, decolorization kinetic constant, k_{app} (min^{-1}) for M1 and M2 were 0.003 and 0.11, respectively at H_2O_2/Fe molar ratio= 100 (pH = 7, magnetite = 2 g L^{-1}). The M2 also revealed higher decomposition rate of H_2O_2 than M1 when normalized to the surface area (k = 3.10^{-4} min^{-1} $(m^2/L)^{-1}$ for M2 and 8.10^{-5} min^{-1} $(m^2/L)^{-1}$) while a reverse trend was found when based on mass basis. Hanna and co-workers[42] evaluated the efficiency of three different kinds of GR including GR(Cl^-), GR(CO_3^{2-}), and GR(SO_4^{2-}) and one type of magnetite to promote Fenton-like oxidation of phenol under similar experimental conditions (30 mM H_2O_2, 1 g L^{-1} of GR or magnetite, pH = 7.1, N_2 atmosphere). The Fe(II) contents were higher in GR(Cl^-) with Fe(II):Fe(III) ratio of 3:1 while this ratio was 2:1 for GR(CO_3^{2-}) and GR(SO_4^{2-}), and 1:2 for magnetite. Obtained results indicated that mineralization rate of phenol as well as the decomposition rate of H_2O_2 was higher for GR(Cl^-) followed by GR(SO_4^{2-}), GR(CO_3^{2-}) or magnetite, mainly due to the higher Fe(II) content of GR(Cl^-). The reaction kinetics were also dependent on the type of the interlayer anion. Pseudo-first order rate constants (k_{surf}) for phenol degradation were 13×10^{-4}, 3.3×10^{-4}, 3.5×10^{-4}, and 0.4×10^{-4} L m^{-2} s^{-1} for GR(Cl^-),

GR(SO_4^{2-}), GR(CO_3^{2-}), and magnetite respectively. Higher efficiency of GR than magnetite was also observed during Fenton-like oxidation of 2,4,6-trinitrotoluene in aqueous phase at circumneutral pH (Figure 22).[504] The obtained values of degradation pseudo-first-order rate constant's (k_{surf}) for GR and magnetite were 2.55×10^{-4} L m^{-2} min^{-1} and 1×10^{-4} L m^{-2} min^{-1} respectively. These results were consistent with higher Fe(II) contents in GR (38%) than magnetite (24%).[504] However, magnetite was found to be more stable than GR as degradation in the latter reached a plateau in 3 h of reaction after a quick start while no such plateau was achieved for magnetite even after 24 h (Figure 22).[504] Moreover, GR was transformed into a mixture of ferrihydrite and lepidocrocite at the end of oxidation process while magnetite retained its structure and catalytic ability.[514] It should be noted that GRs are unstable under oxidizing conditions and their quick reaction with H_2O_2 or atmospheric oxygen transforms them into ferric GR, magnetite or other ferric minerals depending on pH and composition of solution, rate of oxidation, oxidant type and the dehydration rate.[143,183] On the other hand, magnetite exhibits good structural and thermodynamic stability. Due to its ferromagnetic nature, it can be easily separated from aqueous solution by applying an external magnetic field.[521] Therefore, it can be reused for several oxidation cycles with no loss in catalytic efficiency as reported by Xue et al.[455] Recently, magnetite demonstrated strong stability without any significant loss in catalytic ability when it was used in nitrilotriacetic acid-assisted Fenton-like oxidation to degrade TCE for 230 days.[522] Owing to the higher stability and ease of handling offered by magnetite, a major portion of literature is devoted to the use of magnetite to promote chemical oxidation while studies using GR are scarce (Table 12). As a matter of fact, efficiency of GR has never been tested to activate persulfate oxidation.

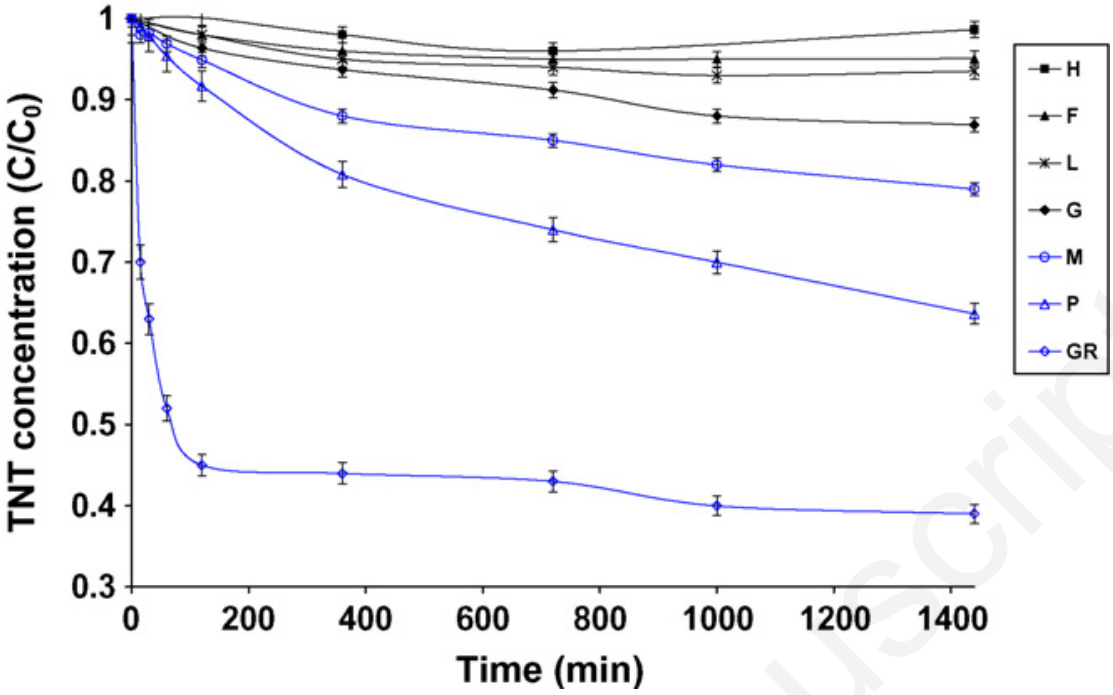

Figure 22: Fenton-like oxidation of TNT (0.11 mM) in the presence of six different iron minerals (2 g L^{-1}) at pH 7: (■) hematite, (▲) ferrihydrite, (*) lepidocrocite, (♦) goethite, (○) magnetite, (△) pyrite, (◊) green rust. H_2O_2 (3%, w/v). Reproduced with permission from Ref. 504. Copyright 2008 Elsevier.

Despite the strong stability of magnetite, several other researchers reported Fe leaching during subsequent oxidation cycles that could affect its reusability and efficiency to some extent (Table 12). Rusevova and co-workers[45] compared the efficiency of three different kinds of nano-magnetite (Fe(II)/Fe(III) ratio of 0.11, 0.52 and 1.44 in M_a, M_b and M_c, respectively) to catalyze Fenton-like oxidation of phenol at neutral pH. It should be noted that, prior to use, M_c was subjected to reductive pretreatment (by reacting with $NaBH_4$) to improve Fe(II) contents. Their results demonstrated similar catalytic ability for all magnetites (42-65% of phenol removal in 24 h) that was correlated to variation in Fe(II) leaching during reaction that lead to different Fe(II)/Fe(III) ratios of 0.10, 0.15 and 1.07 in M_a, M_b and M_c, respectively. It was also correlated to scavenging of radicals by nanoparticle agglomerates. Reusability tests of magnetite for three subsequent oxidation cycles of phenol also

indicated a 20% decrease in oxidation efficiency in 3rd oxidation cycle (negligible effect in second cycle).[45] However, a dramatic decrease in oxidant decomposition rate was reported as evident from R_{25} values of 1200, 500 and 230 mol mol^{-1} obtained for the 1st, 2nd and 3rd cycle. This was not observed in phenol-free reactions where crystalline structure also remained the same in recovered magnetite. Thus, observed instability of the magnetite nanoparticles was attributed to the passivation of the surface iron with intermediates of phenol oxidation.[45] Reusability tests of magnetite over 5 – 8 oxidation cycles showed a loss of 20 – 30% in oxidation efficiency which has been attributed to the loss of catalyst in the form of dissolved Fe(II) and or loss of magnetite particles.[521,523] Hou et al.[524] also deduced decline in degradation efficiency in sequential experiments to the conversion of ≡Fe(II) to ≡Fe(III) on the surface of magnetite.

Recently, natural magnetite has been shown to have strong stability (leached iron concentration of 0.5 mg L^{-1} against applied magnetite dosage of 0.5 g L^{-1}) after six subsequent oxidation cycles while oxidation efficiency remained almost constant.[525] Recently, Munoz et al. reported that natural magnetite showed the best performance over three sequential runs as compared to the natural hematite and ilmenite.[526] Magnetite maintained its catalytic ability as illustrated by 80% mineralization in 3rd oxidation cycle (similar to that in first cycle). Hematite yielded a slight decrease in mineralization (from 80% to 70%) while ilmenite suffered strong deactivation and showed negligible activity (from 78 to 1% mineralization) in 3rd cycle. Until now however, very few studies appeared in literature which report the use of natural magnetite[120,525-527] that exhibited higher catalytic performance than that of the synthetic pure magnetite.[120] Indeed, up to 95% degradation of p-nitrophenol by H_2O_2 was achieved with a natural magnetite, while lab-synthesized magnetite did not cause

any obvious pollutant degradation in one study dedicated to this aspect.[120] It should be noted that most chemical oxidation studies investigated synthetic magnetites rather than natural minerals (Table 12). Furthermore, there are several inconsistencies in the literature regarding the catalytic stability of magnetite. Such inconsistences are not altogether surprising when considering the variety of experimental and analytical approaches adopted in different studies. Indeed, different magnetites are often characterized by contrasting structural properties, morphology, magnetization and stoichiometry. Such differences can often be attributed to the different conditions under which they were synthesized or studied such as in oxic *vs* anoxic controlled atmosphere, batch *vs* column study, solution chemistry, presence of dissolved Fe(II), target compounds, etc.

In this context, it is challenging to develop iron catalysts offering greater stability and lower iron leaching but without compromising the oxidation efficiency. Therefore, various supports or stabilizers have been used to anchor iron on the surface of catalysts to improve the stability of magnetite even after several oxidation cycles including CeO_2,[528] hydrogel,[529] iron oxalate,[530] MWCNTs,[531-533] mesoporous SiO_2,[534] and rGO.[535] Many researchers have tested metal doping for isomorphic substitution of Fe in magnetite structure to improve its stability.[5,536-543] In addition, several other strategies have been developed to decrease iron leaching and to improve catalyst stability such as photo-Fenton,[44,544,545] ultrasound assisted chemical oxidation,[524,546] and UV-LED assisted oxidation.[547] Separation of solid phase is an important issue in photo-Fenton oxidation that can be avoided by using magnetite which offers easy magnetic separation from aqueous solution.[151]

Although the use of magnetite could offer a promising alternative to homogenous Fenton oxidation, its potential application is still limited due to the lack of studies at

field-scale.[497] While most chemical oxidation studies using magnetite as iron source were performed at lab-scale, no report has appeared concerning field applicability. Prior to industrial applications, injection mode, transport of particles in soil or magnetite/soil mixing, eco-toxicity assessment, etc. should be addressed.

Table 12: Summary of studies using mixed-valent iron minerals to promote chemical oxidation in contaminated matrices. Studies are arranged according to their order of appearance.

Oxidant	Catalyst type	Target pollutant and its initial concentration	Medium	Experimental conditions	Extent / rate of pollutant degradation	Mineral stability/Fe leaching	Ref.
H_2O_2	Magnetite (Commercial) 0.675 $m^2\ g^{-1}$ Screened through 0.6 mm sieve.	Pentachlorophenol 250 mg L^{-1}	Spiked sand/ Batch	pH 3, magnetite 10 wt%, H_2O_2 7 wt%	Complete pollutant degradation and mineralization after 24 h. Highest degradation rate constant was in first 8h (5×10^{-4} mol m^{-2} h^{-1}).	N.D.	507,510
H_2O_2	Magnetite (Commercial) Screened through 0.3 mm sieve.	Petroleum hydrocarbons 1000 mg Kg^{-1}	Spiked sand/ Batch	pH 3, magnetite 5 wt%, H_2O_2 15 wt%	50% hydrocarbon removal after 8 days.	N.D.	*a*
H_2O_2	Magnetite (Commercial) 2 $m^2\ g^{-1}$	2,4,6-trinitrotoluene (2 g kg^{-1} when spiked onto soil or 0.11 mM in aqueous phase)	Aqueous medium or soil slurry system/ Batch	pH 3, H_2O_2 80 mM, magnetite 1.76 g L^{-1}	Reaction rate constants k_{surf} = $1.47.10^{-3}$ L min^{-1} m^{-2}.	Fe leaching was 14 mg L^{-1}	503
H_2O_2	Magnetite (lab synthesized) 2.9 μm; 8.6 $m^2\ g^{-1}$	Methyl red 50 μm	Aqueous medium/ Batch	pH 7, T 20 °C H_2O_2/Fe molar ratio of 20	Decolorization rate constant k_s = 2×10^{-4} L min^{-1} m^{-2}	Fe leaching ≤1 mg L^{-1}	517
H_2O_2	- GR(Cl^-) (lab synthesized) 20 $m^2\ g^{-1}$ - Magnetite (lab	2,4,6-trinitrotoluene 0.11 mM	Aqueous medium/ Batch	pH 7, H_2O_2 3% w/v, mineral content 2 g L^{-1}.	Highest degradation (60%) was obtained with GR. Pseudo-first-order rate constant's (*k*) values for	N.D.	504

	synthesized) 2 m^2 g^{-1}				pollutant degradation were: 5.1 × 10^{-3} min^{-1} (GR) > 2.03 × 10^{-4} min^{-1} (magnetite)		
H_2O_2	- GR(Cl^-) (lab synthesized) 21 m^2 g^{-1} - Magnetite (commercial) 2 m^2g^{-1}	Phenol 0.53 mmol L^{-1}	Aqueous medium/ Batch	pH 7, GR or magnetite = 5 g L^{-1}, H_2O_2 155 mM	100% phenol degradation after one minute in the presence of GR while reaction kinetics was much slower with magnetite (<10% after 1h).	GR was transformed into a mixture of ferrihydrite and lepidocrocite after reaction. N.D. for magnetite.	514
H_2O_2	Magnetite (lab synthesized) SSA: 2∼90 m^2 g^{-1}	PAH (phenanthrene) 200 mg kg^{-1}	Spiked sand/ Batch	pH = buffered (2.8) and unbuffered, magnetite 10 wt%, 3 mL of 30% H_2O_2	40% removal in unbuffered and 88 % in buffered system after 16 days.	N.D.	501
H_2O_2	GR(SO_4^{2-}), (lab synthesized) 74 m^2 g^{-1}	Methyl red 0.011 mmol	Aqueous medium/ Batch	pH 7, H_2O_2 9.79 mmol	Complete decolorization was obtained within one hour	GR was transformed into poorly crystallized goethite.	515
H_2O_2	Magnetite (Commercial) 4 μm; 2.4 m^2 g^{-1}	Pentachlorophenol 50 mg L^{-1}	Aqueous medium/ Batch	pH 7, magnetite 2 g L^{-1}, H_2O_2 0.8 M	90% dechlorination after 30 h, total dechlorination after 4 days and complete mineralization after 7 days	Fe leaching (<0.05 mM), good structural stability	455,495
H_2O_2	Nano-magnetite, (lab synthesized) 10 nm	Phenol/aniline 1 mM	Aqueous medium/ Batch	pH 6 – 7, magnetite 5 g L^{-1}, H_2O_2 1.2 M	100% removal of both pollutants after 6h.	80% removal of pollutant after eight times of recycle.	521
H_2O_2	Two kinds of magnetite (Commercial) M1 : <50 nm, 40 m^2 g^{-1} M2 : <5 μm, 2.4 m^2 g^{-1}	Rhodamine B 5 mg L^{-1}	Aqueous medium/ Batch	pH 7, T 20 °C Magnetite 2 g L^{-1} H_2O_2/Fe molar ratio= 100	Higher decolorization kinetic constant, k_{app} (min^{-1}) for M2 (0.011) than M1 (0.003) at	Low iron leaching, good structural and catalytic stabilities.	43

H_2O_2	Three types of GR (lab synthesized): 1) GR(CO_3^{2-}); 39 m^2 g^{-1} 2) GR(SO_4^{2-}); 74 m^2 g^{-1} 3) GR(Cl^-); 25 m^2 g^{-1} **and** Magnetite, 11 m^2 g^{-1}	Phenol 1 mM	Aqueous medium/ Batch	pH 7.1, T 20 °C, 1 g L^{-1} of GR or magnetite; $H2O_2$ 30 mM	Degradation pseudo-first order rate constants (k_{surf}) values: 13×10^{-4}, 3.3×10^{-4}, 3.5×10^{-4}, and 0.4×10^{-4} L m^{-2} s^{-1} for GR(Cl^-), GR(SO_4^{2-}), GR(CO_3^{2-}), and magnetite respectively.	GRs were transformed into ferrihydrite or poorly crystallized goethite. N.D for magnetite.	42
H_2O_2 generated through O_2	Nano-magnetite (Commercial) 30 nm; 48 m^2 g^{-1}	4,6-dinitro-o-cresol 11.4 mg L^{-1}	Aqueous medium/Batch	pH 2.8, magnetite 1 g L^{-1}, Na_2SO_4 0.08 M, 0.025 A of current and 40 mL/min of O_2 flow	Total removal after 60 min, and pseudo second-order degradation rate constant 1.79×10^{-2} μg^{-1}.mL min^{-1}	N.D.	*b*
H_2O_2	Nano-magnetite (Commercial) 30 nm; 48 m^2 g^{-1}	p-Nitrophenol 45 mg L^{-1}	Aqueous medium/Batch	pH 7.0, magnetite 1.5 g L^{-1}, 620 mM H_2O_2	>90% of p-NP was degraded after 10h.	N.D.	512
H_2O_2 + ultrasonics	Nano-magnetite, (lab synthesized) 10-20 nm; 55.7 m^2 g^{-1}	Bisphenol A 20 mg L^{-1}	Aqueous medium/ Batch	pH 3, 7 and 9, T 35 °C, magnetite 585 mg L^{-1}, H_2O_2 160 mmol L^{-1}, under ultrasonics	>95% of BPA was removed at three pH values	25 – 30% decline in efficiency in 2nd cycle which remained steady for 5 cycles.	523
H_2O_2	Three kinds of pure nano-magnetite: M1) Commercial 46 m^2 g^{-1}) M2) $NaBH_4$ Pre-treated M1 to improve Fe(II)	Phenol 25 mg L^{-1}	Aqueous medium/ Batch	pH 7.0, magnetite 3 g L^{-1}, H_2O_2 5 g L^{-1}	42–65%phenol removal in 24 h	20% loss of efficiency in 3rd cycle while negligible decrease in 2nd cycle.	45

	M3) Lab-synthesized 95 $m^2 g^{-1}$ M3) 95 $m^2 g^{-1}$ Particle size for all: 20-30 nm						
H_2O_2 or $Na_2S_2O_8$	Magnetite (lab synthesized) 30 nm; 103 $m^2 g^{-1}$	Petroleum hydrocarbons 4 g Kg^{-1} of crude and weathered oil	Spiked sand/ Batch or Saturated column	pH 6.7, T 20-25 °C, magnetite 10% w/w, oxidant:Fe molar ratio = 10:1 (H_2O_2) and 1:1 ($Na_2S_2O_8$)	80-90% of hydrocarbon removal by both oxidants after one week.	N.D.	200,509
H_2O_2 or $Na_2S_2O_8$	Magnetite (lab synthesized) 30 nm; 103 $m^2 g^{-1}$	PAHs 200 – 300 μg g^{-1} (spiked sand) 1200 – 1300 μg g^{-1} (aged soil)	Spiked sand, real soil/ Batch or Saturated column	pH 7-8, T 20-25 °C, magnetite 10% w/w, oxidant:Fe molar ratio = 20:1 (H_2O_2) and 2:1 ($Na_2S_2O_8$)	80 – 90% of PAH degradation in spiked sand while 50 – 60% of degradation in real soils. (1 week)	N.D.	499,500,509
H_2O_2 or $Na_2S_2O_8$	Magnetite (Commercial) 150 nm; 8 $m^2 g^{-1}$	Ibuprofen 0.1 mM	Aqueous medium/ Batch	pH 6.6, magnetite 1 g L^{-1}, oxidant dose 10 mM	Pollutant removal up to 60% (H_2O_2) and 73% ($Na_2S_2O_8$) after 48h)	N.D.	508
UV irridation + H_2O_2 **Or** + $Na_2S_2O_8$	Four magnetites: M1: 30-50 nm; 75 $m^2 g^{-1}$ M2: Lab-synthesized, 60-80 nm; 26 $m^2 g^{-1}$ M3: 1-2 μm; 1.7 $m^2 g^{-1}$ M4 : 100–300 nm; 8.5 $m^2 g^{-1}$	Phenol 0.1 mM	Aqueous medium/ Batch	pH 3, magnetite 0.2 g L^{-1}, 1 mM H_2O_2 or 0.5 mM $Na_2S_2O_8$	Higher reactivity (e.g. total removal in less than 2h) for magnetites having the highest Fe(II)/Fe(III) ratio (e.g. M2 and M3)	Fe leaching much below 1 mg L^{-1}	44,545
H_2O_2	Five magnetite (natural): M1 : 0.70 $m^2 g^{-1}$ M2 : 3.30 $m^2 g^{-1}$	p-Nitrophenol 10 mg L^{-1}	Aqueous medium/ Batch	pH 7, magnetite 1 g L^{-1}, H_2O_2 10 mmol L^{-1}	M1 showed highest degradation efficiency (95% after 24 h while <30% by others) and $^{\bullet}OH$ generation	N.D.	120

	M3 : 0.54 $m^2 g^{-1}$ M4: 2.46 $m^2 g^{-1}$ M5: 1.41 $m^2 g^{-1}$				(reaction rate constant, *k* = 0.24 300 μg L^{-1} min^{-1}).		
H_2O_2	Magnetite (lab synthesized) 30 nm; 103 $m^2 g^{-1}$	PAHs 1100 mg kg^{-1}	Real soil/ batch	pH 7 – 8, magnetite 10% w/w, oxidant:Fe molar ratio equal to 20:1.	PAH removal efficiency was 31, 36, and 47 % in soil pre-treated at 60, 100, and 150 °C, respectively after one week of chemical oxidation.	N.D.	511
H_2O_2/ $K_2S_2O_8$	Magnetite (lab synthesized) <20 nm; 59.8 $m^2 g^{-1}$	PCBs 5 μg g^{-1}	Spiked sand/ Batch	pH 7.2, T 20 °C, magnetite 0.25 g g^{-1}, H_2O_2 2 M, $K_2S_2O_8$ 180 mM, L/S = 1:1	Degradation extent of PCBs reached 69 – 77% (H_2O_2) and 90 – 99% ($K_2S_2O_8$) in spiked sand.	N.D.	488
$K_2S_2O_8$	Magnetite (natural) 500-1150 μm	Acid Orange 7 15 mg L^{-1}	Aqueous solution/ Recirculating pilot fluidized-bed reactor	pH 5, magnetite 0.5 g L^{-1}, $S_2O_8^{2-}$ 0.2 mM	Almost 75% removal of pollutant after 120 min of reaction.	Fe leaching was 0.5 mg L^{-1}. Degradation efficiency was approximately constant in six oxidation cycles.	525
H_2O_2	Magnetite (natural) 500-1150 μm, 5.15 $m^2 g^{-1}$	Basic Blue 3 5 mg L^{-1}	Aqueous solution/ Recirculating pilot fluidized-bed reactor	pH 5, magnetite 2.27 g L^{-1}, H_2O_2 4 mM	84% of pollutant degradation after 190 min of reaction.	Catalytic performance was maintained over five oxidation cycles (<20% loss in oxidation efficiency)	527
H_2O_2	Magnetite (commercial) 6 $m^2 g^{-1}$	Gallic acid 0.12 mM	Aqueous medium/ Batch	pH 4.3, T 25 °C, magnetite 50 mg L^{-1}, H_2O_2 2.64 mM	Rate constant (*k*) for - pollutant degradation = 0.103 min^{-1} - mineralization = 0.061 min^{-1}. (95% mineralization)	Fe leaching = 0.06 mg L^{-1}	513

Ultrasonics + H_2O_2 **Or** + $Na_2S_2O_8$	Magnetite (commercial) 200-300 nm	Tetracycline 100 mg L^{-1}	Aqueous medium/ Batch	pH 3, magnetite 1 g L^{-1}, H_2O_2 150 mM, Ultrasound power 80 W at 22 °C	93% of pollutant and 32 % of TOC were removed after 60 min.	79% of pollutant removal in 3rd cycle.	524,546
H_2O_2	Magnetite (natural) 8 m^2 g^{-1}	Phenol 100 mg L^{-1}	Aqueous medium/ Batch	pH 3, magnetite 2 g L^{-1}, 500 mg L^{-1} H_2O_2, 75 °C	100% removal of phenol, 80% TOC reduction	3 runs and $X_{TOC\text{-}3rd}$ = 77%	526
H_2O_2	Magnetite (commercial) 0.3–0.5 µm, 7.9 m^2 g^{-1}	Trichloroethylene 20 mg L^{-1}	Aqueous solution fed in column of sand & magnetite	magnetite 0.5 and 7 wt.% feed solution: H_2O_2 50 mM, pH 8.2, nitrilotriacetic acid 2 mM, upflow mode, flow rate of 1.25 mL min^{-1}	74% and 94% of pollutant degradation with 0.5 and 7 wt.% magnetite. (Chelates like EDTA and EDDS had an inhibitory effect)	Magnetite remained stable during whole study (230 days) without any loss in catalytic ability (1mM chelate).	522

[a] Kong, S. H.; Watts, R. J.; Choi, J. H. Treatment of Petroleum-Contaminated Soils Using Iron Mineral Catalyzed Hydrogen Peroxide. *Chemosphere* **1998,** *37*, 1473-1482.
[b] Zeng, X.; Hanna, K.; Lemley, A. T. Cathodic Fenton Degradation of 4,6-Dinitro-o-cresol with Nano-Magnetite. *J. Mol. Catal. A: Chem.* **2011,** *339*, 1-7.

7. Conclusions and outlook

Mixed-valent iron minerals such as magnetite and GR are amongst the most important iron compounds found on Earth due to their impact on biogeochemical cycling of trace elements, their role in controlling the fate and toxicity of environmental pollutants, and their use in various environmental remediation approaches. Magnetite and GR are present in many environmental settings, however, a firm understanding of the mechanisms of their formation and their reactivity remains a major challenge in environmental and applied sciences.

Magnetite and GR can be synthesized *via* a variety of abiotic and microbial pathways. Their chemical composition, crystallinity, morphology, and stoichiometry are controlled by various factors including the nature of the initial substrate, Fe(II)/Fe(III) ratio, reaction pH, and other geochemical conditions. These properties ultimately dictate the stability and reactivity of mixed-valent Fe minerals in aqueous environments. Nevertheless, through the use of diverse synthesis techniques researchers have been able to create novel mineral structures *e.g.* partially substituted, deprotonated or organically modified GRs with enhanced reactivity which could be used to develop new applications of mixed-valent Fe minerals. Further progress in developing new and improved synthesis methods with precise control over product composition (e.g. purity, stability, particle size, sorption capacity, redox activity) or through the application of microbial strategies will further improve the ability to use mixed-valent Fe minerals in environmental applications due to their enhanced reactivity or stability.

Magnetite and GR play key roles for sorption and reductive transformation of metals and organic compounds. Magnetite may also contribute as electron acceptor and electron donor for bacteria to the dynamics of environmental redox processes even

though its significance needs to be further evaluated. Thus, development of *in-situ* methods is needed to determine mixed-valent Fe-minerals in natural settings and to study the dynamics of their formation, transformation and/or decay. Future challenges also include development of predictive models (both thermodynamic and kinetic) to describe and predict formation and reactivity of mixed-valent Fe minerals in natural settings to assess their roles in the cycling of electrons under natural (and thus fluctuating) redox conditions.

The application of magnetite in bioremediation remains a challenge due to aggregation and changing reactivity over time. It would be desirable to maintain or even increase the reactivity of magnetite over time with the help of microorganisms.

Mixed-valent Fe minerals have also shown strong reactivity towards the chemical oxidation of a variety of organic contaminants. In environmental engineering applications (e.g. waste water treatment, soil remediation, etc.), *in situ* or *ex situ*, the decontamination reactions take generally place under ambient environments containing O_2 and H_2O. In these conditions, the stability field of mixed-valent Fe minerals is relatively narrow. GR may quickly transform into other compounds generally less reactive than the parent GR, while magnetite may undergo surface oxidation. Indeed, formation of a passivating layer on the magnetite surface exposed to air alters the redox reactivity, a phenomenon that becomes particularly important for nanoscale particles with a higher surface-to-volume ratio. Consequently, fluctuations in redox and solution chemistry of contaminated systems with respect to the thermodynamic stability of mixed-valent oxides represent a significant level of challenges to engineers. As there is a growing interest in environmentally friendly catalytic processes based on magnetic solids, it would be highly rewarding to develop cheap and effective magnetite-based catalysts with greater stability and higher

reactivity for full-scale applications. However, more knowledge is required to assess their implementation at large-scale, as further research is required regarding the mode of application, mobility, stability and eco-toxicity of such minerals.

Acknowledgments

This work is supported by research grant from the Alexander von Humboldt Foundation of Germany and is gratefully acknowledged. K. Hanna thanks the ADEME (France) for their support. C. Ruby thanks the Institute of Advanced Study of the University of Durham (UK) for providing a Research Fellowship during the writing of this manuscript.

Biography

Muhammad Usman is an Alexander von Humboldt postdoctoral fellow with Stefan Haderlein at the University of Tübingen, Germany. He also holds the position of an Assistant Professor in the Institute of Soil and Environmental Sciences at the University of Agriculture, Faisalabad, Pakistan. He obtained his BS in Soil Science at the later organization. He was, then, awarded a fellowship from Higher Education Commission of Pakistan to pursue further studies from France. He obtained his MS (2008) in environmental sciences from AgroParisTech and PhD (2011) in iron geochemistry and environmental remediation from University of Lorraine under the supervision of Christian Ruby, Khalil Hanna and Pierre Faure. His research concerns iron-mediated remediation of soil and water contaminants. Major focus of his research is the synthesis and use of mixed-valent iron minerals for environmental remediation with an emphasis on advanced oxidation processes (Fenton and persulfate oxidation) and sorption.

James M. Byrne obtained a MPhys in Physics at the University of St Andrews, UK in 2008. He then went on to complete a PhD in 2012 in the field of Geomicrobiology at the University of Manchester, UK under the supervision of Jon Lloyd and Richard Pattrick. He then moved to the University of Tübingen to start a Postdoc and now holds a permanent research position. His research has focused on combining mineralogy, magnetism, geochemistry and microbiology to explore the interactions of iron metabolizing bacteria with mixed-valent iron minerals. His analytical expertise includes magnetic characterisation methods, Mössbauer spectroscopy, electron microscopy and synchrotron based techniques with a strong focus on the development of new bioinspired nanomaterials which could ultimately be used for environmental remediation and biomedical applications.

Aaifa Chaudhary obtained her MS in Environmental Sciences from University of the Punjab, Pakistan in 2011. She, then, joined as Lecturer in Department of Environmental Science and Engineering, Government College University, Faisalabad, Pakistan. Currently, she is pursuing her PhD at the University of Tübingen under the supervision of Prof. Stefan Haderlein. Her research is focused on interactions of metals in iron based redox systems in the presence of organic matter.

Silvia Orsetti obtained a Chemistry Diploma at the University of Buenos Aires in 2004. She completed her PhD in 2010 at the same university in the area of Electrochemistry and Environmental Chemistry. Afterwards, she started a Postdoc at the University of Tübingen in Environmental Mineralogy and Chemistry in Prof. Haderlein´s group. She now holds a research position in the same group, where she focuses on electron transfer processes between natural organic matter and minerals. Her research combines electrochemistry, geochemistry and analytical chemistry to study mechanisms of electron transfer reactions between humic substances and redox active minerals, as well as changes of redox properties of humic substances upon sorption to different sorbents. Her analytical expertise includes photochemistry, electrochemistry and HPLC applied to the optimization of characterizing humic substances' properties.

Khalil Hanna is a Professor of Chemistry at the Graduate School of Chemistry of Rennes and a junior member of the Institut Universitaire de France (IUF). He earned his PhD (2004) in Environmental Science and Technology from INSA of Lyon. His research interests focus on iron-mediated reactions for soil and water treatments and an improved understanding of sorption and heterogeneous redox reactions taking place at oxide/water interface. His research group in Rennes is engaged in elucidating molecular-scale reactions at mineral surfaces, and in translating molecular-level information to observations made at the larger scales using thermodynamics and reactive transport modelling.

Christian Ruby is a full Professor of Materials Science at the University of Lorraine (France). He teaches at the engineering school Polytech Nancy. He obtained PhD in 1997 at the University Henri Poincaré - Nancy 1 and concerned the synthesis of ultra-thin iron oxides layers by molecular beam epitaxy. After postdoctoral training, performed in the MINT Centre at the University of Tuscaloosa in Alabama (USA), he joined the University of Lorraine in 2000 as an Assistant Professor and began his research activity concerning the formation and the chemical reactivity of iron species in aqueous medium at the "Laboratoire de Chimie Physique et Microbiologie pour les Matériaux et l'Environnement" (LCPME -UMR 7564 CNRS-UL). Professor Ruby's research expertise is related to the synthesis and reactivity of iron containing compounds, in particular Fe(II)-Fe(III) layered double hydroxides, more commonly called "green rust". Recently, Christian Ruby managed different research projects

devoted to the use of green rust and related iron containing compounds for wastewater denitrification and dephosphatisation.

Andreas Kappler is a professor for Geomicrobiology at the University of Tübingen. He received his MSc in Chemistry and PhD in Environmental Microbiology from University of Konstanz and had postdoc positions at the EAWAG/ETH Zürich in Environmental Chemistry and at Caltech in Geobiology. The major focus of his research is the biogeochemical cycling of iron and humic substances and the consequences for the environmental fate of toxic metals and nutrients. Other main research areas are the role of microbial iron oxidation in the deposition of Precambrian Banded Iron Formations, biochar as soil amendment and the recovery of precious metals from waste from incineration plants.

Stefan B. Haderlein is a full Professor at the Center for Applied Geosciences (ZAG) of the Eberhard-Karls University Tübingen, Germany. He received his Ph.D. in Environmental Chemistry from the Swiss Federal Institute of Technology (ETH) Zurich, Switzerland in 1992 (Major Professor: René P. Schwarzenbach) and earned his habilitation and venia legendi from the same institution in 1998; he served as research scientist at the Swiss Federal Institute for Water Resources and Water Pollution Control (EAWAG) and ETH Zurich from 1993 to 1999 and was a Postdoctoral Fellow at the Massachusetts Institute of Technology (1996 to 1997; with Philip Gschwend). His research concerns processes at the mineral-water interface such as sorption and oxidation-reduction reactions in the context of contaminant fate and biogeochemistry of subsurface environments.

References

(1) Taylor, S. R. Abundance of Chemical Elements in the Continental Crust: A New Table. *Geochim. Cosmochim. Acta* **1964,** *28*, 1273-1285.

(2) Cornell, R. M.; Schwertmann, U. *The Iron Oxides: Structure, Properties, Reactions, Occurrence and Uses*; Second ed.; Wiley-VCH, **2003**.

(3) Hansen, H. C. B. Environmental Chemistry of Iron(II)-Iron(III) LDHs (Green Rusts). In *Layered Double Hydroxides: Present and Future*; Nova Science Publishers Huntington, NY, 2001, 469-493.

(4) Su, C. Environmental Implications and Applications of Engineered Nanoscale Magnetite and Its Hybrid Nanocomposites: A Review of Recent Literature. *J. Hazard. Mater.* **2017,** *322*, 48-84.

(5) Munoz, M.; de Pedro, Z. M.; Casas, J. A.; Rodriguez, J. J. Preparation of Magnetite-Based Catalysts and Their Application in Heterogeneous Fenton Oxidation – A Review. *Appl. Catal., B* **2015,** *176–177*, 249-265.

(6) Tang, S. C. N.; Lo, I. M. C. Magnetic Nanoparticles: Essential Factors for Sustainable Environmental Applications. *Water Res.* **2013,** *47*, 2613-2632.

(7) Pereira, M. C.; Oliveira, L. C. A.; Murad, E. Iron Oxide Catalysts: Fenton and Fenton Like Reactions- A Review. *Clay Miner.* **2012,** *47*, 285-302.

(8) Trolard, F.; Bourrié, G. Chapter 5 Geochemistry of Green Rusts and Fougerite: A Reevaluation of Fe cycle in Soils. *Adv. Agron.* **2008,** *99*, 227-288.

(9) He, Y. T.; Wilson, J. T.; Su, C.; Wilkin, R. T. Review of Abiotic Degradation of Chlorinated Solvents by Reactive Iron Minerals in Aquifers. *Groundwater Monit. Rem.* **2015,** *35*, 57-75.

(10) Ray, P. Z.; Shipley, H. J. Inorganic Nano-Adsorbents for the Removal of Heavy Metals and Arsenic: A Review. *RSC Adv.* **2015,** *5*, 29885-29907.

(11) Kaur, R.; Hasan, A.; Iqbal, N.; Alam, S.; Saini, M. K.; Raza, S. K. Synthesis and Surface Engineering of Magnetic Nanoparticles for Environmental Cleanup and Pesticide Residue Analysis: A Review. *J. Sep. Sci.* **2014,** *37*, 1805-1825.

(12) Giakisikli, G.; Anthemidis, A. N. Magnetic Materials as Sorbents for Metal/Metalloid Preconcentration and/or Separation. A Review. *Anal. Chim. Acta* **2013,** *789*, 1-16.

(13) Ngomsik, A.-F.; Bee, A.; Draye, M.; Cote, G.; Cabuil, V. Magnetic Nano- and Microparticles for Metal Removal and Environmental Applications: A Review. *C. R. Chim.* **2005,** *8*, 963-970.

(14) Skomurski, F. N.; Kerisit, S.; Rosso, K. M. Structure, Charge Distribution, and Electron Hopping Dynamics in Magnetite (Fe_3O_4) (1 0 0) Surfaces from First Principles. *Geochim. Cosmochim. Acta* **2010,** *74*, 4234-4248.

(15) Gorski, C. A.; Handler, R. M.; Beard, B. L.; Pasakarnis, T.; Johnson, C. M.; Scherer, M. M. Fe Atom Exchange between Aqueous Fe^{2+} and Magnetite. *Environ. Sci. Technol.* **2012,** *46*, 12399-12407.

(16) Jolivet, J.-P.; Tronc, E. Interfacial Electron Transfer in Colloidal Spinel Iron Oxide. Conversion of Fe_3O_4-γFe_2O_3 in Aqueous Medium. *J. Colloid Interface Sci.* **1988,** *125*, 688-701.

(17) Jolivet, J. P.; Belleville, P.; Tronc, E.; Livage, J. Influence of Fe(II) on the Formation of the Spinel Iron Oxide in Alkaline Medium. *Clays Clay Miner.* **1992,** *40*, 531-539.
(18) Tronc, E.; Jolivet, J.-P.; Lefebvre, J.; Massart, R. Ion Adsorption and Electron Transfer in Spinel-Like Iron Oxide Colloids. *J. Chem. Soc., Faraday Trans. 1* **1984,** *80*, 2619-2629.
(19) Ruby, C.; Usman, M.; Naille, S.; Hanna, K.; Carteret, C.; Mullet, M.; François, M.; Abdelmoula, M. Synthesis and Transformation of Iron-Based Layered Double Hydroxides. *Appl. Clay Sci.* **2010,** *48*, 195-202.
(20) Refait, P.; Simon, L.; Génin, J.-M. R. Reduction of SeO_4^{2-} Anions and Anoxic Formation of Iron(II)−Iron(III) Hydroxy-Selenate Green Rust. *Environ. Sci. Technol.* **2000,** *34*, 819-825.
(21) Refait, P.; Abdelmoula, M.; Génin, J. M. R.; Jeannin, M. Synthesis and Characterisation of the Fe(II-III) Hydroxy-Formate Green Rust. *Hyperfine Interact.* **2006,** *167*, 717-722.
(22) Ayala-Luis, K. B.; Koch, C. B.; Hansen, H. C. B. One-Pot Synthesis and Characterization of Fe^{II}–Fe^{III} Hydroxide (Green Rust) Intercalated with C9–C14 Linear Alkyl Carboxylates. *Appl. Clay Sci.* **2010,** *50*, 512-519.
(23) Bourdoiseau, J. A.; Sabot, R.; Jeannin, M.; Termemil, F.; Refait, P. Determination of Standard Gibbs Free Energy of Formation of Green Rusts and Its Application to the Fe(II–III) Hydroxy-Oxalate. *Colloids Surf., A* **2012,** *410*, 72-80.
(24) Simon, L.; François, M.; Refait, P.; Renaudin, G.; Lelaurain, M.; Génin, J.-M. R. Structure of the Fe(II-III) Layered Double Hydroxysulphate Green Rust Two from Rietveld Analysis. *Solid State Sci.* **2003,** *5*, 327-334.
(25) Aissa, R.; Francois, M.; Ruby, C.; Fauth, F.; Medjahdi, G.; Abdelmoula, M.; Génin, J. M. Formation and Crystallographical Structure of Hydroxysulphate and Hydroxycarbonate Green Rusts Synthetised by Coprecipitation. *J. Phys. Chem. Solids* **2006,** *67*, 1016-1019.
(26) Refait, P. H.; Abdelmoula, M.; Génin, J. M. R. Mechanisms of Formation and Structure of Green Rust One in Aqueous Corrosion of Iron in the Presence of Chloride Ions. *Corros. Sci.* **1998,** *40*, 1547-1560.
(27) Bernal, J. D.; Dasgupta, D. R.; Mackay, A. L. The Oxides and Hydroxides of Iron and Their Structural Inter-Relationships. *Clay Miner. Bull.* **1959,** *4*, 15-30.
(28) Génin, J. M. R.; Christy, A.; Kuzmann, E.; Mills, S.; Ruby, C. Structure and Occurrences of ≪ Green Rust ≫ Related New Minerals of the ≪ Fougérite ≫ Group, Trébeurdenite and Mössbauerite, Belonging to the ≪ Hydrotalcite ≫ Supergroup; How Mössbauer Spectroscopy Helps XRD. *Hyperfine Interact.* **2014,** *226*, 459-482.
(29) Refait, P.; Bon, C.; Simon, L.; Bourrié, G.; Trolard, F.; Bessiere, J.; Génin, J.-M. Chemical Composition and Gibbs Standard Free Energy of Formation of Fe(II)-Fe(III) Hydroxysulphate Green Rust and Fe(II) Hydroxide. *Clay Miner.* **1999,** *34*, 499-510.
(30) Christiansen, B. C.; Balic-Zunic, T.; Petit, P. O.; Frandsen, C.; Mørup, S.; Geckeis, H.; Katerinopoulou, A.; Stipp, S. L. S. Composition and Structure of an Iron-Bearing, Layered Double Hydroxide (LDH) – Green Rust Sodium Sulphate. *Geochim. Cosmochim. Acta* **2009,** *73*, 3579-3592.

(31) Ruby, C.; Aïssa, R.; Géhin, A.; Cortot, J.; Abdelmoula, M.; Génin, J.-M. Green Rusts Synthesis by Coprecipitation of Fe^{II}-Fe^{III} ions and Mass-Balance Diagram. *C. R. Geosci.* **2006,** *338*, 420-432.
(32) Bocher, F.; Géhin, A.; Ruby, C.; Ghanbaja, J.; Abdelmoula, M.; Génin, J.-M. R. Coprecipitation of Fe(II–III) Hydroxycarbonate Green Rust Stabilised by Phosphate Adsorption. *Solid State Sci.* **2004,** *6*, 117-124.
(33) Génin, J.-M. R.; Refait, P.; Bourrié, G.; Abdelmoula, M.; Trolard, F. Structure and Stability of the Fe(II)–Fe(III) Green Rust "Fougerite" Mineral and Its Potential for Reducing Pollutants in Soil Solutions. *Appl. Geochem.* **2001,** *16*, 559-570.
(34) Génin, J.; Abdelmoula, M.; Refait, P.; Simon, L. Comparison of the Green Rust Two Lamellar Double Hydroxide Class with the Green Rust One Pyroaurite Class: Fe(II)-Fe(III) Sulphate and Selenate Hydroxides. *Hyperfine Interact.* **1998,** *3*, 313-316.
(35) Gorski, C. A.; Scherer, M. M. Determination of Nanoparticulate Magnetite Stoichiometry by Mossbauer Spectroscopy, Acidic Dissolution, and Powder X-Ray Diffraction: A Critical Review. *Am. Mineral.* **2010,** *95*, 1017-1026.
(36) Zegeye, A.; Abdelmoula, M.; Usman, M.; Hanna, K.; Ruby, C. In Situ Monitoring of Lepidocrocite Bioreduction and Magnetite Formation by Reflection Mossbauer Spectroscopy. *Am. Mineral.* **2011,** *96*, 1410-1413.
(37) Usman, M.; Abdelmoula, M.; Hanna, K.; Grégoire, B.; Faure, P.; Ruby, C. Fe^{II} Induced Mineralogical Transformations of Ferric Oxyhydroxides into Magnetite of Variable Stoichiometry and Morphology. *J. Solid State Chem.* **2012,** *194*, 328-335.
(38) Annersten, H.; Hafner, S. S. Vacancy Distribution in Synthetic Spinels of the Series Fe_3O_4–y-Fe_2O_3. *Z. Kristallogr. Cryst. Mater.* **1973,** *137*, 321-340.
(39) Gorski, C. A.; Nurmi, J. T.; Tratnyek, P. G.; Hofstetter, T. B.; Scherer, M. M. Redox Behavior of Magnetite: Implications for Contaminant Reduction. *Environ. Sci. Technol.* **2010,** *44*, 55-60.
(40) Gorski, C. A.; Scherer, M. M. Influence of Magnetite Stoichiometry on Fe^{II} Uptake and Nitrobenzene Reduction. *Environ. Sci. Technol.* **2009,** *43*, 3675-3680.
(41) Peterson, M. L.; White, A. F.; Brown, G. E.; Parks, G. A. Surface Passivation of Magnetite by Reaction with Aqueous Cr(VI): XAFS and TEM Results. *Environ. Sci. Technol.* **1997,** *31*, 1573-1576.
(42) Hanna, K.; Kone, T.; Ruby, C. Fenton-Like Oxidation and Mineralization of Phenol Using Synthetic Fe(II)-Fe(III) Green Rusts. *Environ. Sci. Pollut. Res.* **2010,** *17*, 124-134.
(43) Xue, X.; Hanna, K.; Deng, N. Fenton-Like Oxidation of Rhodamine B in the Presence of Two Types of Iron (II, III) Oxide. *J. Hazard. Mater.* **2009,** *166*, 407-414.
(44) Minella, M.; Marchetti, G.; De Laurentiis, E.; Malandrino, M.; Maurino, V.; Minero, C.; Vione, D.; Hanna, K. Photo-Fenton Oxidation of Phenol with Magnetite as Iron Source. *Appl. Catal., B* **2014,** *154–155*, 102-109.
(45) Rusevova, K.; Kopinke, F.-D.; Georgi, A. Nano-Sized Magnetic Iron Oxides as Catalysts for Heterogeneous Fenton-Like Reactions—Influence of Fe(II)/Fe(III) Ratio on Catalytic Performance. *J. Hazard. Mater.* **2012,** *241–242*, 433-440.

(46) Da Costa, G.; De Grave, E.; De Bakker, P.; Vandenberghe, R. Influence of Nonstoichiometry and the Presence of Maghemite on the Mössbauer Spectrum of Magnetite. *Clays Clay Miner.* **1995,** *43*, 656-668.
(47) Tronc, E.; Belleville, P.; Jolivet, J. P.; Livage, J. Transformation of Ferric Hydroxide into Spinel by Fe^{II} Adsorption. *Langmuir* **1992,** *8*, 313-319.
(48) Byrne, J. M.; van der Laan, G.; Figueroa, A. I.; Qafoku, O.; Wang, C.; Pearce, C. I.; Jackson, M.; Feinberg, J.; Rosso, K. M.; Kappler, A. Size Dependent Microbial Oxidation and Reduction of Magnetite Nano- and Micro-Particles. *Sci. Rep.* **2016,** *6*, 30969.
(49) Morrall, P.; Schedin, F.; Case, G. S.; Thomas, M. F.; Dudzik, E.; van der Laan, G.; Thornton, G. Stoichiometry of $Fe_{3-\delta}O_4$(111) Ultrathin Films on Pt(111). *Phys. Rev. B* **2003,** *67*, 214408.
(50) Pattrick, R. A. D.; van der Laan, G.; Henderson, C. M. B.; Kuiper, P.; Dudzik, E.; Vaughan, D. J. Cation Site Occupancy in Spinel Ferrites Studied by X-Ray Magnetic Circular Dichroism: Developing a Method for Mineralogists. *Eur. J. Mineral.* **2002,** *14*, 1095-1102.
(51) Usman, M.; Hanna, K.; Abdelmoula, M.; Zegeye, A.; Faure, P.; Ruby, C. Formation of Green Rust Via Mineralogical Transformation of Ferric Oxides (Ferrihydrite, Goethite and Hematite). *Appl. Clay Sci.* **2012,** *64*, 38-43.
(52) Canfield, D. E.; Erik, K.; Bo, T. Thermodynamics and Microbial Metabolism. In *Advances in Marine Biology*; Donald E. Canfield;Kristensen, E.;Bo, T., Eds.; Academic Press, 2005; Vol. 48, 65-94.
(53) White, A. F.; Peterson, M. L.; Hochella, M. F. Electrochemistry and Dissolution Kinetics of Magnetite and Ilmenite. *Geochim. Cosmochim. Acta* **1994,** *58*, 1859-1875.
(54) Gorski, C. A.; Scherer, M. M. Fe^{2+} Sorption at the Fe Oxide-Water Interface: A Revised Conceptual Framework. In *Aquatic Redox Chemistry*; American Chemical Society, 2011; Vol. 1071, 315-343.
(55) Thamdrup, B. Bacterial Manganese and Iron Reduction in Aquatic Sediments. In *Advances in Microbial Ecology*; Schink, B., Ed.; Springer US: Boston, MA, 2000, 41-84.
(56) Linberg, R.; Runnels, D. Ground Water Redox Reactions: An Analysis of Equilibrium State Applied to Eh Measurements and Geochemical Modeling. *Science* **1984,** *225*, 925-927.
(57) Orsetti, S.; Laskov, C.; Haderlein, S. B. Electron Transfer between Iron Minerals and Quinones: Estimating the Reduction Potential of the Fe(II)-Goethite Surface from AQDS Speciation. *Environ. Sci. Technol.* **2013,** *47*, 14161-14168.
(58) Gorski, C. A.; Edwards, R.; Sander, M.; Hofstetter, T. B.; Stewart, S. M. Thermodynamic Characterization of Iron Oxide–Aqueous Fe^{2+} Redox Couples. *Environ. Sci. Technol.* **2016,** *50*, 8538-8547.
(59) Fischer, W. R. Standard Potentials (Eo) of Iron(III) Oxides under Reducing Conditions. *Z. Pflanzenernaehr. Bodenkd.* **1987,** *150*, 286-289.
(60) Sander, M.; Hofstetter, T. B.; Gorski, C. A. Electrochemical Analyses of Redox-Active Iron Minerals: A Review of Nonmediated and Mediated Approaches. *Environ. Sci. Technol.* **2015,** *49*, 5862-5878.
(61) Gorski, C. A.; Klüpfel, L.; Voegelin, A.; Sander, M.; Hofstetter, T. B. Redox Properties of Structural Fe in Clay Minerals. 2. Electrochemical and Spectroscopic Characterization of Electron Transfer Irreversibility in Ferruginous Smectite, SWa-1. *Environ. Sci. Technol.* **2012,** *46*, 9369-9377.

(62) Castro, P. A.; Vago, E. R.; Calvo, E. J. Surface Electrochemical Transformations on Spinel Iron Oxide Electrodes in Aqueous Solutions. *J. Chem. Soc., Faraday Trans.* **1996,** *92*, 3371-3379.
(63) Latta, D. E.; Gorski, C. A.; Boyanov, M. I.; O'Loughlin, E. J.; Kemner, K. M.; Scherer, M. M. Influence of Magnetite Stoichiometry on UVI Reduction. *Environ. Sci. Technol.* **2011,** *46*, 778-786.
(64) Maher, B. A. Rain and Dust: Magnetic Records of Climate and Pollution. *Elements* **2009,** *5*, 229-234.
(65) Evans, M.; Heller, F. *Environmental Magnetism: Principles and Applications of Enviromagnetics*; Academic Press, **2003**.
(66) Dunlop, D. J.; Özdemir, Ö. *Rock Magnetism: Fundamentals and Frontiers*; Cambridge University Press, **2001**.
(67) Coey, J. M. D. Noncollinear Spin Arrangement in Ultrafine Ferrimagnetic Crystallites. *Phys. Rev. Lett.* **1971,** *27*, 1140-1142.
(68) Byrne, J. M.; Coker, V. S.; Cespedes, E.; Wincott, P. L.; Vaughan, D. J.; Pattrick, R. A. D.; van der Laan, G.; Arenholz, E.; Tuna, F.; Bencsik, M.et al. Biosynthesis of Zinc Substituted Magnetite Nanoparticles with Enhanced Magnetic Properties. *Adv. Funct. Mater.* **2014,** *24*, 2518-2529.
(69) Byrne, J. M.; Coker, V. S.; Moise, S.; Wincott, P. L.; Vaughan, D. J.; Tuna, F.; Arenholz, E.; van der Laan, G.; Pattrick, R. A. D.; Lloyd, J. R.et al. Controlled Cobalt Doping in Biogenic Magnetite Nanoparticles. *J. R. Soc. Interface* **2013,** *10*, 20130134.
(70) Céspedes, E.; Byrne, J. M.; Farrow, N.; Moise, S.; Coker, V. S.; Bencsik, M.; Lloyd, J. R.; Telling, N. D. Bacterially Synthesized Ferrite Nanoparticles for Magnetic Hyperthermia Applications. *Nanoscale* **2014,** *6*, 12958-12970.
(71) Verwey, E. Electronic Conduction of Magnetite (Fe_3O_4) and Its Transition Point at Low Temperatures. *Nature* **1939,** *144*, 327-328.
(72) Kąkol, Z.; Sabol, J.; Stickler, J.; Honig, J. Effect of Low-Level Titanium (IV) Doping on the Resistivity of Magnetite near the Verwey Transition. *Phys. Rev. B* **1992,** *46*, 1975.
(73) Kozłowski, A.; Metcalf, P.; Kkol, Z.; Honig, J. M. Electrical Transport and Magnetization Measurements of $Fe_{3-z}Al_zO_4$, $z < 0.06$. *J. Magn. Magn. Mater.* **1996,** *157*, 415-416.
(74) Özdemir, Ö.; Dunlop, D. J. Hallmarks of Maghemitization in Low‐Temperature Remanence Cycling of Partially Oxidized Magnetite Nanoparticles. *J. Geophys. Res.: Solid Earth* **2010,** *115*.
(75) Lee, J.; Kwon, S. G.; Park, J.-G.; Hyeon, T. Size Dependence of Metal–Insulator Transition in Stoichiometric Fe3O4 Nanocrystals. *Nano Lett.* **2015,** *15*, 4337-4342.
(76) Goya, G.; Berquó, T. S.; Fonseca, F. C.; Morales, M. Static and Dynamic Magnetic Properties of Spherical Magnetite Nanoparticles. *J. Appl. Phys.* **2003,** *94*, 3520-3528.
(77) Harrison, R. J.; Feinberg, J. M. Mineral Magnetism: Providing New Insights into Geoscience Processes. *Elements* **2009,** *5*, 209-215.
(78) Beverskog, B.; Puigdomenech, I. Revised Pourbaix Diagrams for Iron at 25–300 °C. *Corros. Sci.* **1996,** *38*, 2121-2135.
(79) Ayala-Luis, K. B.; Koch, C. B.; Hansen, H. C. B. The Standard Gibbs Energy of Formation of Fe(II)Fe(III) Hydroxide Sulfate Green Rust. *Clays Clay Miner.* **2008,** *56*, 633-644.

(80) Refait, P.; Géhin, A.; Abdelmoula, M.; Génin, J. M. R. Coprecipitation Thermodynamics of iron(II-III) Hydroxysulphate Green Rust from Fe(II) and Fe(III) Salts. *Corros. Sci.* **2003,** *45*, 659-676.
(81) Ruby, C.; Géhin, A.; Abdelmoula, M.; Génin, J.-M. R.; Jolivet, J.-P. Coprecipitation of Fe(II) and Fe(III) Cations in Sulphated Aqueous Medium and Formation of Hydroxysulphate Green Rust. *Solid State Sci.* **2003,** *5*, 1055-1062.
(82) McGill, I. R.; McEnaney, B.; Smith, D. C. Crystal Structure of Green Rust Formed by Corrosion of Cast Iron. *Nature* **1976,** *259*, 200-201.
(83) Bearcock, J.; Perkins, W.; Dinelli, E.; Wade, S. Fe (II)/Fe (III) 'Green Rust' Developed within Ochreous Coal Mine Drainage Sediment in South Wales, UK. *Mineral. Mag.* **2006,** *70*, 731-741.
(84) Taylor, R. The Rapid Formation of Crystalline Double Hydroxy Salts and Other Compounds by Controlled Hydrolysis. *Clay Miner.* **1984,** *19*, 591-603.
(85) Trolard, F.; Génin, J. M. R.; Abdelmoula, M.; Bourrié, G.; Humbert, B.; Herbillon, A. Identification of a Green Rust Mineral in a Reductomorphic Soil by Mossbauer and Raman Spectroscopies. *Geochim. Cosmochim. Acta* **1997,** *61*, 1107-1111.
(86) Trolard, F.; Bourrié, G.; Abdelmoula, M.; Refait, P.; Feder, F. Fougerite, a New Mineral of the Pyroaurite-Iowaite Group: Description and Crystal Structure. *Clays Clay Miner.* **2007,** *55*, 323-334.
(87) Feder, F.; Trolard, F.; Klingelhöfer, G.; Bourrié, G. In Situ Mössbauer Spectroscopy: Evidence for Green Rust (Fougerite) in a Gleysol and Its Mineralogical Transformations with Time and Depth. *Geochim. Cosmochim. Acta* **2005,** *69*, 4463-4483.
(88) Christiansen, B. C.; Balic-Zunic, T.; Dideriksen, K.; Stipp, S. L. S. Identification of Green Rust in Groundwater. *Environ. Sci. Technol.* **2009,** *43*, 3436-3441.
(89) Zegeye, A.; Bonneville, S.; Benning, L. G.; Sturm, A.; Fowle, D. A.; Jones, C.; Canfield, D. E.; Ruby, C.; MacLean, L. C.; Nomosatryo, S. Green Rust Formation Controls Nutrient Availability in a Ferruginous Water Column. *Geology* **2012,** *40*, 599-602.
(90) Rennert, T.; Eusterhues, K.; De Andrade, V.; Totsche, K. U. Iron Species in Soils on a Mofette Site Studied by Fe K-Edge X-Ray Absorption near-Edge Spectroscopy. *Chem. Geol.* **2012,** *332–333*, 116-123.
(91) Johnson, C. A.; Freyer, G.; Fabisch, M.; Caraballo, M. A.; Küsel, K.; Hochella, M. F. Observations and Assessment of Iron Oxide and Green Rust Nanoparticles in Metal-Polluted Mine Drainage within a Steep Redox Gradient. *Environ. Chem.* **2014,** *11*, 377-391.
(92) Weatherington-Rice, J.; Bigham, J. M. Buried Pre-Illinoian-Age Lacustrine Deposits with" Green Rust" Colors in Clermont County, Ohio1. *Ohio J. Sci.* **2006,** *106*, 35.
(93) Root, R. A.; Dixit, S.; Campbell, K. M.; Jew, A. D.; Hering, J. G.; O'Day, P. A. Arsenic Sequestration by Sorption Processes in High-Iron Sediments. *Geochim. Cosmochim. Acta* **2007,** *71*, 5782-5803.
(94) Latta, D. E.; Boyanov, M. I.; Kemner, K. M.; O'Loughlin, E. J.; Scherer, M. M. Abiotic reduction of uranium by Fe(II) in soil. *Appl. Geochem.* **2012,** *27*, 1512-1524.
(95) Miyata, S. Anion-Exchange Properties of Hydrotalcite-Like Compounds. *Clays Clay Miner.* **1983,** *31*, 305-311.

(96) Génin, J.-M. R.; Olowe, A. A.; Benbouzid-Rollet, N. D.; Prieur, D.; Confente, M.; Resiak, B. The Simultaneous Presence of Green Rust 2 and Sulfate Reducing Bacteria in the Corrosion of Steel Sheet Piles in a Harbour Area. *Hyperfine Interact.* **1992,** *69*, 875-878.
(97) Sphar, J. Occurrence of Magnetite in the Arkansas River Bed Between Ford and Arkansas City. *Trans. Kans. Acad. Sci.* **1962,** *65*, 257-262.
(98) Maher, B. A. Characterisation of Soils by Mineral Magnetic Measurements. *Phys. Earth Planet. Inter.* **1986,** *42*, 76-92.
(99) Maher, B. A.; Taylor, R. M. Formation of Ultrafine-Grained Magnetite in Soils. *Nature* **1988,** *336*, 368-370.
(100) Auerswald K; Friedl J; Litaor I; H, S. Iron Oxide Mineralogy of a Semi-Arid Wetland. *Mitt. DTCH. Bodenk. Ges.* **2001,** *96*, 677-678.
(101) Fassbinder, J. W. E.; Stanjekt, H.; Vali, H. Occurrence of Magnetic Bacteria in Soil. *Nature* **1990,** *343*, 161-163.
(102) Maher, B. A.; Thompson, R. Mineral Magnetic Record of the Chinese Loess and Paleosols. *Geology* **1991,** *19*, 3-6.
(103) de Jesus Filho, F. M.; Fabris, J. D.; Goulart, A. T.; Coey, J. M. D.; Ferreira, B. A.; Pinto, M. C. F. Ilmenite and Magnetite of a Tholeiitic Basalt. *Clays Clay Miner.* **1995,** *43*, 641-642.
(104) Ramasamy, R.; Gwalani, L. G.; Subramanian, S. P. A Note on the Occurrence and Formation of Magnetite in the Carbonatites of Sevvattur, North Arcot District, Tamil Nadu, Southern India. *J. Asian Earth Sci.* **2001,** *19*, 297-304.
(105) Viana, J. H. M.; Couceiro, P. R. C.; Pereira, M. C.; Fabris, J. D.; Fernandes Filho, E. I.; Schaefer, C. E. G. R.; Rechenberg, H. R.; Abrahão, W. A. P.; Mantovani, E. C. Occurrence of Magnetite in the Sand Fraction of an Oxisol in the Brazilian Savanna Ecosystem, Developed from a Magnetite-Free Lithology. *Soil Res.* **2006,** *44*, 71-83.
(106) Jordanova, D.; Goddu, S. R.; Kotsev, T.; Jordanova, N. Industrial Contamination of Alluvial Soils near Fe–Pb Mining Site Revealed by Magnetic and Geochemical Studies. *Geoderma* **2013,** *192*, 237-248.
(107) Ananthapadmanabha, A. L.; Shankar, R.; Sandeep, K. Rock Magnetic Properties of Lateritic Soil Profiles from Southern India: Evidence for Pedogenic Processes. *J. Appl. Geophys.* **2014,** *111*, 203-210.
(108) Kissel, C.; Liu, Z.; Li, J.; Wandres, C. Magnetic Minerals in Three Asian Rivers Draining into the South China Sea: Pearl, Red, and Mekong Rivers. *Geochem. Geophys. Geosyst.* **2016,** *17*, 1678-1693.
(109) Rijal, M. L.; Porsch, K.; Appel, E.; Kappler, A. Magnetic Signature of Hydrocarbon-Contaminated Soils and Sediments at the Former Oil Field Hänigsen, Germany. *Stud. Geophys. Geod.* **2012,** *56*, 889-908.
(110) Ameen, N. N.; Klueglein, N.; Appel, E.; Petrovský, E.; Kappler, A.; Leven, C. Effect of Hydrocarbon-Contaminated Fluctuating Groundwater on Magnetic Properties of Shallow Sediments. *Stud. Geophys. Geod.* **2014,** *58*, 442-460.
(111) Li, Y.-L.; Konhauser, K. O.; Zhai, M. The Formation of Magnetite in the Early Archean Oceans. *Earth. Planet. Sci. Lett.* **2017,** *466*, 103-114.
(112) Churchman, G. J.; Lowe, D. J. *Alteration, Formation, and Occurrence of Minerals in Soils*; CRC Press, **2012**.
(113) Oldfield, F.; Crowther, J. Establishing Fire Incidence in Temperate Soils Using Magnetic Measurements. *Palaeogeogr., Palaeoclimatol., Palaeoecol.* **2007,** *249*, 362-369.

(114) Geiss, C. E.; Egli, R.; Zanner, C. W. Direct Estimates of Pedogenic Magnetite as a Tool to Reconstruct Past Climates from Buried Soils. *J. Geophys. Res.: Solid Earth* **2008,** *113*, n/a-n/a.
(115) Salazar-Camacho, C.; Villalobos, M.; Rivas-Sánchez, M. d. l. L.; Arenas-Alatorre, J.; Alcaraz-Cienfuegos, J.; Gutiérrez-Ruiz, M. E. Characterization and Surface Reactivity of Natural and Synthetic Magnetites. *Chem. Geol.* **2013,** *347*, 233-245.
(116) Giménez, J.; Martínez, M.; de Pablo, J.; Rovira, M.; Duro, L. Arsenic Sorption onto Natural Hematite, Magnetite, and Goethite. *J. Hazard. Mater.* **2007,** *141*, 575-580.
(117) Marmier, N.; Delisée, A.; Fromage, F. Surface Complexation Modeling of Yb(III), Ni(II), and Cs(I) Sorption on Magnetite. *J. Colloid Interface Sci.* **1999,** *211*, 54-60.
(118) Marmier, N.; Fromage, F. Sorption of Cs(I) on Magnetite in the Presence of Silicates. *J. Colloid Interface Sci.* **2000,** *223*, 83-88.
(119) Villacís-García, M.; Villalobos, M.; Gutiérrez-Ruiz, M. Optimizing the Use of Natural and Synthetic Magnetites with Very Small Amounts of Coarse Fe(0) Particles for Reduction of Aqueous Cr(VI). *J. Hazard. Mater.* **2015,** *281*, 77-86.
(120) He, H.; Zhong, Y.; Liang, X.; Tan, W.; Zhu, J.; Yan Wang, C. Natural Magnetite: An Efficient Catalyst for the Degradation of Organic Contaminant. *Sci. Rep.* **2015,** *5*, 10139.
(121) Stampfl, P. P. Ein Basisches Eisen-II-III-Karbonat in Rost. *Corros. Sci.* **1969,** *9*, 185-187.
(122) Boucherit, N.; Hugot-Le Goff, A.; Joiret, S. Raman Studies of Corrosion Films Grown on Fe and Fe-6Mo in Pitting Conditions. *Corros. Sci.* **1991,** *32*, 497-507.
(123) Abdelmoula, M.; Refait, P.; Drissi, S. H.; Mihe, J. P.; Génin, J. M. R. Conversion Electron Mössbauer Spectroscopy and X-Ray Diffraction Studies of the Formation of Carbonate-Containing Green Rust One by Corrosion of Metallic Iron in $NaHCO_3$ and ($NaHCO_3$ + NaCl) Solutions. *Corros. Sci.* **1996,** *38*, 623-633.
(124) Simard, S.; Odziemkowski, M.; Irish, D. E.; Brossard, L.; Ménard, H. In Situ Micro-Raman Spectroscopy to Investigate Pitting Corrosion Product of 1024 Mild Steel in Phosphate and Bicarbonate Solutions Containing Chloride and Sulfate Ions. *J. Appl. Electrochem.* **2001,** *31*, 913-920.
(125) Refait, P.; Memet, J. B.; Bon, C.; Sabot, R.; Génin, J. M. R. Formation of the Fe(II)-Fe(III) Hydroxysulphate Green Rust During Marine Corrosion of Steel. *Corros. Sci.* **2003,** *45*, 833-845.
(126) Pineau, S.; Sabot, R.; Quillet, L.; Jeannin, M.; Caplat, C.; Dupont-Morral, I.; Refait, P. Formation of the Fe(II–III) Hydroxysulphate Green Rust During Marine Corrosion of Steel Associated to Molecular Detection of Dissimilatory Sulphite-Reductase. *Corros. Sci.* **2008,** *50*, 1099-1111.
(127) Neff, D.; Dillmann, P.; Bellot-Gurlet, L.; Beranger, G. Corrosion of Iron Archaeological Artefacts in Soil: Characterisation of the Corrosion System. *Corros. Sci.* **2005,** *47*, 515-535.
(128) Colomban, P.; Cherifi, S.; Despert, G. Raman Identification of Corrosion Products on Automotive Galvanized Steel Sheets. *J. Raman Spectrosc.* **2008,** *39*, 881-886.

(129) Roh, Y.; Lee, S. Y.; Elless, M. P. Characterization of Corrosion Products in the Permeable Reactive Barriers. *Environ. Geol.* **2000,** *40*, 184-194.
(130) Huang, Y. H.; Zhang, T. C. Effects of Dissolved Oxygen on Formation of Corrosion Products and Concomitant Oxygen and Nitrate Reduction in Zero-Valent Iron Systems with or without Aqueous Fe^{2+}. *Water Res.* **2005,** *39*, 1751-1760.
(131) Massart, R. Préparation de Ferrofluides Aqueux en l'Absence de Surfactant; Comportement en Fonction du pH et de la Nature des Ions Présents en Solution. *CR Acad. Sci. Paris C* **1980,** *1*, t291.
(132) Tamura, H.; Kawamura, S.; Hagayama, M. Acceleration of the Oxidation of Fe^{2+} Ions by Fe(III)-Oxyhydroxides. *Corros. Sci.* **1980,** *20*, 963-971.
(133) Hansen, H. C. B.; Guldberg, S.; Erbs, M.; Bender Koch, C. Kinetics of Nitrate Reduction by Green Rusts--Effects of Interlayer Anion and Fe(II):Fe(III) Ratio. *Appl. Clay Sci.* **2001,** *18*, 81-91.
(134) Vayssières, L.; Chanéac, C.; Tronc, E.; Jolivet, J. P. Size Tailoring of Magnetite Particles Formed by Aqueous Precipitation: An Example of Thermodynamic Stability of Nanometric Oxide Particles. *J. Colloid Interface Sci.* **1998,** *205*, 205-212.
(135) Stumm, W.; Lee, G. F. Oxygenation of Ferrous Iron. *Ind. Eng. Chem.* **1961,** *53*, 143-146.
(136) Davison, W.; Seed, G. The Kinetics of the Oxidation of Ferrous Iron in Synthetic and Natural Waters. *Geochim. Cosmochim. Acta* **1983,** *47*, 67-79.
(137) Millero, F. J.; Sotolongo, S.; Izaguirre, M. The Oxidation Kinetics of Fe(II) in Seawater. *Geochim. Cosmochim. Acta* **1987,** *51*, 793-801.
(138) Morgan, B.; Lahav, O. The effect of pH on the Kinetics of Spontaneous Fe(II) Oxidation by O_2 in Aqueous Solution – Basic Principles and a Simple Heuristic Description. *Chemosphere* **2007,** *68*, 2080-2084.
(139) Feitknecht, v. W.; Keller, G. Über die Dunkelgrünen Hydroxyverbindungen des Eisens. *Z. Anorg. Chem.* **1950,** *262*, 61-68.
(140) Refait, P.; Génin, J. M. R. The oxidation of Ferrous Hydroxide in Chloride-Containing Aqueous Media and Pourbaix Diagrams of Green Rust One. *Corros. Sci.* **1993,** *34*, 797-819.
(141) Detournay, J.; De Miranda, L.; Derie, R.; Ghodsi, M. The Region of Stability of Green Rust II in the Electrochemical Potential-pH Equilibrium Diagram of Iron in Sulphate Medium. *Corros. Sci.* **1975,** *15*, 295-306.
(142) Génin, J. M. R.; Olowe, A. A.; Refait, P.; Simon, L. On the Stoichiometry and Pourbaix Diagram of Fe(II)-Fe(III) Hydroxy-Sulphate or Sulphate-Containing Green Rust 2: An Electrochemical and Mössbauer Spectroscopy Study. *Corros. Sci.* **1996,** *38*, 1751-1762.
(143) Ruby, C.; Upadhyay, C.; Géhin, A.; Ona-Nguema, G.; Génin, J.-M. R. In Situ Redox Flexibility of Fe^{II}-^{III} Oxyhydroxycarbonate Green Rust and Fougerite. *Environ. Sci. Technol.* **2006,** *40*, 4696-4702.
(144) Sada, E.; Kumazawa, H.; Cho, H. M. Formation of Fine Magnetite Particles by Oxidation of Aqueous Auspensions of Ferrous Hydroxide. *Canadian J. Chem. Eng.* **1990,** *68*, 622-626.
(145) Olowe, A.; Pauron, B.; Génin, J. The Influence of Temperature on the Oxidation of Ferrous Hydroxide in Sulphated Aqueous Medium: Activation Energies of Formation of the Products and Hyperfine Structure of Magnetite. *Corros. Sci.* **1991,** *32*, 985-1001.

(146) Domingo, C.; Rodriguez-Clemente, R.; Blesa, M. Kinetics of Oxidative Precipitation of Iron Oxide Particles. *Colloids Surf., A* **1993,** *79*, 177-189.
(147) Sugimoto, T.; Matijević, E. Formation of Uniform Spherical Magnetite Particles by Crystallization from Ferrous Hydroxide Gels. *J. Colloid Interface Sci.* **1980,** *74*, 227-243.
(148) Mürbe, J.; Rechtenbach, A.; Töpfer, J. Synthesis and Physical Characterization of Magnetite Nanoparticles for Biomedical Applications. *Mater. Chem. Phys.* **2008,** *110*, 426-433.
(149) Vereda, F.; De Vicente, J.; Hidalgo-Alvarez, R. Oxidation of Ferrous Hydroxides with Nitrate: A Versatile Method for the Preparation of Magnetic Colloidal Particles. *J. Colloid Interface Sci.* **2013,** *392*, 50-56.
(150) Legrand, L.; Savoye, S.; Chausse, A.; Messina, R. Study of Oxidation Products Formed on Iron in Solutions Containing Bicarbonate/Carbonate. *Electrochim. Acta* **2000,** *46*, 111-117.
(151) Refait, P.; Nguyen, D.; Jeannin, M.; Sable, S.; Langumier, M.; Sabot, R. Electrochemical Formation of Green Rusts in Deaerated Seawater-Like Solutions. *Electrochim. Acta* **2011,** *56*, 6481-6488.
(152) Antony, H.; Labrit, A.; Rouchaud, J.; Legrand, L.; Chaussé, A. Study of Fe^{II}/Fe^{III} Ratio in Thin Films of Carbonate or Sulphate Green Rusts Obtained by Potentiostatic Electrosynthesis. *Electrochim. Acta* **2008,** *53*, 7173-7181.
(153) Legrand, L.; Abdelmoula, M.; Géhin, A.; Chaussé, A.; Génin, J. M. R. Electrochemical Formation of a New Fe(II)-Fe(III) Hydroxy-Carbonate Green Rust: Characterization and Morphology. *Electrochim. Acta* **2001,** *46*, 1815-1822.
(154) Génin, J. M. R.; Mills, S. J.; Christy, A. G.; Guérin; Herbillon, A. J.; Kuzmann, E.; Ona-Nguema, G.; Ruby, C.; Upadhyay, C. Mössbauerite, $Fe^{3+}{}_6O_4(OH)_8[CO_3]\cdot 3H_2O$, the Fully Oxidized 'Green Rust' Mineral from Mont Saint-Michel Bay, France. *Mineral. Mag.* **2014,** *78*, 447-465.
(155) Franger, S.; Berthet, P.; Berthon, J. Electrochemical Synthesis of Fe_3O_4 Nanoparticles in Alkaline Aqueous Solutions Containing Complexing Agents. *J. Solid State Electrochem.* **2004,** *8*, 218-223.
(156) Cabrera, L.; Gutierrez, S.; Menendez, N.; Morales, M.; Herrasti, P. Magnetite Nanoparticles: Electrochemical Synthesis and Characterization. *Electrochim. Acta* **2008,** *53*, 3436-3441.
(157) Fajaroh, F.; Setyawan, H.; Widiyastuti, W.; Winardi, S. Synthesis of Magnetite Nanoparticles by Surfactant-Free Electrochemical Method in an Aqueous System. *Adv. Powder Technol.* **2012,** *23*, 328-333.
(158) Jeen, S.-W.; Jambor, J. L.; Blowes, D. W.; Gillham, R. W. Precipitates on Granular Iron in Solutions Containing Calcium Carbonate with Trichloroethene and Hexavalent Chromium. *Environ. Sci. Technol.* **2007,** *41*, 1989-1994.
(159) Liu, H.; Guo, H.; Li, P.; Wei, Y. The Transformation of Ferrihydrite in the Presence of Trace Fe(II): The Effect of the Anionic Media. *J. Solid State Chem.* **2008,** *181*, 2666-2671.
(160) Pedersen, H. D.; Postma, D.; Jakobsen, R.; Larsen, O. Fast transformation of iron oxyhydroxides by the catalytic action of aqueous Fe(II). *Geochim. Cosmochim. Acta* **2005,** *69*, 3967-3977.
(161) Jeon, B.-H.; Dempsey, B. A.; Burgos, W. D. Kinetics and Mechanisms for Reactions of Fe(II) with Iron(III) Oxides. *Environ. Sci. Technol.* **2003,** *37*, 3309-3315.

(162) Yee, N.; Shaw, S.; Benning, L. G.; Nguyen, T. H. The Rate of Ferrihydrite Transformation to Goethite via the Fe(II) Pathway. *Am. Mineral.* **2006,** *91*, 92-96.
(163) Liu, H.; Li, P.; Lu, B.; Wei, Y.; Sun, Y. Transformation of Ferrihydrite in the Presence or Absence of Trace Fe(II): The Effect of Preparation Procedures of Ferrihydrite. *J. Solid State Chem.* **2009,** *182*, 1767-1771.
(164) Tamaura, Y.; Ito, K.; Katsura, T. Transformation of γ-FeO(OH) to Fe_3O_4 by Adsorption of Iron(II) Ion on γ-FeO(OH). *J. Chem. Soc., Dalton Trans.* **1983**, 189-194.
(165) Ishikawa, T.; Kondo, Y.; Yasukawa, A.; Kandori, K. Formation of Magnetite in the Presence of Ferric Oxyhydroxides. *Corros. Sci.* **1998,** *40*, 1239-1251.
(166) Kahani, S. A.; Jafari, M. A New Method for Preparation of Magnetite from Iron Oxyhydroxide or Iron Oxide and Ferrous Salt in Aqueous Solution. *J. Magn. Magn. Mater.* **2009,** *321*, 1951-1954.
(167) Mann, S.; Sparks, N. H. C.; Couling, S. B.; Larcombe, M. C.; Frankel, R. B. Crystallochemical Characterization of Magnetic Spinels Prepared from Aqueous Solution. *J. Chem. Soc., Faraday Trans. 1* **1989,** *85*, 3033-3044.
(168) Usman, M.; Abdelmoula, M.; Faure, P.; Ruby, C.; Hanna, K. Transformation of Various Kinds of Goethite into Magnetite: Effect of Chemical and Surface Properties. *Geoderma* **2013,** *197-198*, 9-16.
(169) Yang, L.; Steefel, C. I.; Marcus, M. A.; Bargar, J. R. Kinetics of Fe(II)-Catalyzed Transformation of 6-line Ferrihydrite under Anaerobic Flow Conditions. *Environ. Sci. Technol.* **2010,** *44*, 5469-5475.
(170) Larese-Casanova, P.; Scherer, M. M. Abiotic Transformation of Hexahydro-1,3,5-Trinitro-1,3,5-Triazine (RDX) by Green Rusts. *Environ. Sci. Technol.* **2008,** *42*, 3975-3981.
(171) Tamaura, Y. Ferrite Formation from the Intermediate, Green Rust II, in the Transformation Reaction of Ferric Hydroxide Oxide, .Gamma.-FeO(OH), in Aqueous Suspension. *Inorg. Chem.* **1985,** *24*, 4363-4366.
(172) Hansel, C. M.; Benner, S. G.; Neiss, J.; Dohnalkova, A.; Kukkadapu, R. K.; Fendorf, S. Secondary Mineralization Pathways Induced by Dissimilatory Iron Reduction of Ferrihydrite under Advective Flow. *Geochim. Cosmochim. Acta* **2003,** *67*, 2977-2992.
(173) Hansel, C. M.; Benner, S. G.; Fendorf, S. Competing Fe(II)-Induced Mineralization Pathways of Ferrihydrite. *Environ. Sci. Technol.* **2005,** *39*, 7147-7153.
(174) Fredrickson, J. K.; Zachara, J. M.; Kennedy, D. W.; Dong, H.; Onstott, T. C.; Hinman, N. W.; Li, S.-m. Biogenic Iron Mineralization Accompanying the Dissimilatory Reduction of Hydrous Ferric Oxide by a Groundwater Bacterium. *Geochim. Cosmochim. Acta* **1998,** *62*, 3239-3257.
(175) Belleville, P.; Jolivet, J.-P.; Tronc, E.; Livage, J. Crystallization of Ferric Hydroxide into Spinel by Adsorption on Colloidal Magnetite. *J. Colloid Interface Sci.* **1992,** *150*, 453-460.
(176) Handler, R. M.; Beard, B. L.; Johnson, C. M.; Scherer, M. M. Atom Exchange between Aqueous Fe(II) and Goethite: An Fe Isotope Tracer Study. *Environ. Sci. Technol.* **2009,** *43*, 1102-1107.
(177) Williams, A. G. B.; Scherer, M. M. Spectroscopic Evidence for Fe(II)-Fe(III) Electron Transfer at the Iron Oxide-Water Interface. *Environ. Sci. Technol.* **2004,** *38*, 4782-4790.

(178) Frierdich, A. J.; Helgeson, M.; Liu, C.; Wang, C.; Rosso, K. M.; Scherer, M. M. Iron Atom Exchange between Hematite and Aqueous Fe(II). *Environ. Sci. Technol.* **2015,** *49*, 8479-8486.
(179) Handler, R. M.; Frierdich, A. J.; Johnson, C. M.; Rosso, K. M.; Beard, B. L.; Wang, C.; Latta, D. E.; Neumann, A.; Pasakarnis, T.; Premaratne, W. A. P. J.et al. Fe(II)-Catalyzed Recrystallization of Goethite Revisited. *Environ. Sci. Technol.* **2014,** *48*, 11302-11311.
(180) Piepenbrock, A.; Dippon, U.; Porsch, K.; Appel, E.; Kappler, A. Dependence of Microbial Magnetite Formation on Humic Substance and Ferrihydrite Concentrations. *Geochim. Cosmochim. Acta* **2011,** *75*, 6844-6858.
(181) Barrón, V.; Galvez, N.; Hochella, M. F.; Torrent, J. Epitaxial Overgrowth of Goethite on Hematite Synthesized in Phosphate Media; A Scanning Force and Transmission Electron Microscopy Study. *Am. Mineral.* **1997,** *82*, 1091-1100.
(182) Borch, T.; Masue, Y.; Kukkadapu, R. K.; Fendorf, S. Phosphate Imposed Limitations on Biological Reduction and Alteration of Ferrihydrite. *Environ. Sci. Technol.* **2007,** *41*, 166-172.
(183) Benali, O.; Abdelmoula, M.; Refait, P.; Génin, J.-M. R. Effect of Orthophosphate on the Oxidation Products of Fe(II)-Fe(III) Hydroxycarbonate: The Transformation of Green Rust to Ferrihydrite. *Geochim. Cosmochim. Acta* **2001,** *65*, 1715-1726.
(184) Biber, M. V.; dos Santos Afonso, M.; Stumm, W. The Coordination Chemistry of Weathering: IV. Inhibition of the Dissolution of Oxide Minerals. *Geochim. Cosmochim. Acta* **1994,** *58*, 1999-2010.
(185) Dzombak, D. A.; Morel, F. M. *Surface Complexation Modeling: Hydrous Ferric Oxide*; John Wiley & Sons: New York, **1990**.
(186) Rusch, B.; Hanna, K.; Humbert, B. Sorption and Transport of Salicylate in a Porous Heterogeneous Medium of Silica Quartz and Goethite. *Environ. Sci. Technol.* **2010,** *44*, 2447-2453.
(187) Larese-Casanova, P.; Scherer, M. M. Fe(II) sorption on hematite: New insights based on spectroscopic measurements. *Environ. Sci. Technol.* **2007,** *41*, 471-477.
(188) Hiemstra, T.; Van Riemsdijk, W. H. A Surface Structural Approach to Ion Adsorption: The Charge Distribution (CD) Model. *J. Colloid Interface Sci.* **1996,** *179*, 488-508.
(189) Manceau, A.; Nagy, K. L.; Spadini, L.; Ragnarsdottir, K. V. Influence of Anionic Layer Structure of Fe-Oxyhydroxides on the Structure of Cd Surface Complexes. *J. Colloid Interface Sci.* **2000,** *228*, 306-316.
(190) Spadini, L.; Schindler, P. W.; Charlet, L.; Manceau, A.; Vala Ragnarsdottir, K. Hydrous Ferric Oxide: Evaluation of Cd-HFO Surface Complexation Models Combining CdK EXAFS Data, Potentiometric Titration Results, and Surface Site Structures Identified from Mineralogical Knowledge. *J. Colloid Interface Sci.* **2003,** *266*, 1-18.
(191) Weidler, P. G.; Hug, S. J.; Wetche, T. P.; Hiemstra, T. Determination of Growth Rates of (100) And (110) Faces of Synthetic Goethite by Scanning Force Microscopy. *Geochim. Cosmochim. Acta* **1998,** *62*, 3407-3412.
(192) Dixit, S.; Hering, J. G. Sorption of Fe(II) and As(III) on Goethite in Single- and Dual-Sorbate Systems. *Chem. Geol.* **2006,** *228*, 6-15.
(193) Chen, C.; Kukkadapu, R.; Sparks, D. L. Influence of Coprecipitated Organic Matter on $Fe^{2+}_{(aq)}$-Catalyzed Transformation of Ferrihydrite: Implications for Carbon Dynamics. *Environ. Sci. Technol.* **2015,** *49*, 10927-10936.

(194) Eusterhues, K.; Wagner, F. E.; Häusler, W.; Hanzlik, M.; Knicker, H.; Totsche, K. U.; Kögel-Knabner, I.; Schwertmann, U. Characterization of Ferrihydrite-Soil Organic Matter Coprecipitates by X-Ray Diffraction and Mössbauer Spectroscopy. *Environ. Sci. Technol.* **2008,** *42*, 7891-7897.
(195) Chen, C.; Dynes, J. J.; Wang, J.; Sparks, D. L. Probing the Site Occupancies of Co-, Ni-, and Mn-Substituted Biogenic Magnetite Using. *Environ. Sci. Technol.* **2014,** *48*, 13751-13759.
(196) Shimizu, M.; Zhou, J.; Schröder, C.; Obst, M.; Kappler, A.; Borch, T. Dissimilatory Reduction and Transformation of Ferrihydrite-Humic Acid Coprecipitates. *Environ. Sci. Technol.* **2013,** *47*, 13375-13384.
(197) Posth, N. R.; Canfield, D. E.; Kappler, A. Biogenic Fe(III) Minerals: From Formation to Diagenesis and Preservation in the Rock Record. *Earth-Sci. Rev.* **2014,** *135*, 103-121.
(198) Stumm, W.; Sulzberger, B. The Cycling of Iron in Natural Environments: Considerations Based on Laboratory Studies of Heterogeneous Redox Processes. *Geochim. Cosmochim. Acta* **1992,** *56*, 3233-3257.
(199) Boumaiza, H.; Naille, S.; Renard, A.; Grégoire, B.; Mallet, M.; Ruby, C. Chemical Transformation of Ferrihydrite Coating into Green Rust Followed by Raman and X-Ray Photoelectron Spectroscopies. *Desalin. Water Treat.* **2015,** *53*, 1031-1036.
(200) Usman, M.; Faure, P.; Hanna, K.; Abdelmoula, M.; Ruby, C. Application of Magnetite Catalyzed Chemical Oxidation (Fenton-Like and Persulfate) for the Remediation of Oil Hydrocarbon Contamination. *Fuel* **2012,** *96*, 270-276.
(201) Jones, A. M.; Collins, R. N.; Rose, J.; Waite, T. D. The Effect of Silica and Natural Organic Matter on the Fe(II)-Catalysed Transformation and Reactivity of Fe(III) Minerals. *Geochim. Cosmochim. Acta* **2009,** *73*, 4409-4422.
(202) Poulton, S. W.; Canfield, D. E. Ferruginous Conditions: A Dominant Feature of the Ocean through Earth's History. *Elements* **2011,** *7*, 107-112.
(203) Raiswell, R.; Canfield, D. E. The Iron Biogeochemical Cycle Past and Present. *Geochem. Perspect.* **2012,** *1*, 1-220.
(204) Klein, C. Some Precambrian Banded Iron-Formations (BIFs) from around the World: Their Age, Geologic Setting, Mineralogy, Metamorphism, Geochemistry, and Origins. *Am. Mineral.* **2005,** *90*, 1473-1499.
(205) Konhauser, K. O. Bacterial Iron Biomineralisation in Nature. *FEMS Microbiol. Rev.* **1997,** *20*, 315-326.
(206) Caccavo, F.; Lonergan, D. J.; Lovley, D. R.; Davis, M.; Stolz, J. F.; McInerney, M. J. *Geobacter sulfurreducens* sp. nov., A Hydrogen- and Acetate-Oxidizing Dissimilatory Metal-Reducing Microorganism. *Appl. Environ. Microbiol.* **1994,** *60*, 3752-3759.
(207) Lovley, D. R.; Phillips, E. J. P. Novel Mode of Microbial Energy-Metabolism - Organic-Carbon Oxidation Coupled to Dissimilatory Reduction of Iron or Manganese. *Appl. Environ. Microbiol.* **1988,** *54*, 1472-1480.
(208) Lovley, D. R.; Phillips, E. J. P.; Lonergan, D. J. Hydrogen and Formate Oxidation Coupled to Dissimilatory Reduction of Iron or Manganese by *Alteromonas putrefaciens*. *Appl. Environ. Microbiol.* **1989,** *55*, 700-706.
(209) MYERS, C. R.; NEALSON, K. H. Bacterial Manganese Reduction and Growth with Manganese Oxide as the Sole Electron Acceptor. *Science* **1988,** *240*, 1319-1321.

(210) Obuekwe, C. O.; Westlake, D. W. S.; Cook, F. D. Effect of Nitrate on Reduction of Ferric Iron by a Bacterium Isolated from Crude Oil. *Can. J. Microbiol.* **1981,** *27*, 692-697.
(211) Roden, E. E.; Lovley, D. R. Dissimilatory Fe(III) Reduction by the Marine Microorganism *Desulfuromonas acetoxidans*. *Appl. Environ. Microbiol.* **1993,** *59*, 734-742.
(212) Coates, J. D.; Ellis, D. J.; Gaw, C. V.; Lovley, D. R. *Geothrix fermentans* gen. nov., sp. nov., A Novel Fe(III)-Reducing Bacterium from a Hydrocarbon-Contaminated Aquifer. *Int. J. Syst. Evol. Microbiol.* **1999,** *49*, 1615-1622.
(213) Lovley, D. R.; Baedecker, M. J.; Lonergan, D. J.; Cozzarelli, I. M.; Phillips, E. J. P.; Siegel, D. I. Oxidation of Aromatic Contaminants Coupled to Microbial Iron Reduction. *Nature* **1989,** *339*, 297-300.
(214) Lovley, D. R.; Lonergan, D. J. Anaerobic Oxidation of Toluene, Phenol, and p-Cresol by the Dissimilatory Iron-Reducing Organism, GS-15. *Appl. Environ. Microbiol.* **1990,** *56*, 1858-1864.
(215) Nixon, S. L.; Cockell, C. S.; Tranter, M. Limitations to a Microbial Iron Cycle on Mars. *Planet. Space Sci.* **2012,** *72*, 116-128.
(216) Qu, B.; Fan, B.; Zhu, S.; Zheng, Y. Anaerobic Ammonium Oxidation with an Anode as the Electron Acceptor. *Environ. Microbiol. Rep.* **2014,** *6*, 100-105.
(217) Shrestha, J.; Rich, J. J.; Ehrenfeld, J. G.; Jaffe, P. R. Oxidation of Ammonium to Nitrite Under Iron-Reducing Conditions in Wetland Soils: Laboratory, Field Demonstrations, and Push-Pull Rate Determination. *Soil Sci.* **2009,** *174*, 156-164.
(218) Yang, W. H.; Weber, K. A.; Silver, W. L. Nitrogen Loss from Soil through Anaerobic Ammonium Oxidation Coupled to Iron Reduction. *Nature Geosci.* **2012,** *5*, 538-541.
(219) Beal, E. J.; House, C. H.; Orphan, V. J. Manganese- and Iron-Dependent Marine Methane Oxidation. *Science* **2009,** *325*, 184-187.
(220) Riedinger, N.; Formolo, M. J.; Lyons, T. W.; Henkel, S.; Beck, A.; Kasten, S. An Inorganic Geochemical Argument for Coupled Anaerobic Oxidation of Methane and Iron Reduction in Marine Sediments. *Geobiology* **2014,** *12*, 172-181.
(221) Segarra, K. E. A.; Comerford, C.; Slaughter, J.; Joye, S. B. Impact of Electron Acceptor Availability on the Anaerobic Oxidation of Methane in Coastal Freshwater and Brackish Wetland Sediments. *Geochim. Cosmochim. Acta* **2013,** *115*, 15-30.
(222) Lovley, D. R.; Woodward, J. C. Mechanisms for Chelator Stimulation of Microbial Fe(III)-Oxide Reduction. *Chem. Geol.* **1996,** *132*, 19-24.
(223) Roden, E. E. Fe(III) Oxide Reactivity Toward Biological versus Chemical Reduction. *Environ. Sci. Technol.* **2003,** *37*, 1319-1324.
(224) Roden, E. E. Geochemical and Microbiological Controls on Dissimilatory Iron Reduction. *C. R. Geosci.* **2006,** *338*, 456-467.
(225) Roden, E. E.; Zachara, J. M. Microbial Reduction of Crystalline Iron(III) Oxides: Influence of Oxide Surface Area and Potential for Cell Growth. *Environ. Sci. Technol.* **1996,** *30*, 1618-1628.
(226) Cutting, R. S.; Coker, V. S.; Fellowes, J. W.; Lloyd, J. R.; Vaughan, D. J. Mineralogical and Morphological Constraints on the Reduction of Fe(III) Minerals by *Geobacter sulfurreducens*. *Geochim. Cosmochim. Acta* **2009,** *73*, 4004-4022.

(227) Brown, D. A.; Sherriff, B. L.; Sawicki, J. A. Microbial Transformation of Magnetite to Hematite. *Geochim. Cosmochim. Acta* **1997,** *61*, 3341-3348.
(228) Kostka, J. E.; Dalton, D. D.; Skelton, H.; Dollhopf, S.; Stucki, J. W. Growth of Iron(III)-Reducing Bacteria on Clay Minerals as the Sole Electron Acceptor and Comparison of Growth Yields on a Variety of Oxidized Iron Forms. *Appl. Environ. Microbiol.* **2002,** *68*, 6256-6262.
(229) Kostka, J. E.; Nealson, K. H. Dissolution and Reduction of Magnetite by Bacteria. *Environ. Sci. Technol.* **1995,** *29*, 2535-2540.
(230) Kostka, J. E.; Stucki, J. W.; Nealson, K. H.; Wu, J. Reduction of Structural Fe(III) in Smectite by a Pure Culture of *Shewanella putrefaciens* Strain MR-1. *Clays Clay Miner.* **1996,** *44*, 522-529.
(231) Porsch, K.; Rijal, M. L.; Borch, T.; Troyer, L. D.; Behrens, S.; Wehland, F.; Appel, E.; Kappler, A. Impact of Organic Carbon and Iron Bioavailability on the Magnetic Susceptibility of Soils. *Geochim. Cosmochim. Acta* **2014,** *128*, 44-57.
(232) Melton, E. D.; Swanner, E. D.; Behrens, S.; Schmidt, C.; Kappler, A. The Interplay of Microbially Mediated and Abiotic Reactions in the Biogeochemical Fe Cycle. *Nat Rev Micro* **2014,** *12*, 797-808.
(233) Shi, L.; Dong, H.; Reguera, G.; Beyenal, H.; Lu, A.; Liu, J.; Yu, H.-Q.; Fredrickson, J. K. Extracellular Electron Transfer Mechanisms between Microorganisms and Minerals. *Nat Rev Micro* **2016,** *14*, 651-662.
(234) Byrne, J. M.; Telling, N. D.; Coker, V. S.; Pattrick, R. A. D.; van der Laan, G.; Arenholz, E.; Tuna, F.; Lloyd, J. R. Control of Nanoparticle Size, Reactivity and Magnetic Properties During the Bioproduction of Magnetite by *Geobacter sulfurreducens*. *Nanotechnology* **2011,** *22*, 455709.
(235) Dippon, U.; Schmidt, C.; Behrens, S.; Kappler, A. Secondary Mineral Formation During Ferrihydrite Reduction by *Shewanella oneidensis* MR-1 Depends on Incubation Vessel Orientation and Resulting Gradients of Cells, Fe^{2+} and Fe Minerals. *Geomicrobiol. J.* **2015,** *32*, 878-889.
(236) Sundman, A.; Byrne, J. M.; Bauer, I.; Menguy, N.; Kappler, A. Interactions Between Magnetite and Humic Substances: Redox Reactions and Dissolution Processes. *Geochem. Trans.* **2017,** *18*, 6.
(237) Klueglein, N.; Lösekann-Behrens, T.; Obst, M.; Behrens, S.; Appel, E.; Kappler, A. Magnetite Formation by the Novel Fe (III)-Reducing *Geothrix fermentans* Strain HradG1 Isolated from a Hydrocarbon-Contaminated Sediment with Increased Magnetic Susceptibility. *Geomicrobiol. J.* **2013,** *30*, 863-873.
(238) Wu, W.; Li, B.; Hu, J.; Li, J.; Wang, F.; Pan, Y. Iron Reduction and Magnetite Biomineralization Mediated by a Deep‐Sea Iron‐Reducing Bacterium *Shewanella piezotolerans* WP3. *J. Geophys. Res.: Biogeosci.* **2011,** *116*.
(239) Etique, M.; Jorand, F. P.; Ruby, C. Magnetite as a Precursor for Green Rust through the Hydrogenotrophic Activity of the Iron‐Reducing Bacteria *Shewanella putrefaciens*. *Geobiology* **2015,** *14*, 237-254.
(240) Ona-Nguema, G.; Abdelmoula, M.; Jorand, F.; Benali, O.; Géhin, A.; Block, J. C.; Génin, J. M. R. Microbial Reduction of Lepidocrocite γ-FeOOH by *Shewanella putrefaciens*; The Formation of Green Rust. *Hyperfine Interact.* **2002,** *139*, 231-237.
(241) O'Loughlin, E. J.; Larese-Casanova, P.; Scherer, M.; Cook, R. Green Rust Formation from the Bioreduction of γ–FeOOH (Lepidocrocite): Comparison of Several Shewanella Species. *Geomicrobiol. J.* **2007,** *24*, 211-230.

(242) Zhang, C.; Vali, H.; Romanek, C. S.; Phelps, T. J.; Liu, S. V. Formation of Single-Domain Magnetite by a Thermophilic Bacterium. *Am. Mineral.* **1998,** *83*, 1409-1418.
(243) Konhauser, K. O.; Kappler, A.; Roden, E. E. Iron in Microbial Metabolisms. *Elements* **2011,** *7*, 89-93.
(244) Emerson, D. Biogeochemistry and Microbiology of Microaerobic Fe(II) Oxidation. *Biochem. Soc. Trans.* **2012,** *40*, 1211-1216.
(245) Bird, L. J.; Bonnefoy, V.; Newman, D. K. Bioenergetic Challenges of Microbial Iron Metabolisms. *Trends Microbiol.* **2011,** *19*, 330-340.
(246) Barco, R. A.; Emerson, D.; Sylvan, J. B.; Orcutt, B. N.; Jacobson Meyers, M. E.; Ramírez, G. A.; Zhong, J. D.; Edwards, K. J. New Insight into Microbial Iron Oxidation as Revealed by the Proteomic Profile of an Obligate Iron-Oxidizing Chemolithoautotroph. *Appl. Environ. Microbiol.* **2015,** *81*, 5927-5937.
(247) Gault, A. G.; Langley, S.; Ibrahim, A.; Renaud, R.; Takahashi, Y.; Boothman, C.; Lloyd, J. R.; Clark, I. D.; Ferris, F. G.; Fortin, D. Seasonal Changes In Mineralogy, Geochemistry and Microbial Community of Bacteriogenic Iron Oxides (BIOS) Deposited in a Circumneutral Wetland. *Geomicrobiol. J.* **2012,** *29*, 161-172.
(248) Chan, C. S.; Fakra, S. C.; Emerson, D.; Fleming, E. J.; Edwards, K. J. Lithotrophic Iron-Oxidizing Bacteria Produce Organic Stalks to Control Mineral Growth: Implications for Biosignature Formation. *The ISME journal* **2011,** *5*, 717-727.
(249) Amstaetter, K.; Borch, T.; Kappler, A. Influence of Humic Acid Imposed Changes of Ferrihydrite Aggregation on Microbial Fe(III) Reduction. *Geochim. Cosmochim. Acta* **2012,** *85*, 326-341.
(250) Toner, B. M.; Berquó, T. S.; Michel, F. M.; Sorensen, J. V.; Templeton, A. S.; Edwards, K. J. Mineralogy of Iron Microbial Mats from Loihi Seamount. *Front. Microbiol.* **2012,** *3*.
(251) Benz, M.; Brune, A.; Schink, B. Anaerobic and Aerobic Oxidation of Ferrous Iron at Neutral pH by Chemoheterotrophic Nitrate-Reducing Bacteria. *Arch. Microbiol.* **1998,** *169*, 159-165.
(252) Kappler, A.; Schink, B.; Newman, D. K. Fe(III) Mineral Formation and Cell Encrustation by the Nitrate-Dependent Fe(II)-Oxidizer strain BoFeN1. *Geobiology* **2005,** *3*, 235-245.
(253) Lack, J.; Chaudhuri, S.; Chakraborty, R.; Achenbach, L.; Coates, J. Anaerobic Biooxidation of Fe (II) by *Dechlorosoma suillum*. *Microb. Ecol.* **2002,** *43*, 424-431.
(254) Straub, K. L.; Benz, M.; Schink, B.; Widdel, F. Anaerobic, Nitrate-Dependent Microbial Oxidation of Ferrous Iron. *Appl. Environ. Microbiol.* **1996,** *62*, 1458-1460.
(255) Weber, K. A.; Hedrick, D. B.; Peacock, A. D.; Thrash, J. C.; White, D. C.; Achenbach, L. A.; Coates, J. D. Physiological and Taxonomic Description of the Novel Autotrophic, Metal Oxidizing Bacterium, *Pseudogulbenkiania* sp. strain 2002. *Appl. Microbiol. Biotechnol.* **2009,** *83*, 555-565.
(256) Chakraborty, A.; Picardal, F. Induction of Nitrate-Dependent Fe(II) Oxidation by Fe(II) in *Dechloromonas* sp. strain UWNR4 and A*cidovorax* sp. strain 2AN. *Appl. Environ. Microbiol.* **2013,** *79*, 748-752.

(257) Muehe, E. M.; Gerhardt, S.; Schink, B.; Kappler, A. Ecophysiology and the Energetic Benefit of Mixotrophic Fe(II) Oxidation by Various Strains of Nitratereducing Bacteria. *FEMS Microbiol. Ecol.* **2009,** *70*, 335-343.
(258) Byrne-Bailey, K. G.; Weber, K. A.; Bose, S.; Knox, T.; Spanbauer, T. L.; Chertkov, O.; Coates, J. D. Completed Genome Sequence of the Anaerobic Iron-Oxidizing Bacterium *Acidovorax ebreus* strain TPSY. *J. Bacteriol.* **2010,** *192*, 1475-1476.
(259) Coates, J. D.; Chakraborty, R.; Lack, J. G.; O'Connor, S. M.; Cole, K. A.; Bender, K. S.; Achenbach, L. A. Anaerobic Benzene Oxidation Coupled to Nitrate Reduction in Pure Culture by Two Strains of Dechloromonas. *Nature* **2001,** *411*, 1039-1043.
(260) Klueglein, N.; Kappler, A. Abiotic Oxidation of Fe(II) by Reactive Nitrogen Species in Cultures of the Nitrate-Reducing Fe(II) Oxidizer *Acidovorax* sp. BoFeN1 – Questioning the Existence of Enzymatic Fe(II) Oxidation. *Geobiology* **2012,** *11*, 396.
(261) Klueglein, N.; Zeitvogel, F.; Stierhof, Y.-D.; Floetenmeyer, M.; Konhauser, K. O.; Kappler, A.; Obst, M. Potential Role of Nitrite for Abiotic Fe (II) Oxidation and Cell Encrustation During Nitrate Reduction by Denitrifying Bacteria. *Appl. Environ. Microbiol.* **2014,** *80*, 1051-1061.
(262) Hafenbradl, D.; Keller, M.; Dirmeier, R.; Rachel, R.; Roßnagel, P.; Burggraf, S.; Huber, H.; Stetter, K. O. *Ferroglobus placidus* gen. nov., sp. nov., A Novel Hyperthermophilic Archaeum that Oxidizes Fe^{2+} at Neutral pH under Anoxic Conditions. *Arch. Microbiol.* **1996,** *166*, 308-314.
(263) Kumaraswamy, R.; Sjollema, K.; Kuenen, G.; Van Loosdrecht, M.; Muyzer, G. Nitrate-Dependent [Fe(II) EDTA] $^{2-}$ Oxidation by *Paracoccus ferrooxidans* sp. nov., Isolated from a Denitrifying Bioreactor. *Syst. Appl. Microbiol.* **2006,** *29*, 276-286.
(264) Li, B.; Tian, C.; Zhang, D.; Pan, X. Anaerobic Nitrate-Dependent Iron(II) Oxidation by a Novel Autotrophic Bacterium, *Citrobacter freundii* strain PXL1. *Geomicrobiol. J.* **2014,** *31*, 138-144.
(265) Mattes, A.; Gould, D.; Taupp, M.; Glasauer, S. A Novel Autotrophic Bacterium Isolated from an Engineered Wetland System Links Nitrate-Coupled Iron Oxidation to the Removal of as, Zn and S. *Water, Air, Soil Pollut.* **2013,** *224*, 1-15.
(266) Shelobolina, E.; Konishi, H.; Xu, H.; Benzine, J.; Xiong, M.; Wu, T.; Blöthe, M.; Roden, E. Isolation of Phyllosilicate–Iron Redox Cycling Microorganisms from an Illite–Smectite Rich Hydromorphic Soil. *Front. Microbiol.* **2012,** *3*, 1.
(267) Weber, K. A.; Pollock, J.; Cole, K. A.; O'Connor, S. M.; Achenbach, L. A.; Coates, J. D. Anaerobic Nitrate-Dependent Iron(II) Bio-Oxidation by a Novel Lithoautotrophic Betaproteobacterium, Strain 2002. *Appl. Environ. Microbiol.* **2006,** *72*, 686-694.
(268) Zhou, J.; Wang, H.; Yang, K.; Ji, B.; Chen, D.; Zhang, H.; Sun, Y.; Tian, J. Autotrophic Denitrification by Nitrate-Dependent Fe(II) Oxidation in a Continuous up-Flow Biofilter. *Bioprocess Biosyst. Eng.* **2016,** *39*, 277-284.
(269) Su, J. F.; Shao, S. C.; Huang, T. L.; Ma, F.; Yang, S. F.; Zhou, Z. M.; Zheng, S. C. Anaerobic Nitrate-Dependent Iron(II) Oxidation by a Novel Autotrophic Bacterium, *Pseudomonas* sp. SZF15. *J. Environ. Chem. Eng.* **2015,** *3*, 2187-2193.
(270) Schädler, S.; Burkhardt, C.; Hegler, F.; Straub, K.; Miot, J.; Benzerara, K.; Kappler, A. Formation of Cell-Iron-Mineral Aggregates by Phototrophic and

Nitrate-Reducing Anaerobic Fe(II)-Oxidizing Bacteria. *Geomicrobiol. J.* **2009,** *26*, 93-103.

(271) Schmid, G.; Zeitvogel, F.; Hao, L.; Ingino, P.; Flötenmeyer, M.; Stierhof, Y. D.; Schröppel, B.; Burkhardt, C.; Kappler, A.; Obst, M. 3‐D Analysis of Bacterial Cell‐(Iron) Mineral Aggregates Formed During Fe(II) Oxidation by the Nitrate‐Reducing *Acidovorax* sp. Strain BoFeN1 Using Complementary Microscopy Tomography Approaches. *Geobiology* **2014,** *12*, 340-361.

(272) Nordhoff, M.; Tominski, C.; Halama, M.; Byrne, J. M.; Obst, M.; Kleindienst, S.; Behrens, S.; Kappler, A. Insights into Nitrate-Reducing Fe(II) Oxidation Mechanisms by Analyzing Cell-Mineral Associations, Cell Encrustation and Mineralogy in the Chemolithoautotrophic Nitrate-Reducing Fe(II)-Oxidizing Enrichment Culture KS. *Appl. Environ. Microbiol.* **2017,** *83*, e00752-17.

(273) Park, S.; Kim, D.-H.; Lee, J.-H.; Hur, H.-G. Sphaerotilus natans Encrusted with Nanoball-Shaped Fe(III) Oxide Minerals Formed by Nitrate-Reducing Mixotrophic Fe(II) Oxidation. *FEMS Microbiol. Ecol.* **2014,** *90*, 68-77.

(274) Pantke, C.; Obst, M.; Benzerara, K.; Morin, G.; Ona-Nguema, G.; Dippon, U.; Kappler, A. Green Rust Formation during Fe(II) Oxidation by the Nitrate-Reducing Acidovorax sp. Strain BoFeN1. *Environ. Sci. Technol.* **2012,** *46*, 1439-1446.

(275) Etique, M.; Jorand, F. d. r. P.; Zegeye, A.; Grégoire, B.; Despas, C.; Ruby, C. Abiotic Process for Fe (II) Oxidation and Green Rust Mineralization Driven by a Heterotrophic Nitrate Reducing Bacteria (*Klebsiella mobilis*). *Environ. Sci. Technol.* **2014,** *48*, 3742-3751.

(276) Miot, J.; Li, J.; Benzerara, K.; Sougrati, M. T.; Ona-Nguema, G.; Bernard, S.; Jumas, J.-C.; Guyot, F. Formation of Single Domain Magnetite by Green Rust Oxidation Promoted by Microbial Anaerobic Nitrate-Dependent Iron Oxidation. *Geochim. Cosmochim. Acta* **2014,** *139*, 327-343.

(277) Chaudhuri, S. K.; Lack, J. G.; Coates, J. D. Biogenic Magnetite Formation through Anaerobic Biooxidation of Fe(II). *Appl. Environ. Microbiol.* **2001,** *67*, 2844-2848.

(278) Dippon, U.; Pantke, C.; Porsch, K.; Larese-Casanova, P.; Kappler, A. Potential Function of Added Minerals as Nucleation Sites and Effect of Humic Substances on Mineral Formation by the Nitrate-Reducing Fe(II)-Oxidizing Strain *Acidovorac* sp. BoFeN1. *Environ. Sci. Technol.* **2012,** *46*, 6556-6565.

(279) O'Loughlin, E. J.; Gorski, C. A.; Scherer, M. M.; Boyanov, M. I.; Kemner, K. M. Effects of Oxyanions, Natural Organic Matter, and Bacterial Cell Numbers on the Bioreduction of Lepidocrocite (γ-FeOOH) and the Formation of Secondary Mineralization Products. *Environ. Sci. Technol.* **2010,** *44*, 4570-4576.

(280) Coker, V. S.; Pearce, C. I.; Lang, C.; van der Laan, G.; Pattrick, R. A. D.; Telling, N. D.; Schüler, D.; Arenholz, E.; Lloyd, J. R. Cation Site Occupancy of Biogenic Magnetite Compared to Polygenic Ferrite Spinels Determined by X-Ray Magnetic Circular Dichroism. *Eur. J. Mineral.* **2007,** *19*, 707-716.

(281) Lam, K. P.; Hitchcock, A. P.; Obst, M.; Lawrence, J. R.; Swerhone, G. D. W.; Leppard, G. G.; Tyliszczak, T.; Karunakaran, C.; Wang, J.; Kaznatcheev, K.et al. Characterizing Magnetism of Individual Magnetosomes by X-Ray Magnetic Circular Dichroism in a Scanning Transmission X-Ray Microscope. *Chem. Geol.* **2010,** *270*, 110-116.

(282) Kappler, A.; Newman, D. K. Formation of Fe(III)-Minerals by Fe(II)-Oxidizing Photoautotrophic Bacteria. *Geochim. Cosmochim. Acta* **2004,** *68*, 1217-1226.
(283) Wu, W.; Swanner, E. D.; Hao, L.; Zeitvogel, F.; Obst, M.; Pan, Y.; Kappler, A. Characterization of the Physiology and Cell–Mineral Interactions of the Marine Anoxygenic Phototrophic Fe(II) Oxidizer *Rhodovulum iodosum* – Implications for Precambrian Fe(II) Oxidation. *FEMS Microbiol. Ecol.* **2014,** *88*, 503-515.
(284) Jiao, Y.; Kappler, A.; Croal, L. R.; Newman, D. K. Isolation and Characterization of a Genetically Tractable Photoautotrophic Fe(II)-Oxidizing Bacterium, *Rhodopseudomonas palustris* Strain TIE-1. *Appl. Environ. Microbiol.* **2005,** *71*, 4487-4496.
(285) Straub, K. L.; Rainey, F. A.; Widdel, F. *Rhodovulum iodosum* sp. nov. and *Rhodovulum robiginosum* sp. nov., Two New Marine Phototrophic Ferrous-Iron-Oxidizing Purple Bacteria. *Int. J. Syst. Evol. Microbiol.* **1999,** *49*, 729-735.
(286) Crowe, S. A.; Jones, C.; Katsev, S.; Magen, C.; O'Neill, A. H.; Sturm, A.; Canfield, D. E.; Haffner, G. D.; Mucci, A.; Sundby, B. Photoferrotrophs Thrive in an Archean Ocean Analogue. *Proc. Natl. Acad. Sci. U. S. A.* **2008,** *105*, 15938-15943.
(287) Crowe, S. A.; O'Neill, A. H.; Katsev, S.; Hehanussa, P.; Haffner, G. D.; Sundby, B.; Mucci, A.; Fowle, D. A. The Biogeochemistry of Tropical Lakes: A Case Study from Lake Matano, Indonesia. *Limnol. Oceanogr.* **2008,** *53*, 319-331.
(288) Faivre, D.; Godec, T. U. From Bacteria to Mollusks: The Principles Underlying the Biomineralization of Iron Oxide Materials. *Angew. Chem. Int. Ed.* **2015,** *54*, 4728-4747.
(289) Lin, W.; Bazylinski, D. A.; Xiao, T.; Wu, L.-F.; Pan, Y. Life with Compass: Diversity and Biogeography of Magnetotactic Bacteria. *Environ. Microbiol.* **2014,** *16*, 2646-2658.
(290) Blakemore, R. Magnetotactic Bacteria. *Science* **1975,** *190*, 377-379.
(291) Bazylinski, D. A.; Moskowitz, B. M. Microbial Biomineralization of Magnetic Iron Minerals; Microbiology, Magnetism and Environmental Significance. *Rev. Mineral. Geochem.* **1997,** *35*, 181-223.
(292) Bazylinski, D. A.; Frankel, R. B. Magnetosome Formation in Prokaryotes. *Nat. Rev. Microbiol.* **2004,** *2*, 217-230.
(293) Blakemore, R.; Short, K.; Bazylinski, D.; Rosenblatt, C.; Frankel, R. B. Microaerobic Conditions are Required for Magnetite Formation within *Aquaspirillum magnetotacticum*. *Geomicrobiol. J.* **1985,** *4*, 53-71.
(294) Uebe, R.; Schüler, D. Magnetosome Biogenesis in Magnetotactic Bacteria. *Nat. Rev. Microbiol.* **2016,** *14*, 621-637.
(295) Lohße, A.; Borg, S.; Raschdorf, O.; Kolinko, I.; Tompa, É.; Pósfai, M.; Faivre, D.; Baumgartner, J.; Schüler, D. Genetic Dissection of the mamAB and mms6 Operons Reveals a Gene Set Essential for Magnetosome Biogenesis in *Magnetospirillum gryphiswaldense*. *J. Bacteriol.* **2014,** *196*, 2658-2669.
(296) Komeili, A.; Li, Z.; Newman, D. K.; Jensen, G. J. Magnetosomes Are Cell Membrane Invaginations Organized by the Actin-Like Protein MamK. *Science* **2006,** *311*, 242-245.

(297) Komeili, A.; Vali, H.; Beveridge, T. J.; Newman, D. K. Magnetosome Vesicles Are Present before Magnetite Formation, and MamA is Required for Their Activation. *Proc. Natl. Acad. Sci. U. S. A.* **2004,** *101*, 3839-3844.
(298) Raschdorf, O.; Forstner, Y.; Kolinko, I.; Uebe, R.; Plitzko, J. M.; Schüler, D. Genetic and Ultrastructural Analysis Reveals the Key Players and Initial Steps of Bacterial Magnetosome Membrane Biogenesis. *PLOS Genet.* **2016,** *12*, e1006101.
(299) Faivre, D.; Schuler, D. Magnetotactic Bacteria and Magnetosomes. *Chem. Rev.* **2008,** *108*, 4875-4898.
(300) Grünberg, K.; Müller, E.-C.; Otto, A.; Reszka, R.; Linder, D.; Kube, M.; Reinhardt, R.; Schüler, D. Biochemical and Proteomic Analysis of the Magnetosome Membrane in *Magnetospirillum gryphiswaldense*. *Appl. Environ. Microbiol.* **2004,** *70*, 1040-1050.
(301) Bazylinski, D. A.; Frankel, R. B. Biologically Controlled Mineralization in Prokaryotes. *Rev. Mineral. Geochem.* **2003,** *54*, 217-247.
(302) Amor, M.; Busigny, V.; Durand-Dubief, M.; Tharaud, M.; Ona-Nguema, G.; Gélabert, A.; Alphandéry, E.; Menguy, N.; Benedetti, M. F.; Chebbi, I. Chemical Signature of Magnetotactic Bacteria. *Proc. Natl. Acad. Sci. U. S. A.* **2015,** *112*, 1699-1703.
(303) Staniland, S.; Williams, W.; Telling, N. D.; van der Laan, G.; Harrison, A.; Ward, B. Controlled Cobalt Doping of Magnetosomes *In Vivo*. *Nat. Nanotechnol.* **2008,** *3*, 158-162.
(304) Tanaka, M.; Brown, R.; Hondow, N.; Arakaki, A.; Matsunaga, T.; Staniland, S. Highest Levels of Cu, Mn and Co Doped into Nanomagnetic Magnetosomes through Optimized Biomineralisation. *J. Mater. Chem.* **2012,** *22*, 11919-11921.
(305) Bazylinski, D. A.; Frankel, R. B. Magnetic Iron Oxide and Iron Sulfide Minerals within Microorganisms. In *Biomineralization: From Biology to Biotechnology and Medical Application*; Wiley-VCH, 2000, 25-46.
(306) Schüler, D. Formation of Magnetosomes in Magnetotactic Bacteria. *J. Mol. Microbiol. Biotechnol.* **1999,** *1*, 79-86.
(307) Butler, R. F.; Banerjee, S. K. Theoretical Single‐Domain Grain Size Range in Magnetite and Titanomagnetite. *J. Geophys. Res.* **1975,** *80*, 4049-4058.
(308) Blakemore, R. P. Magnetotactic Bacteria. *Annu. Rev. Microbiol.* **1982,** *36*, 217-238.
(309) Guo, F. F.; Yang, W.; Jiang, W.; Geng, S.; Peng, T.; Li, J. L. Magnetosomes Eliminate Intracellular Reactive Oxygen Species in *Magnetospirillum gryphiswaldense* MSR‐1. *Environ. Microbiol.* **2012,** *14*, 1722-1729.
(310) Bazylinski, D. A.; Frankel, R. B.; Konhauser, K. O. Modes of Biomineralization of Magnetite by Microbes. *Geomicrobiol. J.* **2007,** *24*, 465-475.
(311) Simmons, S. L.; Edwards, K. J. Geobiology of Magnetotactic Bacteria. In *Magnetoreception and Magnetosomes in Bacteria*; Springer, 2006, 77-102.
(312) Vali, H.; Kirschvink, J. L. Observations of Magnetosome Organization, Surface Structure, and Iron Biomineralization of Undescribed Magnetic Bacteria: Evolutionary Speculations. In *Iron biominerals*; Springer, 1991, 97-115.
(313) Byrne, J. M.; Klueglein, N.; Pearce, C.; Rosso, K. M.; Appel, E.; Kappler, A. Redox Cycling of Fe(II) and Fe(III) in Magnetite by Fe-Metabolizing Bacteria. *Science* **2015,** *347*, 1473-1476.

(314) Gorby, Y. A.; Beveridge, T. J.; Blakemore, R. P. Characterization of the Bacterial Magnetosome Membrane. *J. Bacteriol.* **1988,** *170*, 834-841.
(315) Chang, S.-B. R.; Kirschvink, J. L. Magnetofossils, the Magnetization of Sediments, and the Evolution of Magnetite Biomineralization. *Annu. Rev. Earth Planet. Sci.* **1989,** *17*, 169.
(316) Kirschvink, J.; Lowenstam, H. Mineralization and Magnetization of Chiton Teeth: Paleomagnetic, Sedimentologic, and Biologic Implications of Organic Magnetite. *Earth. Planet. Sci. Lett.* **1979,** *44*, 193-204.
(317) Stolz, J. F.; Lovley, D. R.; Haggerty, S. E. Biogenic Magnetite and the Magnetization of Sediments. *J. Geophys. Res.: Solid Earth* **1990,** *95*, 4355-4361.
(318) McKay, D. S.; Gibson, E. K.; Thomas-Keprta, K. L.; Vali, H.; Romanek, C. S.; Clemett, S. J.; Chillier, X. D. F.; Maechling, C. R.; Zare, R. N. Search for Past Life on Mars: Possible Relic Biogenic Activity in Martian Meteorite ALH84001. *Science* **1996,** *273*, 924-930.
(319) Treiman, A. Martian Life "Still Kicking" in Meteorite ALH84001. *Trans., Am. Geophys. Union* **1999,** *80*, 205-209.
(320) Kopp, R. E.; Kirschvink, J. L. The Identification and Biogeochemical Interpretation of Fossil Magnetotactic Bacteria. *Earth-Sci. Rev.* **2008,** *86*, 42-61.
(321) Lovley, D. R.; Stolz, J. F.; Nord, G. L.; Phillips, E. J. P. Anaerobic Production of Magnetite by a Dissimilatory Iron-Reducing Microorganism. *Nature* **1987,** *330*, 252-254.
(322) Amor, M.; Busigny, V.; Louvat, P.; Gélabert, A.; Cartigny, P.; Durand-Dubief, M.; Ona-Nguema, G.; Alphandéry, E.; Chebbi, I.; Guyot, F. Mass-Dependent and-Independent Signature of Fe Isotopes in Magnetotactic Bacteria. *Science* **2016,** *352*, 705-708.
(323) Kim, W.; Suh, C.-Y.; Cho, S.-W.; Roh, K.-M.; Kwon, H.; Song, K.; Shon, I.-J. A New Method for the Identification and Quantification of Magnetite–Maghemite Mixture Using Conventional X-Ray Diffraction Technique. *Talanta* **2012,** *94*, 348-352.
(324) Itoh, H.; Sugimoto, T. Systematic Control of Size, Shape, Structure, and Magnetic Properties Of uniform Magnetite and Maghemite Particles. *J. Colloid Interface Sci.* **2003,** *265*, 283-295.
(325) Mikhaylova, A. B.; Sirotinkin, V. P.; Fedotov, M. A.; Korneyev, V. P.; Shamray, B. F.; Kovalenko, L. V. Quantitative Determination of Content of Magnetite and Maghemite in Their Mixtures by X-Ray Diffraction Methods. *Inorg. Mater: Appl. Res.* **2016,** *7*, 130-136.
(326) Faivre, D. *Iron Oxides: From Nature to Applications*; John Wiley & Sons, **2016**.
(327) Pearce, C. I.; Qafoku, O.; Liu, J.; Arenholz, E.; Heald, S. M.; Kukkadapu, R. K.; Gorski, C. A.; Henderson, C. M. B.; Rosso, K. M. Synthesis and Properties of Titanomagnetite ($Fe_{3-x}Ti_xO_4$) Nanoparticles: A Tunable Solid-State Fe(II/III) Redox System. *J. Colloid Interface Sci.* **2012,** *387*, 24-38.
(328) Kone, T.; Hanna, K.; Usman, M. Interactions of Synthetic Fe(II)-Fe(III) Green Rusts with Pentachlorophenol under Various Experimental Conditions. *Colloids Surf., A* **2011,** *385*, 152-158.
(329) Ruby, C.; Abdelmoula, M.; Naille, S.; Renard, A.; Khare, V.; Ona-Nguema, G.; Morin, G.; Génin, J.-M. R. Oxidation Modes and Thermodynamics of Fe^{II-}

^{III} Oxyhydroxycarbonate Green Rust: Dissolution–Precipitation Versus in Situ Deprotonation. *Geochim. Cosmochim. Acta* **2010,** *74*, 953-966.
(330) Guilbaud, R.; White, M. L.; Poulton, S. W. Surface Charge and Growth of Sulphate and Carbonate Green Rust in Aqueous Media. *Geochim. Cosmochim. Acta* **2013,** *108*, 141-153.
(331) Jones, C. J.; Chattopadhyay, S.; Gonzalez-Pech, N. I.; Avendano, C.; Hwang, N.; Lee, S. S.; Cho, M.; Ozarowski, A.; Prakash, A.; Mayo, J. T.et al. A Novel, Reactive Green Iron Sulfide (Sulfide Green Rust) Formed on Iron Oxide Nanocrystals. *Chem. Mater.* **2015,** *27*, 700-707.
(332) Jones, C. *Iron: From Synthesis, Characterization, and Application of Sulfide Green Rust to Viability in Arsenic Water Treatment*; Rice University, **2013**.
(333) Mossbauer, R. L. Kernresonanzfluoreszenz von Gammastrahlung in Ir-191. *Z. Phys.* **1958,** *151*, 124-143.
(334) Klingelhöfer, G.; Morris, R. V.; Bernhardt, B.; Rodionov, D.; de Souza, P. A.; Squyres, S. W.; Foh, J.; Kankeleit, E.; Bonnes, U.; Gellert, R.et al. Athena MIMOS II Mössbauer Spectrometer Investigation. *J. Geophys. Res.: Planets* **2003,** *108*, 8067.
(335) Markovski, C.; Byrne, J. M.; Lalla, E.; Lozano-Gorrín, A.; Klingelhoefer, G.; Rull, F.; Kappler, A.; Hoffmann, T.; Schröder, C. Abiotic Versus Biotic Iron Mineral Transformation Studied by a Miniaturized Backscattering Mössbauer Spectrometer (MIMOS II), X-Ray Diffraction and Raman Spectroscopy. *Icarus* **2017,** *296*, 49-58.
(336) Dyar, M. D.; Agresti, D. G.; Schaefer, M. W.; Grant, C. A.; Sklute, E. C. Mössbauer Spectroscopy of Earth and Planetary Materials. *Annu. Rev. Earth Planet. Sci.* **2006,** *34*, 83-125.
(337) Morice, J. A.; Rees, L. V. C.; Rickard, D. T. Mössbauer Studies of Iron Sulphides. *J. Inorg. Nucl. Chem.* **1969,** *31*, 3797-3802.
(338) Kündig, W.; Steven Hargrove, R. Electron Hopping in Magnetite. *Solid State Commun.* **1969,** *7*, 223-227.
(339) Srivastava, C. M.; Shringi, S. N.; Babu, M. V. Mössbauer Study of the Low-Temperature Phase of Magnetite. *Phys. Status Solidi A* **1981,** *65*, 731-735.
(340) Génin, J.-M. R.; Bourrié, G.; Trolard, F.; Abdelmoula, M.; Jaffrezic, A.; Refait, P.; Maitre, V.; Humbert, B.; Herbillon, A. Thermodynamic Equilibria in Aqueous Suspensions of Synthetic and Natural Fe(II)−Fe(III) Green Rusts: Occurrences of the Mineral in Hydromorphic Soils. *Environ. Sci. Technol.* **1998,** *32*, 1058-1068.
(341) De Faria, D.; Venâncio Silva, S.; De Oliveira, M. Raman Microspectroscopy of Some Iron Oxides and Oxyhydroxides. *J. Raman Spectrosc.* **1997,** *28*, 873-878.
(342) Labbé, J.; Lédion, J.; Hui, F. Infrared Spectrometry for Solid Phase Analysis: Corrosion Rusts. *Corros. Sci.* **2008,** *50*, 1228-1234.
(343) Gotić, M.; Musić, S. Mössbauer, FT-IR and FE SEM Investigation of Iron Oxides Precipitated from $FeSO_4$ Solutions. *J. Mol. Struct.* **2007,** *834*, 445-453.
(344) Pérez, F.; Barrero, C.; Walker, A. H.; García, K.; Nomura, K. Effects of Chloride Concentration, Immersion Time and Steel Composition on the Spinel Phase Formation. *Mater. Chem. Phys.* **2009,** *117*, 214-223.
(345) Pérez, F.; Barrero, C.; García, K. Factors Affecting the Amount of Corroded Iron Converted into Adherent Rust in Steels Submitted to Immersion Tests. *Corros. Sci.* **2010,** *52*, 2582-2591.

(346) Jubb, A. M.; Allen, H. C. Vibrational Spectroscopic Characterization of Hematite, Maghemite, and Magnetite Thin Films Produced by Vapor Deposition. *ACS Appl. Mater. Interfaces* **2010,** *2*, 2804-2812.
(347) Chamritski, I.; Burns, G. Infrared-and Raman-Active Phonons of Magnetite, Maghemite, and Hematite: A Computer Simulation and Spectroscopic Study. *J. Phys. Chem. B* **2005,** *109*, 4965-4968.
(348) Serna, C. J.; Rendon, J. L.; Iglesias, J. E. Infrared Surface Modes in Corundum-Type Microcrystalline Oxides. *Spectrochim. Acta, Part A* **1982,** *38*, 797-802.
(349) Shebanova, O. N.; Lazor, P. Raman Spectroscopic Study of Magnetite ($FeFe_2O_4$): A New Assignment for the Vibrational Spectrum. *J. Solid State Chem.* **2003,** *174*, 424-430.
(350) Shebanova, O. N.; Lazor, P. Raman Study of Magnetite (Fe_3O_4): Laser‐Induced Thermal Effects and Oxidation. *J. Raman Spectrosc.* **2003,** *34*, 845-852.
(351) Dünnwald, J.; Otto, A. An Investigation of Phase Transitions in Rust Layers Using Raman Spectroscopy. *Corros. Sci.* **1989,** *29*, 1167-1176.
(352) Ohtsuka, T.; Kubo, K.; Sato, N. Raman Spectroscopy of Thin Corrosion Films on Iron at 100 to 150 C in Air. *Corrosion* **1986,** *42*, 476-481.
(353) Gasparov, L.; Tanner, D.; Romero, D.; Berger, H.; Margaritondo, G.; Forro, L. Infrared and Raman Studies of the Verwey Transition in Magnetite. *Phys. Rev. B* **2000,** *62*, 7939.
(354) Graves, P. R.; Johnston, C.; Campaniello, J. J. Raman Scattering in Spinel Structure Ferrites. *Mater. Res. Bull.* **1988,** *23*, 1651-1660.
(355) Li, J.-M.; Huan, A. C. H.; Wang, L.; Du, Y.-W.; Feng, D. Interface Effects on Magnetoresistance and Magnetic-Field-Reduced Raman Scattering in Magnetite. *Phys. Rev. B* **2000,** *61*, 6876-6878.
(356) Gupta, R.; Sood, A.; Metcalf, P.; Honig, J. Raman Study of Stoichiometric and Zn-Doped Fe_3O_4. *Phys. Rev. B* **2002,** *65*, 104430.
(357) Bersani, D.; Lottici, P.; Montenero, A. Micro‐Raman Investigation of Iron Oxide Films and Powders Produced by Sol‐Gel Syntheses. *J. Raman Spectrosc.* **1999,** *30*, 355-360.
(358) Ona-Nguema, G.; Carteret, C.; Benali, O.; Abdelmoula, M.; Génin, J.-M.; Jorand, F. Competitive Formation of Hydroxycarbonate Green Rust 1 Versus Hydroxysulphate Green Rust 2 in *Shewanella putrefaciens* Cultures. *Geomicrobiol. J.* **2004,** *21*, 79-90.
(359) Bonin, P. M. L.; Odziemkowski, M. S.; Reardon, E. J.; Gillham, R. W. In Situ Identification of Carbonate-Containing Green Rust on Iron Electrodes in Solutions Simulating Groundwater. *J. Solution Chem.* **2000,** *29*, 1061-1074.
(360) Namduri, H.; Nasrazadani, S. Quantitative Analysis of Iron Oxides Using Fourier Transform Infrared Spectrophotometry. *Corros. Sci.* **2008,** *50*, 2493-2497.
(361) Oh, S. J.; Cook, D.; Townsend, H. Characterization of Iron Oxides Commonly Formed as Corrosion Products On Steel. *Hyperfine Interact.* **1998,** *112*, 59-66.
(362) Legrand, L.; Sagon, G.; Lecomte, S.; Chausse, A.; Messina, R. Raman and Infrared Study of a New Carbonate Green Rust Obtained by Electrochemical Way. *Corros. Sci.* **2001,** *43*, 1739-1749.
(363) Dubois, F.; Mendibide, C.; Pagnier, T.; Perrard, F.; Duret, C. Raman Mapping of Corrosion Products Formed onto Spring Steels During Salt Spray

Experiments. A Correlation between the Scale Composition and the Corrosion Resistance. *Corros. Sci.* **2008,** *50*, 3401-3409.
(364) Pérez, F.; Barreo Meneses, C.; García, K.; Hight Walker, A. Raman Microscopy as a Tool for the Rust Composition Distribution Analysis. *Rev. Colomb. Fís.* **2010,** *42*, 187-190.
(365) Su, X.; Yu, C.; Qiang, C. Synthesis of α-Fe_2O_3 Nanobelts and Nanoflakes by Thermal Oxidation and Study to Their Magnetic Properties. *Appl. Surf. Sci.* **2011,** *257*, 9014-9018.
(366) Zegeye, A.; Ona-Nguema, G.; Carteret, C.; Huguet, L.; Abdelmoula, M.; Jorand, F. Formation of Hydroxysulphate Green Rust 2 as a Single Iron(II-III) Mineral in Microbial Culture. *Geomicrobiol. J.* **2005,** *22*, 389-399.
(367) Peulon, S.; Legrand, L.; Antony, H.; Chaussé, A. Electrochemical Deposition of Thin Films of Green Rusts 1 and 2 on Inert Gold Substrate. *Electrochem. Commun.* **2003,** *5*, 208-213.
(368) Templeton, A.; Knowles, E. Microbial Transformations of Minerals and Metals: Recent Advances in Geomicrobiology Derived from Synchrotron-Based X-Ray Spectroscopy and X-Ray Microscopy. *Annu. Rev. Earth Planet. Sci.* **2009,** *37*, 367-391.
(369) Wilke, M.; Farges, F.; Petit, P.-E.; Brown, G. E.; Martin, F. Oxidation State and Coordination of Fe in Minerals: An Fe *K*-XANES Spectroscopic Study. *Am. Mineral.* **2001,** *86*, 714.
(370) Galoisy, L.; Calas, G.; Arrio, M. A. High-Resolution XANES Spectra of Iron in Minerals and Glasses: Structural Information from the Pre-Edge Region. *Chem. Geol.* **2001,** *174*, 307-319.
(371) ThomasArrigo, L. K.; Mikutta, C.; Byrne, J.; Barmettler, K.; Kappler, A.; Kretzschmar, R. Iron and Arsenic Speciation and Distribution in Organic Flocs from Streambeds of an Arsenic-Enriched Peatland. *Environ. Sci. Technol.* **2014,** *48*, 13218-13228.
(372) Laan, G. v. d. Applications of Soft X-Ray Magnetic Dichroism. *J. Phys.: Conf. Ser.* **2013,** *430*, 012127.
(373) van der Laan, G.; Kirkman, I. W. The 2p Absorption-Spectra of 3d Transition-Metal Compounds in Tetrahedral and Octahedral Symmetry. *J. Phys. Condens. Matter* **1992,** *4*, 4189-4204.
(374) van der laan, G.; Thole, B. T. Strong Magnetic-X-Ray Dichroism in 2p Absorption-Spectra of 3d Transition-Metal Ions. *Phys. Rev. B* **1991,** *43*, 13401-13411.
(375) Pearce, C. I.; Henderson, C. M. B.; Telling, N. D.; Pattrick, R. A. D.; Charnock, J. M.; Coker, V. S.; Arenholz, E.; Tuna, F.; van der Laan, G. Fe Site Occupancy in Magnetite-Ulvöspinel Solid Solutions: A New Approach Using X-Ray Magnetic Circular Dichroism. *Am. Mineral.* **2010,** *95*, 425-439.
(376) Coker, V. S.; Gault, A. G.; Pearce, C. I.; van der Laan, G.; Telling, N. D.; Charnock, J. M.; Polya, D. A.; Lloyd, J. R. XAS and XMCD Evidence for Species-Dependent Partitioning of Arsenic During Microbial Reduction of Ferrihydrite to Magnetite. *Environ. Sci. Technol.* **2006,** *40*, 7745-7750.
(377) Crean, D. E.; Coker, V. S.; van der Laan, G.; Lloyd, J. R. Engineering Biogenic Magnetite for Sustained Cr(VI) Remediation in Flow-through Systems. *Environ. Sci. Technol.* **2012,** *46*, 3352-3359.
(378) Cutting, R. S.; Coker, V. S.; Telling, N. D.; Kimber, R. L.; Pearce, C. I.; Ellis, B. L.; Lawson, R. S.; van der Laan, G.; Pattrick, R. A. D.; Vaughan, D. J.et al.

Optimizing Cr(VI) and Tc(VII) Remediation through Nanoscale Biomineral Engineering. *Environ. Sci. Technol.* **2010,** *44*, 2577-2584.
(379) Telling, N. D.; Coker, V. S.; Cutting, R. S.; van der Laan, G.; Pearce, C. I.; Pattrick, R. A. D.; Arenholz, E.; Lloyd, J. R. Remediation of Cr(VI) by Biogenic Magnetic Nanoparticles: An X-Ray Magnetic Circular Dichroism Study. *Appl. Phys. Lett.* **2009,** *95*, 163701.
(380) Watts, M. P.; Coker, V. S.; Parry, S. A.; Pattrick, R. A. D.; Thomas, R. A. P.; Kalin, R.; Lloyd, J. R. Biogenic Nano-Magnetite and Nano-Zero Valent Iron Treatment of Alkaline Cr(VI) Leachate and Chromite Ore Processing Residue. *Appl. Geochem.* **2015,** *54*, 27-42.
(381) Coker, V. S.; Pearce, C. I.; Pattrick, R. A. D.; van der Laan, G.; Telling, N. D.; Charnock, J. M.; Arenholz, E.; Lloyd, J. R. Probing the Site Occupancies of Co-, Ni-, and Mn-Substituted Biogenic Magnetite Using XAS and XMCD. *Am. Mineral.* **2008,** *93*, 1119-1132.
(382) Coker, V. S.; Telling, N. D.; van der Laan, G.; Pattrick, R. A. D.; Pearce, C. I.; Arenholz, E.; Tuna, F.; Winpenny, R. E. P.; Lloyd, J. R. Harnessing the Extracellular Bacterial Production of Nanoscale Cobalt Ferrite with Exploitable Magnetic Properties. *ACS Nano* **2009,** *3*, 1922-1928.
(383) Coker, V. S.; Bennett, J. A.; Telling, N. D.; Henkel, T.; Charnock, J. M.; van der Laan, G.; Pattrick, R. A. D.; Pearce, C. I.; Cutting, R. S.; Shannon, I. J.et al. Microbial Engineering of Nanoheterostructures: Biological Synthesis of a Magnetically Recoverable Palladium Nanocatalyst. *ACS Nano* **2010,** *4*, 2577-2584.
(384) Chang, L.; Pattrick, R. A. D.; van der Laan, G.; Coker, V. S.; Roberts, A. P. Enigmatic X-Ray Magnetic Circular Dichroism in Greigite (Fe_3S_4). *Can. Mineral.* **2012,** *50*, 667-674.
(385) Letard, I.; Sainctavit, P.; Deudon, C. XMCD at Fe $L_{2,3}$ Edges, Fe and S K Edges on Fe_7S_8. *Phys. Chem. Miner.* **2007,** *34*, 113-120.
(386) Pattrick, R. A. D.; Coker, V. S.; Masood, A.; Azad, M.; Lewis, E.; Haigh, E.; O'Brien, P.; Shafer, P. C.; van der Laan, G. Magnetic Spectroscopy of Nanoparticulate Greigite, Fe_3S_4. *Mineral. Mag.* **2016**.
(387) von der Heyden, B. P.; Roychoudhury, A. N.; Mtshali, T. N.; Tyliszczak, T.; Myneni, S. C. B. Chemically and Geographically Distinct Solid-Phase Iron Pools in the Southern Ocean. *Science* **2012,** *338*, 1199.
(388) Coker, V. S.; Byrne, J. M.; Telling, N. D.; Van Der Laan, G.; Lloyd, J. R.; Hitchcock, A. P.; Wang, J.; Pattrick, R. A. D. Characterisation of the Dissimilatory Reduction of Fe(III)-Oxyhydroxide at the Microbe – Mineral Interface: The Application of STXM–XMCD. *Geobiology* **2012,** *10*, 347-354.
(389) Ona-Nguema, G.; Abdelmoula, M.; Jorand, F.; Benali, O.; Géhin, A.; Block, J. C.; Génin, J. M. R. Iron(II,III) hydroxycarbonate green rust formation and stabilization from lepidocrocite bioreduction. *Environ. Sci. Technol.* **2002,** *36*, 16-20.
(390) Barthélémy, K.; Naille, S.; Despas, C.; Ruby, C.; Mallet, M. Carbonated Ferric Green Rust as a New Material for Efficient Phosphate Removal. *J. Colloid Interface Sci.* **2012,** *384*, 121-127.
(391) Schwertmann, U.; Murad, E. The Influence of Aluminum on Iron Oxides: XIV. Al-Substituted Magnetite Synthesized at Ambient Temperatures. *Clays Clay Miner.* **1990,** *38*, 196-202.
(392) Schwertmann, U.; Cornell, R. M. *Iron Oxides in the Laboratory: Preparation and Characterization*; Wiley-VCH, New York, **2000**.

(393) Heller, F.; Evans, M. E. Loess Magnetism. *Rev. Geophys.* **1995,** *33*, 211-240.
(394) Maher, B. A.; Ahmed, I. A.; Karloukovski, V.; MacLaren, D. A.; Foulds, P. G.; Allsop, D.; Mann, D. M.; Torres-Jardón, R.; Calderon-Garciduenas, L. Magnetite Pollution Nanoparticles in the Human Brain. *Proc. Natl. Acad. Sci. U. S. A.* **2016,** *113*, 10797-10801.
(395) Day, R.; Fuller, M.; Schmidt, V. A. Hysteresis Properties of Titanomagnetites: Grain-Size and Compositional Dependence. *Phys. Earth Planet. Inter.* **1977,** *13*, 260-267.
(396) Dunlop, D. J. Theory and Application of the Day Plot (Mrs/Ms versus Hcr/Hc) 2. Application to Data for Rocks, Sediments, and Soils. *J. Geophys. Res.: Solid Earth* **2002,** *107*, EPM 5-1-EPM 5-15.
(397) Mullins, C. Magnetic Susceptibility of the Soil and its Significance in Soil Science–A Review. *J. Soil Sci.* **1977,** *28*, 223-246.
(398) Porsch, K.; Dippon, U.; Rijal, M. L.; Appel, E.; Kappler, A. In-situ magnetic susceptibility measurements as a tool to follow geomicrobiological transformation of Fe minerals. *Environ. Sci. Technol.* **2010,** *44*, 3846-3852.
(399) Boyd, T. E.; Cusick, M.; Navratil, J. "Ferrite Use in Separation Science and Technology," Rockwell International Corp., Golden, CO (USA), 1983.
(400) Yavuz, C. T.; Mayo, J.; William, W. Y.; Prakash, A.; Falkner, J. C.; Yean, S.; Cong, L.; Shipley, H. J.; Kan, A.; Tomson, M. Low-Field Magnetic Separation of Monodisperse Fe_3O_4 Nanocrystals. *Science* **2006,** *314*, 964-967.
(401) Barriga, C.; Gaitan, M.; Pavlovic, I.; Ulibarri, M. A.; Hermosin, M. C.; Cornejo, J. Hydrotalcites as Sorbent for 2,4,6-Trinitrophenol: Influence of the Layer Composition and Interlayer Anion. *J. Mater. Chem.* **2002,** *12*, 1027-1034.
(402) Pavlovic, I.; Barriga, C.; Hermosín, M. C.; Cornejo, J.; Ulibarri, M. A. Adsorption of Acidic Pesticides 2,4-D, Clopyralid and Picloram on Calcined Hydrotalcite. *Appl. Clay Sci.* **2005,** *30*, 125-133.
(403) Sergent, A. S.; Jorand, F.; Hanna, K. Effects of Si-Bearing Minerals on the Nature of Secondary Iron Mineral Products from Lepidocrocite Bioreduction. *Chem. Geol.* **2011,** *289*, 86-97.
(404) Chowdhury, S. R.; Yanful, E. K. Arsenic and Chromium Removal by Mixed Magnetite-Maghemite Nanoparticles and the Effect of Phosphate on Removal. *J. Environ. Manage.* **2010,** *91*, 2238-2247.
(405) Martínez, M.; Giménez, J.; de Pablo, J.; Rovira, M.; Duro, L. Sorption of Selenium(IV) and Selenium(VI) onto Magnetite. *Appl. Surf. Sci.* **2006,** *252*, 3767-3773.
(406) Dixit, S.; Hering, J. G. Comparison of Arsenic(V) and Arsenic(III) Sorption onto Iron Oxide Minerals: Implications for Arsenic Mobility. *Environ. Sci. Technol.* **2003,** *37*, 4182-4189.
(407) Missana, T.; García-Gutiérrez, M.; Fernńdez, V. Uranium (VI) Sorption on Colloidal Magnetite under Anoxic Environment: Experimental Study and Surface Complexation Modelling. *Geochim. Cosmochim. Acta* **2003,** *67*, 2543-2550.
(408) Missana, T.; Alonso, U.; Scheinost, A. C.; Granizo, N.; García-Gutiérrez, M. Selenite Retention by Nanocrystalline Magnetite: Role of Adsorption, Reduction and Dissolution/Co-Precipitation Processes. *Geochim. Cosmochim. Acta* **2009,** *73*, 6205-6217.

(409) Mayo, J. T.; Yavuz, C.; Yean, S.; Cong, L.; Shipley, H.; Yu, W.; Falkner, J.; Kan, A.; Tomson, M.; Colvin, V. L. The Effect of Nanocrystalline Magnetite Size on Arsenic Removal. *Sci. Technol. Adv. Mater.* **2007,** *8*, 71-75.
(410) Yean, S.; Cong, L.; Yavuz, C. T.; Mayo, J. T.; Yu, W. W.; Kan, A. T.; Colvin, V. L.; Tomson, M. B. Effect of Magnetite Particle Size on Adsorption and Desorption of Arsenite and Arsenate. *J. Mater. Res.* **2005,** *20*, 3255-3264.
(411) Liu, C.-H.; Chuang, Y.-H.; Chen, T.-Y.; Tian, Y.; Li, H.; Wang, M.-K.; Zhang, W. Mechanism of Arsenic Adsorption on Magnetite Nanoparticles from Water: Thermodynamic and Spectroscopic Studies. *Environ. Sci. Technol.* **2015,** *49*, 7726-7734.
(412) Mohan, D.; Pittman Jr, C. U. Arsenic Removal from Water/Wastewater Using Adsorbents—a Critical Review. *J. Hazard. Mater.* **2007,** *142*, 1-53.
(413) Shipley, H. J.; Yean, S.; Kan, A. T.; Tomson, M. B. Adsorption of Arsenic to Magnetite Nanoparticles: Effect of Particle Concentration, pH, Ionic Strength, and Temperature. *Environ. Toxicol. Chem.* **2009,** *28*, 509-515.
(414) Jönsson, J.; Sherman, D. M. Sorption of As(III) and As(V) to Siderite, Green Rust (Fougerite) and Magnetite: Implications for Arsenic Release in Anoxic Groundwaters. *Chem. Geol.* **2008,** *255*, 173-181.
(415) Wang, Y.; Morin, G.; Ona-Nguema, G.; Menguy, N.; Juillot, F.; Aubry, E.; Guyot, F.; Calas, G.; Brown Jr, G. E. Arsenite Sorption at the Magnetite–Water Interface During Aqueous Precipitation of Magnetite: EXAFS Evidence for a New Arsenite Surface Complex. *Geochim. Cosmochim. Acta* **2008,** *72*, 2573-2586.
(416) Wang, Y.; Morin, G.; Ona-Nguema, G.; Juillot, F.; Guyot, F.; Calas, G.; Brown, G. E. Evidence for Different Surface Speciation of Arsenite and Arsenate on Green Rust: An EXAFS and XANES Study. *Environ. Sci. Technol.* **2010,** *44*, 109-115.
(417) Hansen, B. H. C.; Poulsen, I. F. Interaction of Synthetic Sulphate "Green Rust" with Phosphate and the Crystallization of Vivianite. *Clays Clay Miner.* **1999,** *47*, 312-318.
(418) Giraldo, L.; Erto, A.; Moreno-Piraján, J. C. Magnetite Nanoparticles for Removal of Heavy Metals from Aqueous Solutions: Synthesis and Characterization. *Adsorption* **2013,** *19*, 465-474.
(419) Lasheen, M. R.; El-Sherif, I. Y.; Sabry, D. Y.; El-Wakeel, S. T.; El-Shahat, M. F. Removal and Recovery of Cr(VI) by Magnetite Nanoparticles. *Desalin. Water Treat.* **2014,** *52*, 6464-6473.
(420) Lasheen, M. R.; El-Sherif, I. Y.; Tawfik, M. E.; El-Wakeel, S. T.; El-Shahat, M. F. Preparation and Adsorption Properties of Nano Magnetite Chitosan Films for Heavy Metal Ions from Aqueous Solution. *Mater. Res. Bull.* **2016,** *80*, 344-350.
(421) Liu, J.-f.; Zhao, Z.-s.; Jiang, G.-b. Coating Fe_3O_4 Magnetic Nanoparticles with Humic Acid for High Efficient Removal of Heavy Metals in Water. *Environ. Sci. Technol.* **2008,** *42*, 6949-6954.
(422) Singh, B. K.; Jain, A.; Kumar, S.; Tomar, B. S.; Tomar, R.; Manchanda, V. K.; Ramanathan, S. Role of Magnetite and Humic Acid in Radionuclide Migration in the Environment. *J. Contam. Hydrol.* **2009,** *106*, 144-149.
(423) Catalette, H.; Dumonceau, J.; Ollar, P. Sorption of Cesium, Barium and Europium on Magnetite. *J. Contam. Hydrol.* **1998,** *35*, 151-159.

(424) Ebner, A. D.; Ritter, J. A.; Navratil, J. D. Adsorption of Cesium, Strontium, and Cobalt Ions on Magnetite and a Magnetite−Silica Composite. *Ind. Eng. Chem. Res.* **2001,** *40*, 1615-1623.
(425) Aamrani, S. E.; Giménez, J.; Rovira, M.; Seco, F.; Grivé, M.; Bruno, J.; Duro, L.; de Pablo, J. A Spectroscopic Study of Uranium(VI) Interaction with Magnetite. *Appl. Surf. Sci.* **2007,** *253*, 8794-8797.
(426) Rojo, I.; Seco, F.; Rovira, M.; Giménez, J.; Cervantes, G.; Martí, V.; de Pablo, J. Thorium Sorption onto Magnetite and Ferrihydrite in Acidic Conditions. *J. Nucl. Mater.* **2009,** *385*, 474-478.
(427) Ahmed, I. M.; Gamal, R.; Helal, A. A.; Abo-El-Enein, S. A.; Helal, A. A. Kinetic Sorption Study of Cerium (IV) on Magnetite Nanoparticles. *Part. Sci. Technol.* **2017,** *35*, 643-652.
(428) Sagert, N. H.; Ho, C. H.; Miller, N. H. The Adsorption of Uranium(VI) onto a Magnetite Sol. *J. Colloid Interface Sci.* **1989,** *130*, 283-287.
(429) Crane, R. A.; Dickinson, M.; Popescu, I. C.; Scott, T. B. Magnetite and Zero-Valent Iron Nanoparticles for the Remediation of Uranium Contaminated Environmental Water. *Water Res.* **2011,** *45*, 2931-2942.
(430) Das, D.; Sureshkumar, M. K.; Koley, S.; Mithal, N.; Pillai, C. G. S. Sorption of Uranium on Magnetite Nanoparticles. *J. Radioanal. Nucl. Chem.* **2010,** *285*, 447-454.
(431) Singer, D. M.; Chatman, S. M.; Ilton, E. S.; Rosso, K. M.; Banfield, J. F.; Waychunas, G. A. Sorption and Reduction Kinetics on the Magnetite (111) Surface. *Environ. Sci. Technol.* **2012,** *46*, 3821-3830.
(432) Singer, D. M.; Chatman, S. M.; Ilton, E. S.; Rosso, K. M.; Banfield, J. F.; Waychunas, G. A. Identification of Simultaneous U(VI) Sorption Complexes and U(IV) Nanoprecipitates on the Magnetite (111) Surface. *Environ. Sci. Technol.* **2012,** *46*, 3811-3820.
(433) Jordan, N.; Marmier, N.; Lomenech, C.; Giffaut, E.; Ehrhardt, J.-J. Sorption of Silicates on Goethite, Hematite, and Magnetite: Experiments and Modelling. *J. Colloid Interface Sci.* **2007,** *312*, 224-229.
(434) Daou, T. J.; Begin-Colin, S.; Grenèche, J. M.; Thomas, F.; Derory, A.; Bernhardt, P.; Legaré, P.; Pourroy, G. Phosphate Adsorption Properties of Magnetite-Based Nanoparticles. *Chem. Mater.* **2007,** *19*, 4494-4505.
(435) Yang, X.; Roonasi, P.; Jolsterå, R.; Holmgren, A. Kinetics of Silicate Sorption on Magnetite and Maghemite: An In Situ ATR-FTIR Study. *Colloids Surf., A* **2009,** *343*, 24-29.
(436) Mansour, C.; Lefèvre, G.; Pavageau, E. M.; Catalette, H.; Fédoroff, M.; Zanna, S. Sorption of Sulfate Ions onto Magnetite. *J. Colloid Interface Sci.* **2009,** *331*, 77-82.
(437) Roonasi, P.; Holmgren, A. An ATR-FTIR Study of Sulphate Sorption on Magnetite; Rate of Adsorption, Surface Speciation, and Effect of Calcium Ions. *J. Colloid Interface Sci.* **2009,** *333*, 27-32.
(438) Roonasi, P.; Holmgren, A. An ATR–FTIR Study of Carbonate Sorption onto Magnetite. *Surf. Interface Anal.* **2010,** *42*, 1118-1121.
(439) Rakshit, S.; Sarkar, D.; Punamiya, P.; Datta, R. Kinetics of Oxytetracycline Sorption on Magnetite Nanoparticles. *Int. J. Environ. Sci. Technol.* **2014,** *11*, 1207-1214.
(440) Zhang, D.; Niu, H.; Zhang, X.; Meng, Z.; Cai, Y. Strong Adsorption of Chlorotetracycline on Magnetite Nanoparticles. *J. Hazard. Mater.* **2011,** *192*, 1088-1093.

(441) Usman, M.; Martin, S.; Cimetière, N.; Giraudet, S.; Chatain, V.; Hanna, K. Sorption of Nalidixic Acid onto Micrometric and Nanometric Magnetites: Experimental Study and Modeling. *Appl. Surf. Sci.* **2014,** *299C*, 136-145.
(442) Liang, X.; Butler, E. C. Effects of Natural Organic Matter Model Compounds on the Transformation of Carbon Tetrachloride by Chloride Green Rust. *Water Res.* **2010,** *44*, 2125-2132.
(443) Zhao, X.; Shi, Y.; Cai, Y.; Mou, S. Cetyltrimethylammonium Bromide-Coated Magnetic Nanoparticles for the Preconcentration of Phenolic Compounds from Environmental Water Samples. *Environ. Sci. Technol.* **2008,** *42*, 1201-1206.
(444) Ghosh, S.; Badruddoza, A. Z. M.; Hidajat, K.; Uddin, M. S. Adsorptive Removal of Emerging Contaminants from Water Using Superparamagnetic Fe_3O_4 Nanoparticles Bearing Aminated β-Cyclodextrin. *J. Environ. Chem. Eng.* **2013,** *1*, 122-130.
(445) Ayala-Luis, K. B.; Cooper, N. G. A.; Koch, C. B.; Hansen, H. C. B. Efficient Dechlorination of Carbon Tetrachloride by Hydrophobic Green Rust Intercalated with Dodecanoate Anions. *Environ. Sci. Technol.* **2012,** *46*, 3390-3397.
(446) Li-Zhi, H.; Hans Christian, B. H. Synthesis and Reactivity of Surfactant-intercalated Layered Iron(II)Iron(III) Hydroxides. *Current Inorganic Chemistry* **2016,** *6*, 68-82.
(447) Tombácz, E.; Tóth, I. Y.; Nesztor, D.; Illés, E.; Hajdú, A.; Szekeres, M.; L.Vékás. Adsorption of Organic Acids on Magnetite Nanoparticles, pH-Dependent Colloidal Stability and Salt Tolerance. *Colloids Surf., A* **2013,** *435*, 91-96.
(448) Illés, E.; Tombácz, E. The Effect of Humic Acid Adsorption on pH-Dependent Surface Charging and Aggregation of Magnetite Nanoparticles. *J. Colloid Interface Sci.* **2006,** *295*, 115-123.
(449) MacRae, I. C.; Evans, S. K. Removal of Bacteria from Water by Adsorption to Magnetite. *Water Res.* **1984,** *18*, 1377-1380.
(450) Mac Rae, I. C. Removal of Pesticides in Water by Microbial Cells Adsorbed to Magnetite. *Water Res.* **1985,** *19*, 825-830.
(451) Cheng, W.; Marsac, R.; Hanna, K. Influence of Magnetite Stoichiometry on the Binding of Emerging Organic Contaminants. *Environ. Sci. Technol.* **2018,** *52*, 467-473.
(452) Erbs, M.; Hansen, H. C. B.; Olsen, C. E. Reductive Dechlorination of Carbon Tetrachloride using Iron(II) Iron(III) Hydroxide Sulfate (Green Rust). *Environ. Sci. Technol.* **1999,** *33*, 307-311.
(453) Oliveira, L. C. A.; Rios, R. V. R. A.; Fabris, J. D.; Garg, V.; Sapag, K.; Lago, R. M. Activated Carbon/Iron Oxide Magnetic Composites for the Adsorption of Contaminants in Water. *Carbon* **2002,** *40*, 2177-2183.
(454) Pang, K. M.; Ng, S.; Chung, W. K.; Wong, P. K. Removal of Pentachlorophenol by Adsorption on Magnetite-immobilized Chitin. *Water, Air, Soil Pollut.* **2007,** *183*, 355-365.
(455) Xue, X.; Hanna, K.; Abdelmoula, M.; Deng, N. Adsorption and Oxidation of Pcp on the Surface of Magnetite: Kinetic Experiments and Spectroscopic Investigations. *Appl. Catal., B* **2009,** *89*, 432-440.
(456) Stumm, W.; Morgan, J. J. *Aquatic Chemistry: Chemical Equilibria and Rates in Natural Waters*; Thrid ed.; John Wiley and Sons: New York, **1996**.

(457) Haderlein Stefan, B.; Pecher, K. Pollutant Reduction in Heterogeneous Fe(II)-Fe(III) Systems. In *Mineral-Water Interfacial Reactions*; American Chemical Society, 1999; Vol. 715, 342-357.
(458) Williams, A. G. B.; Scherer, M. M. Kinetics of Cr(VI) Reduction by Carbonate Green Rust. *Environ. Sci. Technol.* **2001,** *35*, 3488-3494.
(459) Choi, J.; Batchelor, B. Nitrate Reduction by Fluoride Green Rust Modified with Copper. *Chemosphere* **2008,** *70*, 1108-1116.
(460) Hansen, H. C. B.; Koch, C. B. Reduction of Nitrate to Ammonium by Sulphate Green Rust: Activation Energy and Reaction Mechanism. *Clay Miner.* **1998,** *33*, 87-101.
(461) O'Loughlin, E. J.; Kelly, S. D.; Cook, R. E.; Csencsits, R.; Kemner, K. M. Reduction of Uranium(VI) by Mixed Iron(II)/Iron(III) Hydroxide (Green Rust): Formation of UO_2 Nanoparticles. *Environ. Sci. Technol.* **2003,** *37*, 721-727.
(462) O'Loughlin, E. J.; Kelly, S. D.; Kemner, K. M.; Csencsits, R.; Cook, R. E. Reduction of Ag^{I}, $Au^{III,}$ Cu^{II}, and Hg^{II} by Fe^{II}/Fe^{III} Hydroxysulfate Green Rust. *Chemosphere* **2003,** *53*, 437-446.
(463) Pepper, S. E.; Bunker, D. J.; Bryan, N. D.; Livens, F. R.; Charnock, J. M.; Pattrick, R. A. D.; Collison, D. Treatment of Radioactive Wastes: An X-Ray Absorption Spectroscopy Study of the Reaction of Technetium with Green Rust. *J. Colloid Interface Sci.* **2003,** *268*, 408-412.
(464) Gregory, K. B.; Larese-Casanova, P.; Parkin, G. F.; Scherer, M. M. Abiotic Transformation of Hexahydro-1,3,5-Trinitro-1,3,5-Triazine by Fe^{II} Bound to Magnetite. *Environ. Sci. Technol.* **2004,** *38*, 1408-1414.
(465) Latta, D., E. L; Boyanov, M., I ; Kemner, K., M; O'Loughlin, E., J.; Scherer, M. Reaction of Uranium(VI) with Green Rusts: Effect of Interlayer Anion. *Current Inorganic Chemistry* **2015,** *5*, 156-168.
(466) Klein, C.; Hurlbut Jr, C. *Manual of Mineralogy. /after James D*; John Wiley & Sons, Inc, USA., **1993**.
(467) Skovbjerg, L. L.; Stipp, S. L. S.; Utsunomiya, S.; Ewing, R. C. The Mechanisms of Reduction of Hexavalent Chromium by Green Rust Sodium Sulphate: Formation of Cr-Goethite. *Geochim. Cosmochim. Acta* **2006,** *70*, 3582-3592.
(468) Dhakal, P.; Matocha, C. J.; Huggins, F. E.; Vandiviere, M. M. Nitrite Reactivity with Magnetite. *Environ. Sci. Technol.* **2013,** *47*, 6206-6213.
(469) Loyaux-Lawniczak, S.; Refait, P.; Ehrhardt, J. J.; Lecomte, P.; Génin, J. M. R. Trapping of Cr by Formation of Ferrihydrite During the Reduction of Chromate Ions by Fe(II)-Fe(III) Hydroxysalt Green Rusts. *Environ. Sci. Technol.* **2000,** *34*, 438-443.
(470) Hansen, H. C. B.; Koch, C. B.; Nancke-Krogh, H.; Borggaard, O. K.; Sørensen, J. Abiotic Nitrate Reduction to Ammonium: Key Role of Green Rust. *Environ. Sci. Technol.* **1996,** *30*, 2053-2056.
(471) Myneni, S. C. B.; Tokunaga, T. K.; Brown, G. E. Abiotic Selenium Redox Transformations in the Presence of Fe(II,III) Oxides. *Science* **1997,** *278*, 1106-1109.
(472) Bond, D. L.; Fendorf, S. Kinetics and Structural Constraints of Chromate Reduction by Green Rusts. *Environ. Sci. Technol.* **2003,** *37*, 2750-2757.
(473) Lee, W.; Batchelor, B. Reductive Capacity of Natural Reductants. *Environ. Sci. Technol.* **2003,** *37*, 535-541.

(474) Lee, W.; Batchelor, B. Abiotic Reductive Dechlorination of Chlorinated Ethylenes by Iron-Bearing Soil Minerals. 2. Green Rust. *Environ. Sci. Technol.* **2002,** *36*, 5348-5354.
(475) Jung, Y.; Choi, J.; Lee, W. Spectroscopic Investigation of Magnetite Surface for the Reduction of Hexavalent Chromium. *Chemosphere* **2007,** *68*, 1968-1975.
(476) Klausen, J.; Troeber, S. P.; Haderlein, S. B.; Schwarzenbach, R. P. Reduction of Substituted Nitrobenzenes by Fe (II) in Aqueous Mineral Suspensions. *Environ. Sci. Technol.* **1995,** *29*, 2396-2404.
(477) Amonette, J. E.; Workman, D. J.; Kennedy, D. W.; Fruchter, J. S.; Gorby, Y. A. Dechlorination of Carbon Tetrachloride by Fe(II) Associated with Goethite. *Environ. Sci. Technol.* **2000,** *34*, 4606-4613.
(478) Klupinski, T. P.; Chin, Y.-P.; Traina, S. J. Abiotic Degradation of Pentachloronitrobenzene by Fe(II): Reactions on Goethite and Iron Oxide Nanoparticles. *Environ. Sci. Technol.* **2004,** *38*, 4353-4360.
(479) Hansen, H. C. B.; Borggaard, O. K.; Sørensen, J. Evaluation of the Free Energy of Formation of Fe(II)-Fe(III) Hydroxide-Sulphate (Green Rust) and Its Reduction of Nitrite. *Geochim. Cosmochim. Acta* **1994,** *58*, 2599-2608.
(480) Etique, M.; Zegeye, A.; Grégoire, B.; Carteret, C.; Ruby, C. Nitrate Reduction by Mixed Iron (II-III) Hydroxycarbonate Green Rust in the Presence of Phosphate Anions: The Key Parameters Influencing the Ammonium Selectivity. *Water Res.* **2014,** *62*, 29-39.
(481) Jorand, F. P. A.; Sergent, A. S.; Remy, P. P.; Bihannic, I.; Ghanbaja, J.; Lartiges, B.; Hanna, K.; Zegeye, A. Contribution of Anionic vs. Neutral Polymers to the Formation of Green Rust 1 from γ-FeOOH Bioreduction. *Geomicrobiol. J.* **2013,** *30*, 600-615.
(482) Remy, P. P.; Etique, M.; Hazotte, A. A.; Sergent, A. S.; Estrade, N.; Cloquet, C.; Hanna, K.; Jorand, F. P. A. Pseudo-First-Order Reaction of Chemically and Biologically Formed Green Rusts with Hg^{II} and $C_{15}H_{15}N_3O_2$: Effects of pH and Stabilizing Agents (Phosphate, Silicate, Polyacrylic Acid, and Bacterial Cells). *Water Res.* **2015,** *70*, 266-278.
(483) Legrand, L.; El Figuigui, A.; Mercier, F.; Chausse, A. Reduction of Aqueous Chromate by Fe(II)/Fe(III) Carbonate Green Rust: Kinetic and Mechanistic Studies. *Environ. Sci. Technol.* **2004,** *38*, 4587-4595.
(484) He, Y. T.; Traina, S. J. Cr(VI) Reduction and Immobilization by Magnetite under Alkaline pH Conditions: The Role of Passivation. *Environ. Sci. Technol.* **2005,** *39*, 4499-4504.
(485) Vikesland, P. J.; Heathcock, A. M.; Rebodos, R. L.; Makus, K. E. Particle Size and Aggregation Effects on Magnetite Reactivity toward Carbon Tetrachloride. *Environ. Sci. Technol.* **2007,** *41*, 5277-5283.
(486) Danielsen, K. M.; Hayes, K. F. pH Dependence of Carbon Tetrachloride Reductive Dechlorination by Magnetite. *Environ. Sci. Technol.* **2004,** *38*, 4745-4752.
(487) O'Loughlin, E. J.; Kemner, K. M.; Burris, D. R. Effects of $Ag^{I,}$ Au^{III}, and Cu^{II} on the Reductive Dechlorination of Carbon Tetrachloride by Green Rust. *Environ. Sci. Technol.* **2003,** *37*, 2905-2912.
(488) Rybnikova, V.; Usman, M.; Hanna, K. Removal of PCBs in Contaminated Soils by Means of Chemical Reduction and Advanced Oxidation Processes. *Environ. Sci. Pollut. Res.* **2016,** *23*, 17035–17048.

(489) Fenton, H. J. H. On a New Reaction of Tartaric Acid. *Chem. News* **1876,** *33*, 190.
(490) Fenton, H. J. H. Oxidation of Tartaric Acid in Presence of Iron. *J. Chem. Soc. Trans.* **1894,** *65*, 899-910.
(491) Haber, F.; Weiss, J. The catalytic decomposition of hydrogen peroxide by iron salts. *Proc. R. Soc. London A* **1934,** *147*, 332-351.
(492) Gligorovski, S.; Strekowski, R.; Barbati, S.; Vione, D. Environmental Implications of Hydroxyl Radicals (•OH). *Chem. Rev.* **2015,** *115*, 13051-13092.
(493) De Laat, J.; Gallard, H. Catalytic Decomposition of Hydrogen Peroxide by Fe(III) in Homogeneous Aqueous Solution: Mechanism and Kinetic Modeling. *Environ. Sci. Technol.* **1999,** *33*, 2726-2732.
(494) Sirguey, C.; Tereza de Souza e Silva, P.; Schwartz, C.; Simonnot, M.-O. Impact of Chemical Oxidation on Soil Quality. *Chemosphere* **2008,** *72*, 282-289.
(495) Xue, X.; Hanna, K.; Despas, C.; Wu, F.; Deng, N. Effect of Chelating Agent on the Oxidation Rate of PCP in the Magnetite/H_2O_2 System at Neutral pH. *J. Mol. Catal. A: Chem.* **2009,** *311*, 29-35.
(496) Pardo, F.; Rosas, J.; Santos, A.; Romero, A. Remediation of a Biodiesel Blend-Contaminated Soil by Using a Modified Fenton Process. *Environ. Sci. Pollut. Res.* **2014,** *21*, 12198-12207.
(497) Usman, M.; Hanna, K.; Haderlein, S. Fenton Oxidation to Remediate PAHs in Contaminated Soils: A Critical Review of Major Limitations and Counter-Strategies. *Sci. Total Environ.* **2016,** *569–570*, 179-190.
(498) Tsitonaki, A.; Petri, B.; Crimi, M.; Mosbk, H.; Siegrist, R. L.; Bjerg, P. L. In Situ Chemical Oxidation of Contaminated Soil and Groundwater Using Persulfate: A Review. *Crit. Rev. Environ. Sci. Technol.* **2010,** *40*, 55-91.
(499) Usman, M.; Faure, P.; Ruby, C.; Hanna, K. Remediation of PAH-Contaminated Soils by Magnetite Catalyzed Fenton-Like Oxidation. *Appl. Catal., B* **2012,** *117-118*, 10-17.
(500) Usman, M.; Faure, P.; Ruby, C.; Hanna, K. Application of Magnetite-Activated Persulfate Oxidation for the Degradation of PAHs in Contaminated Soils. *Chemosphere* **2012,** *87*, 234-240.
(501) Jung, Y. S.; Lim, W. T.; Park, J. Y.; Kim, Y. H. Effect of pH on Fenton and Fenton‐like oxidation. *Environ. Technol.* **2009,** *30*, 183-190.
(502) Barreiro, J. C.; Capelato, M. D.; Martin-Neto, L.; Bruun Hansen, H. C. Oxidative Decomposition of Atrazine by a Fenton-Like Reaction in a H_2O_2/Ferrihydrite System. *Water Res.* **2007,** *41*, 55-62.
(503) Matta, R.; Hanna, K.; Chiron, S. Fenton-Like Oxidation of 2,4,6-Trinitrotoluene Using Different Iron Minerals. *Sci. Total Environ.* **2007,** *385*, 242-251.
(504) Matta, R.; Hanna, K.; Kone, T.; Chiron, S. Oxidation of 2, 4, 6-Trinitrotoluene in the Presence of Different Iron-Bearing Minerals at Neutral pH. *Chem. Eng. J.* **2008,** *144*, 453-458.
(505) Kanel, S. R.; Neppolian, B.; Choi, H.; Yang, J. W. Heterogeneous Catalytic Oxidation of Phenanthrene by Hydrogen Peroxide in Soil Slurry: Kinetics, Mechanism, and Implication. *Soil Sediment Contam.* **2003,** *12*, 101-117.
(506) Kanel, S. R.; Neppolian, B.; Jung, H.; Choi, H. Comparative Removal of Polycyclic Aromatic Hydrocarbons Using Iron Oxide and Hydrogen Peroxide in Soil Slurries. *Environ. Eng. Sci.* **2004,** *21*, 741-751.

(507) Watts, R. J.; Udell, M. D.; Kong, S.; Leung, S. W. Fenton-Like Soil Remediation Catalysed by Naturally Occurring Iron Minerals. *Environ. Eng. Sci.* **1999,** *16*, 93-103.
(508) Sabri, N.; Hanna, K.; Yargeau, V. Chemical Oxidation of Ibuprofen in the Presence of Iron Species at near Neutral pH. *Sci. Total Environ.* **2012,** *427-428*, 382-389.
(509) Usman, M.; Faure, P.; Lorgeoux, C.; Ruby, C.; Hanna, K. Treatment of Hydrocarbon Contamination under Flow through Conditions by Using Magnetite Catalyzed Chemical Oxidation. *Environ. Sci. Pollut. Res.* **2013,** *20*, 22-30.
(510) Tyre, B. W.; Watts, R. J.; Miller, G. C. Treatment of Four Biorefractory Contaminants in Soils Using Catalyzed Hydrogen Peroxide. *J. Environ. Qual.* **1991,** *20*, 832-838.
(511) Usman, M.; Chaudhary, A.; Biache, C.; Faure, P.; Hanna, K. Effect of Thermal Pre-Treatment on the Availability of PAHs for Successive Chemical Oxidation in Contaminated Soils. *Environ. Sci. Pollut. Res.* **2016,** *23*, 1371-1380.
(512) Sun, S.-P.; Lemley, A. T. p-Nitrophenol Degradation by a Heterogeneous Fenton-Like Reaction on Nano-Magnetite: Process Optimization, Kinetics, and Degradation Pathways. *J. Mol. Catal. A: Chem.* **2011,** *349*, 71-79.
(513) Fontecha-Cámara, M. A.; Moreno-Castilla, C.; López-Ramón, M. V.; Álvarez, M. A. Mixed Iron Oxides as Fenton Catalysts for Gallic Acid Removal from Aqueous Solutions. *Appl. Catal., B* **2016,** *196*, 207-215.
(514) Matta, R.; Hanna, K.; Chiron, S. Oxidation of Phenol by Green Rust and Hydrogen Peroxide at Neutral pH. *Sep. Purif. Technol.* **2008,** *61*, 442-446.
(515) Kone, T.; Hanna, K.; Abdelmoula, M.; Ruby, C.; Carteret, C. Reductive Transformation and Mineralization of an Azo Dye by Hydroxysulphate Green Rust Preceding Oxidation Using H_2O_2 at Neutral pH. *Chemosphere* **2009,** *75*, 212-219.
(516) Lin, Y.; Yang, C.; Xiu, R.; Wang, J.; Wei, Y.; Sun, Y. Decolorization of Methyl Orange by Green Rusts with Hydrogen Peroxide at Neutral pH. *Water Sci. Technol.* **2014,** *69*, 371-377.
(517) Hanna, K.; Kone, T.; Medjahdi, G. Synthesis of the Mixed Oxides of Iron and Quartz and Their Catalytic Activities for the Fenton-Like Oxidation. *Catal. Commun.* **2008,** *9*, 955-959.
(518) Kwan, W. P.; Voelker, B. M. Rates of Hydroxyl Radical Generation and Organic Compound Oxidation in Mineral-Catalyzed Fenton-like Systems. *Environ. Sci. Technol.* **2003,** *37*, 1150-1158.
(519) Valentine, R. L.; Ann Wang, H. C. Iron Oxide Surface Catalyzed Oxidation of Quinoline by Hydrogen Peroxide. *J. Environ. Eng.* **1998,** *124*, 31-38.
(520) Liu, H.; Bruton, T. A.; Doyle, F. M.; Sedlak, D. L. In Situ Chemical Oxidation of Contaminated Groundwater by Persulfate: Decomposition by Fe(III)- and Mn(IV)-Containing Oxides and Aquifer Materials. *Environ. Sci. Technol.* **2014,** *48*, 10330-10336.
(521) Zhang, S.; Zhao, X.; Niu, H.; Shi, Y.; Cai, Y.; Jiang, G. Superparamagnetic Fe_3O_4 Nanoparticles as Catalysts for the Catalytic Oxidation of Phenolic and Aniline Compounds. *J. Hazard. Mater.* **2009,** *167*, 560-566.
(522) Jia, D.; Sun, S.-P.; Wu, Z.; Wang, N.; Jin, Y.; Dong, W.; Chen, X. D.; Ke, Q. TCE Degradation in Groundwater by Chelators-Assisted Fenton-like Reaction

of Magnetite: Sand Columns Demonstration. *J. Hazard. Mater.* **2018,** *346*, 124-132.
(523) Huang, R.; Fang, Z.; Yan, X.; Cheng, W. Heterogeneous Sono-Fenton Catalytic Degradation of Bisphenol A by Fe_3O_4 Magnetic Nanoparticles under Neutral Condition. *Chem. Eng. J.* **2012,** *197*, 242-249.
(524) Hou, L.; Zhang, H.; Xue, X. Ultrasound Enhanced Heterogeneous Activation of Peroxydisulfate by Magnetite Catalyst for the Degradation of Tetracycline in Water. *Sep. Purif. Technol.* **2012,** *84*, 147-152.
(525) Aghdasinia, H.; Arehjani, P.; Vahid, B.; Khataee, A. Fluidized-Bed Fenton-Like Oxidation of a Textile Dye Using Natural Magnetite. *Res. Chem. Intermed.* **2016,** *42*, 8083-8095.
(526) Munoz, M.; Domínguez, P.; de Pedro, Z. M.; Casas, J. A.; Rodriguez, J. J. Naturally-Occurring Iron Minerals as Inexpensive Catalysts for CWPO. *Appl. Catal., B* **2017,** *203*, 166-173.
(527) Aghdasinia, H.; Khataee, A.; Sheikhi, M.; Takhtfiroozeh, P. Pilot Plant Fluidized-Bed Reactor for Degradation of Basic Blue 3 in Heterogeneous Fenton Process in the Presence of Natural Magnetite. *Environ. Prog. Sustainable Energy* **2017,** *36*, 1039-1048.
(528) Xu, L.; Wang, J. Magnetic Nanoscaled Fe_3O_4/CeO_2 Composite as an Efficient Fenton-Like Heterogeneous Catalyst for Degradation of 4-Chlorophenol. *Environ. Sci. Technol.* **2012,** *46*, 10145-10153.
(529) Wang, W.; Liu, Y.; Li, T.; Zhou, M. Heterogeneous Fenton Catalytic Degradation of Phenol Based on Controlled Release of Magnetic Nanoparticles. *Chem. Eng. J.* **2014,** *242*, 1-9.
(530) Nadejde, C.; Neamtu, M.; Hodoroaba, V. D.; Schneider, R. J.; Paul, A.; Ababei, G.; Panne, U. Green Fenton-Like Magnetic Nanocatalysts: Synthesis, Characterization and Catalytic Application. *Appl. Catal., B* **2015,** *176–177*, 667-677.
(531) Deng, J.; Wen, X.; Wang, Q. Solvothermal in situ synthesis of Fe_3O_4-Multi-Walled Carbon Nanotubes with Enhanced Heterogeneous Fenton-Like Activity. *Mater. Res. Bull.* **2012,** *47*, 3369-3376.
(532) Xu, H.-Y.; Shi, T.-N.; Zhao, H.; Jin, L.-G.; Wang, F.-C.; Wang, C.-Y.; Qi, S.-Y. Heterogeneous Fenton-Like Discoloration of Methyl Orange Using Fe_3O_4/MWCNTs as Catalyst: Process Optimization by Response Surface Methodology. *Front. Mater. Sci.* **2016,** *10*, 45-55.
(533) Hu, X.; Liu, B.; Deng, Y.; Chen, H.; Luo, S.; Sun, C.; Yang, P.; Yang, S. Adsorption and Heterogeneous Fenton Degradation of 17α-Methyltestosterone on Nano Fe_3O_4/MWCNTs in aqueous solution. *Appl. Catal., B* **2011,** *107*, 274-283.
(534) Ferroudj, N.; Nzimoto, J.; Davidson, A.; Talbot, D.; Briot, E.; Dupuis, V.; Bée, A.; Medjram, M. S.; Abramson, S. Maghemite Nanoparticles and Maghemite/Silica Nanocomposite Microspheres as Magnetic Fenton Catalysts for the Removal of Water Pollutants. *Appl. Catal., B* **2013,** *136–137*, 9-18.
(535) Liu, W.; Qian, J.; Wang, K.; Xu, H.; Jiang, D.; Liu, Q.; Yang, X.; Li, H. Magnetically Separable Fe3O4 Nanoparticles-Decorated Reduced Graphene Oxide Nanocomposite for Catalytic Wet Hydrogen Peroxide Oxidation. *J. Inorg. Organomet. Polym. Mater.* **2013,** *23*, 907-916.
(536) Magalhães, F.; Pereira, M. C.; Botrel, S. E. C.; Fabris, J. D.; Macedo, W. A.; Mendonça, R.; Lago, R. M.; Oliveira, L. C. A. Cr-containing Magnetites

$Fe_{3-x}Cr_xO_4$: The Role of Cr^{3+} and Fe^{2+} on the Stability and Reactivity Towards H_2O_2 Reactions. *Appl. Catal., A* **2007,** *332*, 115-123.

(537) Liang, X.; He, Z.; Wei, G.; Liu, P.; Zhong, Y.; Tan, W.; Du, P.; Zhu, J.; He, H.; Zhang, J. The Distinct Effects of Mn Substitution on the Reactivity of Magnetite in Heterogeneous Fenton Reaction and Pb(II) Adsorption. *J. Colloid Interface Sci.* **2014,** *426*, 181-189.

(538) Baldrian, P.; Merhautová, V.; Gabriel, J.; Nerud, F.; Stopka, P.; Hrubý, M.; Beneš, M. J. Decolorization of Synthetic Dyes by Hydrogen Peroxide with Heterogeneous Catalysis by Mixed Iron Oxides. *Appl. Catal., B* **2006,** *66*, 258-264.

(539) Costa, R. C. C.; Lelis, M. F. F.; Oliveira, L. C. A.; Fabris, J. D.; Ardisson, J. D.; Rios, R. R. V. A.; Silva, C. N.; Lago, R. M. Novel Active Heterogeneous Fenton System Based on $Fe_{3-x}M_xO_4$ (Fe, Co, Mn, Ni): The Role of M^{2+} Species on the Reactivity Towards H_2O_2 Reactions. *J. Hazard. Mater.* **2006,** *129*, 171-178.

(540) Zhong, Y.; Liang, X.; He, Z.; Tan, W.; Zhu, J.; Yuan, P.; Zhu, R.; He, H. The Constraints of Transition Metal Substitutions (Ti, Cr, Mn, Co and Ni) in Magnetite on Its Catalytic Activity in Heterogeneous Fenton and UV/Fenton Reaction: From the Perspective of Hydroxyl Radical Generation. *Appl. Catal., B* **2014,** *150–151*, 612-618.

(541) Liang, X.; He, Z.; Zhong, Y.; Tan, W.; He, H.; Yuan, P.; Zhu, J.; Zhang, J. The Effect of Transition Metal Substitution on the Catalytic Activity of Magnetite in Heterogeneous Fenton Reaction: In Interfacial View. *Colloids Surf., A* **2013,** *435*, 28-35.

(542) Liang, X.; Zhong, Y.; He, H.; Yuan, P.; Zhu, J.; Zhu, S.; Jiang, Z. The Application of Chromium Substituted Magnetite as Heterogeneous Fenton Catalyst for the Degradation of Aqueous Cationic and Anionic Dyes. *Chem. Eng. J.* **2012,** *191*, 177-184.

(543) Liu, J.; Zhao, Z.; Ding, Z.; Fang, Z.; Cui, F. Degradation of 4-Chlorophenol in a Fenton-Like System Using Au-Fe_3O_4 Magnetic Nanocomposites as the Heterogeneous Catalyst at near Neutral Conditions. *RSC Adv.* **2016,** *6*, 53080-53088.

(544) Lima, M. J.; Leblebici, M. E.; Dias, M. M.; Lopes, J. C. B.; Silva, C. G.; Silva, A. M. T.; Faria, J. L. Continuous Flow Photo-Fenton Treatment of Ciprofloxacin in Aqueous Solutions Using Homogeneous and Magnetically Recoverable Catalysts. *Environ. Sci. Pollut. Res.* **2014,** *21*, 11116-11125.

(545) Avetta, P.; Pensato, A.; Minella, M.; Malandrino, M.; Maurino, V.; Minero, C.; Hanna, K.; Vione, D. Activation of Persulfate by Irradiated Magnetite: Implications for the Degradation of Phenol under Heterogeneous Photo-Fenton-Like Conditions. *Environ. Sci. Technol.* **2014,** *49*, 1043-1050.

(546) Hou, L.; Wang, L.; Royer, S.; Zhang, H. Ultrasound-Assisted Heterogeneous Fenton-Like Degradation of Tetracycline over a Magnetite Catalyst. *J. Hazard. Mater.* **2016,** *302*, 458-467.

(547) Zazo, J. A.; Pliego, G.; García-Muñoz, P.; Casas, J. A.; Rodriguez, J. J. UV-LED Assisted Catalytic Wet Peroxide Oxidation with a Fe(II)-Fe(III)/Activated Carbon Catalyst. *Appl. Catal., B* **2016,** *192*, 350-356.

Table of content graphic